AD_____

Award Number: DAMD17-02-1-0638

TITLE: Preclinical Mouse Models of Neurofibromatosis

PRINCIPAL INVESTIGATOR: Kevin M. Shannon, M.D.
Andrea McClatchey, Ph.D.
Luis Parada, Ph.D.
Marco Giovannini, M.D., Ph.D.
Tyler Jacks, Ph.D.
Judy Small.Ph.D.

CONTRACTING ORGANIZATION: The University of California, San Francisco
San Francisco, CA 94143-0962

REPORT DATE: November 2005

TYPE OF REPORT: Final

PREPARED FOR: U.S. Army Medical Research and Materiel Command
Fort Detrick, Maryland 21702-5012

REPORT DOCUMENTATION PAGE

Form Approved
OMB No. 0704-0188

1. REPORT DATE *(DD-MM-YYYY)*	**2. REPORT TYPE**	**3. DATES COVERED** *(From - To)*
01-11-2005	Final	1 Oct 2002 - 31 Oct 2005

4. TITLE AND SUBTITLE
Preclinical Mouse Models of Neurofibromatosis

5a. CONTRACT NUMBER

5b. GRANT NUMBER
DAMD17-02-1-0638

5c. PROGRAM ELEMENT NUMBER

6. AUTHOR(S)
Kevin M. Shannon, M.D. , Andrea McClatchey, Ph.D., Luis Parada, Ph.D., Marco Giovannini, M.D., Ph.D., Tylr Jacks, Ph.D., Judy Small.Ph.D.

E-mail: shannonk@peds.ucsf.edu

5d. PROJECT NUMBER

5e. TASK NUMBER

5f. WORK UNIT NUMBER

7. PERFORMING ORGANIZATION NAME(S) AND ADDRESS(ES)

The University of California, San Francisco
San Francisco, CA 94143-0962

8. PERFORMING ORGANIZATION REPORT NUMBER

9. SPONSORING / MONITORING AGENCY NAME(S) AND ADDRESS(ES)
U.S. Army Medical Research and Materiel Command
Fort Detrick, Maryland 21702-5012

10. SPONSOR/MONITOR'S ACRONYM(S)

11. SPONSOR/MONITOR'S REPORT NUMBER(S)

12. DISTRIBUTION / AVAILABILITY STATEMENT
Approved for Public Release; Distribution Unlimited

13. SUPPLEMENTARY NOTES

14. ABSTRACT
This report describes three years of research by a Consortium of investigators who worked to develop, characterize, and utilize strains of mice that accurately model tumors found in persons with NF1 and NF2. This Consortium has generated novel models of NF1 and NF2-associated tumors and has exploited these strains to investigate biologic and preclinical questions. The Consortium also organized scientific conferences on the pathologic classification of murine NF-associated neural tumors and on the use of mouse models of NF-associated tumors to test new therapies, and published the proceedings of the pathologic classification conference. The novel strains that have been developed have been shared widely with the research community. The investigators have collaborated closely with each other and have shared expertise and reagents extensively. This NF Consortium is a member of the Moue Models of Human Cancer Consortium of the National Cancer Institute and is participating fully in the activities of the group. A new award from the CDMRP for Neurofibromatosis that received a high priority score will support the continuing efforts of this research group from 2005-2008.

15. SUBJECT TERMS
Neurofibromatosis, cancer, mouse models

16. SECURITY CLASSIFICATION OF:			**17. LIMITATION OF ABSTRACT**	**18. NUMBER OF PAGES**	**19a. NAME OF RESPONSIBLE PERSON**
					USAMRMC
a. REPORT	**b. ABSTRACT**	**c. THIS PAGE**			**19b. TELEPHONE NUMBER** *(include area code)*
U	U	U	UU	127	

Standard Form 298 (Rev. 8-98)
Prescribed by ANSI Std. Z39.18

NSN 7540-01-280-5500

Standard Form 298 (Rev. 2-89)
Prescribed by ANSI Std. Z39-18
298-102

TABLE OF CONTENTS

INTRODUCTION

Benign and malignant tumors are a major cause of morbidity and mortality in individuals afflicted with NF1 and NF2. The *NF1* and *NF2* genes function as tumor suppressors in humans and in mice. Although a great deal has been learned about the genetics, biochemistry, and cell biology of NF1 and NF2-associated tumors, it has proven difficult to translate these advances into new treatments. The development of accurate, well-characterized mouse models of NF-associated tumors NF1 and NF2 would provide an invaluable resource for bringing improved treatments to NF patients. The overall purpose of this consortium, which has been in existence for 6 years, is to develop such models so that they will serve as permanent resources for the scientific community. These efforts are timely for a number of reasons.

First, advances in gene targeting technologies have made it feasible to introduce many types of alterations into the mouse germline. Indeed, the members of this research consortium developed the initial strains of *Nf1* and *Nf2* mutant mice, which provided major insights into a number of the complications seen in human NF1 and NF2 patients. Since the inception of this consortium effort, we have made dramatic progress in improving and extending these models, specifically in the area of engineering conditional mutant alleles of both *Nf1* and *Nf2.* Second, much has been learned about the genetic and biochemical basis of deregulated growth in *NF1* and *NF2*-deficient human cells and in cells from *Nf1* and *Nf2* mutant mice. Genetic analysis of human and murine tumors has provided compelling evidence that *NF1/Nf1* and *NF2/Nf2* function as tumor suppressor genes (TSGs) *in vivo.* Biochemical data have suggested target proteins and pathways for rational drug design. The improved mouse models developed by this consortium now provide invaluable platforms for rigorous preclinical trials of these innovative approaches. Third, new therapies are urgently needed for many of the tumors that arise in individuals with NF1 and NF2. The current treatments for neurofibroma, optic nerve glioma, vestibular schwannoma, and for NF1 and NF2-asociated malignancies are frequently ineffective and carry a substantial risk of long-term morbidity. This consortium is highly complementary to the ongoing efforts to undertake human clinical trials because it will facilitate testing novel agents and approaches in a controlled preclinical setting. The quantity of drug required, expense, and potential liability are all either greatly reduced or eliminated when mouse models are used for preclinical studies. This will facilitate testing a wide range of new therapies that might benefit NF patients. Finally, the Mouse Models of Human Cancer Consortium (MMHCC) of the National Cancer Institute (NCI) is providing an opportunity for interactions among ~20 research groups that are working to develop, validate, and enhance models of a variety of human cancers. NF is the only inherited cancer predisposition represented within the MMHCC as a discrete disease entity. Our group was admitted to the MMHCC in 2000 and has been participating in its activities. Drs. Jacks, Parada, and Shannon are members of the MMHCC Steering Committee, with Dr. Parada serving as the designated representative of the NF Consortium. Dr. Jacks was Co-Chair of the Steering Committee from its inception until last year, and Dr. Shannon served as Co-Chairs from 2002-2005. Thus, this award has provided the NF research community with an exceptional level of representation within the mouse modeling community. The MMHCC is spearheading efforts in areas such as building repositories, devising pathologic classification schemes, imaging mouse tumors, and stimulating interactions with industry in the area of preclinical therapeutics that are of general importance to NF research. The laboratory researchers in this consortium are working with the Children's Tumor Foundation (CTF; formerly the National Neurofibromatosis Foundation). This interaction facilitates research in NF1 and NF2

and links basic and clinical researchers with patients. Our work under this awared focused on the technical objectives (aims) listed below. Progress in each area is summarized in the following sections.

(1) To enhance existing lines of *Nf1* and *Nf2* mutant mice and to develop new *in vivo* models of NF-associated tumors. We will fully characterize lesions that arise in these mice, focusing on how closely they reproduce the phenotypic, genetic, and biochemical alterations seen in comparable human tumors.

(2) To perform *in vitro* and *in vivo* studies to elucidate biochemical pathways underlying the proliferative advantage of *Nf1* and *Nf2*-deficient cells as a way of identifying molecular targets for therapeutic interventions.

(3) To use these models to perform preclinical trials that will test the efficacy and toxicities of rational therapies for tumors that arise in individuals with NF1 and NF2.

(4) To organize specialized working group meetings that will address: (1) Pathologic Classification of Tumors in NF Mouse Models, and (2) Preclinical Therapeutics in NF Mouse Models, and to develop a pilot program to support preclinical testing of promising treatments in mouse models of NF1 and NF2.

BODY

Background

Tumor Spectrum in NF1 and NF2 Patients. Persons with NF1 are predisposed to benign neurofibromas, optic nerve gliomas, and to specific malignant neoplasms. Individuals with NF1 typically develop multiple neurofibromas that can result in cosmetic, orthopedic, and neurologic disabilities. Optic nerve gliomas are another vexing clinical problem. Although histologically benign, these tumors frequently cause visual impairment or blindness because of their anatomic location. The malignant neoplasms seen in NF1 patients include astrocytoma, malignant peripheral nerve sheath tumor (MPNST), pheochromocytoma, and juvenile myelomonocytic leukemia (JMML). NF2 affects 1 in 40,000 persons worldwide. Other NF2-related tumors include meningiomas, gliomas, and ependymomas.

Production and Characterization of *Nf1* and *Nf2* Mutant Mice. Drs. Jacks and Parada independently disrupted *Nf1* by inserting a neomycin *(neo)* cassette into exon 31 (1, 2). Homozygous *Nf1* mutant ($Nf1^{-/-}$) embryos die *in utero* with cardiac anomalies, which precludes the use of these mice to study important aspects of NF1 pathology, including the formation of many tumor types. To circumvent this problem, Dr. Parada's lab harnessed *Cre-loxP* technology to create a conditional *Nf1* allele (3). Importantly, the Parada's lab showed that the $Nf1^{flox}$ allele functions as a wild-type allele in spite of harboring *loxP* sites and a *neo* gene within its intronic sequences. The $Nf1^{flox}$ allele is readily recombined *in vivo* to make a null allele through co-expression of *Cre* recombinase. Drs. McClatchey, Jacks, and Giovannini used gene targeting to disrupt the *Nf2* locus (4, 5). Homozygous *Nf2* mutant embryos failed without initiating

gastrulation. Although heterozygous *Nf2* mutant mice are cancer prone, these animals do not develop schwannoma or meningioma. To circumvent the early embryonic-lethal phenotype associated with homozygous inactivation of *Nf2* and to test the hypothesis that the tumor spectrum might be modulated by the rate of the loss of the normal allele in specific tissues, Dr. Giovannini and his colleagues generated a conditional mutant *Nf2* allele (6). As expected, mice homozygous for the $Nf2^{flox2}$ mutant allele ($Nf2^{flox2/flox2}$) were viable and fertile suggesting that the introduction of *loxP* sites did not hamper *Nf2* expression. Induced expression of *Cre* recombinase in $Nf2^{flox2/flox2}$ mice results in biallelic inactivation of *Nf2* in specific tissues. The major research goals of this Consortium include exploiting these conditional mutant alleles of *Nf1* and *Nf2* to develop tractable models of NF-associated tumors for use in our labs and by other investigators. A list of investigators who have received these mice appears in the Reportable Outcomes section.

Models of NF1 and NF2-Associated Tumors. In work published prior to 2004, the participants in this consortium reported the phenotypic and biologic features of NF1-associated mouse tumor models of MPNST/Triton tumor, astrocytoma, JMML, plexiform neurofibroma, and chemotherapy-induced leukemia (7-12) and of NF2-associated tumors such as vestibular Schwannoma and meningioma (5, 6). These data are also described in detail in previous annual reports.

Progress Report

Technical Objective (Aim) 1: To enhance existing lines of Nf1 and Nf2 mutant mice and to develop new in vivo models of NF-associated tumors

An Enhanced Model of JMML. JMML is a lethal myeloproliferative disorder (MPD) characterized by over-production of infiltrative myeloid cells (13). JMML has been modeled in mice by transferring *Nf1*-deficient fetal liver cells into irradiated recipients (14, 15). However, this system is cumbersome and expensive because it requires embryo dissections around E13 and injecting fetal liver cells into irradiated hosts. To circumvent these problems, Drs. Shannon and Parada collaborated to breed $Nf1^{flox}$ and *Mx1-Cre* mice and then induced somatic *Nf1* inactivation in hematopoietic cells. The results of these studies are presented in detail in a paper by Le, *et al.* (16). Briefly, the Cre recombinase is expressed from the interferon-inducible *Mx1* promoter in the *Mx1-Cre* strain. Injecting *Mx1-Cre,* $Nf1^{flox/flox}$ mice with polyinosinic-polycytidylic acid (pIpC*)* induced endogenous interferon production and efficiently ablated *Nf1* in the hematopoietic compartment. These mice consistently developed MPD, which was associated with elevated myeloid cell counts and progressive splenomegaly.

Mx1-Cre, $Nf1^{flox/flox}$ bone marrow cells showed a modest increase in baseline Ras-GTP levels, but phosphorylation of the downstream effectors MEK and Akt were similar in mutant and control cells (data not shown). Exposing *Mx1-Cre,* $Nf1^{flox/flox}$ and wild-type bone marrow to granulocyte-macrophage colony stimulating factor (GM-CSF) induced robust Ras-GTP, MEK, and Akt activation from baseline levels that was equivalent in both genotypes (data not shown). Because *Nf1-/-* and wild-type bone marrows showed marked differences with respect to the relative proportions of different cell types, the Shannon lab isolated Mac1+ cells and compared MEK activation in this myeloid subpopulation. In these experiments, *Nf1-/-* cells showed sustained activation of MEK after exposure to GM-CSF (16). *Mx1-Cre,* $Nf1^{flox/flox}$ mice and cells from these animals can be used to examine the biochemical consequences of *Nf1* inactivation in

primary cells and to test molecularly targeted agents with pharmacodynamic monitoring of relevant biochemical endpoints. As summarized under Technical Objectives 2 and 3, the Shannon lab has launched major initiatives in these areas.

Plexiform Neurofibroma Formation in *Nf1*$^{flox/flox}$ Conditional Mutant Mice. The Parada lab has continued to pursue the novel plexiform neurofibroma models developed in prior fund years. They have generated convincing genetic evidence that the etiology of plexiform neurofibromas requires homozygous inactivation of *Nf1* in Schwann cell (SC) precursors. Thus, *Nf1*-deficient SC in the context of wild type cells cannot give rise to frank tumors. The Parada lab is investigating the source of the heterozygous (haploinsufficient) contribution to these tumors. The first suspect is the mast cell due to their presence in peripheral nerves that contain null, but not heterozygous, SC (8). To examine the potential causal role of hematopoieitc cells in tumor formation, the Parada lab initiated adoptive transfer experiments in collaboration with Dr. Wade Clapp (Indiana U.). *Nf1*$^{flox/flox}$*;Krox20Cre* mice do not form neurofibromas whereas *Nf1*$^{flox/-}$*;Krox20Cre* mice do. Therefore, bone marrow from *Nf1*$^{+/-}$ mice was adoptively transferred into irradiated *Nf1*$^{flox/flox}$*;Krox20Cre* mice. The recipient mice were maintained for 4 months and then necropsied to analyze mast cell infiltration in peripheral nerves. The recipient mice exhibit enlarged peripheral nerves reminiscent of the tumor bearing *Nf1*$^{flox/-}$*;Krox20Cre* mice and histological examination demonstrates mast cell infiltration and evidence of incipient tumor formation. These data provide a compelling demonstration of a non-cell autonomous contribution to tumor formation by transplanted bone marrow. The presence of infiltrating mast cells in pripheral nerves supports the "mast cell hypothesis" of neurofibroma pathogenesis and give direct insight into potential therapeutic windows for therapeutic intervention.

The Giovannini and Parada labs have also collaborated to generate a novel model of neurofibroma in which use of a P0-cre mice gives a different type of neurofibroma. These tumors project peripherally rather than centrally and may provide additional new clues into mechanisms of tumor formation.

Modeling Optic Track Glioma and Astrocytoma in *Nf1* Mice. Approximately 15-20% of children with NF1 develop pilocytic astrocytomas, which predominantly occur within the optic pathway and hypothalamus (17, 18). The Parada lab recently published their initial studies into the origin of these tumors. As summarized in the attached pdf file, ablating *Nf1* with a *h*-GFAP-Cre transgene results in fully penetrant hyperplasia of the optic nerve and a 20% incidence of optic glioma. Thus, although *Nf1* loss is necessary for optic glioma, it is apparently not sufficient. The Parada lab has also studied the developmental biology of optic nerve formation. Interestingly, normal development relies on requisite interactions between differing cell types and this may provide insight into therapeutic windows.

Glioblastoma is the most common malignant tumor of the CNS and no effective therapies are available. Patients with NF1 have a 5-10-fold increase in the incidence of glioblastoma over the general population. Thus, germ line *NF1* mutations also predisposes to this malignant tumor. Basing our work on the known oncogene and tumor suppressor mutations in sporadic glioma, the Parada lab constructed mice lacking both *Nf1* and *p53* in CNS precursor cells. These mice develop gliomas with 100% penetrance. However, 1 to 3 tumors are detected in each brain suggesting that at the cellular level, the penetrance is actually rare. The gliomas resemble sporadic human gliomas at all levels analyzed from histopathological to molecular (19). Study of presymptomatic mice indicates that the earliest lesions associate with stem cell niches.

Therefore, Dr. Parada and his colleagues propose that the origin of the glioma is a stem cell. They are intensively investigating these "cancer stem cells" and characteristics that might afford therapeutic windows of opportunity.

Nf2 and *p53* Mutations Cooperate in Neural Crest Tumor Formation. Schwannomas are frequent in NF2 patients and also occur as sporadic tumors. Both familial and sporadic schwannomas show mutations of the *NF2* gene. Specific biallelic *Nf2* gene mutation in the mouse neural crest cell lineage results in Schwann cell hyperplasia at high frequency, but schwannomas are rare. This suggests that additional mutations are required for progression from hyperplasia to schwannoma. Dr. Giovannini's lab has evidence that the *Nf2* and *p53* tumor suppressor genes cooperate in neural crest tumorigenesis. The time window in which mutations are induced/occur determines whether malignant Schwann cell or osteogenic tumors arise, indicating its critical importance for accurate tumor modelling. In particular, they assessed the role of *p53* hemizygosity in conditional *Nf2* knockout mice and found strong synergy between *Nf2* and *p53* mutations in development of malignant tumors of neural crest origin. Nearly all P0Cre^{B};$Nf2^{flox2/flox2}$;$p53^{+/-}$ mice rapidly died starting at a median age 4.5 months and developed malignant peripheral nerve sheath tumors (MPNSTs). Benign Schwann cell tumors were also seen, including schwannomas in 3 of 26 (11%) and neurofibromas in 2 of 26 (8%) animals (the distinction between the two entities in the mouse could not always be established with certainty following the criteria of human pathology).

Osteogenic Tumors Predominate in P0*Cre*;$Nf2^{flox2/+}$;$p53^{+/-}$ *cis* Mice. Dr. Giovannini found that the great majority of P0*Cre*;$Nf2^{flox2/+}$;$p53^{+/-}$ *cis* mice (81%) developed osteogenic tumors, both osteosarcomas (63%) and osteomas (25%) that all arose in the neural crest-derived bone at a mean age of 5.5 months. So, in contrast to the P0*Cre*;$Nf2^{flox2/+}$;$p53^{+/-}$ *cis* mice, P0*Cre*;$Nf2^{flox2/flox2}$;$p53^{+/-}$ mice did not develop osteogenic tumors suggesting that early loss of schwannomin may lead to compensatory signaling thereby preventing the generation of osteogenic tumors. Loss of merlin at a later developmental stage may disable this compensatory signaling leading to the generation of osteogenic tumors. Although the developmental stage of Schwann cells may determine their susceptibility to tumor-initiating alterations (20, 21), a concomittant modification of the tumor spectrum has not been described yet. Dr. Giovannini's observations may indicate that the proliferation rate and the probability of LOH are higher in homozygous than in heterozygous *Nf2* mutant cells or that functional loss of *Nf2* increases the risk of abnormal chromosomal segregation. Moreover, these data infer that the time window in which gene inactivation occurs is critical for accurate tumor modeling.

Construction of Drug-Inducible Cre Mice to Locally and Temporally Control Deletion of the *Nf2* Gene. In addition to using conventional transgenic Cre lines to inactivate the conditional $Nf2^{flox}$ allele generated by Dr. Giovannini, the Jacks lab has generated drug-inducible Cre mice that will permit local ablation and desired time points. They have inserted a modified Cre, $CreER^{T2}$ (Cre fused to an altered human estrogen receptor that is activated by the drug tamoxifen), downstream of the ubiquitous Rosa26 promoter. $CreER^{T2}$ is ten times more sensitive to tamoxifen than the first generation of CreER constructs; therefore, it will avoid confounding issues related to tamoxifen toxicity. The Jacks lab has demonstrated that the $CreER^{T2}$ construct is functional in ES cells, and has generated mice that have $CreER^{T2}$ in the germ line. By crossing the Rosa26-$CreER^{T2}$ mice to mice containing a Cre reporter (Rosa26-LSL-$LacZ^{2lox}$), they have determined

the pattern of Cre expression. In the absence of tamoxifen no background Cre activity was detected. After intraperitoneal injection of 9 mg tamoxifen/40 g body weight for 5 consecutive days, Cre activity was detected throughout the liver and intestine and in a mosaic fashion within the brain and other organs (data not shown).

The Jacks lab intercrossed Rosa26-CreER^{T2} and *Nf2^{flox}* mice to generate Rosa26-CreER^{T2}; *Nf2$^{flox/flox}$* mice. A single intraperitoneal injection of 3 mg/40 g body weight of tamoxifen into pregnant female mice at E8.5 resulted in neural tube defects in the subset of embryos with the genotype Rosa26-CreER^{T2}; *Nf2$^{flox/flox}$*. Thus, acute inactivation of *Nf2* in development can recapitulate the tissue fusion defects observed in Nestin-Cre^{p};*Nf2$^{flox/1lox}$* mice (see below). The Jacks lab has also injected adult Rosa26-CreER^{T2}; *Nf2$^{flox/flox}$* mice with a single intraperitoneal tamoxifen dose of 4.5 mg/40 g body weight. At 1 month post injection, these mice appear healthy and are being monitored closely for signs of tumor formation.

Generation and Characterization of Mouse Models of Ependymoma. Brain tumors are the second most frequent malignancy of childhood and are the leading cause of death from childhood cancer. Ependymoma, a type of primary brain tumor that arises from the specialized glial cells (ependymal cells) that line the ventricular system, may develop at any age. However, ependymomas are particularly common in young children, accounting for 6-12% of pediatric brain tumors, and this tumor type occurs at increased frequency in children with NF2. Although ependymomas are slow growing and histologically classified as WHO grade II/IV, the 5-year progression free survival is only 50%, with children under two years of age having a particularly dismal prognosis. Since mutation of the *NF2* gene is the only well documented genetic alteration in human ependymomas, the Jacks laboratory is generating mouse models of ependymoma in which the initiating event is loss of *Nf2*. Previous work from the Jacks lab has shown that *Nf2$^{-/-}$* mice die in early embryogenesis secondary to defects in the extraembryonic tissues, and that *Nf2$^{+/-}$* mice develop malignant tumors but not the tumor types characteristic of the human disease (schwannoma, meningioma, and ependymoma). Therefore, all of the mouse models now under construction are making use of the conditional *Nf2^{flox}* allele generated by Dr. Giovannini. At this time, no ependymal cell-specific promoter has been characterized. Such a promoter would be the ideal way to drive Cre expression in ependymal cells. In the absence of such a promoter, the Jacks laboratory is using Cre transgenic mice in which Cre is expressed within ependymal cells but also within other cells of the body and/or brain. Like neurons and other glial cells that form the brain, ependymal cells develop from neuroepithelial cells, which express the intermediate filament nestin. Neuroepithelial cells are thought give rise to radial glial cells, which in turn give rise to immature ependymal cells (tanycytes). Tanycytes mature into ependymal cells that continue to express nestin and in the mouse but not in humans, express another intermediate filament glial fibrillary acidic protein (GFAP). A few tanycytes remain in adult animals. Both Nestin-Cre and *h*GFAP-Cre transgenic mice are currently available.

By crossing Nestin-Cre and *h*GFAP-Cre mice to mice containing a Cre reporter (Rosa26-LSL-LacZ), Jacks laboratory has confirmed that both Nestin-Cre and *h*GFAP-Cre mice do express Cre within the ependymal cell layer. Nestin-Cre is highly expressed in neurons and other glial cells in the brain and throughout most tissues of the body. Nestin-Cre expression is detected as early as E8.5. *h*GFAP-Cre expression is restricted to neurons and glial cells, and is detected as early as E14.5. The *h*GFAP-Cre transgenic mouse was constructed with the human GFAP promoter; therefore, the pattern of Cre expression more closely resembles that of human GFAP.

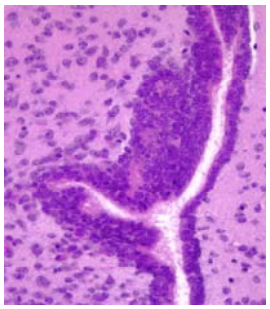

Figure 1 "Mini" ependymoma with true rosettes arising in the wall of the third ventricle in a postnatal day 11 Nestin-Cre^{m};*Nf2*$^{flox/flox}$ mouse.

Nestin-Cre^{p};*Nf2*$^{flox/flox}$ mice in which the neural tube has closed (70% of all mutants) showed diffuse hyperproliferation of ependymal cells around the ventricles and central canal of the spinal cord (Fig. 1). A single Nestin-Cre^{m};*Nf2*$^{flox/flox}$ mouse that survived past birth had a focal lesion arising from the wall of the third ventricle in which the ependymal cells formed tubules resembling the true rosettes of human ependymomas. This lesion appears to represent the earliest stage of ependymoma. By contrast, the Jacks laboratory has generated 25 *h*GFAP-Cre;*Nf2* $^{flox/flox}$ mice, and to date none of the mice analyzed histologically has shown evidence of ependymal cell hyperproliferation. These studies suggest that Nestin-Cre-expressing neuroepithelial cells or ependymal cells, not *h*GFAP-Cre-expressing radial glia or tanycytes, are the most likely cells of origin of ependymomas.

Since *h*GFAP-Cre;*Nf2* $^{flox/flox}$ mice do not develop ependymoma, the Jacks lab generated cohorts of 25 *h*GFAP-Cre;*Nf2* $^{flox/flox}$;*p53*$^{flox/flox}$ mice and 25 *h*GFAP-Cre;*Nf2* $^{flox/flox}$;*APC*$^{flox/flox}$ mice, as both *p53* and *APC* mutations have been implicated in the pathogenesis of human ependymomas. To date, none of these mice have developed ependymomas. Given the recent data from other groups suggesting that ependymomas may arise from distinct subpopulations of radial glia, we are investigating other strategies to inactivate *Nf2* in the radial glia, such as Rosa26-CreER^{T2} and Nestin-CreER^{T2}.

Modeling the Interaction between *Nf1* Inactivation and Genotoxins in the Pathogenesis of Therapy-Induced Cancers. Therapy-induced malignant neoplasms are a severe late complication of mutagenic therapies. The pathogenesis of these cancers is obscure, and there is a lack of relevant animal models. The risk of therapy-induced cancers is of great importance to persons with NF1 and NF2 because they are predisposed to tumors that often require aggressive treatment and because they might be prone to therapy-induced cancers if chemotherapy and radiation induce mutations that cooperate with inactivation of *NF1* or *NF2.* Indeed, there is clinical evidence that patients with NF1 are susceptible to therapy-induced cancers. A systematic review of 64 children with NF1 who received chemotherapy and/or radiation (RAD) to treat a primary cancer revealed 11% with a second malignant neoplasm (SMN), all of which were either myeloid malignancies or sarcomas (22). Two adults with NF1 have also been reported who developed therapy-related myelodysplastic syndrome (MDS) after treatment for *de novo* acute myeloid leukemia (AML) (23). These observations suggest that therapeutic exposure to genotoxic agents cooperates with germline *NF1* mutations in the genesis of common SMNs found in the general population, namely myeloid leukemia and sarcoma.

In studies that were initiated under US Army NF Research Project DAMD 17-02-1-0638, the Shannon and Jacks lab investigated tumor induction by RAD, the alklyating agent cyclophosphamide (CY), or both modalities in heterozygous *Nf1* mutant (*Nf1*+/-) mice. The results of these studies are summarized briefly here because they were published last month (24). *Nf1*+/- mice that were exposed to these mutagens developed a spectrum of secondary cancers that are common in human patients, including myeloid malignancies, soft tissue sarcomas, and breast cancers. A total of 192 wild-type (WT) and *Nf1*+/- mice that were assigned to one of four groups: no treatment, CY alone, RAD alone, or CY followed by RAD were followed for tumor development for 18 months after exposure. Pathologic analysis was performed on 91% of the

study cohort, including 95 of 104 WT mice and 77 of 86 *Nf1-/-* mice. Heterozygous inactivation of *Nf1* was strongly associated with an increased risk of premature death with a survival rate of 30% after 15 months in *Nf1*+/- mice compared with 78% in WT littermates. Tumor types that occurred significantly more often in *Nf1+/-* mice included sarcomas with features of human MPNST (p=0.001), myeloid malignancies (p=0.0005), and pheochromocytomas (p=0.0007). Myeloid malignancies and sarcomas, which are the most common SMNs in human patients, accounted for 24 of the 52 cancers found in *Nf1+/-* mice. Four *Nf1*+/- mice unexpectedly developed breast cancer versus no cases in the WT animals (p=0.04, Fisher's exact test).

We found that RAD cooperates strongly with heterozygous *Nf1* inactivation in tumorigenesis whether administered alone or after CY. By contrast, the incidence of cancer was similar in untreated *Nf1+/-* mice and in animals that received CY only. Interestingly, the nature of the mutagen exposure influenced the tumor spectrum in *Nf1*+/- mice. In particular, RAD alone resulted in a greater frequency of myeloid malignancies, whereas exposure to RAD in combination with CY resulted in a high incidence of solid tumors, including breast cancer. Molecular analysis revealed loss of the WT C57Bl/6 *Nf1* allele in 6 of 8 soft tissue sarcomas, confirming the important role of biallelic inactivation of *Nf1* in tumorigenesis (data not shown). LOH also occurred in 3 of 3 pheochromocytomas and in 4 of 4 breast cancers. By contrast, PCR analysis did not reveal LOH in any of the myeloid malignancies. Drs. Jacks and Parada found that inactivation of *Trp53* and *Nf1* cooperate in tumorigenesis, particularly sarcoma development (7, 25). The loci for these two genes are approximately 7 cM apart on mouse chromosome 11, while the human homologs are separated by approximately 22 Mb on chromosome 17. Surprisingly, while LOH at *Trp53* occurred in all of the breast tumors, most of the sarcomas from *Nf1+/-* mice retained both *Trp53* alleles. Biochemical analysis of three cell lines generated from mutagen-induced breast cancers demonstrated prolonged Ras activation, which is consistent with a recent report (26). Levels of phosphorylated ERK and Akt changed in parallel with Ras•GTP (24).

These data establish a robust and tractable mouse model of common human SMNs. *Nf1+/-* mice can be harnessed to address the mutagenic potential of chemotherapeutic agents given alone and in combination and to test preventive strategies. This work has implications for treating tumors that arise in the patients with NF1. In particular, a single low dose of RAD cooperated strongly with heterozygous *Nf1* inactivation in tumorigenesis. Children with NF1 are strongly predisposed to optic tract gliomas and low-grade astrocytomas, which may be difficult to manage. Data in *Nf1+/-* mice suggest that the potential risk of SMN should be considered when deciding when to irradiate these and other NF1-associated tumors, and that patients who require RAD should be followed carefully for subsequent treatment-induced cancers.

Technical Objective (Aim) 2: To perform in vitro and in vivo experiments that will elucidate molecular targets for therapeutic interventions.

Functions of Neurofibromin and Merlin. The identification and validation of molecular targets remains a significant rate-limiting step in the discovery of effective therapies for the complications of NF1 and NF2 disease. Addressing this central question ultimately depends on having accurate cellular systems for interrogating how specific biochemical pathways are perturbed in *Nf1* and *Nf2* deficient cells. Cells from the strains of mice engineered by the members of this Consortium now provide robust systems for performing genetic, biochemical,

and cell biologic experiments to uncover genes that cooperate in generating NF-associated tumors and to characterize proteins that might be targets for therapeutic intervention.

Considerable work from our laboratories and others has shown that loss of *NF1/Nf1* function leads to hyperactivation of the Ras signaling pathway. Post-translational processing of Ras proteins has attracted interest as a potential target for drug discovery in various cancers and in NF1. Processing is initiated by farnesyltransferase (Ftase), which attaches a farnesyl lipid to the thiol group of the cysteine (the "C" of the CAAX motif). Prenylation targets Ras to membranes, and is required for biologic activity. However, K-Ras and N-Ras are substrates for geranylgeranyltransferase 1 (GGTase 1) and are processed by this alternative pathway when Ftase is inhibited and the initial clinical experience with Ftase inhibitors has been disappointing. Indeed, extensive data now support the view that non-Ras C*AAX* proteins are critical *in vivo* targets of the Ftase inhibitors (reviewed in (27)). After prenylation, the carboyxl terminal three amino acids are released by Rce1, an integral membrane endoprotease of the endoplasmic reticulum. The final step in Ras processing involves methylation of the prenylcysteine by isoprenylcysteine carboxyl methyltransferase *(Icmt).* Genetic experiments performed by Dr. Shannon's lab showed no detectable effects of ablating *Rce1* on normal hematopoiesis (28).

Agents that interfere with various signaling pathways downstream of Ras (such as the Raf1-MEK-MAPK and phosphoinositide-3-OH kinase (PI3K)-protein kinase B (PKB; also known as Akt) cascades) are of obvious interest in the treatment of NF1-associated tumors. Upstream receptor tyrosine kinases and their ligands may also be required for the growth of specific *NF1/Nf1* mutant tumors, including GM-CSF in the case of myeloid leukemia and epidermal growth factor receptor (EGFR) for MPNSTs (29, 30). It is important to note that genetic experiments in *Drosophila* have also demonstrated link between loss of neurofibromin function and PKA signaling.

Until recently, much less was known about the biochemical consequences of *Nf2* inactivation. However, data from the McClatchey, Giovannini and Jacks laboratories are providing key insights into the molecular function of merlin and have identified several potential therapeutic targets. For example, accumulating evidence indicates a reciprocal relationship between merlin and the small GTPase Rac1. Drs. McClatchey and Jacks demonstrated that Rac1 activation leads to phosphorylation, reduced membrane:cytoskeleton association and impaired growth suppressing activity of merlin (31). Conversely, merlin overexpression blocks Rac activation and $Nf2^{-/-}$ cells exhibit features of excessive Rac signaling. A similar reciprocal relationship between the closely related ERM proteins and Rho has been demonstrated. Dr. Jacks and others went on to demonstrate that the Rac effector kinase Pak1 can phosphorylate merlin; indeed, recent work from the Jacks laboratory has now shown that merlin can bind to and inhibit PAK1 (32-34). Inhibitors of Rac/PAK1 signaling exist and represent attractive candidates for the treatment of *NF2*-deficient tumors.

Genetically engineered mice are a valuable source of primary cells for studying the consequences of gene deficiency. Dr. McClatchey's group found that a signature of *Nf2*-deficiency across several different types of cells is loss of contact-dependent inhibition of proliferation and abnormal cell:cell communication (35). Specifically, $Nf2^{-/-}$ cells do not form stable cadherin-based cell:cell junctions known as adherens junctions (AJs) and merlin normally localizes to these structures in wild-type cells. Merlin may normally stabilize the interaction between nascent AJs and the actin cytoskeleton either by controlling Rac activity or stabilizing actin filaments, both of which are required for AJ assembly (31, 36). Accumulating evidence indicates that AJ assembly results in silencing of membrane tyrosine kinase receptors such as the

epidermal growth factor receptor (EGFR) (37-39). Indeed, Dr. McClatchey's group has found that EGFR silencing is defective in several types of confluent *Nf2*$^{-/-}$ cells. Their data indicate that merlin complexes with the EGFR and controls its surface availability upon cell:cell contact; this, in turn, controls EGFR internalization and association with its immediate downstream targets (i.e. Grb2/Sos/PLC-γ; Fig. 2). These data not only provide mechanistic insight into the molecular basis of merlin's function as a tumor suppressor, but also suggests potential therapeutic targets for NF2.

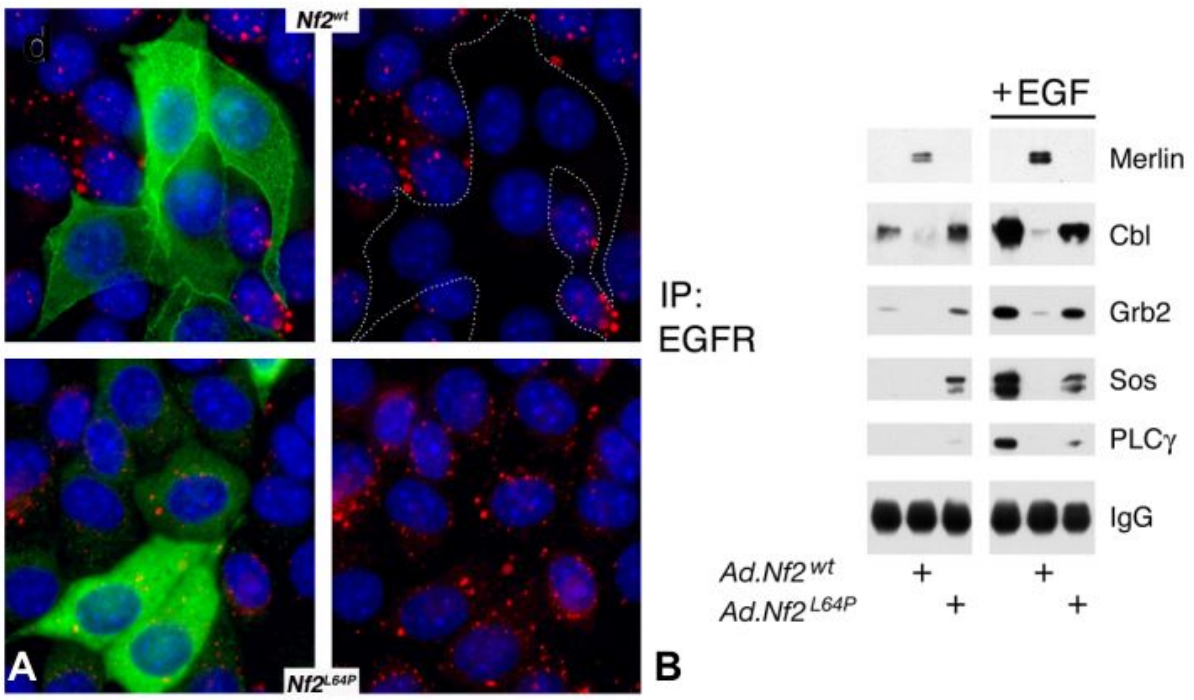

Figure 2. Merlin prevents EGFR internalization and effector association. **A**. Internalization of fluorescent Tr-EGF (red) in confluent *Nf2*$^{-/-}$ liver cells into which wild-type (top, green) or mutant (L64P ; bottom, green) have been reintroduced at low efficiency to produce mosaic cultures. Vesicles containing internalized Tr-EGF are apparent in virtually every *Nf2*$^{-/-}$ cell ; however, internalized Tr-EGF was rarely observed in cells expressing Nf2^{wt}, which concentrates along cell :cell boundaries (top, green). In contrast, Tr-EGF internalization was rarely seen in cells expressing Nf2^{L64P} (bottom, green), which fails to concentrate along cell :cell boundaries. **B**, After reintroduction into *Nf2*$^{-/-}$ liver cells, Nf2^{wt} but not Nf2^{L64P} complexes with the EGFR and prevents its interaction with multiple signaling effectors in response to EGF.

Indeed, Dr. McClatchey's group has also found that EGFR inhibitors such as gefitinib (Iressa, AstraZeneca) can restore contact inhibition to *Nf2*$^{-/-}$ cells (Fig. 3). Several inhibitors of the EGFR (ErbB1) and its close family members (ErbB2, 3, and 4) have been developed and some are being evaluated in clinical trials for other types of cancer and therefore may be excellent candidates for therapeutic intervention in NF2 (40). Indeed, given the plethora of phenotypes associated with *NF2*-deficiency in different mammalian cell types *in vivo*, merlin may also control the endocytic trafficking of other membrane receptors. This work has been submitted for publication.

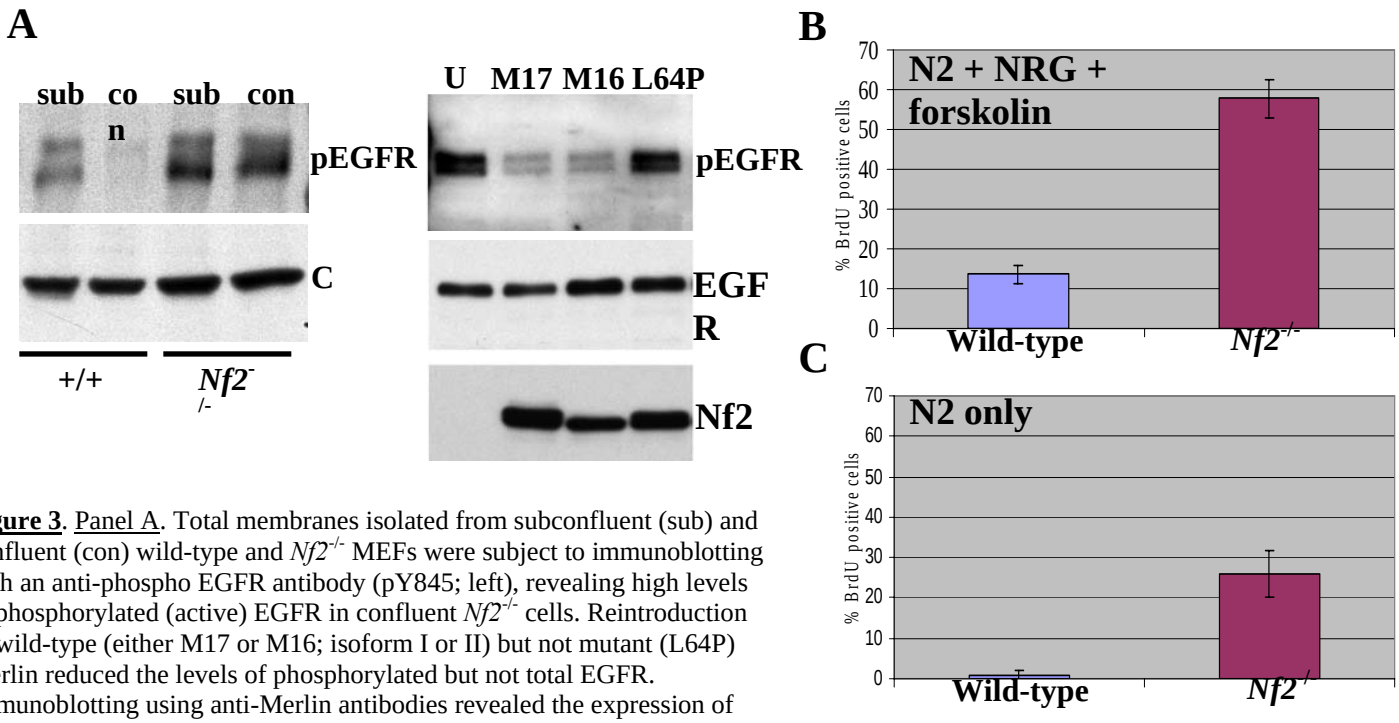

Figure 3. Panel A. Total membranes isolated from subconfluent (sub) and confluent (con) wild-type and *Nf2*$^{-/-}$ MEFs were subject to immunoblotting with an anti-phospho EGFR antibody (pY845; left), revealing high levels of phosphorylated (active) EGFR in confluent *Nf2*$^{-/-}$ cells. Reintroduction of wild-type (either M17 or M16; isoform I or II) but not mutant (L64P) Merlin reduced the levels of phosphorylated but not total EGFR. Immunoblotting using anti-Merlin antibodies revealed the expression of each Merlin isoform. U, uninfected. Panels B and C. Schwann cells isolated from E12.5 *Nf2*$^{lox/lox}$ DRG were infected with empty adenovirus (left, wild-type) or Ad-Cre (right, *Nf2*$^{-/-}$) and grown to confluence in either N2 plus NRG plus forskolin (B) or in N2 medium alone without NRG (C). Cells were exposed to Brd for 2 hours.

Signal Transduction in Primary *Nf1*-Deficient Hematopoietic Cells. A previous biochemical investigation of *Mx1-Cre, Nf1*$^{flox/flox}$ mice with MPD surprisingly revealed only modestly elevated levels of phopsho-MEK and phospho-ERK in the Mac1^{+} fraction of bone marrow and spleen cells (16). By contrast, myeloid cell lines generated from *Nf1-/-* fetal liver cells show markedly elevated levels of Ras-GTP and hyperactivation of MEK and Akt, which infer that components of the Raf1-MEK-ERK and PI3 kinase/Akt/mTOR sigaling cascades are rational targets for drug development (41). The Shannon lab is exploiting bone marrow cells from *Mx1-Cre, Nf1*$^{flox/flox}$ mice in a concerted effort to extend their observations in *Nf1-/-* cell lines to primary cells. They considered a number of possible explanations for the subtle signaling differences that were detected in primary *Nf1-/-* bone marrow cells. First, the experimental conditions used to collect, starve, and stimulate primary cells might have obscured *in vivo* differences in the activation status of Ras and its downstream effectors between *Nf1*-deficient and normal bone marrow. Alternatively, because hematopoietic cells at various stages of differentiation are present in *Mx1-Cre, Nf1*$^{flox/flox}$ mice with MPD, aberrant activation of effector cascades within a minor subpopulation of immature myeloid cells would not be detected in lysates of whole bone marrow or spleen. Finally, primary *Nf1*-deficient cells might respond to hyperactive Ras by remodeling signaling networks over time. These potential explanations are not mutually exclusive, and all three may be operative at some level.

To address these issues, the Shannon lab first interrogated the activation status of a series of signaling molecules downstream of Ras in bone marrow cells *Mx1-Cre, Nf1*$^{flox/flox}$ mice under a variety of experimental conditions. They discovered that incubating cells with even a low concentration of serum (0.1%) increased basal signaling and blunted the response to GM-CSF stimulation (data not shown). They went on to define serum-free culture conditions under which wild-type and mutant cells down-regulated Ras-dependent pathways that could be robustly activated by adding serum and GM-CSF. These studies showed that optimal conditions for short-term culture include the use of serum-free medium supplemented with 1% BSA. Signaling experiments performed under these optimized conditions surprisingly uncovered two distinct profiles in bone marrow cells from *Nf1* mutant mice with MPD. Approximately half of the animals showed activation of multipe downstream effectors for Ras-GTP (Fig. 4A). A second group of mice that typically had long survival showed attenuated RSK and Akt signaling, which was dramatic in some cases (Fig. 4B). Attenuation was also observed in Mac1+ cells and in cultured macrophages from these mice (data not shown). Together, these provocative data, whihc raise the possibility that *Nf1* mutant hematopoietic cells adapt to chronic hyperactive Ras by remodeling signaling pathways, have profound implications for the use of molecularly targeted therapeutics to treat complications of NF1 disease.

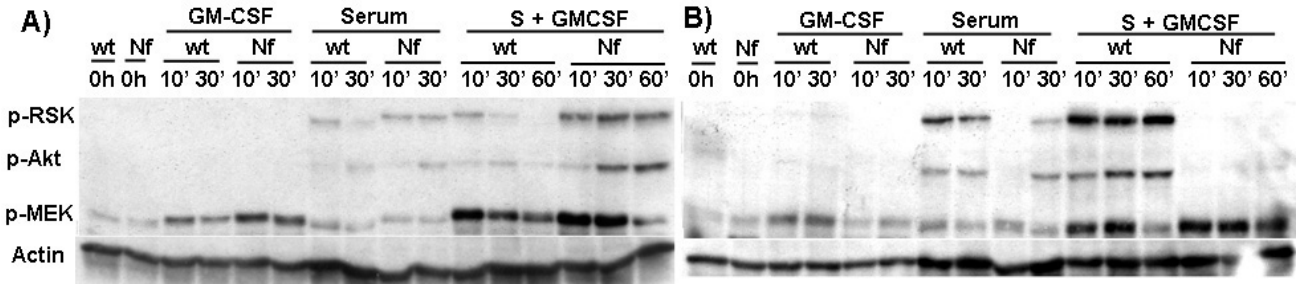

Figure 4. Representative experiments showing primary bone marrow cells from *Nf1-/-* mutant mice with (A) hyperphosphorylated RSK, and Akt; and (B) mice with attenuated p-RSK and p-Akt.

Addressing the general question of how *Nf1* inactivation perturbs the activation status of Ras effector pathways over time requires methodologies for accurately assessing the phosphorylation status of signaling molecules in small subpopulations of primary cells. To achieve this goal, the Shannon lab is collaborating with Dr. Garry Nolan (Stanford) to utilize flow cytometry to measure the activation status of Ras effectors in subpopulations of blood, marrow, and spleen cells at defined time points after *Nf1* inactivation. The Nolan lab pioneered this technology (42). Dr. Shannon selected a model of MPD induced by somatic activation of an oncogenic *Kras* allele by *Mx1-Cre*-mediated excision of a lox-stop-lox cassette (43) for pilot experiments because Ras signaling pathways are consistently activated in *Kras* mutant bone marrow cells (data not shown). His laboratory discovered that the higher levels of phospho-ERK observed in *Kras* mutant bone marrow cells after GM-CSF stimulation are due to increased numbers of responding cells rather than a higher maximal response of these cells (Fig. 5, left panel). By contrast, *Kras* mutant c-kit+/lineage^{lo} cells, which comprise <1% of nucleated BM cells and include CFU-GM progenitors, show a robust response to GM-CSF versus c-kit+/lineage^{lo} cells in WT control cells and a higher maximal response to the combination of PMA + ionomycin (Fig. 5, right panel).

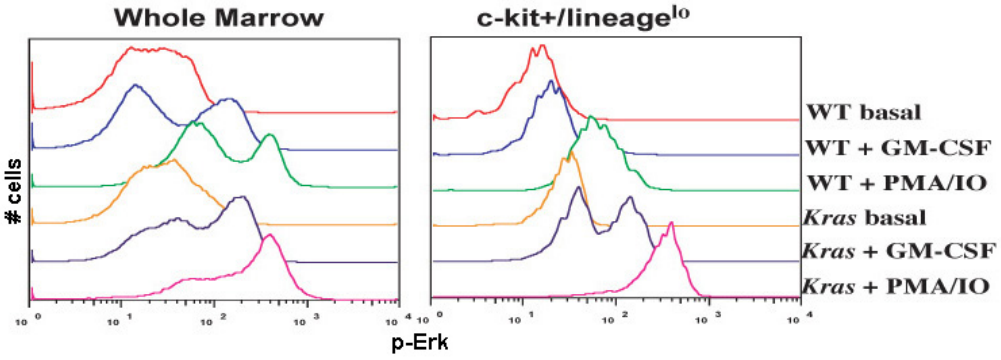

Figure 5: Intracellular signaling at single cell level obtained by multiparametric flow citometry. p-Erk levels are compared between wt and mutant Kras in total bone marrow (Left) and ckit+/lineage^{lo} (Right).

These data illustrate the power of using this flow cytometry phospho-signaling technique to uncover novel signaling aberrations in rare cells that are relevant to the *in vivo* disease phenotype. The Shannon lab is extending this analysis to primary hematopoeitic cells collected from *Mx1-Cre, Nf1*$^{flox/flox}$ mice with and without overt MPD at various times after treatment with pIpC. These studies will define the signaling networks of each cell subpopulation in wild-type mice and *Nf1* mutant mice at different stages of the disease, which should uncover pathways that are deregulated directly by *Nf1* before the development of overt MPD. A major consideration for using mouse models of NF1 and NF2 disease as platforms for preclinical testing involves the need to correlate clinical and pharmacodynamic endpoints. Sensitive flow cytometric assays would allow investigators to measure inhibition of relevant biochemical targets by therapeutic agents in small numbers of blood cells without sacrificing the animal. Thus, developing assays of this type has general applicability for testing NF therapeutics with circulating blood cells serving as surrogate markers of tissue bioavailability.

Ongoing Studies of Ras Processing and Upstream Adapter Molecules as Therapeutic Targets in NF1 Disease. Gab2 is an adapter molecule that links activated hematopoietic growth factor receptors to Ras. Although *Gab2* mutant mice are normal, the ability of the *BCR-ABL* oncogene to induce MPD was recently shown to be Gab2-dependent (44). Since signaling from the GM-CSF receptor plays a central role in the MPD that results from *Nf1* inactivation (15), we reasoned that Gab2 might similarly be required to induce leukemia in *Nf1* mice. The Shannon lab is pursuing a cross between *Mx1-Cre, Nf1*$^{flox/flox}$ and *Gab2* mutant mice to test this hypothesis. If these studies reveal a requirement for Gab2 in disease pathogenesis, this would identify a new class of potential therapeutic targets upstream of Ras and neurofibromin. Compound mutant mice have been generated and are being observed for evidence of MPD. In addition to analyzing the phenotypes of these mice, the Shannon lab will perform detailed cell biologic and biochemical studies.

Merlin Restricts Epithelial Detachment and Anoikis to the Leading Edge of Epithelial Sheets Undergoing Tissue Fusion. Because *Nf2*$^{-/-}$ mouse embryos die early in gestation due to an extraembryonic defect, the consequences of *Nf2* loss in the embryo proper were unknown. To examine merlin's role in development, the Jacks laboratory has again taken advantage of Cre/Lox technology. Through a series of crosses, they have generated mutant embryos that contain one copy of a conditional *Nf2*^{flox} allele, which behaves like the wild-type allele until exposure to Cre recombinase, and one copy of the *Nf2*^{1lox} allele in which the floxed exon 2 has already been deleted. The *Nf2*^{1lox} allele behaves like the null. In addition, the mutant embryos contain a Nestin-Cre transgene. The Nestin-Cre transgene is unusual in that it inserted into an

imprinted locus. Thus, mice that inherit paternally derived Nestin-Cre (Nestin-Cre^{p}) lose *Nf2* in virtually all cells within the brain and are mosaic for *Nf2* loss in the body, whereas mice that inherit maternally derived Nestin-Cre (Nestin-Cre^{m}) are mosaic for *Nf2* loss in the brain and body.

Nestin-Cre^{p};*Nf2*$^{flox/1lox}$ mice exhibit a range of neural tube defects, including craniorachischisis, a condition in which the entire neural tube fails to close. Strikingly, tissue fusion fails at several other sites within the mutant embryos, suggesting that there may be a global requirement for merlin in tissue fusion. To understand on a molecular level the reason for the failure in tissue fusion, the Jacks laboratory studied two tissue fusion events, neural tube closure and eyelid fusion, in detail. Histologically, the mutant neuroepithelium exhibited foci of ectopic epithelial detachment. Loss of adherens junctions was noted in these foci by immunofluoresence for β-catenin and by electron microscopy. Similarly, in the eyelid ridge there was increased intercellular space between epidermal cells, and away from the ridge there was ectopic detachment of peridermal cells. These findings suggest that ectopic epithelial detachment resulting in a paucity of cells was the primary reason for failure of tissue fusion.

By *in situ* hybridization, the Jacks lab found that *Nf2* is dynamically regulated during tissue fusion, with decreased levels of *Nf2* at the leading front prior to fusion and increased levels across the fused tissue bridge. Together these data suggest a new model of tissue fusion in which the dynamic regulation of *Nf2*, and thereby cell-cell adhesion, restricts physiologic detachment and detachment-induced apoptosis (anoikis) to the leading front. In this model, anoikis may serve a quality control function, ensuring that only those epithelial cells that form stable cell-cell contacts survive to contribute to the tissue bridge.

Merlin is an Inhibitor of the p21-Activated Kinase PAK1. Until recently, little was known about the biochemical consequences of *Nf2* inactivation. However, data from the McClatchey, Giovannini and Jacks laboratories are providing key insights into the molecular function of merlin and have identified several potential therapeutic targets. For example, accumulating evidence indicates a reciprocal relationship between merlin and the small GTPase Rac1. Drs. McClatchey and Jacks demonstrated that Rac1 activation leads to phosphorylation, reduced membrane:cytoskeleton association and impaired growth suppressing activity of merlin (31). Conversely, merlin overexpression blocks Rac activation and *Nf2*$^{-/-}$ cells exhibit features of excessive Rac signaling. A similar reciprocal relationship between the closely related ERM proteins and Rho has been demonstrated. The Jacks lab has recently shown that merlin expression inversely correlates with the activity of p21 activated kinases (PAKs), which are downstream regulators of Rac and other signaling pathways (see attached reprint by Kissel, *et al)*. Experiments utilizing conditional over-expression of *Nf2* in a human schwannoma cell line, and conditional deletion of *Nf2* in MEFs have led to this discovery of PAK activity regulation by merlin. In addition, merlin can form physical complexes with PAK, providing a possible mechanism of regulation. The Jacks lab has gone on to demonstrate that the interaction of merlin and PAK1 is dynamic and influenced by cellular adhesion and cell density (34). Complementary data have been published by the group of Maruta (32). These results provide a new therapeutic target for *Nf2* mutant tumors.

Growth and Survival of *Nf2*$^{-/-}$ Schwann cells (SC). Dr. Giovannini's lab used primary mouse SC cultures to study the consequences of *Nf2* loss *in vitro* in a cell autonomous manner and found that loss of merlin expression results in 3 major phenotypes. Firstly, *Nf2*$^{-/-}$ cells show an altered

morphology. Wild-type *Nf2* SCs are usually bipolar, with two cytoplamic extensions emanating from a small cellular body. In contrast, *Nf2*$^{-/-}$ cells show multiple extensions and display a flatter morphology. Staining of the actin cytoskeleton using fluorescent phalloidin reveals profound alteration of actin filaments, which are usually thicker and less organized than in wild-type SCs. Staining with an antibody to tubulin also shows important modifications in the organization of microtubules. Given the reported interactions of merlin with actin and tubulin, these effects are likely to be direct. Secondly, although *Nf2*$^{-/-}$ SCs don't grow appreciably faster than their wild-type counterparts, they reach a much higher density. Dr. Giovannini's lab investigated whether this could be due to the loss of cell to cell junctions, as it was observed for *Nf2*$^{-/-}$ primary fibroblasts, and found that AJs, although abnormal in shape, are present in the *Nf2*$^{-/-}$ SCs. Therefore, loss of contact inhibition in *Nf2*$^{-/-}$ SCs does not seem to be the consequence of AJ loss but could still be the result of their altered organization. Thirdly, a senescent phenotype was not observed in *Nf2*$^{-/-}$ SCs in culture whereas wild-type SCs stop proliferating after 5 to 8 passages in culture suggesting that loss of *Nf2* induces immortalization. Also, *Nf2*$^{-/-}$ SCs that have been propagated *in vitro* 1-10 times do not form colonies in agar or tumors in mice indicating that they are not transformed at that point. Beyond passage 10, *Nf2*-/- cells do form colonies in agar and tumor in mice, hallmarks of transformation. The >P10 *Nf2*$^{-/-}$ SCs typically show loss of cell cycle regulators like p21 or p16. Upon extended periods in culture, wild-type Schwann cells also lose p16 or p21 and become immortalized. In conclusion, it appears that immortalization of SCs in culture requires the loss of one tumor suppressor (*Nf2* or p21/p16) but that transformation requires the loss of at least two of them.

The mechanisms by which merlin might control immortalization were also investigated. Consistent with role of merlin in regulating EGFR/ErbB1 signaling in other cell types, many receptor tyrosine kinases (RTKs) accumulate at the cytoplasmic membrane of *Nf2*$^{-/-}$ SCs including *erbB2*. This leads to an increase in signaling from this receptor. Previously published data (20) have shown that expression of a constitutively active form of *ErbB2* receptor in primary SCs is sufficient to promote their immortalization and subsequent transformation. These data support the idea that spontaneous immortalization of *Nf2*$^{-/-}$ SCs in culture is due to the increase in *erbB2* receptor signaling from the membrane. We also used gene expression profiling to investigate the mechanisms of RTKs accumulation in *Nf2*$^{-/-}$ SCs. No increase in RTK expression was observed suggesting that accumulation of RTKs is likely due to a change in recycling and degradation. This is also consistent with the aforementioned role of merlin in EGFR/ErbB1 trafficking in other cell types. Dr. Giovannini and his colleagues are currently investigating this possibility. Altogether, these studies have uncovered the major phenotypes that result from the inactivation of *Nf2* in primary SCs *in vitro* cultures and their probable mechanisms.

Transcriptome Analysis of *Nf2* Mutant SC. To identify genes that are altered secondary to *Nf2* loss and that might be relevant to peripheral nerve tumorigenesis, Dr. Giovannini has compared the transcriptome of wild type and *Nf2* mutant SC samples using microarray technology. Transcriptome analysis was performed on wild-type *Nf2*$^{-/-}$ and on *P0NF2*Δ*39-121* adult mouse SC. Cross comparison of differentially expressed genes in *Nf2*$^{-/-}$ or *P0NF2*Δ*39-121* SC compared to their *Nf2*$^{+/+}$ counterparts showed an overlap of 70% genes thus arguing for a dominant negative function of the *NF2*Δ*39-121* mutant protein, and revealing a molecular signature of *Nf2* loss *in vitro* (Fig. 6). Affymetrix CEL files included in this study were preprocessed using the Robust Multiarray Analysis (RMA) algorithm implemented in GeneSpring 7.1

(SiliconGenetics/Agilent Technologies, San Jose, CA). Data was then normalized: *i*) per chip to 50% percentile and *ii*) per gene using global normalization. All probe sets present on the GeneChip®s were then filtered across all samples using GeneSpring 7.1. Genes with expression intensities of at least 1.25 in a minimum 5% of the samples were used in the analysis. This approach allowed disregarding genes with low variation across samples. Then, ANOVA coupled to false discovery rate correction was used to identify genes with different expression levels between conditions. Differentially expressed genes are now being validated by real time PCR in a validation series of cell and tumor samples. Dr. Giovannini's group plans to publish the results of these studies in the next year.

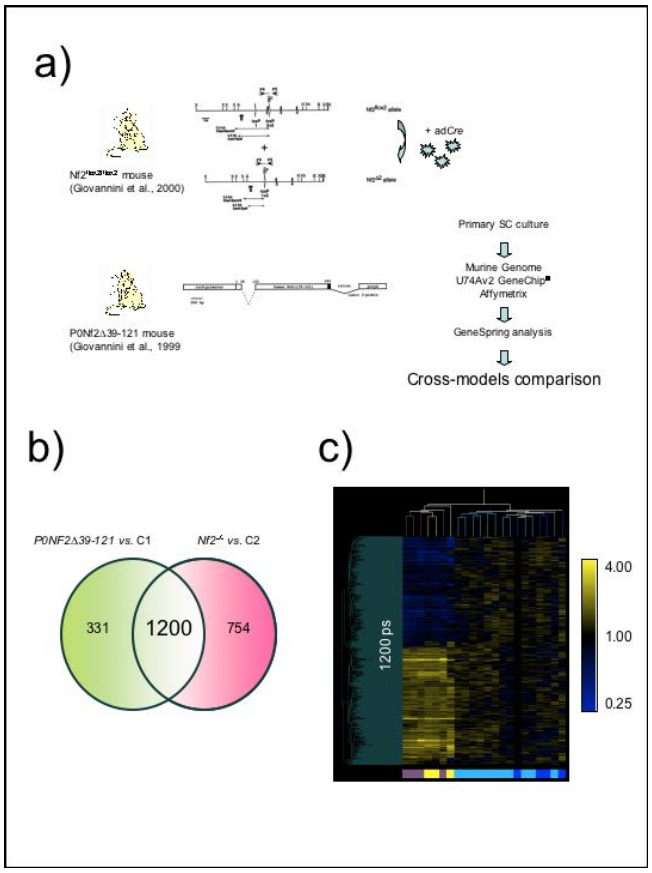

Figure 6. Comparison of NF2 mouse models shows 70% overlap in transcriptome modifications (a), infers a dominant negative function of the *NF2Δ39-121* form of the protein (b), and reveals a molecular signature of *Nf2* loss *in vitro* (c).

Aim 3. Preclinical Studies of Experimental Therapeutics in Mouse Models

Preclinical Evaluation of a MEK Inhibitor in Mx1-Cre, $Nf1^{flox/flox}$ Mice with MPD and Acute Myeloid Leukemia (AML). MEK is a dual specificity kinase that catalyzes the phosphorylation of $p44^{MAPK}$ (ERK1) and of $p42^{MAPK}$ (ERK2). MEK is a component of the canonical mitogen activated protein (MAP) kinase pathway that transduces proliferative signals from Ras-GTP to the nucleus in many cell types. In myeloid cells, Ras-GTP binds to the Raf1 kinase, which, in turn, phosphorylates and activates MEK. CI-1040 (also known as PD184352) was identified in a screen for small molecule inhibitors of MEK (45). Biochemical studies infer an allosteric mechanism of action. CI-1040 is a potent inhibitor of MAPK activation in cancer cell lines, and

it induces regression of explanted tumors in nude mice that correlated with in vivo effects on MAPK phosphorylation (45). We obtained CI-1040 from Pfizer, Inc. and first performed preclinical studies in Mx1-Cre, $Nf1^{flox/flox}$ mice. We found that 25-50 μM of CI-1040 abrogated CFU-GM colony formation in response to GM-CSF from normal and Mx1-Cre, $Nf1^{flox/flox}$ bone marrow; however, there was no therapeutic index as CFU-GM growth from wild-type bone marrow was inhibited at similar concentrations (Fig 7A). Furthermore, Mx1-Cre, $Nf1^{flox/flox}$ mice with MPD (n=10) that were treated at the maximal tolerated dose of CI-1040 (100 mg/kg twice a day) showed no improvement in leukocyte counts, splenomegaly, or survival. As reported in previous Progress Reports, we observed transient inhibition of MEK kinase activity in bone marrow cells from CI-1040-treated mice, which was assessed by measuring the ability of GM-CSF to phosphorylate ERK. Whereas ERK phosphorylation was markedly decreased 2 hours following a CI-1040 dose, inhibition was estimated to be ~50% after 4 hours and was no longer detected after 8 hours (data not shown)

In studies that are also supported by NIH grant R01 CA72614, the Shannon lab is exploiting retroviral insertional mutagenesis to conduct a forward genetic screen to isolate genes that might cooperate with loss of *Nf1* in progression from MPD to AML. In these experiments, *Mx1-Cre, Nf1*$^{flox/flox}$ pups are injected with both pIpC and the MOL4070LTR retrovirus at birth and observed for subsequent development of leukemia. Whereas *Mx1-Cre, Nf1*$^{flox/flox}$ pups that are injected with pIpC alone never develop AML, ~25% of mice that receive pIpC + MOL4070LTR develop AML with reduced latency compared to MPD (data not shown). They Shannon lab evaluated the *in vitro* responses of MOL4070LTR-induced AMLs from *Mx1-Cre Nf1* $^{flox/flox}$ mice to CI-1040. Unexpectedly, colony growth was completely abrogated at much lower drug concentrations (0.25- 5 μM) than wild-type or *Nf1* mutant bone marrow cells (Fig 7B), suggesting that *Mx1-Cre Nf1* $^{flox/flox}$ AMLs are more sensitive to MEK inhibition. (Fig 7B). To test this hypothesis *in vivo*, the Shannon lab performed a second randomized trial in 25 recipient mice that were transplanted with 4 independent leukemias. Mice were randomized and received either CI-1040 or control vehicle when flow cytometry revealed blast cells in the peripheral blood, which occurred 2-4 weeks after transplantation. CI-1040 had dramatic effects in this setting. Whereas the leukocyte counts of vehicle-treated mice increased progressively, all of the mice that were randomized to CI-1040 showed transient fall in leukocyte counts (Fig7B). Treatment with CI-1040 was also associated with markedly prolonged survival (24 versus 7 days in the vehicle-treated cohort; odds ratio 3.5, 95% CI 3.0-3.8) (Fig 7C). These data suggest that the biologic response to a molecularly-targeted inhibitor is strongly modulated by the genetic context in which a disease-initiating mutation occurs. Specifically, although the MPD induced by *Nf1* inactivation was resistant to CI-1040, progression to AML was associated with enhanced sensitivity to this agent. These data have important implications for NF-associated tumors as they suggest that early stage lesions such as neurofibromas or optic gliomas may respond differently to targeted therapeutics than MPNSTs or other advanced cancers.

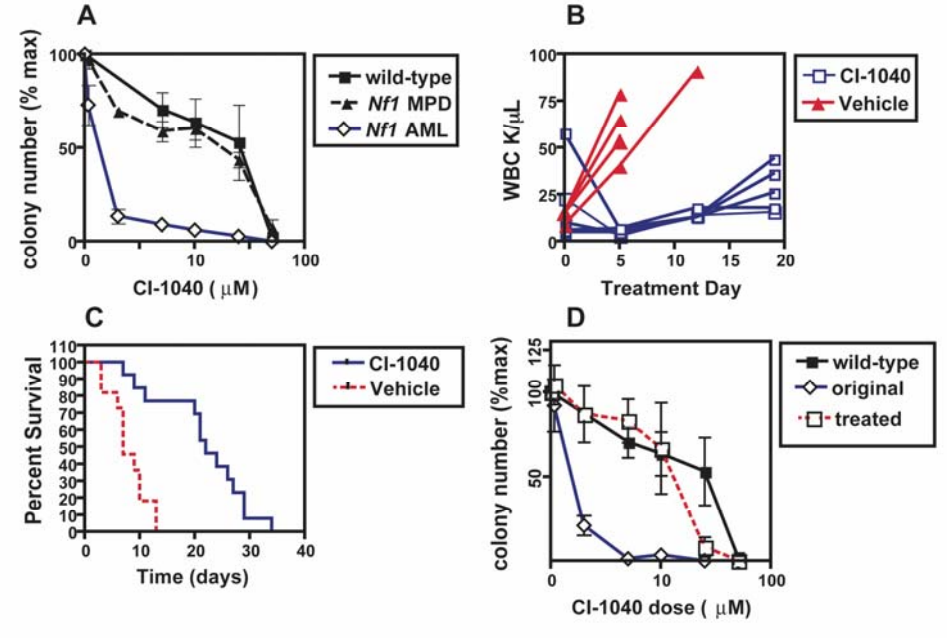

Figure 7. Preclinical evaluation of CI-1040. CFU-GM colony formation in Nf1 AML, NF1 MPD and wild-type bone marrow in presence CI-1040 (A), White Blood Cell (WBC) count (B) and survival (C) in mice with AML treated with CI-1040 or vehicle, relapsed AMLs show robust CFU-GM growth compared to original leukemias in presence of CI-1040.

Despite objective responses based on criteria that included a decrease in peripheral white blood cell counts with reappearance of mature myeloid cells, improved physical condition, and prolonged survival, all of the mice that received CI-1040 eventually developed leukocytosis with reemergence of peripheral blood blasts, and died from AML. Importantly, these leukemias were remarkably less sensitive to CI-1040 *in vitro* than the parental AMLs (Fig. 7D), and did not respond to treatment in secondary recipients (data not shown). Together, these data strongly support the hypothesis that these AMLs undergo clonal selection *in vivo* during treatment with a molecularly targeted inhibitor. The Shannon lab is working to clone genes that underlie acquired resistance to CI-1040.

Preclinical Studies in the *Krox20 Nf1*$^{flox/flox}$ Model of Neurofibroma. BMS 354825 is a selective inhibitor of a subfamily of tyrosine kinases including c-Kit; c-abl, and the platelet derived growth factor receptor. In a collaborative agreement with Bristol Meyer Squibb, preclinical mouse trials are underway in the Parada lab to determine potential effectiveness of this drug to impede mast cell invasion into peripheral nerves. Preliminary culture experiments indicate activity of this drug on cultured mast cells, as presence of inhibitor reduces proliferative index and migratory capacity (data not shown). The mouse studies should be completed in the coming months.

Aim 4. To sponsor specialized working group meetings and to support preclinical testing in mouse models of NF1 and NF2.

Workshop on Pathologic Classification of Tumors in NF Mouse Models. Dr. Giovannini organized a meeting of pathologists and basic scientists on February 8-10, 2003, in Boston, Massachusetts, to review all available genetically engineered murine (GEM) models of NF1 and NF2, and to draft a pathological classification of murine peripheral nerve sheath tumors to characterize these lesions in a uniform and consistent manner. The meeting and pathological classification followed a format successfully adopted by similar workshops for murine models of

other organ systems. Dr. Anat Stemmer-Rachamimov (Harvard University), who has extensive expertise in NF-associated tumors, led a panel of 10 pathologists that reviewed lesions from most published and unpublished NF mouse models and compared their histological features with the corresponding human tumors.

The panel members, who have different areas of expertise, reviewed 56 lesions from 8 laboratories. In formulating the GEM classification of peripheral nerve sheath tumors, the panel referred to criteria and terminology devised by the World Health Organization for classifying human nervous system tumors (46). However, although the WHO classification served as a useful point of reference, it was not adopted for the classification of the GEM lesions because of some important differences between the human and murine tumors. The WHO classification of human peripheral nerve sheath tumors (PNSTs) is based on both histological and clinical characteristics (and describes clinico-pathological entities), whereas the GEM classification must necessarily be based on histological features alone, as clinical features of murine PNSTs are not yet known. Furthermore, although many of the histological features displayed by GEM PNSTs were similar to those observed in human tumors, some GEM lesions presented unique and distinct morphology, and did not fit into the human classification by histological criteria.

In addition, because the human tumor nomenclature refers to histological features as well as predicted clinical behavior of tumors, some of these terms were deemed inappropriate for description of GEM tumors, in which biological behavior is still unknown. The panel therefore proposed a novel classification for GEM nerve sheath tumors based purely on morphological features. Although the term "grade" is used in the GEM classification, it is applied as a histological descriptor only and has no predictable bearing on the biological behavior of the tumor in the animals. In other words, as opposed to the WHO classification where grade is an indicator of biological behavior, grading in the GEM classification refers merely to the presence or absence of specific histological features such as high cellularity, necrosis, nuclear pleomorphism and brisk mitotic activity.

This classification represents a valuable tool for standardization and validation of tumors arising in NF mouse models, as it facilitates direct comparisons between models and enables effective design and interpretation of preclinical trials that are directly relevant to human NF disease. Finally, the panel also recommended general guidelines for the work-up and morphological evaluation of peripheral nerve sheath lesions in GEM models. A manuscript describing the guidelines developed through this highly interactive and collaborative effort was published in *Cancer Research.*

Workshop on Preclinical Therapeutics in NF Mouse Models. Dr. Shannon organized a workshop entitled *"Barriers and Solutions in the Use of Mouse Models to Develop Therapeutic Strategies for NF1 and NF2-Associated Tumors"* with Drs. D David Gutmann (Washington U.) and Kim Hunter-Schaedle (CTF). This meeting, which was held at the Banbury Conference Center, Cold Spring Harbor National Laboratory from November 3-5, emphasized an informal "think tank" format with extensive discussion. In addition to prominent NF researchers, the attendees included outstanding investigators such as Scott Lowe, Daivd Tuveson, and Eric Holland. The attendees identified a number of practical strategies to achieve the goal of of using mouse models of NF-associated tumors to facilitate the goal of bringing new treatments to patients. The organizers are preparing a review article that summarizes many of the principles discussed at the meeeting.

KEY RESEARCH ACCOMPLISHMENTS

(a) The investigators continue to extensively share expertise and reagents to pursue common research goals.

(b) The NF Modeling Group is participating in the activities of the MMHCC and is contributing to achieving the goals of this national cancer research inititative.

(c) We developed accurate models of most NF1 and NF2-assocated tumors, characterized these lesions, and pursued the goals of developing additional models and of enhancing existing mutant strains.

(d) We have developed a robust model for MPNST. These mice are now being placed in preclinical trials for prevention and tumor arrest therapies.

(e) We have developed a robust model for NF1 associated Optic Glioma. These mice are now being placed in preclinical trials for prevention and tumor arrest therapies.

(f) We have developed a robust model for NF1 associated astrocytoma. These mice are now being placed in preclinical trials for prevention and tumor arrest therapies.

(g) A new method was developed for isolating mitotically active Schwann cells.

(h) Progress was made toward engineering a mouse model of ependymona.

(i) A novel strain of drug-inducible Cre mice was constructed that will permit regulated deletions between loxP elements. These mice are being harnessed to inactivate of the *Nf2* gene in specific tissues at defined time points.

(j) *Mx1-Cre Nf1*$^{flox/flox}$ mice provide a tractable model of JMML that is being harnessed to fully characterize the biochemical consequences of *Nf1* inactivation in primary cells and to test an inhibitor of MEK *in vivo* with correlative biochemical (pharmacodynamic) monitoring.

(k) Radiation was shown to cooperate strongly with heterozygous *Nf1* inactivation in tumorigenesis. Radiation-induced cancers included myeloid leukemia, sarcoma, and breast cancers.

(l) Strains of mutant mice have been shared widely with the NF research community (see list below in Reportable Outcomes). Through these collaborative experiments, the scientific value of this Consortium has extended well beyond the studies being pursued in the participant's laboratories.

REPORTABLE OUTCOMES

(a) Research Articles and Reviews from Previous Consortium Award (2000 – 2002)

Parada LF. Neurofibromatosis Type 1. *BBA,* 2000, 147, M13-M19.

Zhu Y, Romero M, Ghosh P, Charnay P, Rushing EJ, Marth J and Parada LF. Ablation of NF1 function in neurons induces abnormal development of cerebral cortex and reactive gliosis in the CNS and PNS. *Genes & Dev.,* 2000, 5:859-876.

McClatchey AI and Cichowski K. Mouse models of neurofibromatosis. *Biochim. Biophys. Acta* 2001;1471:M73-80.

Shannon KM, Le Beau MM, Largaespada DA and Killeen N. Modeling myeloid leukemia tumor suppressor gene inactivation in the mouse. *Semin. Cancer Biol.* 2001; 11: 191-199.

Shaw RJ, Paez JG, Curto M, Yaktine A, Pruitt WM, Saotome I, O'Bryan JP, Gupta V, Ratner N, Der CJ, Jacks T and McClatchey AI. The Nf2 tumor suppressor, merlin, functions in Rac-dependent signaling. *Dev. Cell,* 2001, 1:63-72.

Zhu Y and Parada LF. Neurofibromin, a tumor suppressor of the nervous system. *Exp. Cell Research,* 2001, 264, 19-28.

Bajenaru ML*, Zhu Y*, Hedrick NM, Donahoe J, Parada LF and Gutmann DH. Astrocyte-specific inactivation of the neurofibromatosis 1 (Nf1) gene is insufficient for astrocytoma formation. *Mol. Cell Biology,* 2002, 22:5100-5113 (*co-first authors).

Donovan S, Shannon KM and Bollag GE. GTPase activating proteins: critical regulators of intracellular signaling. *Biochem. Biophy.s Acta,* 2002, 1602:23-45.

Gautreau A, Manent J, Fievet B, Louvard D, Giovannini M and Arpin M. Mutant products of the NF2 tumor suppressor gene are degraded by the ubiquitin-proteasome pathway. *J Biol Chem*., 2002, 277:31279-82.

Gutmann D and Giovannini M. Mouse models of neurofibromatosis type 1 and 2. *Neoplasia,* 2002; 4: 279-290.

Gutmann D, Wu YL, Hedrick NM, Zhu Y, Guha A and Parada LF. Heterozygosity for the neurofibromatosis 1 *(Nf1)* tumor suppressor results in abnormalities in cell attachment, spreading and motility in astrocytes. *Human Molecular Genetics,* 2002, 10:3009-3016.

Johnson KC, Kissil JL Fry JL and Jacks T. Cellular transformation by a FERM domain mutant of the NF2 tumor suppressor gene. *Oncogene* 2002, 21:5990-97.

Kalamarides M, Niwa-Kawakita M, Leblois H, Abramowski V, Perricaudet M, Janin A, Thomas G, Gutmann D and Giovannini M. *Nf2* gene inactivation in arachnoidal cells is rate-limiting for meningioma development in the mouse. *Genes & Development,* 2002, 16:1060-1065.

Kissil JL, Johnson KC, Eckman MS and Jacks T. Merlin Phosphorylation by p21-activated Kinase 2 and Effects of Phosphorylation on Merlin Localization. *J Biol Chem*. 2002; 277:10394-99.

Le DT and Shannon KM. Ras processing as a therapeutic target in hematologic malignancies. *Curr. Opin. Hematol.,* 2002, 9:308-315.

Li H, Velasco-Miguel S, Vass WC, Parada LF and DeClue JE. Epidermal growth factor receptor (EGFR) signaling pathways are associated with tumorigenesis in *Nf1:p53* mouse tumor-derived cell lines. *Cancer Res.,* 2002, 8:616-26.

Messerli SM, Tang Y, Giovannini M, Bronson R, Weissleder R and Breakefield XO. Detection of spontaneous schwannomas by MRI in a transgenic murine model of neurofibromatosis type 2. *Neoplasia*, 2002, 4:501-509.

Sun CX, Haipek C, Scoles DR, Pulst SM, Giovannini M, Komada M and Gutmann DH. Functional analysis of the relationship between the neurofibromatosis 2 (NF2) tumor suppressor and its binding partner, hepatocyte growth factor-regulated tyrosine kinase substrate (HRS/HGS). *Hum. Mol. Gen.,* 2002, 11:3167-3178.

Weiss WA, Israel M, Cobbs C, Holland E, James CD, Louis DN, Marks C, McClatchey AI, Roberts T, Van Dyke T, Wetmore C, Chiu IM, Giovannini M, Guha A, Higgins RJ, Marino S, Radovanovic I, Reilly K, Aldape K. Neuropathology of genetically engineered mice: consensus report and recommendations from an international forum. *Oncogene*, 2002, 21(49):7453-63.

Zhu Y, Ghosh P, Charnay P, Burns DK, and Parada LF. Neurofibromas in NF1:Schwann cell origin and role of tumor environment. *Science,* 2002, 296:920-2.

Zhu Y and Parada LF. The molecular and genetic basis of neurologic tumours. *Nature Reviews on Cancer,* 2002, 8:616-26.

Publications Supported by the Award (* denotes papers included in the appendix)

2003

Aiyagari A, Taylor B, Aurora V, Young SG and Shannon KM. Hematologic effects of inactivating the Ras processing enzyme *Rce1. Blood* 2003; 101: 2250-2252.

Cichowski K, Santiago S, Jardim M, Johnson BW, Jacks T. Dynamic regulation of the Ras pathway via proteolysis of the NF1 tumor suppressor. *Genes Dev*. 2003. 17(4):449-54

Crone SA, Negro A, Trumpp A, Giovannini M, and Lee KF. Colonic Epithelial Expression of ErbB2 Is Required for Postnatal Maintenance of the Enteric Nervous System. *Neuron*, 2003, 37(1):29-40.

Denisenko-Nehrbass N, Goutebroze L, Galvez T, Bonnon C, Stankoff B, Ezan P, Giovannini M, Faivre-Sarrailh C, and Girault JA. Association of Caspr/paranodin with tumor suppressor schwannomin/merlin and 1 integrin in the CNS. *J. Neurochem*., 2003, 84 :209-221.

Fleury-Feith J, Lecomte C, Renier A, Matrat M, Kheuang L, Abramowski A, Levy F, Janin A, Giovannini M and Jaurand M-C. Hemizygosity of Nf2 is associated with increased susceptibility to asbestos-induced peritoneal tumours. *Oncogene*, 2003, 22:3799-3805.

Gitler, A.D.*, Zhu, Y.*, Lu, M.M., Parada, L.F., and Epstein, J.A. Nf1 has an essential role in endothelial cells. *Nat. Genet,* 2003*,* 33(1):75-9. (*co-first authors).

Gutmann DH, Baker SJ, Giovannini M, Garbow J and Weiss W. Mouse models of human cancer consortium symposium on nervous system tumors. *Cancer Res*., 2003, 63(11):3001-4.

Ingram DJ, Wenning MJ, Shannon K and Clapp DW. Leukemic potential of doubly mutant *Nf1* and W^v hematopoietic cells. *Blood* 2003; 101: 1984-1986.

Kissil JL, Wilker EW, Johnson KC, Eckman MS, Yaffe M, and Jacks T. Merlin, the product of the *Nf2* tumor suppressor gene, is an inhibitor of the p21-activated kinase Pak1. *Mol Cell* 2003; 12(4):841-849.

Lallemand D, Curto M, Saotome I, Giovannini M and McClatchey AI. *NF2* deficiency promotes tumorigenesis and metastasis by destabilizing adherens junctions. *Genes & Dev*., 2003, 17(9):1090-100.

Leneuve P, Colnot S, Hamard G, Francis F, Niwa-Kawakita M, Giovannini M and Holzenberger M. Cre-mediated germline mosaicism: A new transgenic mouse for the selective removal of residual markers from tri-low conditional alleles. *Nucleic Acids Res.,* 2003, 31(5):1-8.

Manent J, Oguievetskaia X, Bayer J, Ratner N and Giovannini M. Magnetic cell sorting for enriching Schwann cells from adult mouse peripheral nerves. *J. Neuroscience Meth.*, 2003, 123:167-173.

McLaughlin, ME and Jacks, T. Progesterone receptor expression in neurofibromas. *Cancer Research,* 2003; 63 (4): 752-755.

McLaughlin, ME and Jacks, T. 2002. Thinking beyond the tumor cell: *Nf1* haploinsufficiency in the tumor environment. *Cancer Cell: June 2002*

McLaughlin, ME and Jacks, T. Neurofibromatosis type 1. *Methods Mol Biol.* 2003; 222:223-37.

McLaughlin, ME, Robson, CD, Kieran, MW, Jacks T, Pomeroy, SL, Cameron, S. Marked regression of metastatic pilocytic astrocytoma during treatment with imatinib mesylate (STI-571, Gleevec): a case report and laboratory investigation. *J Pediatr Hematol Oncol*. 2003; 25(8):644-8

McClatchey AI. Merlin and ERM proteins: unappreciated roles in cancer development? *Nat. Rev. Cancer,* 2003, 3:877-883.

Utermark T, Aleko A, Lerche H, Abramowski V, Giovannini M and Hanemann CO. Quinidine reduces proliferation in human malignant mesothelioma cell lines lacking Schwannomin/Merlin but not in those expressing the neurofibromatosis type 2 tumor suppressor gene. *Cancer* 2003, **97:**1955-1962.

Weiss BG and Shannon KM. Mouse cancer models as a platform for performing preclinical therapeutic trials. *Curr. Opin. Genet. Dev.,* 2003, **13:** 84-9.

Yajnik V, Paulding C, Sordella R, McClatchey AI, Saito M, Wahrer DC, Reynolds P, Bell DW, Lake R, van den Heuvel S, Settleman J and Haber DA. DOCK4, a GTPase activator, is disrupted during tumorigenesis. *Cell* 2003; **112:** 673-84.

2004

*Le DT, Kong N, Zhu Y, Aiyigari A, Braun BS, Wang E, Kogan SC, Le Beau MM, Parada L, Shannon KM. Somatic inactivation of *Nf1* in hematopoietic cells results in a progressive myeloproliferative disorder. *Blood* 2004; **103:** 4243-4250.

*Reilly KM, Tuskan RG, Christy E, Loisel DA, Ledger J, Bronson RT, Smith CD, Tsang S, Munroe DJ, Jacks T. Susceptibility to astrocytoma in mice mutant for Nf1 and Trp53 is linked to chromosome 11 and subject to epigenetic effects. *PNAS USA* 2004; **101:** 3008-13013.

Robanus-Maandag E.*, Giovannini M.*, van der Valk M., Niwa-Kawakita M., Abramowski V., Woodruff J.M., Thomas G., Berns A. Early *Nf2* inactivation in neural crest-derived cells hemizygous for *p53* converts the tumor spectrum from osteogenic to peripheral nerve sheath tumors. *Oncogene* 2004, 23 :6541-6547. *these two authors contributed equally

*Saotome I., Curto M., McClatchey A.I. Ezrin is essential for epithelial organization and villus morphogenesis in the developing intestine. *Developmental Cell* 2004; 6: 855-64.

Stemmer-Rachamimov A., Louis D., Nielsen P., Antonescu C.R., Borowsky A., Bronson R., Burns D, Cervera P., McLaughlin M., Reifenberger G., Schmale M., MacCollin M., Chao R., Cichowski K., Kalamarides M., Messerli S., McClatchey A.I., Niwa-Kawakita M., Ratner N., Reilly K.M., Zhu Y., Giovannini M. Comparative pathology of nerve sheath tumors in mouse models and humans. *Cancer Research* 2004, 64: 3718-3724.

Weiss BG, Shannon KM. Preclinical trials in mouse cancer models *in* Holland EC (ed): Mouse Models of Human Cancer, Wiley-Liss, Hoboken NJ, 2004: pp. 437-446.

2005

*Chao RC, Pyzel U, Fridlyand J, Kuo, Y-M, Teel L, Haaga J, Borowsky A, Horvai A, Kogan SC, Bonifas J, Huey B, Jacks TE, Albertson D, Shannon K. Therapy-induced malignant neoplasms in *Nf1* mutant mice. *Cancer Cell* 2005; **8:** 337-48.

Curto, M, Liu, C, Lallemand, D and McClatchey, AI. The *Nf2* tumor suppressor, Merlin, controls contact-dependent EGFR silencing. (in revision)

*McClatchey A. and M. Giovannini. Membrane organization and tumorigenesis – the *NF2* tumor suppressor, merlin. *Genes and Development* 2005, 19 :2265-77.

*Kuns R, Kissil JL, Newsham IF, Jacks T, Gutmann DH, Sherman LS. Protein 4.1B expression is induced in mammary epithelial cells during pregnancy and regulates their proliferation. *Oncogene* 2005, 24:6502-15.

Parada, L.F., Kwon, C.H., and Zhu, Y. Modeling Neurofibromatosis Type 1 Tumors in the Mouse for Therapeutic Intervention. Cold Spring Harbor Symposia on Quantitative Biology: *Molecular Approaches to Controlling Cancer.* (in press)

Romero M.I., Zhu Y., Lush, M.E., and Parada, L.F. Neuron-specific deletion of NF1 enhances functional recovery after spinal cord sensory denervation. *Neuron* (in revision)

*Zhu, Y., Guignard, F., Zhao, D., Burns, D.K., Mason, R.P., and Parada, L.F. Early inactivation of p53 tumor suppressor gene cooperating with NF1 loss induces malignant astrocytoma. *Cancer Cell* 2005; **8:** 119-130.

*Zhu, Y., Harada, T., Guignard, F., Harada, C., Burns, D. K., Bajenaru, M.L, Gutmann, D.H., Messing, A., and Parada, L.F. Ablation of NF1 in CNS causes transient neural progenitor hyperplasia and is sufficient to induce optic gliomas. *Development* 2005; **132:** 5577-5588.

(b) Model Development and Distribution to the Research Community

Studies conducted to date have established a number of novel models of NF1 and NF2-associated tumors and have generated several new strains of mice. *Nf1* and *Nf2* mutant mice have been deposited in the MMHCC Repository where they are readily available to the research community. In addition, the participants in this Consortium have provided strains directly to the investigators listed below.

Karlene Reilly (National Cancer Institute)
Jeffrey DeClue (National Cancer Institute)
Jonathan Epstein (University of Pennsylvania)
D. Wade Clapp (Indiana University)
David Guttmann (Washington University)
David Largaespada (University of Minnesota)

Jeffrey Lawrence (UCSF)
Alcino Silva (UCLA)
Gerard Karsenty (Baylor)
Shaojun Tang (UC Irvine)
Shalom Avraham (Beth Israel)
James Bieker (Mount Sinai, New York)
Abhijit Guha (Labatt Brain Tumor Research Center, Tornoto)
Andreas Kurtz, (Harvard)
Jim Gussella (Harvard)
Dan Haber (Harvard)
Antonio Chiocca (Harvard)
Isidro Sanchez-Garcia (IBMCC)
Victor Tybulewicz (National Institute for Medical Research, London)
Lindsay Hinck (UC Santa Cruz)
Keqiang Ye (Emory University School of Medicine)
Lynda Chin (Dana Farber Cancer Institute)
Joseph Testa (Fox Chase Cancer Center)
Nancy Ratner (U. of Cincinnati)
Stefan Mundlos (U. of Berlin)
Juha Peltonen (U. of Helsinki, Finland)
Warren Pear (University of Pennsylvania)
David Beebe (Washington University)
Filippo Giancotti (MSKCC, New York)
Joe Kissil (Wistar Institute, Philadelphia)
Long Sheng Chang (Ohio State University, Columbus)
Cristina Fernandez Valle (University of Central Florida, Orlando)
Silvia Espejel (University of California, San Francisco)
Karen Cichowski, (Harvard)
Sean J. Morrison, (University of Michigan)
John J. Ryan, (Virginia Commonwealth University)
Isa Hussaini, (University of Virginia)
William Pu, (Children's Hospital, Boston)
Filippo G. Giancotti (Sloan-Kettering Institute for Cancer Research)
David Wilkes (Cornell University Medical College)
Ivan Radovanovic (Geneva)
Brian Weiss (University of Cincinnati)
Arturo Alvarez-Buylla (University of California, San Francisco)
Jonathan Chernoff, (Fox Chase Cancer Center
Laurent Elefteriou (UT San Antonio)
David Kaplan (Toronto)
Hong Wu (UCLA)
Ugur Ozerdem (La Jolla Insitiute)
David Ingram (Indiana)
Takayuki Harada (Tokyo)
Alison Lloyd (London)

(c) Employment and Research Opportunities

This award has provided salary support for technical personnel in each of participating labs.

CONCLUSIONS

During the fourth year of its existence, this consortium made progress in accomplishing its primary goal of generating and characterizing mouse models of NF1 and NF2-associated tumors for biologic and preclinical therapeutic trials. A number of novel strains have been developed and reported, innovative strategies were deployed to make optimal use of these resources, and our recent research has provided a number of novel insights regarding mechanisms of tumor formation in Nf1 and NF2 patients, and have suggested potential therapeutic targets in NF disease. The investigators have collaborated closely and have shared expertise and reagents extensively. The proceedings of the meeting on Pathologic Classification of Mouse Models of NF-Associated Tumors, which Dr. Giovanini organized, were published in *Cancer Research* a highly successful meeting that focused. This NF Consortium is a full participant in the Mouse Models of Human Cancer Consortium of the NCI.

REFERENCES

1. Brannan CI, Perkins AS, Vogel KS, Ratner N, Nordlund ML, Reid SW, et al. Targeted disruption of the neurofibromatosis type 1 gene leads to developmental abnormalities in heart and various neural crest-derived tissues. Genes and Development 1994;8:1019-1029.
2. Jacks T, Shih S, Schmitt EM, Bronson RT, Bernards A, Weinberg RA. Tumorigenic and developmental consequences of a targeted *Nf1* mutation in the mouse. Nat Genet 1994;7:353-361.
3. Zhu Y, Romero MI, Ghosh P, Ye Z, Charnay P, Rushing EJ, et al. Ablation of NF1 function in neurons induces abnormal development of cerebral cortex and reactive gliosis in the brain. Genes Dev 2001;15(7):859-76.
4. McClatchey AI, Saotome I, Ramesh V, Gusella JF, Jacks T. The Nf2 tumor suppressor gene product is essential for extraembryonic development immediately prior to gastrulation. Genes Dev 1997;11(10):1253-65.
5. Giovannini M, Robanus-Maandag E, Niwa-Kawakita M, van der Valk M, Woodruff JM, Goutebroze L, et al. Schwann cell hyperplasia and tumors in transgenic mice expressing a naturally occurring mutant NF2 protein. Genes Dev 1999;13(8):978-86.
6. Giovannini M, Robanus-Maandag E, van der Valk M, Niwa-Kawakita M, Abramowski V, Goutebroze L, et al. Conditional biallelic Nf2 mutation in the mouse promotes manifestations of human neurofibromatosis type 2. Genes Dev 2000;14(13):1617-30.
7. Cichowski K, Shih TS, Schmitt E, Santiago S, Reilly K, McLaughlin ME, et al. Mouse models of tumor development in neurofibromatosis type 1. Science 1999;286(5447):2172-6.
8. Zhu Y, Ghosh P, Charnay P, Burns DK, Parada LF. Neurofibromas in NF1: Schwann cell origin and role of tumor environment. Science 2002;296(5569):920-2.
9. Zhu Y, Parada LF. Neurofibromin, a tumor suppressor in the nervous system. Exp Cell Res 2001;264(1):19-28.
10. Mahgoub N, Taylor B, Le Beau M, Gratiot M, Carlson K, Jacks T, et al. Myeloid malignancies induced by alkylating agents in Nf1 mice. Blood 1999;93:3617-3623.
11. Mahgoub N, Taylor BR, Gratiot M, Kohl NE, Gibbs JB, Jacks T, et al. In vitro and In vivo effects of a farnesyltransferase inhibitor on Nf1- deficient hematopoietic cells. Blood 1999;94(7):2469-76.
12. Reilly KM, Loisel DA, Bronson RT, McLaughlin ME, Jacks T. Nf1;Trp53 mutant mice develop glioblastoma with evidence of strain- specific effects. Nat Genet 2000;26(1):109-13.
13. Arico M, Biondi A, Pui C-H. Juvenile myelomonocytic leukemia. Blood 1997;90:479-488.
14. Largaespada DA, Brannan CI, Jenkins NA, Copeland NG. *Nf1* deficiency causes Ras-mediated granulocyte-macrophage colony stimulating factor hypersensitivity and chronic myeloid leukemia. Nat Genet 1996;12:137-143.

15. Birnbaum RA, O'Marcaigh A, Wardak Z, Zhang YY, Dranoff G, Jacks T, et al. Nf1 and Gmcsf interact in myeloid leukemogenesis. Mol Cell 2000;5(1):189-95.

16. Le DT, Kong N, Zhu Y, Lauchle JO, Aiyigari A, Braun BS, et al. Somatic inactivation of Nf1 in hematopoietic cells results in a progressive myeloproliferative disorder. Blood 2004;103(11):4243-50.

17. Listernick R, Charrow J, Gutmann DH. Intracranial gliomas in neurofibromatosis type 1. Am J Med Genet 1999;89(1):38-44.

18. Listernick R, Louis DN, Packer RJ, Gutmann DH. Optic pathway gliomas in children with neurofibromatosis 1: consensus statement from the NF1 Optic Pathway Glioma Task Force. Ann Neurol 1997;41(2):143-9.

19. Zhu Y, Guignard F, Zhao D, Liu L, Burns DK, Mason RP, et al. Early inactivation of p53 tumor suppressor gene cooperating with NF1 loss induces malignant astrocytoma. Cancer Cell 2005;8(2):119-30.

20. Sherman L, Sleeman JP, Hennigan RF, Herrlich P, Ratner N. Overexpression of activated neu/erbB2 initiates immortalization and malignant transformation of immature Schwann cells in vitro. Oncogene 1999;18(48):6692-9.

21. Jin JJ, Nikitin A, Rajewsky MF. Schwann cell lineage-specific neu (erbB-2) gene expression in the developing rat nervous system. Cell Growth Differ 1993;4(3):227-37.

22. Maris JM, Wiersma SR, Mahgoub N, Thompson P, Geyer RJ, Lange BJ, et al. Monosomy 7 myelodysplastic syndrome and other second malignant neoplasms in children with neurofibromatosis type 1. Cancer 1997;79:1438-46.

23. Papageorgio C, Seiter K, Feldman EJ. Therapy-related myelodysplastic syndrome in adults with neurofibromatosis. Leuk Lymphoma 1999;32(5-6):605-8.

24. Chao RC, Pyzel U, Fridlyand J, Kuo YM, Teel L, Haaga J, et al. Therapy-induced malignant neoplasms in Nf1 mutant mice. Cancer Cell 2005;8(4):337-48.

25. Vogel KS, Klesse LJ, Velasco-Miguel S, Meyers K, Rushing EJ, Parada LF. Mouse tumor model for neurofibromatosis type 1. Science 1999;286(5447):2176-9.

26. Cichowski K, Santiago S, Jardim M, Johnson BW, Jacks T. Dynamic regulation of the Ras pathway via proteolysis of the NF1 tumor suppressor. Genes Dev 2003;17(4):449-54.

27. Le DT, Shannon KM. Ras processing as a therapeutic target in hematologic malignancies. Curr Opin Hematol 2002;9(4):308-15.

28. Aiyagari AL, Taylor BR, Aurora V, Young SG, Shannon KM. Hematologic effects of inactivating the Ras processing enzyme Rce1. Blood 2003;101(6):2250-2.

29. DeClue JE, Heffelfinger S, Benvenuto G, Ling B, Li S, Rui W, et al. Epidermal growth factor receptor expression in neurofibromatosis type 1- related tumors and NF1 animal models. J Clin Invest 2000;105(9):1233-41.

30. Ling BC, Wu J, Miller SJ, Monk KR, Shamekh R, Rizvi TA, et al. Role for the epidermal growth factor receptor in neurofibromatosis-related peripheral nerve tumorigenesis. Cancer Cell 2005;7(1):65-75.

31. Shaw R, Paez J, Curto M, Taktine A, Pruitt W, Sadtome I, et al. The neurofibromatosis type 2 tumor suppressor protein, merlin, functions in Rac-dependent signaling. Dev Cell 2001;1:63-72.

32. Hirokawa Y, Tikoo A, Huynh J, Utermark T, Hanemann CO, Giovannini M, et al. A clue to the therapy of neurofibromatosis type 2: NF2/merlin is a PAK1 inhibitor. Cancer J 2004;10(1):20-6.

33. Kissil JL, Johnson KC, Eckman MS, Jacks T. Merlin phosphorylation by p21-activated kinase 2 and effects of phosphorylation on merlin localization. J Biol Chem 2002;277(12):10394-9.

34. Kissil JL, Wilker EW, Johnson KC, Eckman MS, Yaffe MB, Jacks T. Merlin, the product of the Nf2 tumor suppressor gene, is an inhibitor of the p21-activated kinase, Pak1. Mol Cell 2003;12(4):841-9.

35. Lallemand D, Curto M, Saotome I, Giovannini M, McClatchey AI. NF2 deficiency promotes tumorigenesis and metastasis by destabilizing adherens junctions. Genes Dev 2003;17(9):1090-100.

36. James MF, Manchanda N, Gonzalez-Agosti C, Hartwig JH, Ramesh V. The neurofibromatosis 2 protein product merlin selectively binds F-actin but not G-actin, and stabilizes the filaments through a lateral association. Biochem J 2001;356(Pt 2):377-86.

37. Takahashi K, Suzuki K. Density-dependent inhibition of growth involves prevention of EGF receptor activation by E-cadherin-mediated cell-cell adhesion. Exp Cell Res 1996;226(1):214-22.

38. Lampugnani MG, Zanetti A, Breviario F, Balconi G, Orsenigo F, Corada M, et al. VE-cadherin regulates endothelial actin activating Rac and increasing membrane association of Tiam. Mol Biol Cell 2002;13(4):1175-89.

39. Qian X, Karpova T, Sheppard AM, McNally J, Lowy DR. E-cadherin-mediated adhesion inhibits ligand-dependent activation of diverse receptor tyrosine kinases. Embo J 2004;23(8):1739-84.

40. Noble ME, Endicott JA, Johnson LN. Protein kinase inhibitors: insights into drug design from structure. Science 2004;303(5665):1800-5.

41. Donovan S, See W, Bonifas J, Stokoe D, Shannon KM. Hyperactivation of protein kinase B and ERK have discrete effects on survival, proliferation, and cytokine expression in Nf1-deficient myeloid cells. Cancer Cell 2002;2(6):507-14.

42. Perez OD, Nolan GP. Simultaneous measurement of multiple active kinase states using polychromatic flow cytometry. Nat Biotechnol 2002;20(2):155-62.

43. Braun BS, Tuveson DA, Kong N, Le DT, Kogan SC, Rozmus J, et al. Somatic activation of oncogenic Kras in hematopoietic cells initiates a rapidly fatal myeloproliferative disorder. Proc Natl Acad Sci U S A 2004;101(2):597-602.

44. Sattler M, Mohi MG, Pride YB, Quinnan LR, Malouf NA, Podar K, et al. Critical role for Gab2 in transformation by BCR/ABL. Cancer Cell 2002;1(5):479-92.

45. Sebolt-Leopold JS, Dudley DT, Herrera R, Van Becelaere K, Wiland A, Gowan RC, et al. Blockade of the MAP kinase pathway suppresses growth of colon tumors in vivo [see comments]. Nat Med 1999;5(7):810-6.

46. Kleihues P, Sobin LH. World Health Organization classification of tumors. Cancer 2000;88(12):2887.

Children's Tumor Foundation
Ending Neurofibromatosis Through Research

Banbury Conference Center
Cold Spring Harbor, NY
http://www.cshl.edu/banbury/

November 3rd-5th, 2005

Barriers and Solutions in the Use of Mouse Models to Develop Therapeutic Strategies for NF1 and NF2-Associated Tumors

Organizers: David Gutmann, *Washington University*
Kevin Shannon, *University of California, San Francisco*
Kim Hunter-Schaedle, *Children's Tumor Foundation*

Purpose: Overall, an informal discussion-oriented forum to address and identify potential solutions to barriers in the drive to develop therapeutics for neurofibromatosis (NF). The advantages, limitations and potential new directions of using mouse models of neurofibromatosis 1 and neurofibromatosis 2 (NF1 and NF2) to achieve this goal will be analyzed.

Participants: Approximately 25 leading experts in the field of NF research; invited experts from relevant fields outside NF research; NF program leadership representatives from Children's Tumor Foundation (CTF), National Institutes of Health, and Department of Defense. The small group format is anticipated to stimulate extensive discussion.

Format: The evening of Day 1 will set the stage for the meeting. On Day 2, there are a series of defined sessions within which each presenter is limited to 20 minutes. Presentations should not be 'form talks', but aim to raise key issues within that topic area and provoke discussion with colleagues. Each block of presentation will be followed by a round-table open discussion session. On Day 3 all participants are assigned to one of six breakout groups each assigned a specific question/issue for which to develop key recommendations. The meeting will then reconvene and each group will share their recommendations.

Outcome Goal: To define the key barriers and identify potential solutions that will ultimately accelerate the number of drugs screened in mouse models of NF and increase the likelihood of identifying potential NF therapeutics.
A report on the outcome recommendations of the meeting will be prepared by CTF in conjunction with the organizers for publication in a high-visibility journal.

****

This meeting is made possible with support from the Department of Defense and the Children's Tumor Foundation

Agenda

Thursday - November 3rd, 2005

5:00 pm:	*Registration and cocktails*
6:30pm:	*Dinner*
7:45 pm:	*Walk to Conference Room*

****

Session I: Setting the Stage

8 pm:	Overview of meeting purpose and goals: 'throwing down the gauntlet'	Kevin Shannon
8:15pm:	Report from the CDMRP NF program	Melissa Kaime
8:30pm:	The Use of Mouse Models to Probe Drug Sensitivity and Resistance	Scott Lowe
9:15pm:	A Prototype Mouse Hospital for Performing Preclinical Trials	David Tuveson
10pm:	Discussion moderated by Dr. Shannon; *adjourn*	

****

Friday - November 4th, 2005

Buffet Breakfast served in conference room

****

Session II:	**NF1 and NF2-Associated Tumors: Clinical and Pathologic Features and Current Treatments**	
	<u>Chair</u>: Wade Clapp	
7:30am:	Clinical aspects of neurofibromatosis demanding attention	Mia MacCollin
7:50am:	Vestibular schwannoma xenografts in the SCID mouse	Brad Welling
8:10am:	Challenges in clinical trial development for childhood cancer and applicability to neurofibromatosis-related malignancies	Susan Blaney
8:30am:	Of Mice and Men - Pathology of Neurofibromatosis-Associated Lesions	Anat Stemmer-Rachamimov
8:50am:	Endpoints for clinical trials in NF	Brigitte Widemann

9:10am: Discussion moderated by Dr. Clapp

****

9:30 –9:50am: Refreshments Break

****

Session III: ***Therapeutic Targets and Drug Discovery in NF1, Part 1***
Chair: Mia MacCollin

9:50am:	NF1 drug targets from a fly's perspective	Andre Bernards
10:10am:	Transgenic and cell culture models of NF1	Nancy Ratner
10:30am:	Targeting endothelial cells and pericytes in the neurofibroma microenvironment	David Ingram

****

10:50 – 11:10am: Break

****

Session IV: **Targets and Drug Discovery in NF1, Part 2**
Chair: Brigitte Widemann

11:10am:	mTOR signalling in NF1	Karen Cichowski
11:30pm:	Thinking beyond Ras GTPase	Jay Gibbs
11:50pm:	Kinase Inhibitors for the Potential Treatment of NF1	Gideon Bollag

12:10pm: Discussion moderated by Dr. MacCollin and Dr. Widemann

****

12:30 – 1:30 pm: Lunch (Robertson House)

****

Session V: **Therapeutic Targets and Drug Discovery in NF2**
Chair: Brad Welling

1:30pm:	A Search for Allosteric Inhibitors of p21-Activated Kinases	Jon Chernoff
1:50pm:	Context-dependent function of Merlin	Andrea McClatchey
2:10pm:	Small molecule inhibitors of Pak for the treatment of NF2	Ruihong Chen

2:30-2:50 pm: Discussion moderated by Dr. Welling

****

2:50pm – 3:10pm: *Refreshments Break*

****

Session VI: **Mouse Models and Preclinical Data**
Chair: Andre Bernards

3:10pm:	Gliomas	Eric Holland
3:30pm:	Mouse models of NF1-associated optic glioma	David Gutmann
3:50pm:	PET/CT imaging as a tool to evaluate cellular, genetic, and molecular targets for the treatment of plexiform neurofibromas	Wade Clapp
4:10pm:	Stage specific response of *Nf1* mutant myeloid malignancies to a targeted agent	Kevin Shannon
4:30pm:	Understanding NF2: insights from mouse models	Marco Giovannini
4:50pm:	Discussion moderated by Dr. Korf	

5.30pm *PROMPT – ADJOURN*

****

6:30pm: *Cocktails (Meier House)*

7:30pm: *Buffet Dinner (Meier House)*

****

Saturday - November 5th, 2005

Buffet Breakfast served in conference room

****

7:30am: **Children's Tumor Foundation Drug Discovery Partnerships: a proposed partnering & funding initiative** — Kim Hunter-Schaedle

7:45am: **Session VII: Breakout sessions: Introduction by Moderators: Dr. Shannon & Dr. Gutmann**

8:am: **Breakouts convene**

Each participant has been assigned by the organizers to a breakout session as follows:

GROUP 1: **What additional information do we need have regarding drug targets in NF1 and NF2? How can we use tissues from genetically engineered mice to address this problem?**

Assigned:
Andre Bernards (Moderator)
Jonathan Chernoff
Karen Cichowski
Andrea McClatchey
Nancy Ratner

GROUP 2: **What are the major barriers to conducting therapeutic trials in NF patients?**

Assigned:
Gideon Bollag (Moderator)
Mia MacCollin
Anat Stemmer-Rachimimov
Peter Bellermann

GROUP 3: **What questions can we address with mouse models that we cannot address by studying human tumors?**

Assigned:
Marco Giovannini (Moderator)
David Gutmann
Meg McLaughlin
Wade Clapp

GROUP 4: **How can we maximize interactions with industry to identify and evaluate new therapies for NF?**

Assigned:
Jay Gibbs (Moderator)
Ruihong Chen
Eric Holland
Cheryl Marks
Kim Hunter-Schaedle

GROUP 5: **How can we design preclinical trials to provide useful information for human clinical trials?**

Assigned:
Susan Blaney (Moderator)
Kevin Shannon
David Tuveson
Brigitte Widemann
Jill Heemskerk

9:45 – 10am: Refreshments Break

****

Session VIII: Final Recommendations

10am:	Group 1 Report	Andre Bernards
10:15am:	Group 2 Report	David Ingram
10:30am:	Group 3 Report	Marco Giovannini
10:45am:	Group IV Report	Jay Gibbs
11am:	Group V Report	Susan Blaney

11:15 – 12:30pm: **Open discussion & final recommendations**
Moderators: Kevin Shannon David Gutmann

What are the Barriers and Solutions in the Use of Mouse Models to Develop Therapeutic Strategies for NF1 and NF2-Associated Tumors?

What types of funding initiatives should DOD and NIH consider to encourage preclinical studies that lead to rational clinical trials in human patients?

How can mouse model efforts be dovetailed with planned human clinical efforts (DOD clinical trials program)?

- **PRIORITIES**
- **RECOMMENDATIONS**

****

12:30pm: Lunch (Robertson House)

****

Meeting adjourns

Therapy-induced malignant neoplasms in *Nf1* mutant mice

Richard C. Chao,[1,8,11] Urszula Pyzel,[1] Jane Fridlyand,[2] Yien-Ming Kuo,[1,3] Lewis Teel,[1] Jennifer Haaga,[1] Alexander Borowsky,[9] Andrew Horvai,[4] Scott C. Kogan,[5,6] Jeannette Bonifas,[1] Bing Huey,[6] Tyler E. Jacks,[10] Donna G. Albertson,[5,6,7] and Kevin M. Shannon[1,6,*]

[1]Department of Pediatrics, University of California, San Francisco, San Francisco, California 94143
[2]Department of Epidemiology and Biostatistics, University of California, San Francisco, San Francisco, California 94143
[3]Department of Medicine, University of California, San Francisco, San Francisco, California 94143
[4]Department of Pathology, University of California, San Francisco, San Francisco, California 94143
[5]Department of Laboratory Medicine, University of California, San Francisco, San Francisco, California 94143
[6]Comprehensive Cancer Center, University of California, San Francisco, San Francisco, California 94143
[7]Cancer Research Institute, University of California, San Francisco, San Francisco, California 94143
[8]Department of Medicine, Division of Hematology/Oncology, Department of Veterans' Affairs Medical Center, San Francisco, California 94121
[9]Medical Pathology Center for Comparative Medicine, University of California, Davis, Davis, California 95616
[10]Center for Cancer Research, Massachusetts Institute of Technology, Cambridge, Massachusetts 02139
[11]Present address: Pfizer Global Research and Development, 10578 Science Center Drive (B95), San Diego, California 92121
*Correspondence: kevins@itsa.ucsf.edu

Summary

Therapy-induced cancers are a severe complication of genotoxic therapies. We used heterozygous *Nf1* mutant mice as a sensitized genetic background to investigate tumor induction by radiation (RAD) and cyclophosphamide (CY). Mutagen-exposed *Nf1*$^{+/-}$ mice developed secondary cancers that are common in humans, including myeloid malignancies, sarcomas, and breast cancers. RAD cooperated strongly with heterozygous *Nf1* inactivation in tumorigenesis. Most of the solid tumors showed loss of the wild-type *Nf1* allele but retained two *Trp53* alleles. Comparative genomic hybridization demonstrated distinct patterns of copy number aberrations in sarcomas and breast cancers from *Nf1* mutant mice, and tumor cell lines showed deregulated Ras signaling. *Nf1*$^{+/-}$ mice provide a tractable model for investigating the pathogenesis of common mutagen-induced cancers and for testing preventive strategies.

Introduction

Therapy-induced malignant neoplasms, also known as second malignant neoplasms (SMNs), are a severe complication of genotoxic cancer treatments including radiation (RAD) and chemotherapeutic agents (Bhatia and Sklar, 2002; Matesich and Shapiro, 2003; Smith et al., 2003). SMNs have a substantial public health impact, as they account for most of the ~90,000 new cancers that are diagnosed in the United States each year in persons who had a previous histologically distinct malignancy (Bhatia and Sklar, 2002). Whereas early reports emphasized the risk of SMNs in patients with Hodgkin's disease and other hematopoietic malignancies (Le Beau et al., 1986; Rowley et al., 1977; Tucker et al., 1988), these cancers are increasingly recognized after intensive treatment for breast cancer and other solid tumors (Matesich and Shapiro, 2003; Smith et al., 2003). Myeloid leukemia, lymphoma, and sarcoma are the most common SMNs found in survivors of hematologic and nonhematologic cancers (Bhatia and Sklar, 2002; Matesich and Shapiro, 2003; Smith et al., 2003). With prolonged follow-up, cancer survivors are also at elevated risk of developing epithelial tumors of the breast, uterus, and gastrointestinal tract (de Vathaire et al., 1989a, 1989b; Hawkins et al., 1987; Tucker et al., 1988). Importantly, many SMNs are resistant to treatment, and previous exposure to cytotoxic agents may limit the use of intensive salvage regimens. The lack of relevant animal models of SMNs has impeded efforts to understand how mutagenic cancer therapeutics induce tumors in vivo, and to test preventive strategies.

Studies of familial cancer syndromes have provided fundamental insights into mechanisms that underlie tumorigenesis. In addition to markedly increasing the incidence of primary ma-

SIGNIFICANCE

Cancers induced by genotoxic treatments are a major clinical problem; however, the long-term mutagenic potential of specific therapeutic regimens may not be known until many years from now. We used *Nf1* mutant mice to recapitulate the dynamic interaction between mutagen exposure and tumorigenesis that underlies the development of human therapy-induced malignancies. These animals develop a similar spectrum of malignancies as human patients who are treated with radiation and alkylating agents, and provide a tractable system for performing mechanistic studies, for comparing the mutagenic potential of different regimens, and for testing preventive strategies. Our data also have translational implications for assessing the potential risks of genotoxic modalities, particularly in persons with neurofibromatosis type 1.

lignancies, some inherited cancer predispositions confer a high risk of SMNs. For example, persons with the Li-Fraumeni syndrome carry germline *TP53* mutations, which leads to an elevated risk of both primary malignancies and SMNs (Li and Fraumeni, 1982; Malkin et al., 1992; Nichols et al., 2001). Similarly, most children with a germline *RB1* mutation develop one or more retinoblastoma tumors and are predisposed to osteosarcoma and other cancers later in life (Wong et al., 1997). The incidence of osteosarcoma is dramatically increased in areas exposed to RAD in the course of treating the initial retinoblastoma (Wong et al., 1997). As in de novo cancers, investigating how heritable mutations cooperate with genotoxic cancer therapies will likely provide mechanistic insights that are relevant to tumorigenesis in individuals who develop SMNs without a known genetic predisposition.

Mutations in the *NF1* tumor suppressor gene cause neurofibromatosis type 1 (NF1), an inherited cancer syndrome that affects 1 in 3500 persons (Cichowski and Jacks, 2001; Dasgupta and Gutmann, 2003). *NF1* encodes neurofibromin, a GTPase-activating protein that negatively regulates Ras signaling (Boguski and McCormick, 1993; Donovan et al., 2002b). Affected individuals are predisposed to specific benign and malignant tumors, particularly in tissues derived from the embryonic neural crest (Side and Shannon, 1998). In addition, the incidence of juvenile myelomonocytic leukemia (JMML) and other myeloid malignancies is increased 200- to 500-fold in children with NF1 (Stiller et al., 1994). Clinical data suggest that persons with NF1 are also predisposed to SMNs. Maris and coworkers (Maris et al., 1997) reported five children with NF1 who developed myeloid malignancies and performed a systematic review of 64 children with NF1 who received chemotherapy and/or RAD to treat a primary cancer. This study revealed an 11% incidence of SMNs, with an especially high risk in children who had a primary embryonal cancer. Two adults with NF1 also developed therapy-related myelodysplastic syndrome (MDS) after treatment for de novo acute myeloid leukemia (AML) (Papageorgio et al., 1999). These reports suggested that therapeutic exposure to genotoxic agents might cooperate with germline *NF1* mutations in the genesis of common SMNs found in the general population, namely myeloid leukemia and sarcoma.

Based on these clinical observations, we reasoned that heterozygous *Nf1* mutant mice (*Nf1*$^{+/-}$) might be harnessed to investigate the pathogenesis of SMNs in vivo. *Nf1*$^{+/-}$ mice spontaneously develop pheochromocytoma and a myeloproliferative disorder (MPD) that resembles JMML with incomplete penetrance (Jacks et al., 1994b). In a previous study, exposing these mice to the alkylating agent cyclophosphamide (CY) increased the incidence of MPD and reduced the latency (Mahgoub et al., 1999). Here, we show that RAD alone or in combination with CY induces a spectrum of SMNs in *Nf1*$^{+/-}$ mice that includes soft tissue sarcomas and breast carcinomas. The normal *Nf1* allele is inactivated in most of these solid tumors, and some also demonstrate loss of heterozygosity (LOH) at the *Trp53* locus. Comparative genomic hybridization (CGH) uncovered tumor-specific patterns of copy number aberrations, which implies the existence of distinct pathways of cooperating genetic lesions in different cancers. Biochemical investigation of cell lines developed from a subset of these malignant tumors revealed deregulated Ras signaling. *Nf1*$^{+/-}$ mice provide a tractable in vivo model for understanding how RAD and alkylating agents induce cancer, and for testing preventive strategies.

Results

CY and RAD induce reversible myelosuppression

We selected CY for investigation because this alkylating agent is a component of many front-line therapeutic regimens. To model the myelosuppression that occurs in human patients, we intercrossed wild-type C57Bl/6 and 129/Sv mice to generate cohorts of five to ten F1 animals that were exposed to different CY doses. Mice injected with a weekly intraperitoneal CY dose of 200 mg/kg for 6 consecutive weeks reproducibly developed anemia and leukopenia that resolved after the drug was discontinued (data not shown). This regimen was not otherwise associated with obvious morbidity. A single RAD dose of 3 Gy, which was selected on the basis of previous data showing that this dose was leukemogenic in CBA mice (Major, 1979; Major and Mole, 1978; Mole et al., 1983), was administered 2 weeks after the last dose of CY. In a pilot experiment that assessed the combination of CY at 200 mg/kg/week for 6 weeks followed by 3 Gy of RAD, we found that mice tolerated sequential treatment without significant toxicity (data not shown).

Based on these preliminary data, 192 wild-type and *Nf1*$^{+/-}$ mice were assigned to one of four groups at 8–17 weeks of age: no treatment, CY only, RAD only, or CY followed by RAD. Treatment with CY, RAD, or the combination resulted in reversible myelosuppression (Figure S1 in the Supplemental Data available with this article online). Mice that received six weekly injections of CY developed anemia with decreases in hemoglobin concentration (from 16.2 ± 1.0 g/dl to 12.3 ± 1.3 g/dl; $p < 0.00001$) and white blood cell count (from $7.4 \pm 3.0 \times 10^3$ to $1.5 \pm 0.7 \times 10^3$ cells/μl; $p < 0.00001$). Animals assigned to receive RAD alone entered the study cohort concurrently and were irradiated at the same time as mice that had been treated with CY. RAD induced a significant reduction in leukocyte counts and a modest fall in the hemoglobin concentration that was not statistically significant (Figure S1). Myelosuppression was similar in wild-type and *Nf1*$^{+/-}$ mice, and peripheral blood cell counts recovered quickly after cessation of CY and/or RAD. The only early treatment-related deaths occurred 19 and 20 days after RAD in two wild-type mice that received both CY and RAD (~1% of the cohort).

Survival and tumorigenesis in wild-type and *Nf1*$^{+/-}$ mice

Pathologic analysis was performed on 91% of the study cohort, including 97 of 104 wild-type mice and 77 of 86 *Nf1*$^{+/-}$ mice. Three wild-type and four *Nf1*$^{+/-}$ mice were considered evaluable without complete pathologic analysis, including two mice with treatment-related mortality, two mice with massive splenomegaly in which there was no histologic analysis of other organs, and three mice with tumors of the Harderian gland, which secretes lipid and porphyrins over the eye. Eleven mice that died unexpectedly could not be analyzed for tumor formation. Heterozygous inactivation of *Nf1* was strongly associated with an increased risk of premature death following treatment with a survival rate of only 30% after 15 months in *Nf1*$^{+/-}$ mice compared with 78% in wild-type littermates (Figure 1, left panel; $p < 0.001$). Death was due to cancer in 96% of evaluable mice. We identified 51 malignancies in 81 *Nf1*$^{+/-}$ ani-

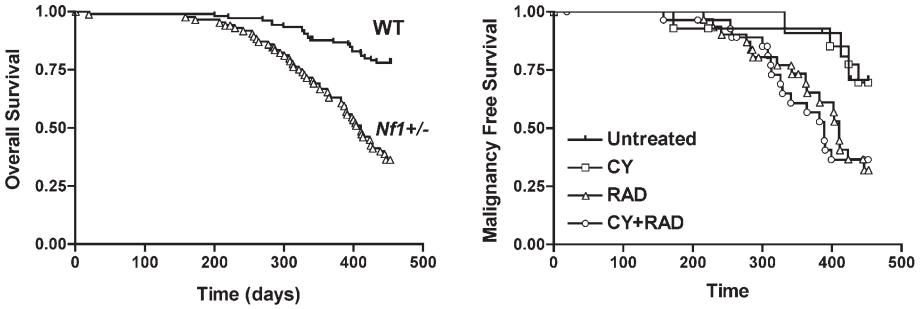

Figure 1. Reduced survival and increased incidence of cancer in *Nf1*$^{+/-}$ mice

Kaplan-Meier analysis was performed to analyze survival and tumor formation in the entire cohort from the date that mice assigned to receive radiation were treated. Left panel: analysis of overall survival demonstrates an increased risk of death in *Nf1*$^{+/-}$ versus wild-type (WT) mice with a hazard ratio of death of 3.83 (confidence interval: 2.52–6.40). The survival plots include control (untreated) and genotoxin-exposed mice of each genotype. Right panel: *Nf1*$^{+/-}$ mice that were exposed to RAD alone (p = 0.0043) or RAD in combination with CY displayed a significantly higher risk of cancer than *Nf1*$^{+/-}$ mice that were not irradiated. The incidence of cancer was not significantly different in control and CY-treated *Nf1*$^{+/-}$ mice. In these plots, the latency to death or tumor was measured from the date of radiation treatment.

mals that were available for pathologic examination compared with 17 cancers in 100 wild-type mice (Table 1; $p < 0.0001$). Tumor types that occurred significantly more often in *Nf1*$^{+/-}$ mice included soft tissue sarcomas ($p = 0.001$), myeloid malignancies ($p = 0.0005$), and pheochromocytomas ($p = 0.0007$). Myeloid malignancies and sarcomas, which are the most common SMNs in human patients, accounted for 24 of the 52 cancers found in *Nf1*$^{+/-}$ mice. We also unexpectedly detected breast cancers in four female *Nf1*$^{+/-}$ mice but observed none in the wild-type animals ($p = 0.04$, Fisher's exact test).

RAD cooperated strongly with heterozygous *Nf1* inactivation in tumorigenesis whether administered alone or after CY (Figure 1, right panel; $p = 0.002$). By contrast, the incidence of cancer was similar in untreated *Nf1*$^{+/-}$ mice and in animals that received CY only (Figure 1, right panel). Interestingly, the nature of the mutagen exposure influenced the tumor spectrum in *Nf1*$^{+/-}$ mice. In particular, RAD alone resulted in a greater frequency of myeloid malignancies, whereas exposure to RAD in combination with CY resulted in a high incidence of solid tumors, including breast cancer (Table 2).

Tumor phenotypes

Sixteen *Nf1*$^{+/-}$ mice developed tumors of presumed neural crest origin, which included soft tissue sarcomas, pheochromocytoma, neuroblastoma, and paraganglioma (Table 1). Pheochromocytomas occurred in both untreated *Nf1*$^{+/-}$ mice and in animals that were exposed to genotoxins, whereas sarcomas, neuroblastomas, and paragangliomas only developed after exposure to CY and/or RAD. None of these tumors occurred in wild-type animals ($p = 0.000001$). Soft tissue sarcomas from *Nf1*$^{+/-}$ mice demonstrated a spindle cell pattern, and some were positive by S100 staining (Figures 2A–2F), which is typical of the malignant peripheral nerve sheath tumors (MPNSTs) that occur in NF1 patients (Weiss et al., 1983; Wick et al., 1987). Most of these tumors arose in close proximity to peripheral nerves, were deep-seated, and ranged from morphologically low-grade spindle cell proliferations with $\leq$1 mitotic figure (mf) per 10 high-power fields (hpf) and minimal nuclear atypia to highly malignant tumors with >50 mf per 10 hpf and highly atypical nuclei. The low-grade tumors were uniformly S100-positive, whereas higher-grade lesions were S100-negative, which is consistent with the pattern of S100 expression in human MPNSTs. Interestingly, areas that were architecturally and cytologically reminiscent of benign Schwann cell proliferations were found immediately adjacent to some of the high-grade sarcomas. We also assessed these tumors for epidermal growth factor receptor (EGFR), p16, and p21 expression. Interestingly, none expressed detectable surface EGFR or nuclear p16, whereas seven of eight were positive for nuclear p21 (Figure 3).

Consistent with previous reports (Jacks et al., 1994b; Mahgoub et al., 1999), *Nf1*$^{+/-}$ mice were predisposed to myeloid malignancies ($p = 0.0065$ versus wild-type littermates). Although the overall incidence of these cancers did not differ in *Nf1*$^{+/-}$ mice according to treatment group, exposure to RAD was associated with an unexpectedly diverse spectrum of myeloid diseases, which included cases that were classified as AML, MDS, or cytopenias without definitive criteria for AML or MDS (Kogan et al., 2002). In addition, two *Nf1*$^{+/-}$ mice that died suddenly without a confirmed cause of death had massive splenomegaly, which suggests an underlying myeloid malignancy (Table 1). All of the wild-type mice with myeloid malignancies were from the RAD treatment group. Interestingly, sequential administration of CY and RAD was associated with fewer myeloid malignancies in heterozygous *Nf1* mutant mice than exposure to either modality alone (Table 1).

Four of twenty-one female *Nf1*$^{+/-}$ mice that received CY + RAD were diagnosed with breast cancers. These tumors were characterized by cytokeratin (Figures 2G–2I), which is consis-

Table 1. Tumor spectra in untreated and genotoxin-exposed mice according to genotype

Type of neoplasm	Wild-type (n = 100)	*Nf1*$^{+/-}$ (n = 81)
Neural crest tumors	0	16
Soft tissue sarcomas	0	8
Pheochromocytoma	0	6
Neuroblastoma/paraganglioma	0	2
Myeloid malignancies*	4	17*
Breast cancer	0	4
Poorly differentiated malignant tumors	0	3
Other	13	11
Total	17	51

Tumors identified in mice that were examined pathologically. The neural crest tumors were further classified as soft tissue sarcoma, pheochromocytoma, or neuroblastoma/paraganglioma. *The myeloid disorders identified included MPD (n = 9), MDS (n = 1), AML (n = 3), histiocytic sarcoma (n = 1), and refractory cytopenia with splenomegaly (n = 3). Two additional *Nf1*$^{+/-}$ mice with massive splenomegaly (>1 g) but no other gross abnormalities were not classified as having a myeloid malignancy as the cause of death.

Table 2. Tumors in *Nf1*$^{+/-}$ mice according to treatment group

Tumor type	Untreated (n = 12)	CY (n = 14)	RAD (n = 31)	CY + RAD (n = 29)	Latency (range in days)
Neural crest tumors	2	3	5	6	
Soft tissue sarcomas	0	2	2	4	172–469
Pheochromocytomas	1	1	2	2	382–494
Neuroblastoma/paraganglioma	1	0	1	0	467
Myeloid malignancies	2	1	10	4	215–519
Poorly differentiated tumors	0	1	1	1	389–410
Breast cancer	0	0	0	4	308–389
Other	1	1	4	5	158–467
Total	5	6	20	20	158–519

Tumors developing in *Nf1* mutant mice were subdivided according to exposure to radiation (RAD), cyclophosphamide (CY), or both modalities (RAD + CY), and the number of mice assigned to each group is also shown. The corresponding numbers of wild-type mice were as follows: control (n = 20), RAD (n = 32), CY (n = 17), and RAD + CY (n = 37). The neural crest tumors were further subclassified as soft tissue sarcoma, pheochromocytoma, or neuroblastoma/paraganglioma. Latency refers to the number of days from RAD treatment to when a tumor was detected. The mean latency was the same in mice that developed soft tissue sarcomas (359 days), myeloid malignancies (347 days), or breast cancer (341 days).

tent with epithelial origin. The histology of these breast cancers was remarkably uniform between cases. In general, areas of adenocarcinoma in situ were identified adjacent to infiltrating ductal carcinoma with both glandular and more solid growth patterns. The invasive component demonstrated high-grade nuclear features and abundant mitotic activity (>20 mf/10 hpf). Most of the breast cancers invaded into the underlying skeletal muscle. Overall, the pathologic features of these murine breast cancers were very similar to those of high-grade adenocarcinoma of the breast in humans.

Three *Nf1*$^{+/-}$ mice developed poorly differentiated malignant tumors that could not be characterized with precision. In addition, we incidentally detected benign bronchiolo/alveolar adenomas in the lungs of many older wild-type and *Nf1*$^{+/-}$ mice. Similar findings have been reported in other mouse strains (Dixon and Maronpot, 1991). These lesions were excluded from the analysis of malignancies, with the exception that six very large lung tumors (four in treated wild-type mice and two in treated *Nf1*$^{+/-}$ mice) that resulted in premature death were classified as malignant. Other tumor types noted included lymphoma (four wild-type, five *Nf1*$^{+/-}$), Harderian gland (three wild-type, two *Nf1*$^{+/-}$), osteosarcoma (two wild-type), and liver (one *Nf1*$^{+/-}$). Most of the wild-type and *Nf1*$^{+/-}$ mice that developed these tumors were exposed to CY, RAD, or both.

CGH analysis of primary tumors and tumor-derived cell lines

We performed CGH on primary sarcomas and breast cancers to identify copy number changes that might contribute to tumorigenesis. These studies uncovered multiple genomic changes

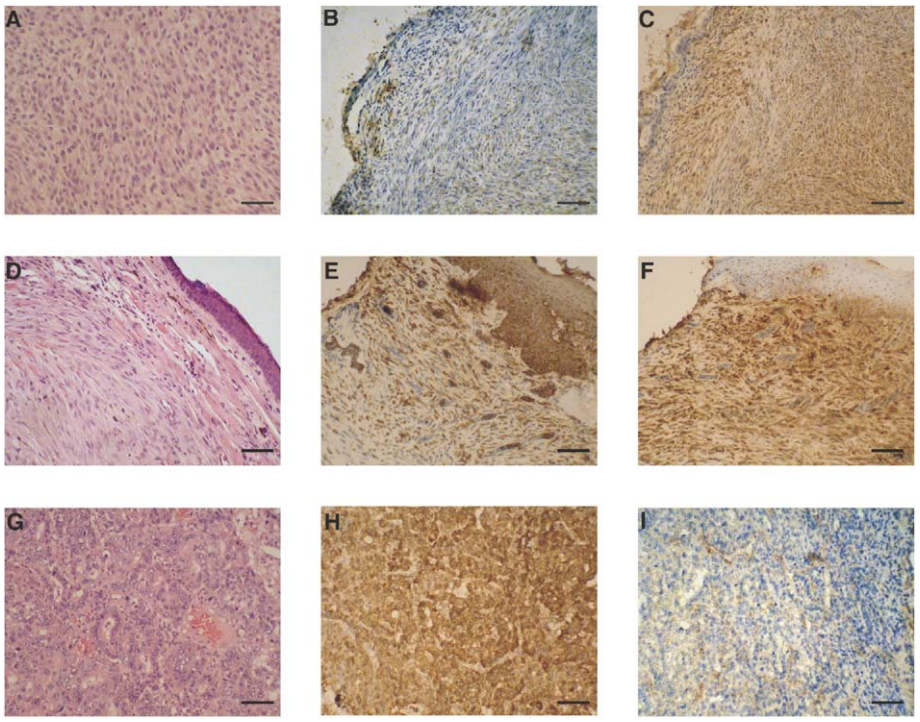

Figure 2. Histologic and immunocytochemical analysis of malignant tumors from *Nf1*$^{+/-}$ mice

Tumor tissues were stained with hematoxylin and eosin (**A**, **D**, and **G**), cytokeratin (CK; **B**, **E**, and **H**), or S100 (**C**, **F**, and **I**). **A**–**C** depict a spindle cell tumor from an *Nf1* mutant mouse that was exposed to CY and RAD. Immunohistochemical staining for CK was negative, while staining for S100 revealed intense cytoplasmic staining of a large proportion of spindle cells. **D**–**F** are sections of a spindle cell neoplasm from an *Nf1*$^{+/-}$ that was exposed to RAD. This tumor displayed positive staining for both CK and S100, with islands of CK-positive cells found in a background of predominantly S100-positive cells. **G**–**I** are from a breast adenocarcinoma that developed in a female *Nf1*$^{+/-}$ mouse exposed to both CY and RAD. This tumor displayed staining for CK but not S100. The scale bars are 50 μm in length.

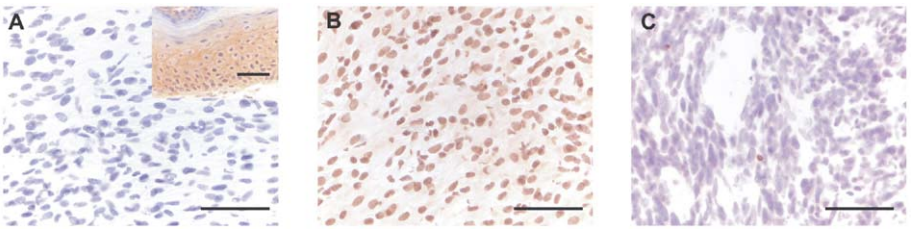

Figure 3. EGFR, p21, and p16 staining of genotoxin-induced sarcomas

A: A sarcoma section stained with an anti-EGFR antibody is negative for surface EGFR expression, while skin from the same mouse shows positive staining in the epidermis (insert).

B: Staining with an antibody against p21 demonstrates nuclear staining of the tumor cells.

C: A section stained with anti-p16 antibody is negative for staining in tumor cells. Note the positive staining seen in rare infiltrating leukocytes.

The scale bars are 50 μm in length.

in four of six sarcomas and in all of the breast cancers (see Table S1). Two independent clustering methodologies were employed to classify four sarcomas and four breast cancers that developed in mice exposed to CY + RAD based on their genomic profiles (see the Experimental Procedures). Both approaches led to a perfect separation of the sarcomas from the breast tumors (Figure 4). To evaluate the relative similarities of individual tumors grouped within each cluster, we performed within sum of squares analyses and found that this difference for breast tumors was less than half of that for the sarcomas. These results demonstrate that the genomic profiles of the breast cancers and sarcomas are distinct and that unsupervised approaches are capable of separating them into two groups, with the breast tumors showing a higher degree of similarity than the sarcomas. We were able to establish stable cell lines from four genotoxin-induced tumors that developed in *Nf1*$^{+/-}$ mice. Three were derived from breast cancers, and the fourth was from a soft tissue sarcoma. When we included these cell lines and performed hierarchical clustering analysis as before, the separation between breast cancers and sarcomas was preserved, and each cell line clustered together with the corresponding primary tumor with the exception of breast cancer B1 and cell line B1CL (Figure 4).

LOH at the *Nf1* and *Trp53* loci in tumors from *Nf1*$^{+/-}$ mice

Molecular investigation of tumors that develop spontaneously in persons with NF1 and in strains of *Nf1* mutant mice frequently demonstrates somatic loss of constitutional heterozygosity (Jacks et al., 1994b; Side and Shannon, 1998). Similarly, Southern blot analysis showed loss of the wild-type C57Bl/6 *Nf1* allele in six of eight soft tissue sarcomas, confirming the important role of biallelic inactivation of *Nf1* in tumorigenesis (Figure 5A). We also observed LOH in three of three pheochromocytomas and in four of four breast cancers. By contrast, polymerase chain reaction (PCR) genotyping did not reveal LOH in any of the myeloid malignancies.

Inactivation of *Trp53* and *Nf1* cooperate in tumorigenesis, particularly sarcoma development (Cichowski et al., 1999; Vogel et al., 1999). The loci for these two genes are approximately 7 cM apart on mouse chromosome 11, whereas the human homologs are separated by approximately 22 Mb on chromosome 17. We assayed the D11Mit29 polymorphic microsatellite marker, which is tightly linked to the *Trp53* locus, to determine if *Trp53* and *Nf1* are coordinately lost in malignancies that arise after mutagen exposure. Surprisingly, while LOH occurred in each of the breast tumors and in some pheochromocytomas, all of the sarcomas that developed in *Nf1*$^{+/-}$ mice retained both *Trp53* alleles (Figure 5B).

Chromosome 11 demonstrated copy number losses spanning the *Nf1* locus in all of the breast cancers and in two of the sarcomas (Figure 5C). Each tumor with copy number loss showed LOH at *Nf1.* While these data exclude amplification of

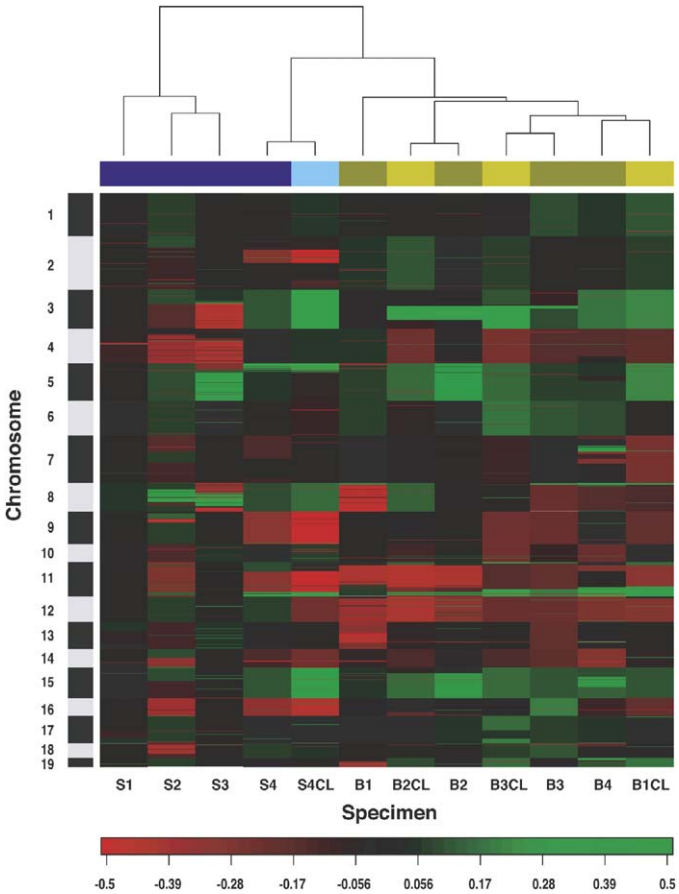

Figure 4. Hierarchical clustering of CGH data generated from SMNs and tumor cell lines in *Nf1* mice

The sarcomas are labeled "S1," "S2," "S3," and "S4" and are shown in dark blue; the sarcoma cell line is labeled "S4CL" and is shown in light blue; the breast cancers are labeled "B1," "B2," "B3," and "B4" and are shown in dark green; and the corresponding breast cancer cell lines are labeled "B1CL," "B2CL," and "B3CL" and are shown in light green. A red-to-green scale indicates the relative change in copy number, with losses shown in red and gains shown in green. The sarcomas and breast cancers form distinct clusters, and the cell lines are closely related to the primary tumors from which they were derived. Note the shared pattern of genomic changes within each tumor type (e.g., all of the breast cancers and cell lines show copy number reductions spanning chromosome 12).

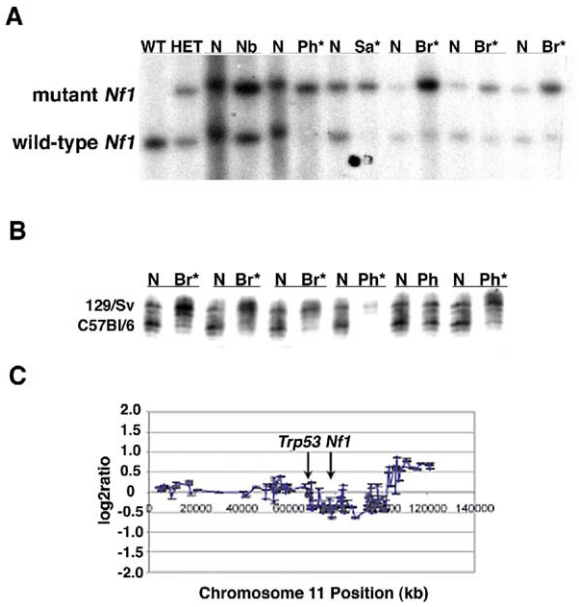

Figure 5. Molecular analysis at the *Nf1* and *Trp53* loci

A: Representative data from Southern blot analysis of tumors from *Nf1* mutant mice using a probe that distinguishes the wild-type (WT) and mutant *Nf1* alleles. Lanes 1 and 2 show analysis of normal tissues from wild-type and heterozygous *Nf1* mutant (HET) mice. The remaining lanes show paired normal (N) and tumor tissues from $Nf1^{+/-}$ mice that developed neuroblastoma (Nb), pheochromocytoma (Ph), sarcoma (Sa), or breast cancer (Br). Asterisks denote tumors with loss of the wild-type C57Bl/6 *Nf1* allele. Overall, 14 of 18 solid tumors that developed in $Nf1^{+/-}$ mutant mice showed loss of the normal *Nf1* allele (includes data not shown).

B: Representative data from analysis at the *Trp53* locus with the microsatellite marker D11Mit29 showing paired normal tissue (N) with tumor specimens from mice with breast cancer (Br) or pheochromocytoma (Ph). Tumors with LOH are marked with an asterisk. Whereas LOH was detected consistently in the breast cancers and was seen in most of the pheochromocytomas, it was uncommon in the sarcomas (data not shown). In each tumor with LOH, the *Trp53* allele was deleted from the C57Bl/6 chromosome, which carries a normal *Nf1* allele in *cis*.

C: Copy number gains and losses across chromosome 11 in sarcoma S4 that showed LOH at *Nf1* but retained two alleles at *Trp53*. The CGH data reveal reduced copy number spanning a DNA segment that includes *Nf1*, but not *Trp53*.

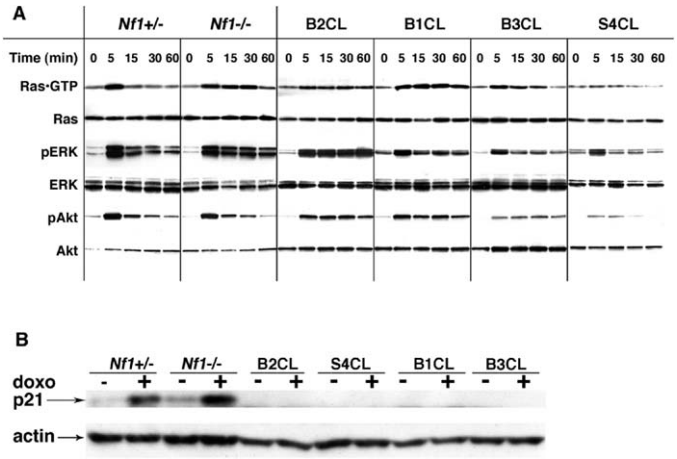

Figure 6. Biochemical analysis of MEFs and tumor cell lines developed from $Nf1^{+/-}$ mice

A: EGF induces a transient spike in Ras-GTP levels in $Nf1^{+/-}$ MEFs, which is followed by a rapid return to baseline values. By contrast, $Nf1^{-/-}$ MEFs show a sustained Ras-GTP response and prolonged ERK phosphorylation. Three breast cancer cell lines also show prolonged Ras-GTP levels as well as prolonged ERK and Akt phosphorylation.

B: Doxorubicin induces p21 expression in heterozygous and homozygous *Nf1* mutant MEFs. By contrast, p21 was not detected in any of the cell lines before or after doxorubicin exposure.

the mutant *Nf1* allele in tumor tissues, none of the copy number changes in the *Nf1* or *Trp53* regions is equivalent to a single-copy loss in a diploid cell. This could be due to the presence of some normal cells admixed with the tumor samples or, alternatively, to loss of the normal C57Bl/6 allele with duplication of the 129/Sv chromosome in a polyploid tumor genome with duplication of the 129/Sv chromosome.

Biochemical characterization of tumor cell lines

Based on previous data implicating aberrant EGFR signaling in NF1-associated sarcomagenesis (DeClue et al., 2000; Li et al., 2002), we compared EGF-induced activation of Ras and phosphorylation of the downstream effectors MEK and Akt in the four cell lines derived from genotoxin-induced cancers. Mouse embryonic fibroblasts (MEFs) were assessed in parallel. $Nf1^{+/-}$ MEFs that were plated, serum starved, and stimulated with EGF displayed a marked increase in Ras-GTP levels with a rapid return to baseline levels (Figure 6A). By contrast, $Nf1^{-/-}$ MEFs showed slightly higher peak levels of Ras-GTP in response to EGF and demonstrated prolonged Ras activation, which is consistent with a previous report (Cichowski et al., 2003). Levels of phosphorylated ERK and Akt changed in parallel with Ras-GTP. While there was some variability among the three breast cancer cell lines with respect to the degree and duration of Ras-GTP, ERK, and Akt activation, all of these cell lines showed elevated Ras-GTP levels for at least 30 min after EGF stimulation and persistence of phosphorylated Akt and ERK above baseline levels for 60 min (Figure 6A). By contrast, basal and EGF-induced Ras activation showed no consistent differences between the one sarcoma cell line and control $Nf1^{+/-}$ MEFS (Figure 6A).

We also compared the functional status of the p53 damage response pathway in MEFs and in tumor cell lines. *Nf1* mutant MEFs induced p21 expression in response to either doxorubicin (Figure 6B) or 5 Gy of RAD, which is expected in cells with an intact p53 pathway. The three breast cancer cell lines demonstrated LOH at the *Trp53* locus, whereas the sarcoma line retained both *Trp53* alleles. Each tumor cell line had high basal p53 expression, which is commonly associated with expression of mutant proteins, and failed to induce p21 in response to either doxorubicin (Figure 6B) or RAD (data not shown).

Discussion

Therapy-induced cancers are an increasing concern as more patients are surviving after receiving intensive regimens to treat a primary malignancy (Armitage et al., 2003; Bhatia and Sklar, 2002; Curtis et al., 1992; Kushner et al., 1998; Matesich and

Shapiro, 2003; Neglia et al., 1991; Smith et al., 2003; Tucker et al., 1988; van Leeuwen et al., 1994). Molecularly targeted therapeutics are appealing in principle as an alternative to genotoxic agents; however, the paucity of tractable biochemical targets and the frequent occurrence of de novo and acquired resistance imply that RAD and conventional chemotherapy will remain mainstays of therapeutic protocols for the foreseeable future. The experience in childhood cancers, where survival rates of ~75% have been achieved through the use of intensive chemotherapy and/or RAD, illustrates that success in curing primary cancers is associated with an increased incidence of SMNs (Bhatia and Sklar, 2002; de Vathaire et al., 1989a, 1989b). Unfortunately, the long-term toxicity of a therapeutic regimen may only become apparent years after many patients have been treated. Given these considerations, tractable animal models of SMN would be valuable for comparing the mutagenic potential of specific agents, for uncovering mechanisms of DNA damage in vivo, and for evaluating prevention strategies.

SMNs are problematic to model accurately in animals because the causative mutations result from exposure to genotoxins. By contrast, conventional strategies for generating tumor-prone mice involve engineering cancer-associated mutations into the germline. Although this is a powerful approach for investigating biologic effects of known therapy-related mutations such as *MLL* gene fusions in epipodophyllotoxin-induced leukemias (Dobson et al., 1999), introducing these cancer-associated mutations into the germline does not recapitulate the dynamic interaction between mutagen exposure and the host genome that underlies tumorigenesis. However, exposing wild-type mice to various doses and combinations of genotoxins is an inefficient and nonselective strategy for generating SMNs. The sensitized genetic background of *Nf1*$^{+/-}$ mice allowed us to develop a tractable and penetrant model of common SMNs that affect human patients. Moreover, the highly significant increase in tumor formation in *Nf1* mutant mice and the frequent loss of the normal *Nf1* allele in genotoxin-induced tumors reveals a direct mechanistic interaction between mutagen exposure and somatic mutations at this locus.

Myeloid malignancies and sarcomas were the most common SMNs detected in *Nf1*$^{+/-}$ mice. These data are consistent with observations in NF1 patients and, importantly, represent two of the most common sporadic SMNs (Armitage et al., 2003; Bhatia and Sklar, 2002; Matesich and Shapiro, 2003; Smith et al., 2003). We previously found that CY cooperates with heterozygous loss of *Nf1* to increase the incidence of MPD, with a substantially higher penetrance in inbred 129/Sv strain mice than in F1 129/Sv × C57Bl/6 animals (Mahgoub et al., 1999). Genetic analysis of bone marrow and splenic DNA from mice with MPD revealed a higher frequency of LOH at *Nf1* in the 129/Sv background. The genetic mechanism, which involves deletion of the normal *Nf1* allele and duplication of the mutant allele (Mahgoub et al., 1999), is also seen in most of the myeloid malignancies that arise in patients with NF1 (K. Stephens, M.M. Le Beau, and K.M.S., unpublished data). Based on these results, we speculate that the low rate of myeloid malignancies that we observed in CY-treated mice is due to the F1 strain background and might be related to a reduced rate of mitotic recombination between 129/Sv and C57Bl/6 chromosome 11 homologs. In the current study, we investigated F1 mice to increase the probability of obtaining nonhematologic cancers and to induce tumors that were heterozygous at multiple genetic loci. It is striking that exposing *Nf1*$^{+/-}$ mice to RAD or to the combination of RAD + CY induced a wide spectrum of myeloid disorders, including refractory cytopenias, MDS, and AML, whereas control and CY-treated *Nf1*$^{+/-}$ mice almost always develop MPD (Mahgoub et al., 1999). Similarly, Japanese atomic bomb survivors are predisposed to chronic myeloid leukemia (CML), AML, and MDS (Imamura et al., 2002; Preston et al., 1994), and patients who are treated with alkylating agents and/or RAD develop both MDS and AML (Armitage et al., 2003; Le Beau et al., 1986; Thirman and Larson, 1996). Because MDS can be difficult to diagnose in both humans and mice, we may have underestimated the incidence of myeloid malignancies by excluding two mice that died with splenomegaly without a definitive diagnosis. Although the number of animals assigned to each treatment group is too small to compare individual regimens, there is no evidence that RAD and CY cooperate in this model, and our data raise the intriguing possibility that RAD may be more leukemogenic than RAD + CY. One potential explanation for this apparent paradox is that the probability of a mutant leukemia-initiating cell surviving and inducing disease in vivo might be higher after RAD only if the combination of CY + RAD induces severe DNA damage that results in cell death or senescence. It is interesting that we did not detect LOH at *Nf1* in bone marrow from mice that developed myeloid malignancies, which contrasts with the solid tumors. Similarly, five therapy-induced human leukemias from NF1 patients retained both alleles (Maris et al., 1997). It is possible that the wild-type *Nf1* allele is inactivated by point mutations or other subtle alterations in humans and mice; alternatively, genotoxin-induced mutations may cooperate with haploinsufficiency at the *Nf1* locus in the F1 genetic background. Consistent with this hypothesis, heterozygous inactivation of *Nf1* has phenotypic consequences in mast cells and melanocytes (Ingram et al., 2000), and therapy-related myeloid malignancies from NF1 patients demonstrate acquired chromosomal abnormalities such as monosomy 7 (Maris et al., 1997; Papageorgio et al., 1999).

In addition to inducing myeloid malignancies, RAD is strongly associated with subsequent development of sarcomas within the RAD portals of patients treated for nonmalignant diseases and for a variety of cancers (Beck, 1922; Boice et al., 1988; Darby et al., 1987; Doherty et al., 1986; Halperin et al., 1984; Marsche, 1922; Murray et al., 1999; Pendlebury et al., 1995; Smith and Doll, 1982). Many of these tumors are high-grade osteosarcomas or malignant fibrous histiocytomas that have a poor prognosis (Huvos et al., 1985; Inwards and Unni, 1995; Laskin et al., 1988; Murray et al., 1999). Although *TP53* inactivation is common in RAD-induced sarcomas (Brachman et al., 1991; Nakanishi et al., 1998), the other molecular lesions are largely unknown (Beech et al., 1998; Cowan et al., 1990; Remmelink et al., 1998; Sekyi-Otu et al., 1995; Wang et al., 1994). MPNST, the most common sarcoma that arises de novo in persons with NF1, has also been reported as a SMN (Li et al., 2002). MPNSTs typically display complex karyotypes and may also show loss of the normal *NF1* allele, mutations that deregulate the pRb and p53 pathways, and aberrant expression of EGFR (Birindelli et al., 2001; DeClue et al., 2000; Halling et al., 1996; Liapis et al., 1999; Plaat et al., 1999). A few small studies of human RAD-induced sarcomas have suggested the existence of nonrandom cytogenetic aberr-

ations including translocation breakpoints involving chromosome band 1p13 and 7p22, gain of 7q1, and losses of 9p2, 1p3, and 21p1-q2 (Bridge et al., 2004; Mertens et al., 1995; Plaat et al., 1999). Human chromosome band 7q1 is orthologous to two segments of mouse chromosome 5. Interestingly, our CGH analysis revealed a discrete region of amplification in four of six sarcomas and in the four breast cancers at BAC RP23-281N22, which is within the segment of mouse chromosome 5 that is syntenic to human 7q1. This BAC includes a number of putative genes including a homolog of the *Drosophila* frizzled gene, a FK506 binding protein, and a putative zinc finger transcription factor. We also identified a region of amplification on mouse chromosome 8 in breast cancer samples that corresponds to an interval of human chromosome 13q34 that is amplified in hepatocellular carcinoma and some other epithelial cancers (Yasui et al., 2002). This segment includes the *TFDP1*, *CUL4A*, and *CDC16* genes.

Two groups crossed *Nf1* and *Trp53* mutant mice to generate recombinant founders that carried both mutant alleles on the same chromosomal homolog (i.e., in *cis* configuration) in order to recapitulate the simultaneous loss of *NF1* and *TP53* frequently seen in NF1-associated MPNSTs. Whereas heterozygous and homozygous *Trp53* mutant mice spontaneously develop tumors (primarily lymphomas) at 30–50 weeks of age (Donehower et al., 1992; Jacks et al., 1994a), many *cis* and *trans* $Nf1^{+/-};Trp53^{+/-}$ mice developed early-onset sarcomas that resembled human MPNSTs. Molecular analysis revealed LOH at both *Nf1* and *Trp53* in at least 70% of the soft tissue tumors from *cis* $Nf1^{+/-};Trp53^{+/-}$ mice. Based on these data, we were surprised that RAD- and CY-induced sarcomas with LOH at *Nf1* generally retained both *Trp53* alleles. Residual p53 function may underlie the failure of most of these tumors to grow as permanent cell lines, which is in contrast to sarcomas from *cis* $Nf1^{+/-};Trp53^{+/-}$ mice (L. Parada, personal communication). In this regard, it is of interest that the sarcoma cell line that we obtained had abnormal p53 pathway function as assessed by elevated p53 expression and failure to induce p21 in response to RAD and doxorubicin. Although we cannot exclude similar defects in other RAD- and CY-induced tumors, our data suggest the existence of one or more p53-independent pathways to sarcoma development. This hypothesis is consistent with studies of NF1-associated de novo MPNSTs, which uncovered either LOH at *TP53* or a somatic mutation in less than half of the tumors (Birindelli et al., 2001; Halling et al., 1996; Lothe et al., 2001; Menon et al., 1990). Aberrant expression of the EGF receptor has also been implicated in the development of MPNST in humans and in mouse models (DeClue et al., 2000; Li et al., 2002; Ling et al., 2005), and a recent study demonstrated that reducing EGFR signaling by ~90% dramatically reduced the incidence of sarcoma in *cis* $Nf1^{+/-};Trp53^{+/-}$ mice (Ling et al., 2005). By contrast, none of the genotoxin-induced soft tissue tumors that developed in $Nf1^{+/-}$ mice expressed detectable level of EGFR. These data are consistent with the observation that ~30% of MPNSTs from NF1 patients do not express EGFR mRNA (Watson et al., 2004). The expression profiles of this subset of tumors were characterized by elevated levels of neuroglial markers and by relatively low expression of transcripts that are associated with proliferation. Together, our molecular and immunohistochemical data support a distinct pathway of genotoxin-induced sarcomagenesis that involves loss of *Nf1*, normal p53 activity, and a lack of EGFR amplification. The recurring copy number changes detected by CGH analysis of these tumors imply that limited numbers of cooperating events promote clonal outgrowth in vivo.

The observation that female $Nf1^{+/-}$ mice developed breast cancer after exposure to RAD or RAD in combination with CY was unexpected and intriguing. The incidence of SMNs has been investigated over many decades in patients who were treated for Hodgkin's disease as adolescents or young adults. Among these individuals, breast cancer is the most common solid SMN in women, with a cumulative probability of up to 42% after 30 years (Bhatia et al., 1996). Although RAD dose, combined treatment with chemotherapy, and age at the time of treatment strongly influence the risk of subsequent development of secondary breast cancer, the genetic pathways that underlie malignant transformation are poorly understood. CGH analysis of these tumors uncovered a striking pattern of recurring copy number changes involving chromosome 12 and other DNA segments (Figure 3 and Supplemental Data). Together, our data imply that loss of *Trp53* and hyperactive Ras cooperate with a common series of secondary genetic changes in mammary tumorigenesis after genotoxin exposure.

Hyperactivation of the PI3 kinase/Akt cascade underlies growth factor-independent survival in immortalized *Nf1*-deficient hematopoietic cells, whereas aberrant MAP kinase signaling drives proliferation and autocrine production of granulocyte-macrophage colony stimulating factor (GM-CSF) (Donovan et al., 2002a). In addition, recent studies in *Nf1*-deficient astrocytes and MEFs have uncovered deregulated activation of S6 kinase, a downstream effector of mTOR (Dasgupta et al., 2005; Johannessen et al., 2005). Dephosphorylation of tuberin (the protein encoded by the *TSC2* tumor suppressor gene) by activated Akt is an important mechanism that contributes to hyperactive mTOR/S6 kinase in *Nf1*-deficient cells (Johannessen et al., 2005). We found that breast cancer cell lines from $Nf1^{+/-}$ mice responded to EGF with prolonged activation of Ras, ERK, and Akt, and it will be of interest to determine how this modulates the activation status of downstream effectors and contributes to specific cellular phenotypes. Based on the data of Li and colleagues (Li et al., 2002) showing elevated levels of EGFR expression in most sarcoma cell lines from *cis* $Nf1^{+/-};Trp53^{+/-}$ mice, we investigated signaling in response to EGF in the S4CL cell line. The modest increase in ERK phosphorylation that we observed in response to EGF is consistent with our data showing that sarcomas that arise in $Nf1^{+/-}$ mice that are exposed to genotoxins do not express detectable levels of EGFR.

$Nf1^{+/-}$ mice are a robust and tractable in vivo system that can be harnessed to address the mutagenic potential of cancer treatments and to test preventive strategies. This "first generation" model can also be refined further; for example, it is feasible to selectively administer a range of RAD doses to the mammary glands of mice, and to test how age, previous pregnancies, and hormonal manipulations modulate tumorigenesis. A more challenging experimental question involves investigating if the therapy-induced cancers that develop in this model are largely refractory to conventional chemotherapeutic agents, and if this is true, this model may prove useful for testing novel therapeutic strategies. Unlike hematopoietic cancers, there are no simple techniques for transplanting primary solid tumors into immunocompetent recipients, which would greatly facilitate studies of this nature. Our data also have implications for

treating tumors that arise in the patients with NF1. In particular, we found that a single low dose of RAD cooperated strongly with heterozygous *Nf1* inactivation in tumorigenesis. Children with NF1 are predisposed to optic track gliomas and low-grade astrocytomas, which may be difficult to manage. Our data suggest that the potential risk of SMN should be considered when deciding whether to irradiate these and other NF1-associated tumors and that patients who require RAD should be followed carefully for subsequent treatment-induced cancers.

Experimental procedures

Mouse stains, breeding, and treatment

All experimental procedures involving mice were reviewed and approved by the UCSF Committee on Animal Research. Heterozygous *Nf1* mutant mice that were maintained in the 129/Sv strain background (Jacks et al., 1994b) were mated with wild-type C57Bl/6 mice (Jackson Labs, Bar Harbor, ME) to generate wild-type and $Nf1^{+/-}$ mice. These mice were genotyped and assigned to one of the four experimental groups. Study mice were housed in a pathogen-free environment at the UCSF Animal Care Facility. Mice exposed to CY (Mead Johnson Oncology Products) received intraperitoneal injections of CY (200 mg/ml in sterile water) medial to the proximal aspect of the femur. RAD-treated mice received a single dose of 3 Gy, which was administered using a cesium-137 source (JL Shepherd & Associates, San Fernando, CA) at a rate of ~250 cGy/min.

Pathologic analysis

Complete blood counts (CBCs) were measured on blood samples taken premortem from tail vein bleeding and postmortem by intracardiac puncture in Hema-Vet 850 hematology analyzer (CDC Technologies, Inc., Oxford, CT). Blood and bone marrow smears were made on glass slides, and cytospin slides were prepared by suspending 100,000 viable cells in 200 μl of PBS and centrifuging them for 10 min at 400 rpm. The slides were stained with Wright-Giemsa (Fisher) and examined using a Nikon Eclipse E400 microscope. Tumor tissues were fixed in 10% formalin (Fisher) and embedded in paraffin, cut, and stained with hematoxylin and eosin. Slides of tumor tissues were stained with antibodies against CK and S100 (Dako, Carpinteria, CA) according to the manufacturer's instructions. EGFR expression, p16 expression, and p21 expression were assessed on 10 μm thick cryostat sections cut from frozen tumor specimens. Briefly, the slides were fixed in cold acetone or 4% paraformaldehyde and then blocked with serum followed by incubation with avidin then biotin blocking reagents (Vector Laboratories). Sections were immunostained using standard procedures with rabbit antibodies against EGFR (SC-03), p16 (SC-1207), and p21 (SC-397) (Santa Cruz Biotechnology) and enhanced with ABC Elite Vector Stain Substrate Kit (Vector Laboratories) using the manufacturer's protocol. Staining was visualized with 3,3′-diaminobenzidine (DAB Substrate Kit, Vector Laboratories) and counterstained with Gill's hematoxylin (Santa Cruz Biotechnology). Blood, bone marrow, and spleen sections from mice with hematopoietic malignancies were reviewed by a hematopathologist with expertise in murine myeloid malignancies (S.C.K.). A veterinary pathologist with experience in evaluating mouse cancer models (A.B.) and a pathologist with expertise in human sarcomas (A.H.) independently reviewed the solid tumor slides.

Genotyping and mutation analysis

Mice were genotyped at the *Nf1* locus, and LOH was performed on solid tumor specimens using Southern blot analysis as described elsewhere (Jacks et al., 1994b). A PCR-based assay was employed to assess myeloid malignancies for LOH at *Nf1*. LOH analysis was performed at the D11Mit29 locus amplifying tumor DNA samples with 3′ and 5′ γ-^{33}P-labeled primers (Research Genetics, Carlsbad, CA). The amplification products were resolved on a polyacrylamide gel and visualized by autoradiography.

Cell culture

Cells were maintained at 37°C in humidified incubator with 5% CO_2. To generate tumor cell lines, a 10–100 mm^3 piece tissue was first washed with Dulbecco's modified essential medium (DMEM) containing penicillin and streptomycin and minced with a sterile scalpel. After adding 2–3 ml of DMEM with 10% FBS (Hyclone, Logan, UT), the tissue was passed through a 16G needle (Becton-Dickinson, Franklin Lakes, NJ), plated in two wells of a six-well plate (Corning, Corning, NY), and cultured at 37°C. The medium was changed every 1–3 days, and cells that proliferated in culture were trypsinized, passaged, and frozen. MEFs were generated from E13.6 F1 embryos by first dissecting the fetal liver and head, and then mincing and trypsinizing the remaining tissues, and culturing the cells in DMEM supplemented with 10% FBS, glutamine, and β-mercaptoethanol (Sigma, St. Louis, MO).

Acquisition and analysis of CGH data

Array CGH was carried out on arrays of 2500 mouse BACs as described previously (Snijders et al., 2005). Briefly, test and reference DNA samples from 129/Sv × C57Bl/6 female F1 mice were labeled by random priming to incorporate Cy3- and Cy5-dUTP, respectively. The labeled DNAs together with Cot-1 DNA (Invitrogen) were hybridized to the arrays for 48 hr. Following washing 16 bit 1024 × 1024 pixel DAPI, Cy3 and Cy5 images were collected with a custom-built CCD camera system as described previously (Pinkel et al., 1998). "UCSF SPOT" software (Jain et al., 2002) was used to automatically segment the spots based on the DAPI images, perform local background correction, and calculate various measurement parameters, including log2 ratios of the total integrated Cy3 and Cy5 intensities for each spot. A second custom program, SPROC, was used to obtain averaged ratios of the triplicate spots for each clone, standard deviations of the triplicates, and plotting position for the BACs on the May 2004 freeze of the mouse genome sequence (http://genome.ucsc.edu/). Data files were edited to remove ratios on clones for which only one of the triplicates remained after SPROC analysis and/or the standard deviation of the log2 ratios of the triplicates was >0.2.

To address the distinction between types of tumors based on their genomic profiles, we applied clustering approaches (Fridlyand et al., 2004). The clones missing in more than 20% of the samples were filtered out, and each sample was segmented using DNA copy (Olshen et al., 2004). The tumor-specific experimental error was estimated as median absolute deviation (MAD) of the differences between the observed log2 ratios and the means of their corresponding segments. The clones with log2 ratios further away from their segment mean than 4 × MAD retained their original log2 ratios, whereas the rest of the clones were assigned the value of their segment mean. The distance between a pair of samples was computed as 1 – Pearson correlation calculated over the autosomal clones. The resulting distance matrix was used as an input to hierarchical (see Figure 3) and k-means clustering with two groups. To evaluate the relative similarity of the two clusters we compared the within sum of squares of each cluster, which is an output of the k-means procedure in the R statistical package.

Biochemical analysis

Cell lines or MEFs were plated a density of 1.5–2 × 10^6 cells per 10 cm plate in DMEM with 10% FBS. After 16–20 hr, the cells were washed and transferred to DMEM without serum. After 24 hr, the cells were stimulated with EGF (Peprotech, Rocky Hill, NJ) at 10 ng/ml for 5–60 min. The cells were lysed in Holstrom buffer, protein levels were quantified using the modified Bradford assay (Bio-Rad, Hercules, CA), and the samples were resolved using SDS-PAGE in 10%–12.5% precast gels (Bio-Rad). The proteins were transferred to an Immobilon filter (Amersham, Piscataway, NJ) and probed with antibodies labeled with horseradish peroxidase. The filters were incubated with ECL (Amersham) reagent and then exposed to film. We used the following primary antibodies to detect specific proteins: anti-pan-Ras antibody (Oncogene Research Products, San Diego, CA), anti-pERK (Santa Cruz Biotechnology, Santa Cruz, CA), anti-ERK antibody (Cell Signaling, Beverly, MA), anti-pAkt antibody (a kind gift from David Stokoe), anti-Akt antibody (Cell Signaling). Ras-GTP levels were quantified using an excess of Raf1 RBD-GST conjugated agarose beads (Upstate, Charlottesville, VA) according to the manufacturer's instructions. For studies of p53 function, cells that were irradiated to a dose of 5 Gy were incubated at 37°C for 3 hr or incubated with doxorubicin for approximately 16 hr. The cells were lysed, and Western blotting was performed as described above with antibodies that recognize p53 (Santa Cruz Biotechnology) and p21 (Santa Cruz Biotechnology).

Sample size and statistical analysis

The primary endpoint for statistical analysis was the effect of RAD, alone or in combination with CY, on the incidence of cancer in *Nf1*$^{+/-}$ mice. Based on previous data, we estimated the risk of tumor development in untreated F1 *Nf1*$^{+/-}$ mice to be 10% over 16 months. Since the primary goal was to examine if RAD cooperates with heterozygous *Nf1* inactivation in tumorigenesis, we allocated twice as many mice to the RAD cohorts in order to conserve resources.

Supplemental data

The Supplemental Data include two figures and one table and can be found with this article online at http://www.cancercell.org/cgi/content/full/8/4/337/DC1/.

Acknowledgments

We are grateful to Abigail Aiyagari, Charles Fezzie, Ben Yen, Robert Cardiff, Angell Shieh, and Doan Le for advice and for assisting with various aspects of this study. We are also indebted to David Stokoe, who provided the anti-pAkt antibody that we used in these studies. This work was supported by US Army Neurofibromatosis Research Program projects DAMD 17-02-1-0638 and DAMD17-98-1-8608, NIH grants R01 CA72614 and U01 CA84221, and the Jeffrey and Karen Peterson Family Foundation (all to K.M.S.); by NIH training grant T32ES07106 (R.C.C.); and by NIH grants U01 CA84118 and R01 CA101359 (D.G.A.). S.C.K. is a Scholar of the Leukemia and Lymphoma Society of America, and T.E.J. is an Investigator of the Howard Hughes Medical Institute.

Received: February 9, 2005
Revised: June 24, 2005
Accepted: August 26, 2005
Published: October 17, 2005

References

Armitage, J.O., Carbone, P.P., Connors, J.M., Levine, A., Bennett, J.M., and Kroll, S. (2003). Treatment-related myelodysplasia and acute leukemia in non-Hodgkin's lymphoma patients. J. Clin. Oncol. *21*, 897–906.

Beck, A. (1922). Zur Frage des Röntgensarkoms, Zugleich ein Beitrag zur Pathogenese des Sarkoms. Munch. Med. Wochenschr. *69*, 623–624.

Beech, D., Pollock, R.E., Tsan, R., and Radinsky, R. (1998). Epidermal growth factor receptor and insulin-like growth factor-I receptor expression and function in human soft-tissue sarcoma cells. Int. J. Oncol. *12*, 329–336.

Bhatia, S., and Sklar, C. (2002). Second cancers in survivors of childhood cancer. Nat. Rev. Cancer *2*, 124–132.

Bhatia, S., Robison, L.L., Oberlin, O., Greenberg, M., Bunin, G., Fossati-Bellani, F., and Meadows, A.T. (1996). Breast cancer and other second neoplasms after childhood Hodgkin's disease. N. Engl. J. Med. *334*, 745–751.

Birindelli, S., Perrone, F., Oggionni, M., Lavarino, C., Pasini, B., Vergani, B., Ranzani, G.N., Pierotti, M.A., and Pilotti, S. (2001). Rb and TP53 pathway alterations in sporadic and NF1-related malignant peripheral nerve sheath tumors. Lab. Invest. *81*, 833–844.

Boguski, M., and McCormick, F. (1993). Proteins regulating Ras and its relatives. Nature *366*, 643–653.

Boice, J.D., Jr., Engholm, G., Kleinerman, R.A., Blettner, M., Stovall, M., Lisco, H., Moloney, W.C., Austin, D.F., Bosch, A., Cookfair, D.L., et al. (1988). Radiation dose and second cancer risk in patients treated for cancer of the cervix. Radiat. Res. *116*, 3–55.

Brachman, D.G., Hallahan, D.E., Beckett, M.A., Yandell, D.W., and Weichselbaum, R.R. (1991). p53 gene mutations and abnormal retinoblastoma protein in radiation-induced human sarcomas. Cancer Res. *51*, 6393–6396.

Bridge, R.S., Jr., Bridge, J.A., Neff, J.R., Naumann, S., Althof, P., and Bruch, L.A. (2004). Recurrent chromosomal imbalances and structurally abnormal breakpoints within complex karyotypes of malignant peripheral nerve sheath tumour and malignant triton tumour: a cytogenetic and molecular cytogenetic study. J. Clin. Pathol. *57*, 1172–1178.

Cichowski, K., and Jacks, T. (2001). NF1 tumor suppressor gene function: Narrowing the GAP. Cell *104*, 593–604.

Cichowski, K., Shih, T.S., Schmitt, E., Santiago, S., Reilly, K., McLaughlin, M.E., Bronson, R.T., and Jacks, T. (1999). Mouse models of tumor development in neurofibromatosis type 1. Science *286*, 2172–2176.

Cichowski, K., Santiago, S., Jardim, M., Johnson, B.W., and Jacks, T. (2003). Dynamic regulation of the Ras pathway via proteolysis of the NF1 tumor suppressor. Genes Dev. *17*, 449–454.

Cowan, J.M., Beckett, M.A., Tarbell, N., and Weichselbaum, R.R. (1990). Symmetrical chromosome rearrangements in cell lines established from human radiation-induced sarcomas. Cancer Genet. Cytogenet. *50*, 125–137.

Curtis, R.E., Boice, J.D., Jr., Stovall, M., Bernstein, L., Greenberg, R.S., Flannery, J.T., Schwartz, A.G., Weyer, P., Moloney, W.C., and Hoover, R.N. (1992). Risk of leukemia after chemotherapy and radiation treatment for breast cancer. N. Engl. J. Med. *326*, 1745–1751.

Darby, S.C., Doll, R., Gill, S.K., and Smith, P.G. (1987). Long term mortality after a single treatment course with X-rays in patients treated for ankylosing spondylitis. Br. J. Cancer *55*, 179–190.

Dasgupta, B., and Gutmann, D.H. (2003). Neurofibromatosis 1: Closing the GAP between mice and men. Curr. Opin. Genet. Dev. *13*, 20–27.

Dasgupta, B., Yi, Y., Chen, D.Y., Weber, J.D., and Gutmann, D.H. (2005). Proteomic analysis reveals hyperactivation of the mammalian target of rapamycin pathway in neurofibromatosis 1-associated human and mouse brain tumors. Cancer Res. *65*, 2755–2760.

DeClue, J.E., Heffelfinger, S., Benvenuto, G., Ling, B., Li, S., Rui, W., Vass, W.C., Viskochil, D., and Ratner, N. (2000). Epidermal growth factor receptor expression in neurofibromatosis type 1-related tumors and NF1 animal models. J. Clin. Invest. *105*, 1233–1241.

de Vathaire, F., Francois, P., Hill, C., Schweisguth, O., Rodary, C., Sarrazin, D., Oberlin, O., Beurtheret, C., Dutreix, A., and Flamant, R. (1989a). Role of radiotherapy and chemotherapy in the risk of second malignant neoplasms after cancer in childhood. Br. J. Cancer *59*, 792–796.

de Vathaire, F., Schweisguth, O., Rodary, C., Francois, P., Sarrazin, D., Oberlin, O., Hill, C., Raquin, M.A., Dutreix, A., and Flamant, R. (1989b). Long-term risk of second malignant neoplasm after a cancer in childhood. Br. J. Cancer *59*, 448–452.

Dixon, D., and Maronpot, R.R. (1991). Histomorphologic features of spontaneous and chemically-induced pulmonary neoplasms in B6C3F1 mice and Fischer 344 rats. Toxicol. Pathol. *19*, 540–556.

Dobson, C.L., Warren, A.J., Pannell, R., Forster, A., Lavenir, I., Corral, J., Smith, A.J., and Rabbitts, T.H. (1999). The mll-AF9 gene fusion in mice controls myeloproliferation and specifies acute myeloid leukaemogenesis. EMBO J. *18*, 3564–3574.

Doherty, M.A., Rodger, A., and Langlands, A.O. (1986). Sarcoma of bone following therapeutic irradiation for breast carcinoma. Int. J. Radiat. Oncol. Biol. Phys. *12*, 103–106.

Donehower, L., Harvey, M., Slagle, B., McArthur, M., Montgomery, C., Butel, J., and Bradley, A. (1992). Mice deficient for p53 are developmentally normal but susceptible to spontaneous tumours. Nature *356*, 215–221.

Donovan, S., See, W., Bonifas, J., Stokoe, D., and Shannon, K.M. (2002a). Hyperactivation of protein kinase B and ERK have discrete effects on survival, proliferation, and cytokine expression in Nf1-deficient myeloid cells. Cancer Cell *2*, 507–514.

Donovan, S., Shannon, K.M., and Bollag, G. (2002b). GTPase activating proteins: critical regulators of intracellular signaling. Biochim. Biophys. Acta *1602*, 23–45.

Fridlyand, J., Snijders, A.M., Pinkel, D., Albertson, D.G., and Jain, A.N. (2004). Hidden Markov models approach to the analysis of array CGH data. J. Multivariate Anal., in press.

Halling, K.C., Scheithauer, B.W., Halling, A.C., Nascimento, A.G., Ziesmer, S.C., Roche, P.C., and Wollan, P.C. (1996). p53 expression in neurofibroma

and malignant peripheral nerve sheath tumor. An immunohistochemical study of sporadic and NF1-associated tumors. Am. J. Clin. Pathol. *106*, 282–288.

Halperin, E.C., Greenberg, M.S., and Suit, H.D. (1984). Sarcoma of bone and soft tissue following treatment of Hodgkin's disease. Cancer *53*, 232–236.

Hawkins, M.M., Draper, G.J., and Kingston, J.E. (1987). Incidence of second primary tumours among childhood cancer survivors. Br. J. Cancer *56*, 339–347.

Huvos, A.G., Woodard, H.Q., Cahan, W.G., Higinbotham, N.L., Stewart, F.W., Butler, A., and Bretsky, S.S. (1985). Postradiation osteogenic sarcoma of bone and soft tissues. A clinicopathologic study of 66 patients. Cancer *55*, 1244–1255.

Imamura, N., Abe, K., and Oguma, N. (2002). High incidence of point mutations of p53 suppressor oncogene in patients with myelodysplastic syndrome among atomic-bomb survivors: a 10-year follow-up. Leukemia *16*, 154–156.

Ingram, D.A., Yang, F.C., Travers, J.B., Wenning, M.J., Hiatt, K., New, S., Hood, A., Shannon, K., Williams, D.A., and Clapp, D.W. (2000). Genetic and biochemical evidence that haploinsufficiency of the Nf1 tumor suppressor gene modulates melanocyte and mast cell fates in vivo. J. Exp. Med. *191*, 181–188.

Inwards, C.Y., and Unni, K.K. (1995). Classification and grading of bone sarcomas. Hematol. Oncol. Clin. North Am. *9*, 545–569.

Jacks, T., Remington, L., Williams, B.O., Schmitt, E.M., Halachmi, S., Bronson, R.T., and Weinberg, R.A. (1994a). Tumor spectrum analysis in p53-mutant mice. Curr. Biol. *4*, 1–7.

Jacks, T., Shih, S., Schmitt, E.M., Bronson, R.T., Bernards, A., and Weinberg, R.A. (1994b). Tumorigenic and developmental consequences of a targeted *Nf1* mutation in the mouse. Nat. Genet. *7*, 353–361.

Jain, A.N., Tokuyasu, T.A., Snijders, A.M., Segraves, R., Albertson, D.G., and Pinkel, D. (2002). Fully automatic quantification of microarray image data. Genome Res. *12*, 325–332.

Johannessen, C.M., Reczek, E.E., James, M.F., Brems, H., Legius, E., and Cichowski, K. (2005). The NF1 tumor suppressor critically regulates TSC2 and mTOR. Proc. Natl. Acad. Sci. USA *102*, 8573–8578.

Kogan, S.C., Ward, J.M., Anver, M.R., Berman, J.J., Brayton, C., Cardiff, R.D., Carter, J.S., de Coronado, S., Downing, J.R., Fredrickson, T.N., et al. (2002). Bethesda proposals for classification of nonlymphoid hematopoietic neoplasms in mice. Blood *100*, 238–245.

Kushner, B.H., Heller, G., Cheung, N.K., Wollner, N., Kramer, K., Bajorin, D., Polyak, T., and Meyers, P.A. (1998). High risk of leukemia after short-term dose-intensive chemotherapy in young patients with solid tumors. J. Clin. Oncol. *16*, 3016–3020.

Laskin, W.B., Silverman, T.A., and Enzinger, F.M. (1988). Postradiation soft tissue sarcomas. An analysis of 53 cases. Cancer *62*, 2330–2340.

Le Beau, M.M., Albain, K.S., Larson, R.A., Vardiman, J.W., Davis, E.M., Blough, R.R., Golomb, H.M., and Rowley, J.D. (1986). Clinical and cytogenetic correlations in 63 patients with therapy-related myelodysplastic syndromes and acute nonlymphocytic leukemia: further evidence for characteristic abnormalities of chromosomes no. 5 and 7. J. Clin. Oncol. *4*, 325–345.

Li, F.P., and Fraumeni, J.F., Jr. (1982). Prospective study of a family cancer syndrome. JAMA *247*, 2692–2694.

Li, H., Velasco-Miguel, S., Vass, W.C., Parada, L.F., and DeClue, J.E. (2002). Epidermal growth factor receptor signaling pathways are associated with tumorigenesis in the Nf1:p53 mouse tumor model. Cancer Res. *62*, 4507–4513.

Liapis, H., Marley, E.F., Lin, Y., and Dehner, L.P. (1999). p53 and Ki-67 proliferating cell nuclear antigen in benign and malignant peripheral nerve sheath tumors in children. Pediatr. Dev. Pathol. *2*, 377–384.

Ling, B.C., Wu, J., Miller, S.J., Monk, K.R., Shamekh, R., Rizvi, T.A., Decourten-Myers, G., Vogel, K.S., DeClue, J.E., and Ratner, N. (2005). Role for the epidermal growth factor receptor in neurofibromatosis-related peripheral nerve tumorigenesis. Cancer Cell *7*, 65–75.

Lothe, R.A., Smith-Sorensen, B., Hektoen, M., Stenwig, A.E., Mandahl, N., Saeter, G., and Mertens, F. (2001). Biallelic inactivation of TP53 rarely contributes to the development of malignant peripheral nerve sheath tumors. Genes Chromosomes Cancer *30*, 202–206.

Mahgoub, N., Taylor, B., Le Beau, M., Gratiot, M., Carlson, K., Jacks, T., and Shannon, K.M. (1999). Myeloid malignancies induced by alkylating agents in Nf1 mice. Blood *93*, 3617–3623.

Major, I.R. (1979). Induction of myeloid leukaemia by whole-body single exposure of CBA male mice to x-rays. Br. J. Cancer *40*, 903–913.

Major, I.R., and Mole, R.H. (1978). Myeloid leukaemia in x-ray irradiated CBA mice. Nature *272*, 455–456.

Malkin, D., Jolly, K.W., Barbier, N., Look, A.T., Friend, S.H., Gebhardt, M.C., Andersen, T.I., Borresen, A.L., Li, F.P., Garber, J., et al. (1992). Germline mutations of the p53 tumor-suppressor gene in children and young adults with second malignant neoplasms. N. Engl. J. Med. *326*, 1309–1315.

Maris, J.M., Wiersma, S.R., Mahgoub, N., Thompson, P., Geyer, R.J., Hurwitz, C.G., Lange, B.J., and Shannon, K.M. (1997). Monosomy 7 myelodysplastic syndrome and other second malignant neoplasms in children with neurofibromatosis type 1. Cancer *79*, 1438–1446.

Marsche, E. (1922). Tuberkulose und Sarkom. Zentralbl. Chir. *49*, 1057–1060.

Matesich, S.M., and Shapiro, C.L. (2003). Second cancers after breast cancer treatment. Semin. Oncol. *30*, 740–748.

Menon, A.G., Anderson, K.M., Riccardi, V.M., Chung, R.Y., Whaley, J.M., Yandell, D.W., Farmer, G.E., Freiman, R.N., Lee, J.K., Li, F.P., et al. (1990). Chromosome 17p deletions and p53 gene mutations associated with the formation of malignant neurofibrosarcomas in von Recklinghausen neurofibromatosis. Proc. Natl. Acad. Sci. USA *87*, 5435–5439.

Mertens, F., Rydholm, A., Bauer, H.F., Limon, J., Nedoszytko, B., Szadowska, A., Willen, H., Heim, S., Mitelman, F., and Mandahl, N. (1995). Cytogenetic findings in malignant peripheral nerve sheath tumors. Int. J. Cancer *61*, 793–798.

Mole, R.H., Papworth, D.G., and Corp, M.J. (1983). The dose-response for x-ray induction of myeloid leukaemia in male CBA/H mice. Br. J. Cancer *47*, 285–291.

Murray, E.M., Werner, D., Greeff, E.A., and Taylor, D.A. (1999). Postradiation sarcomas: 20 cases and a literature review. Int. J. Radiat. Oncol. Biol. Phys. *45*, 951–961.

Nakanishi, H., Tomita, Y., Myoui, A., Yoshikawa, H., Sakai, K., Kato, Y., Ochi, T., and Aozasa, K. (1998). Mutation of the p53 gene in postradiation sarcoma. Lab. Invest. *78*, 727–733.

Neglia, J.P., Meadows, A.T., Robison, L.L., Kim, T.H., Newton, W.A., Ruymann, F.B., Sather, H.N., and Hammond, G.D. (1991). Second neoplasms after acute lymphoblastic leukemia in childhood. N. Engl. J. Med. *325*, 1330–1336.

Nichols, K.E., Malkin, D., Garber, J.E., Fraumeni, J.F., Jr., and Li, F.P. (2001). Germ-line p53 mutations predispose to a wide spectrum of early-onset cancers. Cancer Epidemiol. Biomarkers Prev. *10*, 83–87.

Olshen, A.B., Venkatraman, E.S., Lucito, R., and Wigler, M. (2004). Circular binary segmentation for the analysis of array-based DNA copy number data. Biostatistics *5*, 557–572.

Papageorgio, C., Seiter, K., and Feldman, E.J. (1999). Therapy-related myelodysplastic syndrome in adults with neurofibromatosis. Leuk. Lymphoma *32*, 605–608.

Pendlebury, S.C., Bilous, M., and Langlands, A.O. (1995). Sarcomas following radiation therapy for breast cancer: a report of three cases and a review of the literature. Int. J. Radiat. Oncol. Biol. Phys. *31*, 405–410.

Pinkel, D., Segraves, R., Sudar, D., Clark, S., Poole, I., Kowbel, D., Collins, C., Kuo, W.L., Chen, C., Zhai, Y., et al. (1998). High resolution analysis of DNA copy number variation using comparative genomic hybridization to microarrays. Nat. Genet. *20*, 207–211.

Plaat, B.E., Molenaar, W.M., Mastik, M.F., Hoekstra, H.J., te Meerman, G.J., and van den Berg, E. (1999). Computer-assisted cytogenetic analysis of 51 malignant peripheral-nerve-sheath tumors: sporadic vs. neurofibromatosis-type-1-associated malignant schwannomas. Int. J. Cancer *83*, 171–178.

Preston, D.L., Kusumi, S., Tomonaga, M., Izumi, S., Ron, E., Kuramoto, A., Kamada, N., Dohy, H., Matsuo, T., Matsui, T., et al. (1994). Cancer incidence in atomic bomb survivors. Part III. Leukemia, lymphoma and multiple myeloma, 1950–1987. Radiat. Res. *137*, S68–S97.

Remmelink, M., Decaestecker, C., Darro, F., Goldschmidt, D., Gebhart, M., Pasteels, J.L., Kiss, R., and Salmon, I. (1998). The in vitro influence of eight hormones and growth factors on the proliferation of eight sarcoma cell lines. J. Cancer Res. Clin. Oncol. *124*, 155–164.

Rowley, J.D., Golomb, H.M., and Vardiman, J. (1977). Nonrandom chromosomal abnormalities in acute nonlymphocytic leukemia in patients treated for Hodgkin disease and non-Hodgkin lymphoma. Blood *50*, 759.

Sekyi-Otu, A., Bell, R.S., Ohashi, C., Pollak, M., and Andrulis, I.L. (1995). Insulin-like growth factor 1 (IGF-1) receptors, IGF-1, and IGF-2 are expressed in primary human sarcomas. Cancer Res. *55*, 129–134.

Side, L.E., and Shannon, K.M. (1998). The NF1 gene as a tumor suppressor. In Neurofibromatosis Type 1, M. Upashyaya and D.N. Cooper, eds. (Oxford: Bios Scientific Publishers), pp. 133–152.

Smith, P.G., and Doll, R. (1982). Mortality among patients with ankylosing spondylitis after a single treatment course with x rays. Br. Med. J. (Clin. Res. Ed.) *284*, 449–460.

Smith, S.M., Le Beau, M.M., Huo, D., Karrison, T., Sobecks, R.M., Anastasi, J., Vardiman, J.W., Rowley, J.D., and Larson, R.A. (2003). Clinical-cytogenetic associations in 306 patients with therapy-related myelodysplasia and myeloid leukemia: the University of Chicago series. Blood *102*, 43–52.

Snijders, A.M., Nowak, N.J., Huey, B., Fridlyand, J., Law, S., Conroy, J., Tokuyasu, T., Demir, K., Chiu, R., Mao, J.H., et al. (2005). Mapping segmental and sequence variations among laboratory mice using BAC array CGH. Genome Res. *15*, 302–311.

Stiller, C.A., Chessells, J.M., and Fitchett, M. (1994). Neurofibromatosis and childhood leukemia/lymphoma: A population-based UKCCSG study. Br. J. Cancer *70*, 969–972.

Thirman, M.J., and Larson, R.A. (1996). Therapy-related myeloid leukemia. Hematol. Oncol. Clin. North Am. *10*, 293–320.

Tucker, M.A., Coleman, C.N., Cox, R.S., Varghese, A., and Rosenberg, S.A. (1988). Risk of second cancers after treatment for Hodgkin's disease. N. Engl. J. Med. *318*, 76–81.

van Leeuwen, F.E., Klokman, W.J., Hagenbeek, A., Noyon, R., van den Belt-Dusebout, A.W., van Kerkhoff, E.H., van Heerde, P., and Somers, R. (1994). Second cancer risk following Hodgkin's disease: a 20-year follow-up study. J. Clin. Oncol. *12*, 312–325.

Vogel, K.S., Klesse, L.J., Velasco-Miguel, S., Meyers, K., Rushing, E.J., and Parada, L.F. (1999). Mouse tumor model for neurofibromatosis type 1. Science *286*, 2176–2179.

Wang, J., Coltrera, M.D., and Gown, A.M. (1994). Cell proliferation in human soft tissue tumors correlates with platelet-derived growth factor B chain expression: an immunohistochemical and in situ hybridization study. Cancer Res. *54*, 560–564.

Watson, M.A., Perry, A., Tihan, T., Prayson, R.A., Guha, A., Bridge, J., Ferner, R., and Gutmann, D.H. (2004). Gene expression profiling reveals unique molecular subtypes of Neurofibromatosis Type I-associated and sporadic malignant peripheral nerve sheath tumors. Brain Pathol. *14*, 297–303.

Weiss, S.W., Langloss, J.M., and Enzinger, F.M. (1983). Value of S-100 protein in the diagnosis of soft tissue tumors with particular reference to benign and malignant Schwann cell tumors. Lab. Invest. *49*, 299–308.

Wick, M.R., Swanson, P.E., Scheithauer, B.W., and Manivel, J.C. (1987). Malignant peripheral nerve sheath tumor. An immunohistochemical study of 62 cases. Am. J. Clin. Pathol. *87*, 425–433.

Wong, F.L., Boice, J.D., Jr., Abramson, D.H., Tarone, R.E., Kleinerman, R.A., Stovall, M., Goldman, M.B., Seddon, J.M., Tarbell, N., Fraumeni, J.F., Jr., and Li, F.P. (1997). Cancer incidence after retinoblastoma. Radiation dose and sarcoma risk. JAMA *278*, 1262–1267.

Yasui, K., Arii, S., Zhao, C., Imoto, I., Ueda, M., Nagai, H., Emi, M., and Inazawa, J. (2002). TFDP1, CUL4A, and CDC16 identified as targets for amplification at 13q34 in hepatocellular carcinomas. Hepatology *35*, 1476–1484.

Oncogene (2005) 24, 6502–6515

www.nature.com/onc

Protein 4.1B expression is induced in mammary epithelial cells during pregnancy and regulates their proliferation

Robin Kuns[1,2], Joseph L Kissil[3], Irene F Newsham[4], Tyler Jacks[5], David H Gutmann[6] and Larry S Sherman*[,1]

[1]*Division of Neuroscience, Oregon National Primate Research Center, Oregon Health & Science University, 505 NW 185th Ave., Beaverton, OR 97006, USA;* [2]*Department of Cell Biology, Neurobiology & Anatomy, University of Cincinnati School of Medicine, Cincinnati, OH 45267, USA;* [3]*Molecular and Cellular Oncogenomics Program, The Wistar Institute, Philadelphia, PA 19104, USA;* [4]*Department of Neurosurgery, David and Doreen Hermelin Laboratory of Molecular Oncogenetics, Hermelin Brain Tumor Center, Henry Ford Hospital, Detroit, MI 48202, USA;* [5]*Department of Biology and Center for Cancer Research, and Howard Hughes Medical Institute, Massachusetts Institute of Technology, Cambridge, MA 02139, USA;* [6]*Department of Neurology, Washington University School of Medicine, St Louis, MO 63110, USA*

4.1B is a member of the protein 4.1 superfamily of proteins that link transmembrane proteins to the actin cytoskeleton. The *4.1B* gene localizes to chromosome 18p11.3, which undergoes loss of heterozygosity in mammary tumors. Here, we examine the expression of 4.1B in murine mammary epithelium and find that 4.1B is dramatically upregulated in mammary epithelial cells during pregnancy when there is extensive cell proliferation. In contrast, 4.1B is not expressed in virgin, lactating, or involuting mammary epithelium. To examine the consequence of 4.1B loss on mammary epithelial cell proliferation, we analysed mammary glands in 4.1B-null mice. 4.1B loss results in a significant increase in mammary epithelial cell proliferation during pregnancy, but has no effect on mammary epithelial cell proliferation, in virgin or involuting mice. Furthermore, we show that 4.1B inhibits the proliferation of mammary epithelial cell lines by inducing a G_1 cell cycle arrest, characterized by decreased cyclin A expression and reduced Rb phosphorylation, and accompanied by reduced erbB2 phosphorylation. This cell cycle arrest does not involve alterations in the activities of MAPK, JNK, or Akt. Collectively, our findings demonstrate that 4.1B regulates mammary epithelial cell proliferation during pregnancy and suggest that its loss may influence mammary carcinoma pathogenesis in multiparous women.
Oncogene (2005) **24,** 6502–6515. doi:10.1038/sj.onc.1208813; published online 20 June 2005

Keywords: protein 4.1B; erbB2; mammary epithelial cells; pregnancy; mammary carcinoma

Introduction

Members of the protein 4.1 superfamily of proteins share structural homology with band 4.1R, a spectrin-binding protein that was originally isolated from human erythrocytes (Tyler *et al*., 1979). This superfamily consists of five subgroups, including the 4.1 proteins (4.1R, 4.1N, 4.1G, 4.1O, and 4.1B) and the ERM proteins (ezrin, radixin, moesin, and merlin). All 4.1 family members are characterized by the presence of a conserved N-terminal membrane-association FERM (Fourpoint-one, Ezrin, Radixin, Moesin) domain (Chishti *et al*., 1998). In addition, most 4.1 proteins can associate with the spectrin–actin cytoskeleton by virtue of an actin-binding domain (Parra *et al*., 2000; Gimm *et al*., 2002). Both 4.1 and ERM proteins can act as structural proteins that link the plasma membrane to the actin cytoskeleton (Tsukita *et al*., 1994).

A number of signaling functions have been attributed to 4.1 family members. In particular, growth suppressive functions have been identified for protein 4.1R and the merlin tumor suppressor protein, as overexpression of these proteins results in decreased cell proliferation (Lutchman and Rouleau, 1995; Robb *et al*., 2003). Loss or inactivation of merlin, which shares high homology with ezrin, radixin, and moesin, is linked to neurofibromatosis type 2 (NF2), a disease characterized by the development of multiple nervous system tumors including schwannomas and meningiomas (Rouleau *et al*., 1993; Trofatter *et al*., 1993).

Several lines of evidence suggest that protein 4.1B may also function as a tumor suppressor. Protein 4.1B is a brain-enriched ortholog of 4.1R that localizes to points of cell–cell contact at the plasma membrane (Peters *et al*., 1998; Parra *et al*., 2000). Several studies have indicated that 4.1B expression is lost or reduced in numerous malignant and benign tumors, including 54% of non-small cell lung carcinomas (NSCLC) (Tran *et al*., 1999). 4.1B is also reduced in 60% of sporadic meningiomas and 30% of ependymomas (Gutmann *et al*., 2000; Singh *et al*., 2002). The *4.1B* gene is located on band 18p11.3, a chromosomal region that has been shown to undergo frequent loss of heterozygosity (LOH) in these tumors (Tran *et al*., 1999; Gutmann *et al*., 2000; Singh *et al*., 2002). Re-expression of 4.1B in NSCLC and meningioma cell lines causes in growth suppression, further supporting the possibility that 4.1B acts as a tumor suppressor (Tran *et al*., 1999; Gutmann *et al*., 2001).

*Correspondence: LS Sherman; E-mail: shermanl@ohsu.edu
Received 22 January 2005; revised 8 April 2005; accepted 2 May 2005; published online 20 June 2005

4.1B has also been implicated as a tumor suppressor protein in mammary carcinomas, which also frequently develop LOH at band 18p11.3 (Tran *et al*., 1999; Kittiniyom *et al*., 2004). Because loss of this region occurs with relatively high frequency in ductal carcinomas *in situ* (56%), it has been proposed to be an early event in tumor progression in the breast (Kittiniyom *et al*., 2001). Furthermore, re-introduction of the minimal growth inhibitory domain of 4.1B, called DAL-1 (differentially expressed in adenocarcinoma of the lung), results in growth suppression in a number of mammary carcinoma cell lines (Charboneau *et al*., 2002).

In order to elucidate the role of 4.1B in the normal mammary gland and how its loss might contribute to mammary tumorigenesis, we examined the expression pattern of 4.1B during postpubertal mammary gland development. Because the mammary gland is a dynamic tissue that undergoes extensive remodeling during its postpubertal development, it is an excellent model system in which to study a protein involved in growth regulation (Daniel and Smith, 1999). The mature virgin mammary gland consists of a ductal tree that is comprised of generally quiescent epithelial cells that surround a central lumen, with some of these ductal branches ending in rudimentary alveolar buds. During pregnancy, the epithelial cells undergo a massive burst of proliferation in order to form more alveolar buds and differentiated alveoli that ultimately fill nearly the entire fat pad. During late pregnancy and lactation, these alveoli become fully differentiated and begin to secrete milk. Upon weaning, the mammary gland enters involution, a stage in which the secretory epithelial cells of the alveoli undergo apoptosis and the entire gland is remodeled so that it resembles the virgin gland (Richert *et al*., 2000). Although the epithelium of the mammary gland undergoes a proliferative phase during pregnancy, the proliferation that occurs is tightly controlled and lasts for a defined period of time.

In this report, we show that 4.1B is not expressed in the epithelium of the virgin mouse mammary gland, but is dramatically upregulated during pregnancy and then downregulated again in the lactating and involuting glands. Exogenous expression of 4.1B in both mammary epithelial and carcinoma cell lines causes a significant inhibition of proliferation that results in a G_1 cell cycle arrest. Interestingly, although 4.1B-null mice do not form tumors of the mammary gland (Kissil *et al*., manuscript in preparation), loss of 4.1B in these mice results in a significant increase in mammary epithelial cell proliferation during pregnancy. Collectively, our results demonstrate that 4.1B regulates cell cycle progression in proliferating mammary epithelium through a novel mechanism.

Results

Protein 4.1B expression is induced in mammary epithelia during pregnancy

Previous reports have suggested that protein 4.1B may function as a tumor suppressor protein whose expression is lost in breast cancers (Tran *et al*., 1998; Kittiniyom *et al*., 2001; Charboneau *et al*., 2002). However, the role of 4.1B in normal mammary epithelium had not been previously tested. We therefore examined the expression of 4.1B in mammary glands from prepubertal virgin (day 16, data not shown), mature virgin (week 8), pregnant (13.5 days postcoitum (dpc)), lactating (9 days postpartum (dpp)), and involuting (1 day postweaning (dpw), data not shown, and 5 dpw) C57BL/6 mice to determine whether 4.1B expression changes in mammary epithelial cells that are quiescent, proliferating, fully differentiated, or undergoing apoptosis. Immunohistochemistry of paraffin-embedded sections revealed that 4.1B expression is virtually absent from epithelial cells in the mammary glands of virgin mice, but is dramatically induced in these cells during pregnancy (compare Figure 1a and b). By midlactation, however, 4.1B expression is significantly reduced or absent from these cells (Figure 1c) and is absent from the epithelial cells in involuting glands (Figure 1d). Nearly all epithelial cells examined during pregnancy (12.5–14.5 dpc) were positive for 4.1B expression, indicating that the upregulation of this protein occurs throughout mammary gland epithelium. Specific labeling of 4.1B by the antibody used in these experiments was confirmed by staining mammary gland sections from pregnant (13.5 dpc) 4.1B-null mice (Figure 1b, inset). Using this 4.1B antibody, weak immunoreactivity was detected in the lumen of some acini of both wild-type and 4.1B-null mice, indicating that this luminal staining was nonspecific (data not shown). Immunofluorescence of the wild-type pregnant (13.5 dpc) gland for 4.1B (Figure 1e) and E-cadherin (Figure 1f) and their overlay (Figure 1g) shows that 4.1B localizes predominantly to regions of cell–cell contact (Figure 1g, arrows) as well as at apical membranes, with some limited cytoplasmic expression.

We next quantified the changes in 4.1B expression during different phases of mammary development. The specificity of the 4.1B antibody was further verified by Western blot analysis of mammary gland lysates from wild-type and 4.1B-null mice at 13.5 dpc. Major bands with the predicted sizes of 4.1B isoforms were detected in the wild-type but not the 4.1B-null lysate, with only a limited number of nonspecific bands appearing in both lysates (Figure 1h). Similar results were obtained in Western blots of wild-type lysates when the antibody was preincubated with 4.1B peptide (data not shown). The upregulation of 4.1B during pregnancy was then confirmed by Western blot analysis of stage-matched wild-type virgin, pregnant, lactating, and involuting whole mammary gland lysates. As shown in Figure 1i, 4.1B is dramatically induced during pregnancy coincident with the increased expression of the epithelial cell marker, E-cadherin. Weak 4.1B bands from nonpregnant mammary tissues can be detected with increased protein loading (not shown), likely resulting from 4.1B expression by vascular endothelial cells (Gutmann *et al*., 2000).

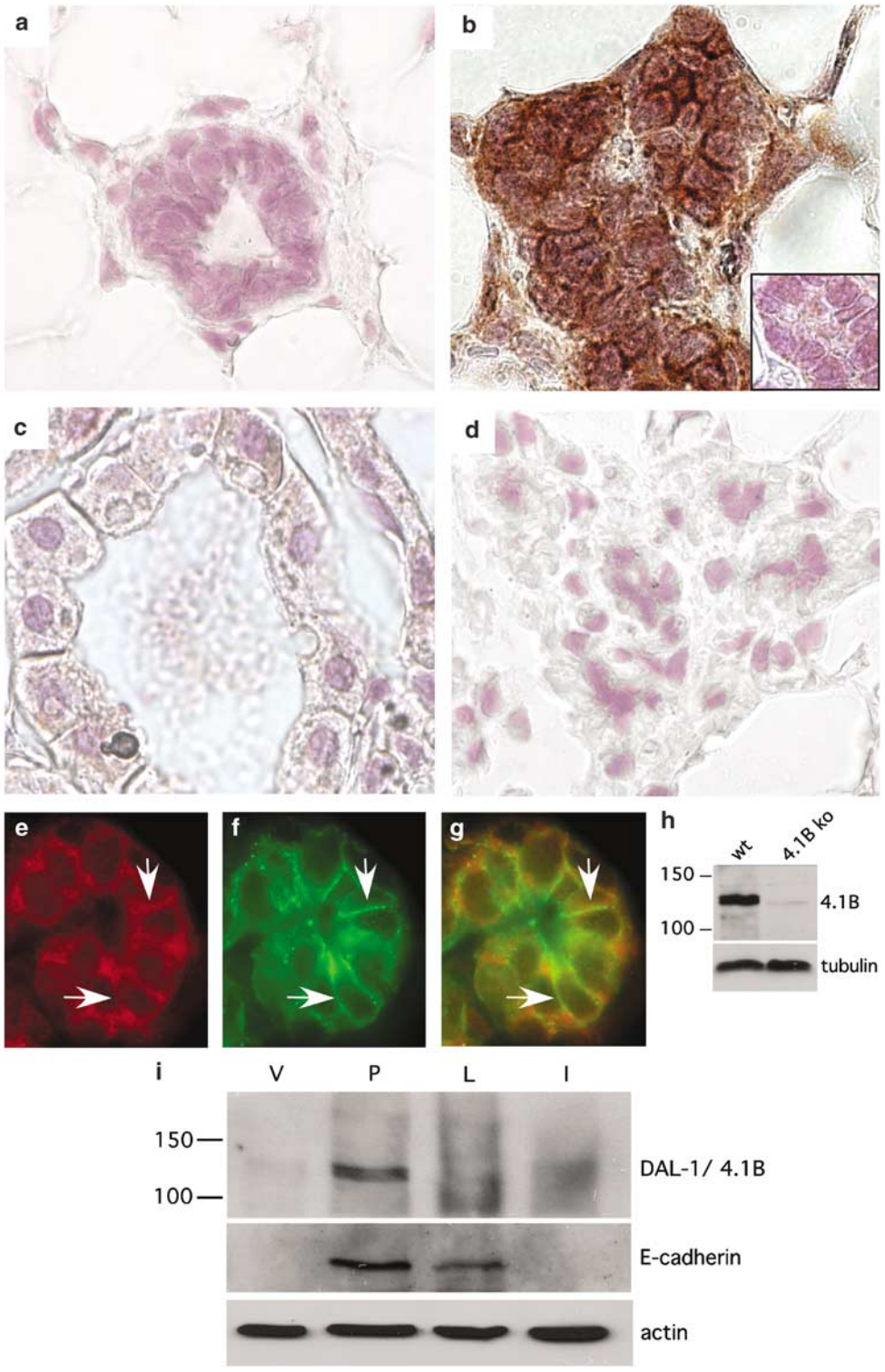

Figure 1 Protein 4.1B expression in the normal mouse mammary gland. (**a**) Virgin (8 weeks), (**b**) pregnant (13.5 dpc), (**c**) lactating (9 dpp), and (**d**) involuting (5 dpw) mouse mammary glands were sectioned and stained for protein 4.1B. The inset (**b**) shows protein 4.1B staining of a mammary gland section from a 13.5 dpc pregnant 4.1B-null mouse to demonstrate the specificity of the protein 4.1B antibody. (**e**–**g**) Sections from the pregnant gland (13.5 dpc) were stained for protein 4.1B (**e**) and E-cadherin (**f**), and the images were overlaid to show localization of protein 4.1B at cell junctions (**g**, arrows). (**h**, **i**) Immunoblotting of lysates from wild-type and 4.1B-null pregnant mammary glands (13.5 dpc) was performed to demonstrate (**h**) the specificity of the protein 4.1B antibody and (**i**) to quantify changes in the levels of protein 4.1B expression. Whole tissue lysates from 8 weeks virgin (V), 13.5 dpc pregnant (P), 9 dpp lactating (L), and 5 dpw involuting (I) glands were probed with an anti-4.1B antibody, an anti-E-cadherin antibody (to demonstrate epithelial cell contribution), and an anti-actin antibody (as a loading control). Note that, consistent with the immunostaining in panels a–d, a band specific for 4.1B is only detectable at significant levels during pregnancy

ERM proteins are downregulated during pregnancy

Although primarily known for its role as a structural protein, ezrin has been implicated in metastatic progression (Hunter, 2004). Ezrin upregulation has been documented in a number of metastatic tumors (Akisawa *et al*., 1999), and its overexpression may be both necessary and sufficient for metastatic progression of some pediatric tumors (Khanna *et al*., 2004; Yu *et al*., 2004). In order to determine whether 4.1B expression is regulated in mammary epithelia in a similar manner to ERM proteins, we examined the expression pattern of the ERM proteins during postpubertal mammary gland development. Using an antibody that recognizes ezrin and crossreacts with radixin and moesin, these proteins were found to be present at high levels at the apical membranes in the virgin mammary gland (Figure 2a, arrow). We further found that ERM expression decreases dramatically during the proliferative stage of pregnancy and the differentiated stage of lactation before returning to high levels during late involution (Figure 2b–d). These results are interesting because the ERM proteins are downregulated in other tissues during times of active proliferation and differentiation. ERM proteins, therefore, are expressed at distinct times compared to 4.1B in the postpubertal developing mammary gland.

Protein 4.1B is expressed at low levels in normal and carcinogenic mammary cell lines

The notion that 4.1B functions as a tumor suppressor is based, in part, on previous findings indicating that its expression was not detectable in a variety of tumors or tumor cell lines, including mammary carcinoma cell lines (Tran *et al*., 1999; Gutmann *et al*., 2000; Kittiniyom *et al*., 2001; Charboneau *et al*., 2002; Singh *et al*., 2002). We have found, however, that this protein is either not expressed or expressed at very low levels in the normal nonpregnant mouse mammary gland and that its expression increases during pregnancy. To gain a better understanding of the role of 4.1B in various mammary cell lines and to determine which of these cell lines could be used to further study the function of 4.1B, we compared 4.1B expression in two immortalized mammary epithelial cell lines (MCF-10A and Eph4-3) to that in several mammary carcinoma cell lines (MDA-MB 231, MDA-MB 435, MDA-MB 436, SKBR3,

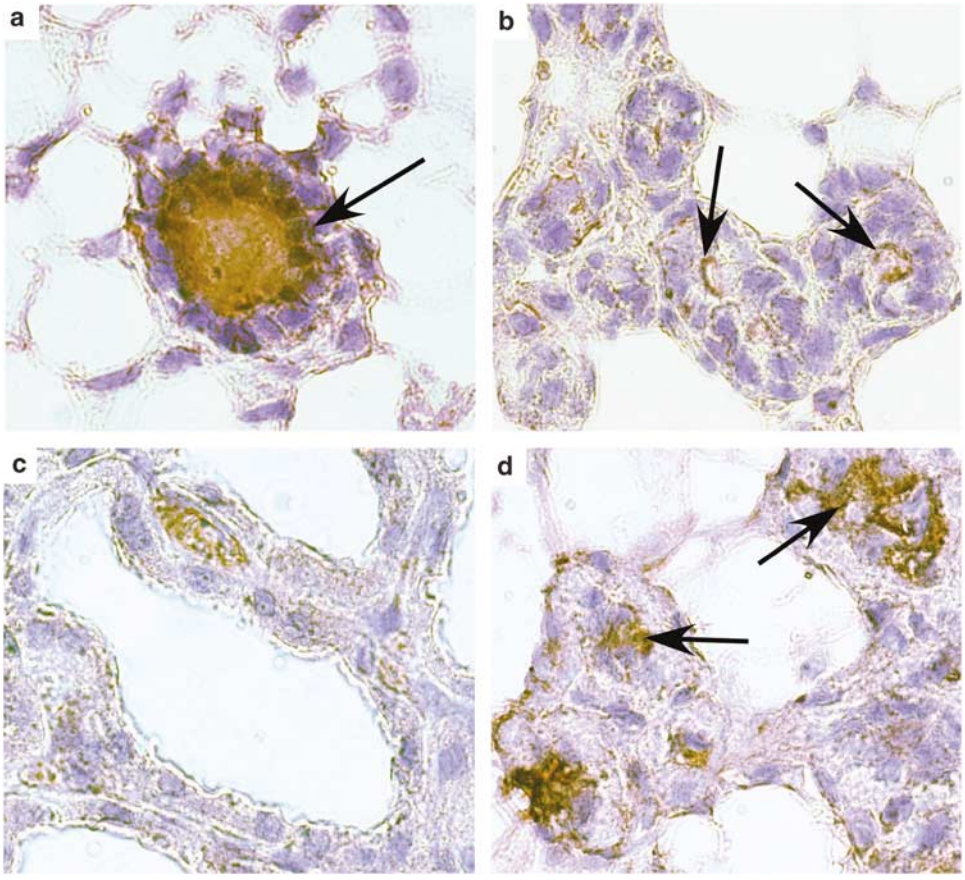

Figure 2 ERM protein expression in the normal mouse mammary gland. (**a**) Virgin (8 weeks), (**b**) pregnant (13.5 dpc), (**c**) lactating (9 dpp), and (**d**) involuting (5 dpw) mouse mammary glands were sectioned and immunolabeled with an anti-ezrin antibody that crossreacts with radixin and moesin. Note that, in contrast to protein 4.1B, ERM proteins are expressed in virgin and involuting ductal epithelia, but less so in proliferating epithelia during pregnancy. ERM proteins are also only weakly expressed during lactation. Arrows indicate ERM staining at apical membranes

Hs578T, and MDA-MB 175) by Western blot analysis. By loading high amounts of protein, we found that 4.1B is expressed at very low levels in both carcinoma and immortalized epithelial cell lines (data not shown for Eph4-3 cells), with the exception of MDA-MB 436 cells, which constitutively express higher levels of 4.1B (Figure 3a). The different-sized bands recognized by the 4.1B antibody in MDA-MB 436 cells are consistent with the predicted sizes of different 4.1B splice variants. Taken together, our results indicate that 4.1B is not absent from mammary carcinoma cell lines, and is not expressed at significant levels in normal mammary epithelia.

Although 4.1B localizes primarily to regions of cell–cell contact (Tran *et al*., 1999; Parra *et al*., 2000; Charboneau *et al*., 2002), we found that 4.1B also localizes to the membrane and cytoplasm in individual MDA-MB 436 cells, which do not form normal cell–cell contacts (Figure 3b), and is concentrated at the tips of cell processes at apparent points of adhesion to the culture dish. Interestingly, 4.1B expression could be detected around and in the nuclei of these cells even though no such nuclear localization was apparent in mammary tissue sections. Similar results were seen with other mammary cell lines (data not shown). 4.1B contains a putative nuclear localization signal (NLS) (KRRK), as well as an upstream casein kinase II site (SAAE), a common feature in proteins containing an NLS (Kittiniyom *et al*., 2004). Furthermore, 4.1B has been shown to translocate from the plasma membrane into the nucleus in PC12 cells following differentiation (Gascard *et al*., 2004), and the 4.1 family members merlin, ezrin, and 4.1R localize within the nucleus under some conditions (Mattagajasingh *et al*., 1999; Batchelor *et al*., 2004; Muranen *et al*., 2005). To exclude the possibility that the observed nuclear localization of 4.1B was due to nonspecific staining by the 4.1B antibody, we created a GFP-4.1B fusion construct (pEFGP-4.1B) in order to monitor the localization of the exogenous protein without having to rely on the antibody. MCF-10A cells, which also exhibit nuclear staining for this protein, were transfected with pEGFP-4.1B or pEGFP alone and fixed 24 h post-transfection. GFP (Figure 3d and g) and 4.1B (Figure 3e and h) localization were determined by immunofluorescence, and nuclei were stained with Hoechst 33342 (Figure 3f and i). Our results indicate that although transfection with pEGFP alone results in GFP localization throughout the cell, GFP tagged with 4.1B is excluded from the nucleus. Similar results were seen in other mammary cell lines (data not shown). Consistent with these findings, Western blots of nuclear and cytoplasmic fractions of MDA-MB 436 and MCF-10A cell lines indicated that the nuclear fractions contained a distinct set of bands, including a prominent band of over 210 kDa, that were not present in the cytoplasmic fractions. Reprobing these blots with a 4.1B antibody that had been preincubated with the full-length protein confirmed that these distinct nuclear bands were in fact nonspecific (data not shown). We conclude, therefore, that although 4.1B contains a putative NLS, it does not localize to the nucleus in mammary cell lines under any of the conditions used in the experiments described here.

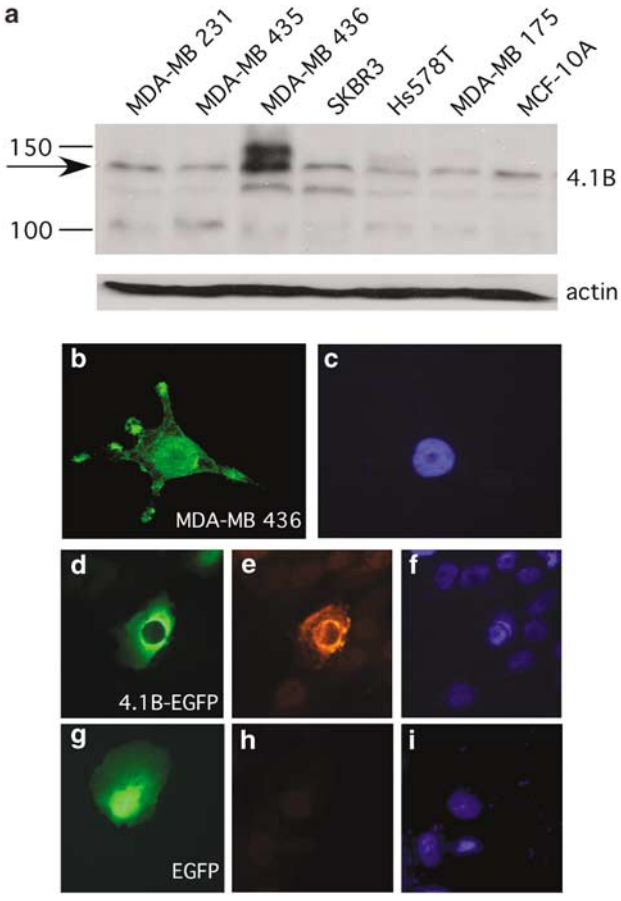

Figure 3 Protein 4.1B is expressed at low levels by immortalized mammary epithelial and carcinoma cell lines. (**a**) Lysates from a series of breast cancer cell lines (MDA-MB 231, MDA-MB 435, MDA-MB 436, SKBR3, Hs578T, and MDA-MB 175) and the immortalized mammary epithelial cell line MCF-10A were immunoblotted for 4.1B (arrow indicates specific band). Actin serves as the loading control. Note that all cell lines express low levels of 4.1B and that the MDA-MB 436 carcinoma cell line expresses constitutively elevated 4.1B levels. (**b**, **c**) MDA-MB 436 cells were fixed and immunolabeled for 4.1B (**b**) and Hoechst 33342 (**c**). (**d**–**i**) MCF-10A cells were transfected with pEGFP-4.1B (**d**–**f**) or pEGFP alone (**g**–**i**). GFP expression (**d**, **g**) marks transfected cells. The cells were immunostained for 4.1B (**e**, **h**) and Hoechst 33342 (**f**, **i**). Note that 4.1B localizes to filopodial regions of the membrane and cytoplasm but not to the nucleus in these cells

4.1B inhibits mammary epithelial cell proliferation but does not influence cell survival

Previous reports have indicated that cells transfected with a cDNA encoding the partial 4.1B construct, DAL-1, demonstrate growth suppression as measured by cell counts and growth curve analysis (Tran *et al*., 1999; Gutmann *et al*., 2001; Charboneau *et al*., 2002; Robb *et al*., 2005). One report showed a slight induction in apoptosis in cells overexpressing DAL-1 (Charboneau *et al*., 2002). Given our findings that 4.1B is expressed by mammary epithelia during pregnancy, a period of active

cell proliferation, but not during involution, a period of extensive apoptosis, we sought to better understand the mechanism by which 4.1B regulates cell growth and survival.

To determine whether 4.1B expression results in increased apoptosis, we first induced overexpression of DAL-1 in the inducible cell line MCF7-DAL1 (Charboneau *et al*., 2002) by the addition of muristerone for 96 h. Lysates were collected and immunoblotted for 4.1B to insure overexpression of the protein, and for cleaved-PARP, whose expression increases during the induction of apoptosis (Figure 4a). Our results indicate no increase in cleaved-PARP protein levels. We also assessed the total percentage of cells undergoing apoptosis 48 and 96 h postinduction by the TUNEL assay to measure DNA fragmentation. Pycnotic TUNEL-positive nuclei, as shown in Figure 4b, were counted (Figure 4c). Although there was a slight increase in the percentage of apoptotic cells 96 h after the induction of apoptosis, the increase was small (<1% of total cells counted; $P=0.0545$).

We next determined the effect of overexpression of 4.1B on proliferation as measured by BrdU incorporation and Ki67 expression. MCF7-DAL1 cells induced to overexpress DAL-1 for 48 or 96 h were pulsed with BrdU for 2 h, fixed, immunolabeled for BrdU, and counterstained with Hoechst 33342. We found a decrease in the percentage of BrdU-positive cells 96 h postinduction ($P=0.048$) (Figure 5a). MCF7-DAL1 cells were also immunolabeled for Ki67 expression, another marker of cell proliferation (Gerdes *et al*., 1984), 48 and 96 h postinduction. We found a significant decrease in the percentage of Ki67-positive cells both at 48 ($P=0.03$) and 96 ($P=0.008$) h postinduction (Figure 5b). Taken together, these results quantitatively indicate that the overexpression of DAL-1 in MCF7-DAL1 cells causes a significant reduction in cellular proliferation.

To determine whether intact protein 4.1B also inhibits proliferation, we repeated the BrdU and Ki67 assays with full-length 4.1B in MCF-10A and SKBR3 cells. Cells were transiently transfected with pEGFP or pEGFP-4.1B and pulsed for 2 h with BrdU 48 or 96 h post-transfection. For these assays, we immunolabeled for BrdU and then examined the number of BrdU-labeled GFP-positive cells. Compared to cells expressing only pEGFP, cells expressing elevated levels of 4.1B demonstrated a significant decrease in the percentage of BrdU-positive cells at both 48 and 96 h postinduction in both the MCF-10A (48 h: $P=0.004$; 96 h: $P=0.004$) and the SKBR3 (48 h: $P=0.009$; 96 h: $P=0.004$) mammary lines (Figure 5c and e). The percentage of Ki67-labeled GFP-positive cells at both 48 and 96 h post-transfection was also significantly reduced in both the MCF-10A (48 h: $P=0.005$; 96 h: $P=0.047$) and the SKBR3 (48 h: $P=0.02$; 96 h: $P=0.004$) cell lines (Figure 5d and f). Our results indicate that 4.1B mediates growth suppression primarily through the inhibition of proliferation. Although we did observe a slight increase in apoptosis in cells that had been induced to overexpress DAL-1, the percentage of cells undergoing apoptosis

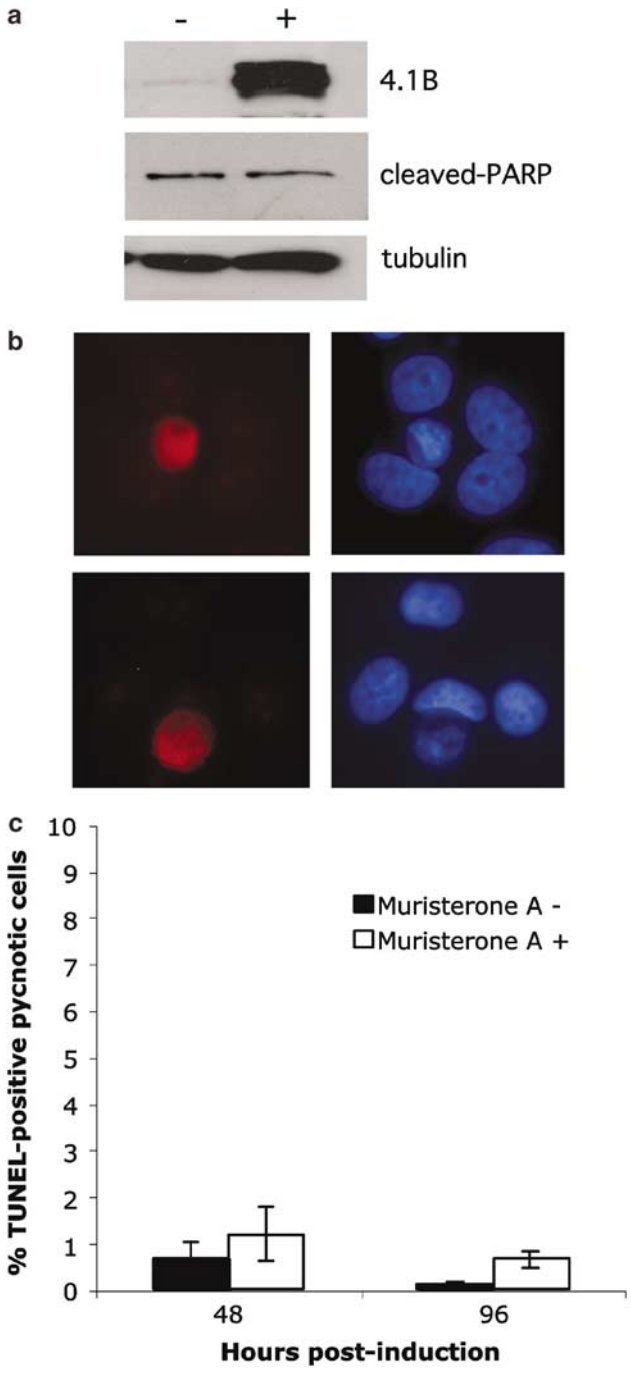

Figure 4 Effect of 4.1B on apoptosis. A clone of MCF-7 cells carrying an ecdysone-inducible DAL-1 construct (MCF7-DAL1 cells) was grown in the presence or absence of 2 μM muristerone in ethanol for 48 or 96 h. (**a**) Immunoblots of lysates collected 96 h after the addition of muristerone (+) or ethanol alone (−) for cleaved-PARP. Tubulin was used as a loading control. (**b**, **c**) TUNEL assays of MCF7-DAL1 cells fixed 48 or 96 h after the addition of 2 μM muristerone or ethanol alone. (**b**) Fragmented nuclei were labeled in red by terminal deoxynucleotidyl transferase and all nuclei were labeled in blue with Hoechst 33342. (**c**) TUNEL-positive pycnotic cells were counted and are shown ±s.e.m. Results shown include data from three independent experiments. Note that overexpression of DAL-1 does not result in a significant induction of apoptosis

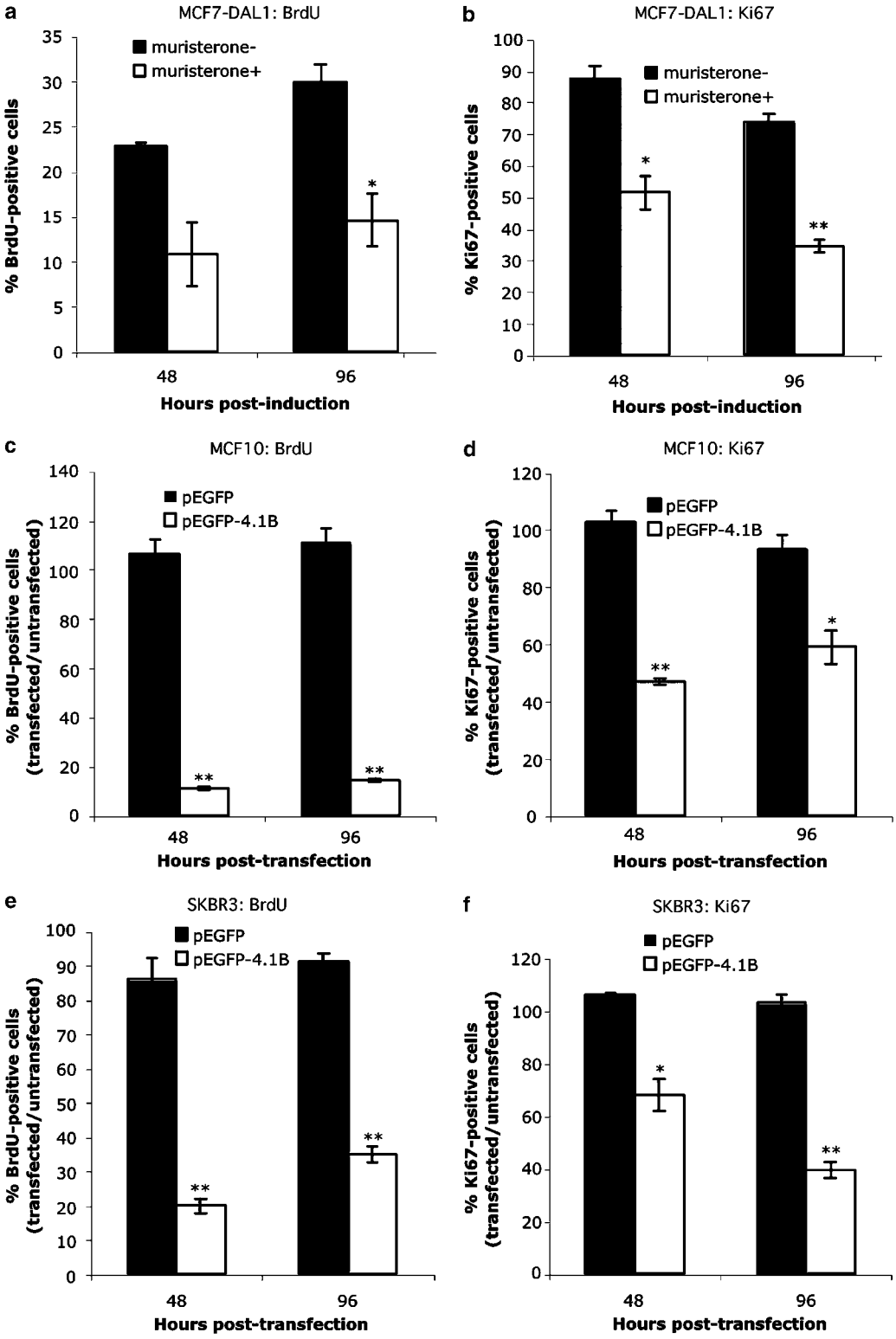

Figure 5 Effect of 4.1B on BrdU incorporation and Ki67 expression in mammary epithelial and carcinoma cell lines. (**a**, **b**) MCF7-DAL1 cells were induced to overexpress DAL-1 by the addition of 2 μM muristerone for 48 or 96 h. Cells were either (**a**) pulsed with 10 μM BrdU for 2 h and then immunolabeled for BrdU or (**b**) immunolabeled for Ki67. Cells were counterstained with Hoechst 33342, and the percentage of BrdU-positive or Ki67-positive cells was then determined. (**c**–**f**) Cell lines were transiently transfected with pEGFP or pEGFP-4.1B and then examined, as above, for BrdU incorporation and Ki67 expression. After 48 or 96 h, MCF-10A cells (**c**, **d**) and SKBR3 cells (**e**, **f**) demonstrated marked reduction in both BrdU incorporation and Ki67 labeling, indicating that 4.1B inhibits mammary epithelial cell proliferation. Results include data from two or three independent experiments and are shown $\pm$s.e.m. $^{*}P<0.05$, $^{**}P<0.005$

was relatively small, especially in comparison to the level of reduction in both BrdU incorporation and Ki67 expression. These data also further confirm that DAL-1 contains the essential protein sequences of 4.1B required for growth suppression.

Exogenous 4.1B expression in mammary cell lines results in G_1 cell cycle arrest

The decreased incorporation of BrdU in 4.1B-overexpressing cells suggests that these cells are becoming arrested at some point in the cell cycle, as they are not progressing through S phase. Furthermore, because Ki67 is expressed throughout all stages of the cell cycle except early G_1 and G_0 (Gerdes *et al*., 1984), the significant reduction in Ki67 expression observed in 4.1B-overexpressing mammary cells suggests that this protein induces a G_0/G_1 cell cycle arrest. Cell cycle progression through the G_1/S transition requires pRb to be hyperphosphorylated, allowing it to dissociate from and permit the activation of the transcription factor E2F (Chau and Wang, 2003). Cells arrested in G_0/G_1 thus exhibit a decrease in pRb hyperphosphorylation. We assessed the pRb levels in MCF7-DAL1 cells after 72 h of induction with muristerone by Western blot analysis, and found a decrease in the level of hyperphosphorylated pRb (Figure 6a), supporting the idea that 4.1B overexpression results in a G_0/G_1 arrest. In addition, we examined the levels of cyclin A and cyclin D. Cyclin A expression is induced by E2F-mediated transcription during late G_1 and forms a complex with cdk2, which is necessary for progression into and through S phase. Cyclin A is upregulated in S and G_2 phase and downregulated in G_1. Cyclin D expression is induced during early G_1 as cells exit G_0, when it forms a complex with cdk4/6 and phosphorylates pRb, and is thus critical for cell cycle activation (Stull *et al*., 2004). Levels of cyclin D remain high throughout the remainder of the cell cycle. We found no change in cyclin D levels in cells overexpressing DAL-1, but observed a marked inhibition of cyclin A expression. Collectively, our findings indicate that 4.1B functions by causing cells to arrest in G_1.

Protein 4.1B does not mediate its growth inhibitory effect through the MAPK, Akt, or JNK signaling pathways

We have demonstrated that 4.1B mediates its growth suppressive function by inducing a G_1 cell cycle arrest. Two signal transduction pathways that are commonly implicated in mediating cell cycle progression through G_1 are the MAPK and PI3K/Akt pathways. The 4.1 family members ezrin and merlin have been shown to regulate these signaling cascades (Gautreau *et al*., 1999; Fraenzer *et al*., 2003). In addition, DAL-1 can induce JNK phosphorylation in IOMM-Lee meningioma cells (Robb *et al*., 2005). To determine whether 4.1B mediates its growth inhibitory effect by altering MAPK, Akt, or JNK signaling, we analysed lysates from MCF7-DAL1 cells that had been induced to overexpress DAL-1 by Western blot analysis using phospho-specific antibodies against p44/42 MAPK, Akt, and JNK. We found no changes in the levels of either total or phosphorylated forms of p44/42 or Akt (Figure 6b) or JNK (Figure 6c), indicating that changes in MAPK, Akt, and JNK activity are not required in mammary carcinoma cells to induce G_1 arrest.

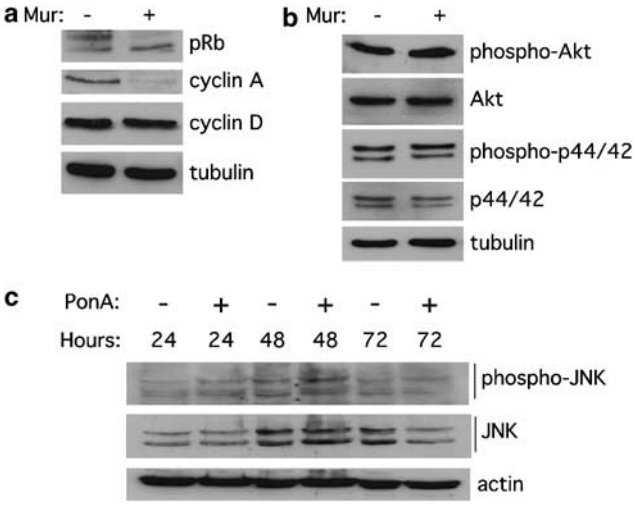

Figure 6 Effect of 4.1B overexpression on cell cycle and cell signaling molecules. MCF7-DAL1 cells were induced to overexpress DAL-1 for 72 h (**a**, **b**) or for 24, 48, and 72 h (**c**). Equal concentrations of cell lysates were subjected to Western blot analysis, and blots were probed for (**a**) the cell cycle proteins pRb, cyclin A, and cyclin D, (**b**) the signal transduction molecules phospho-Akt, total Akt, phospho-p44/42 MAPK, and total p44/42 MAPK, or (**c**) phospho-JNK and total JNK. All blots were stained with Ponceau S and probed for a loading control, and tubulin or actin was included as a representative loading control from one of the blots in each panel. Note that pRb hyperphosphorylation and cyclin A levels were decreased in cells induced to overexpress DAL-1 (**a**), while no change was seen in cyclin D (**a**), phospho-Akt, Akt, phospho-p44/42, p44/42 (**b**), phospho-JNK or total JNK levels (**c**) in DAL-1-overexpressing cells

4.1B inhibits erbB2 phosphorylation

ErbB2 (also called HER2) is a member of the erbB family of receptor tyrosine kinases that includes the epidermal growth factor receptor (EGFR, also called erbB1 and HER1), erbB3 (HER3), and erbB4 (HER4). These receptors are activated by EGF- and neuregulin-related proteins. Upon ligand binding, EGFR, erbB3, and erbB4 form heterodimers, with erbB2 being the preferred heterodimerization partner (Tzahar *et al*., 1996). The expression and activation of erbB2 and EGFR are necessary for normal mammary ductal growth and increase in mammary epithelia during puberty and pregnancy, times when mammary epithelial cells are undergoing high rates of proliferation (Sebastian *et al*., 1998; Stern, 2003). Furthermore, erbB2 is a major target of breast cancer treatments, as overexpression of this protein occurs in 20–40% of breast tumors and is associated with poor prognosis (Allred and Mohsin, 2000).

ErbB2 may indirectly interact with 4.1B through the CD44 transmembrane glycoprotein, which interacts

with erbB2 and EGFR in mammary carcinoma cells (Wobus *et al*., 2002; Ghatak *et al*., 2005) and with 4.1 proteins through its C-terminal domain (Ponta *et al*., 2003). As loss of erbB2 expression or activity can inhibit proliferation of mammary carcinoma cells (Jhabvala-Romero *et al*., 2003; Faltus *et al*., 2004; Chu *et al*., 2005), including the MCF-7 cell line, we tested the possibility that 4.1B regulates mammary epithelial cell proliferation at least in part by regulating erbB2 activity. Compared to controls, MCF-7 cells induced to express DAL-1 demonstrated a nearly total reduction in erbB2 phosphorylation without any decrease in the total levels of erbB2 (Figure 7a). We therefore tested whether 4.1B disrupted the formation of erbB2–EGFR or erbB2–erbB3 heterodimers. In both the absence and presence of induced levels of 4.1B, EGFR remained associated with erbB2 (Figure 7b). In contrast to EGFR, erbB3 did not constitutively associate with erbB2 in these cells. However, following the addition of neuregulin, we did observe erbB2–erbB3 heterodimers, but they also were not dissociated in the presence of 4.1B (data not shown). We were unable to detect significant quantities of erbB4 in these cells. These data suggest that although 4.1B can inhibit erbB2 phosphorylation, it does so without disrupting the formation of erbB receptor heterodimers.

We next tested the possibility that 4.1B disrupted interactions between erbB2 and CD44. However, in co-immunoprecipitation assays, the induction of 4.1B had no effect on CD44–erbB2 interactions in MCF-7 cells (Figure 7c). Thus, reduced erbB2 phosphorylation resulting from 4.1B induction may contribute to 4.1B-mediated cell cycle arrest without disrupting erbB receptor heterodimers or other erbB2 interactions with transmembrane proteins that promote erbB2 activation and signaling.

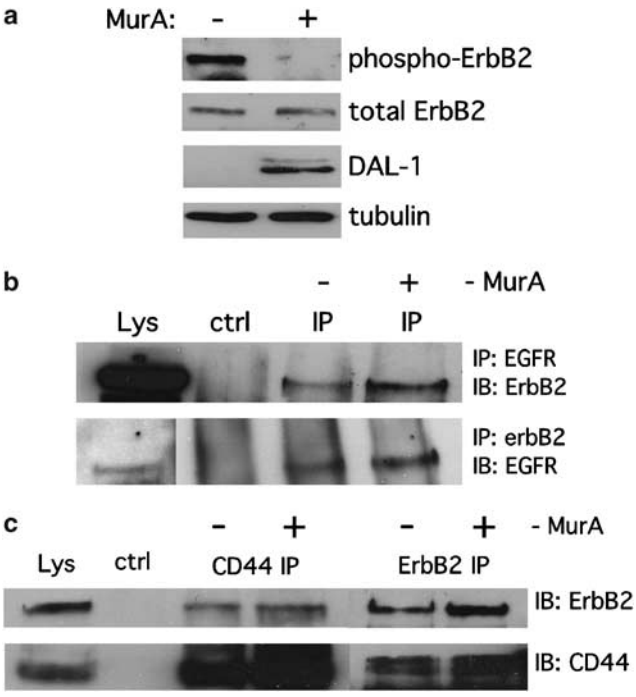

Figure 7 Effects of 4.1B on erbB2 phosphorylation. (**a**) MCF7-DAL1 cells were induced to overexpress DAL-1 by the addition of Muristerone A for 48 h. Equal concentrations of cell lysates from induced (+) and uninduced (−) cells were subjected to Western blot analysis, and the resulting blots were probed for phospho-erbB2, total erbB2, DAL-1, or tubulin as a loading control. Note that in the presence of DAL-1, erbB2 phosphorylation is dramatically reduced while total erbB2 levels are unchanged. (**b**) MCF7-DAL1 cells were induced as above and then equal concentrations of lysates were immunoprecipitated for erbB2 and EGFR and subjected to Western blot analysis. The resulting blots were probed for erbB2 and EGFR. Note that ErbB2 and EGFR co-immunoprecipitate both in the absence (−) and presence (+) of DAL-1. (**c**) MCF7-DAL1 cells were induced to overexpress DAL-1, and then equal concentrations of lysates were immunoprecipitated for erbB2 and CD44. Lysates and immunoprecipitates were then assessed for erbB2 and CD44 expression by Western blot analysis. Note that erbB2 and CD44 co-immunoprecipitate both in the absence (−) and presence (+) of DAL-1

Loss of protein 4.1B results in increased mammary epithelial cell proliferation during pregnancy

To determine if loss of protein 4.1B leads to proliferative abnormalities *in vivo*, we examined mammary glands from different postpubertal developmental stages in 4.1B knockout mice. These mice have an apparently normal phenotype and do not develop tumors of the mammary gland (Kissil *et al*., manuscript in preparation). Indeed, we found no significant morphological differences between the virgin mammary glands of wild-type and 4.1B-null animals (compare Figure 8a and d). However, we did observe dramatic differences in pregnant glands compared to stage-matched wild-type controls (compare Figure 8b and e). The appearance of the tissues indicated an overall increase in the numbers of alveoli and ducts during pregnancy. This phenotype did not persist into lactation (compare Figure 8c and f). In order to determine whether this altered morphology was due to an increase in epithelial cell proliferation, we assessed Ki67 expression in the epithelium of these glands as Ki67 is a frequently used marker of proliferation in tissues (Scholzen and Gerdes, 2000). Although we found no effect on cell proliferation as measured by Ki67 expression in the mature virgin or lactating mammary gland (data not shown), we did observe a significant increase (from 49.6 ± 1.3 to $80.2 \pm 4.8\%$; $P = 0.0009$) in the percentage of proliferating epithelial cells in the pregnant wild-type gland in comparison to region-matched 4.1B knockout glands (Figure 9a–c). At no point in any stage of mammary development did we observe altered levels of apoptosis, as assessed by TUNEL labeling (data not shown). Together, our results suggest that the upregulation of 4.1B during pregnancy regulates the proliferative levels of luminal epithelial cells by regulating the progression of these cells through G_1.

Discussion

We demonstrate here that 4.1B is not expressed in the normal mouse virgin mammary gland epithelium and

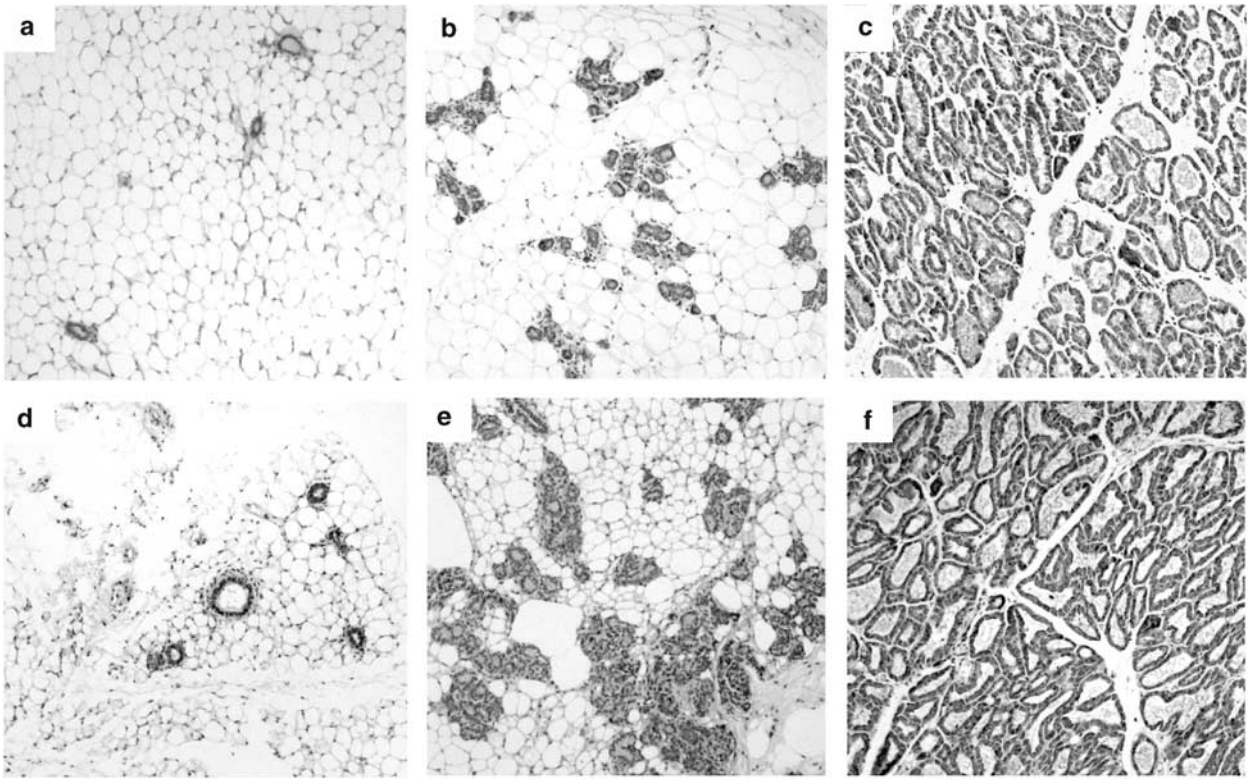

Figure 8 Morphology of virgin, pregnant, and lactating mammary glands in the wild-type and 4.1B knockout mice. The fourth pair of mammary glands from (**a**, **d**) 8 weeks virgin, (**b**, **e**) 13.5 dpc pregnant, and (**c**, **f**) 9 dpp lactating wild-type (**a**–**c**) and 4.1B-null (**d**–**f**) mice were paraffin-embedded and sectioned. Nuclei were stained with hematoxylin. Images were taken with a 5× objective to show the overall morphology of the glands. Note the apparent increase in the density of ductal and alveolar epithelial cells in the 4.1B-null *versus* wild-type glands

that loss of 4.1B does not influence cell proliferation in virgin 4.1B-null mice. In contrast, 4.1B expression is dramatically induced in mammary epithelium during pregnancy, and pregnant 4.1B-null mice demonstrate increased mammary epithelial proliferation. As cells pass this highly proliferative state and move into the fully differentiated state of lactation, 4.1B expression is no longer evident, and remains undetectable during the apoptotic involuting stage. Furthermore, loss of 4.1B does not affect proliferation of epithelial cells in the lactating or involuting mammary glands. In support of these data, we find that 4.1B is expressed at very low levels in both immortalized mammary epithelial and carcinoma cell lines and that overexpression of 4.1B in these cells causes them to arrest in G_1. These results demonstrate a unique role for 4.1B in the regulation of epithelial cell proliferation in the mammary gland.

Our findings suggest that 4.1B may not function to suppress cell growth in a manner that is analogous to merlin or other tumor suppressor proteins. Since it is not expressed in virgin mouse mammary epithelial cells, 4.1B does not appear to function by maintaining or inducing epithelial cell quiescence. Furthermore, the lack of mammary tumors in 4.1B-null mice indicates that loss of 4.1B is not likely to be sufficient to promote tumorigenesis. In contrast, loss or mutational inactivation of merlin is sufficient to induce tumor formation (Rouleau *et al*., 1993; Trofatter *et al*., 1993; McClatchey *et al*., 1998). It is nonetheless possible that 4.1B cooperates with other tumor suppressor genes, including other members of the 4.1 family, to promote tumor formation. In addition, because multiparity has been associated with increased breast cancer risk (Whiteman *et al*., 2004; Hall *et al*., 2005), it is possible that loss of 4.1B may promote mammary gland tumors after multiple pregnancies, although this has not yet been observed in 4.1B-null mice (Kissil *et al*., manuscript in preparation).

It has been previously reported that ectopic expression of DAL-1, which contains the growth suppressive function of full-length 4.1B, results in the induction of apoptosis, with 5–8% of DAL-1-overexpressing cells becoming apoptotic as assessed by TUNEL or Annexin V labeling (Charboneau *et al*., 2002; Robb *et al*., 2005). It was concluded from these findings that DAL-1 may reduce growth, in part, by altering cell survival. Here, we measured apoptotic induction by assaying cleaved-PARP expression levels as well as DNA fragmentation by TUNEL labeling and did not observe the same significant increase in apoptosis. Although 4.1B may indeed induce apoptosis, our data suggest that this is not the case under all conditions.

We have shown, however, through BrdU and Ki67 labeling studies that exogenous 4.1B significantly inhibits cellular proliferation at a specific stage of the cell cycle. The BrdU results, which indicate that 4.1B-overexpressing cells are significantly inhibited in their ability to progress through S-phase, are supported by the observation that cyclin A levels are decreased in 4.1B-overexpressing cells. The Ki67 results, obtained both *in vitro* and *in vivo*, indicate that 4.1B-overexpressing cells are either entering G_0 or arresting in the G_1 phase of the cell cycle and are supported by the decrease observed in pRb hypophosphorylation. The change in pRb phosphorylation levels indicates that cells are not progressing through the G1/S-phase transition. Furthermore, cyclin D levels did not change upon 4.1B overexpression, indicating that cells are not exiting the cell cycle and entering G_0. Taken together, these results indicate that 4.1B mediates a cell cycle arrest in G_1 in mammary cell lines. Although G_1 cell cycle arrest can be mediated in some systems through the JNK, MAPK, and/or Akt pathways, we did not observe changes in phospho-JNK, phospho-Akt, or phospho-p44/42 levels upon 4.1B overexpression, suggesting that other signaling mechanisms are affected by 4.1B to regulate growth suppression. In contrast, recent studies from one of our laboratories have suggested that 4.1B functions to regulate cell growth in meningioma cells by modulating JNK signaling (Robb *et al*., 2005). 4.1B may therefore mediate its growth inhibitory effect differently in mammary cells compared to meningioma cells.

It has also recently been shown that 4.1B interacts with protein arginine *N*-methyltransferase 3 (PRMT3) and inhibits its ability to methylate its substrates (Singh *et al*., 2004). 4.1B may mediate its growth inhibitory effect by interacting with PRMT3 and thus modulating its ability to methylate its substrates. Another possibility is that the interaction between 4.1B and the tumor suppressor in lung cancer-1 (TSLC1) is required for 4.1B-mediated growth suppression (Yageta *et al*., 2002). In addition to being lost in NSCLCs, TSLC1 has recently been shown to be lost in meningiomas; both of these tumor types also exhibit frequent 4.1B loss (Surace *et al*., 2004). Interestingly, we have found that, similar to 4.1B, TSLC1 is expressed at low levels in virgin and involuting mouse mammary glands, but is upregulated during pregnancy as well as during lactation (data not shown).

Our finding that DAL-1 can inhibit the constitutive phosphorylation of erbB2 in MCF-7 cells suggests that 4.1B may regulate mammary epithelial cell proliferation in part by regulating erbB2 activation. However, erbB2 signals through the MAPK and Akt pathways to influence cell proliferation (Yarden and Sliwkowski,

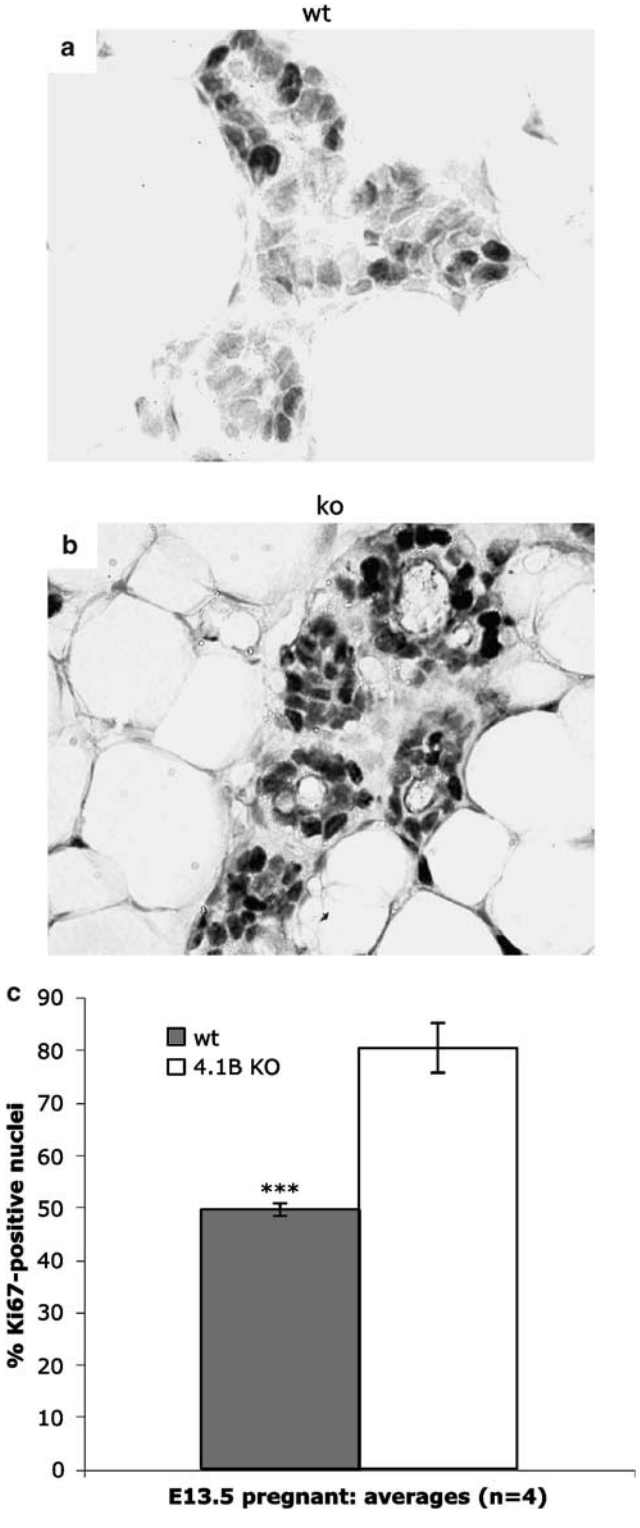

Figure 9 Ki67 expression in wild-type and 4.1B knockout pregnant mammary glands. The fourth pair of mammary glands from E13.5 pregnant wild-type and 4.1B knockout mice were dissected, and the approximately 3 mm region closest to the nipple was removed, paraffin-embedded, and sectioned. The sections were immunolabeled for Ki67 (black) and counterstained with hematoxylin (gray). Shown are epithelial regions from (**a**) wild-type and (**b**) 4.1B knockout glands. (**c**) At least 500 epithelial nuclei were counted in random fields, and the counts from both the right and left glands were then averaged to determine the percentage of Ki67-postive nuclei for each mouse. Four wild-type and 4.1B knockout mice were used to obtain the results, which are shown $\pm$s.e.m. ***$P<0.001$. Note the significant upregulation in Ki67 expression in the mammary epithelium of the pregnant 4.1B-null *versus* wild-type mice

2001) and our data indicate that 4.1B induces a G_1 arrest independent of altered MAPK or Akt activity. It is therefore possible that other signaling cascades that influence pRb are also regulated by erbB2. Alternatively, the loss of erbB2 phosphorylation may be an indirect effect of 4.1B induction that could amplify a number of signals that result in cell cycle arrest. Nonetheless, our studies raise the intriguing possibility that 4.1B can influence erbB receptor activation during pregnancy and in mammary carcinoma cells with elevated levels of EGFR or erbB2 through a mechanism that does not influence receptor heterodimerization. Although it is unclear how 4.1B influences erbB2 phosphorylation, one possible way could be through the recruitment of a protein tyrosine phosphatase that, like 4.1B, possesses a FERM domain and could bind the C-terminus of 4.1B (e.g. Cuppen *et al*., 1999).

Although 4.1B has previously been reported to localize to the nucleus, it has only been shown to do so in nonproliferating, differentiated cells (Gascard *et al*., 2004), in contrast to the highly proliferative mammary cell lines used here and the undifferentiated mammary epithelia in the nonpregnant mammary gland. It is therefore possible that, like other 4.1 family members, 4.1B does localize to the nucleus but only under distinct cellular conditions. Although we never observed nuclear 4.1B at any stage of mammary development, it is possible that 4.1B translocates to the nucleus of other cell types after the transition from proliferative to differentiated states.

In summary, our results suggest that 4.1B may only be functional when mammary epithelial cells become highly proliferative during pregnancy. We therefore propose that 4.1B is upregulated during pregnancy, and possibly similar states of increased proliferation in other cell types, as a means of modulating external proliferative signals. Furthermore, we hypothesize that although loss of the *4.1B* gene in mammary epithelia does not itself result in tumor formation, it may exacerbate the rate of tumor cell proliferation by relieving cells of an antiproliferative signal that would otherwise prevent continued cell growth. Further studies utilizing the 4.1B-null mice will be required to better understand the role of 4.1B in mammary carcinogenesis.

Materials and methods

Mice

Female 8-week-old wild-type C57BL/6 and C57BL/6-129Sv/J mice were purchased from Jackson Laboratories. Generation of the 4.1B-null mice is described elsewhere (Kissil, 2005). Dams were euthanized using a lethal dose of isoflurane and tissues were harvested as described below from 8-week-old virgin, 13.5 dpc pregnant, 9 dpp lactating, and 5 dpw involuting animals.

Immunohistochemistry

For quantitative analyses, an approximately 3 mm region nearest the nipple of the right and left fourth mammary glands was dissected from animals at each stage of mammary gland maturation. In some cases, whole mammary tissues were also dissected. Tissues were fixed overnight in 4% paraformaldehyde at 4°C and washed three times for 20 min per wash in PBS before being embedded in paraffin. Sections (5 μm) were deparaffinized with xylene followed by rehydration with a graded ethanol series. Antigen retrieval was performed with DAKO target retrieval solution (S1700, DAKO Corporation) as per the manufacturer's instructions. The sections were blocked in 3% hydrogen peroxide/PBS for 15 min and in 10% normal goat serum (NGS) in PBS for 60 min, and then incubated overnight with the following primary antibodies at 4°C: a rabbit anti-4.1B polyclonal antibody (Ezequiel Surace and David Gutmann, unpublished results, 2005; 1 : 500), a rabbit anti-ezrin (C-19) polyclonal antibody (Santa Cruz; 1 : 100), rabbit anti-E-cadherin (H-108) polyclonal antibody (Santa Cruz; 1 : 250), or a mouse anti-Ki67 monoclonal antibody (NCL-L-Ki67-MMI, Novocastra; 1 : 50) in 10% NGS at 4°C. After being washed, the sections were incubated with biotinylated secondary antibodies (BA-1000, BA-9500, BA-9500; Vector Laboratories; 1 : 200) for 25 min. The sections were then incubated with the Vectastain Elite ABC reagent (PK-6100; Vector Laboratories), developed with the Vector NovaRed Substrate Kit (SK-4800; Vector Laboratories), and counterstained with hematoxylin (H-3401, Vector Laboratories) or processed for immunofluorescence with Alexa-Fluor-conjugated secondary antibodies (A-11029, A-11030, A-11034, A-11035, Molecular Probes; 1 : 500) and Hoechst 33342 (Molecular Probes; 1 : 2000). Images were obtained with a Zeiss Axioskop 40 microscope using a $\times 63$ oil-immersion objective (Carl Zeiss Inc.).

Cell culture

All cell lines were obtained from and grown according to the specifications of ATCC except the MCF7-DAL1 cell line, which was grown as previously described (Charboneau *et al*., 2002). DAL-1 expression was induced in the MCF7-DAL1 cell line by the addition of 2 μM Muristerone A (Invitrogen) or 5 μM Ponasterone A (Invitrogen) for the indicated length of time. In some experiments, cells were pulsed with 10 ng/ml neuregulin-1β (R&D Systems) for 10 min.

Western blot analysis and immunoprecipitations

Cultured cells were washed in PBS and lysed (20 mM Tris-HCl pH 7.4, 25 mM NaCl, 3 mM $MgCl_2$, and 0.5% NP-40 plus protease inhibitors); mammary tissues were lysed by sonication in the same lysate buffer. Lysates were cleared by centrifugation (14 000 r.p.m. at 4°C) for 10 min, and the protein concentration of the resulting supernatant was obtained by the Bradford assay before Laemmli buffer was added. The samples were boiled for 5 min before being loaded in equal concentrations onto a 5.5, 7.5, or 12% SDS–polyacrylamide gel. The protein was transferred onto nitrocellulose membrane and probed overnight with the indicated antibodies at 4°C. Two different rabbit anti-4.1B polyclonal antibodies were used as previously described (Tran *et al*., 1999) at 1 : 2000. Additional antibodies used were mouse anti-cleaved-PARP monoclonal antibody (19F4, Cell Signaling Technology; 1 : 2000), mouse anti-alpha-tubulin monoclonal antibody (DM1A, NeoMarkers; 1 : 1000), rabbit anti-E-cadherin (H-108) polyclonal antibody (Santa Cruz; 1 : 1000), goat anti-actin (I-19) polyclonal antibody (Santa Cruz; 1 : 1000), rabbit anti-pRb (C-15) polyclonal antibody (Santa Cruz; 1 : 100), mouse anti-cyclin D1 (DCS6) monoclonal antibody (2926, Cell Signaling; 1 : 2000), rabbit anti-phospho-p44/42 MAP kinase polyclonal antibody (9101, Cell Signaling; 1 : 1000), mouse

anti-EGFR monoclonal antibody (Upstate; 1 : 500), mouse anti-erbB2 monoclonal antibody (Calbiochem; 1 : 500), rabbit anti-phospho-erbB2 polyclonal antibody (Upstate; 1 : 2000), and mouse anti-human CD44 monoclonal antibody (Hermes-3; ATCC; 1 : 50). The following antibodies were generously provided: rabbit anti-cyclin A (C-19) polyclonal antibody (Santa Cruz; 1 : 1000) from Erik Knudsen (University of Cincinnati); rabbit anti-phospho-JNK polyclonal antibody (Cell Signaling; 1 : 1000) and rabbit anti-JNK polyclonal antibody (Cell Signaling; 1 : 500) from Mihail Iordanov (Oregon Health & Science University); rabbit anti-phospho-Akt polyclonal antibody (9271, Cell Signaling; 1 : 1000), rabbit anti-Akt rabbit polyclonal antibody (9272, Cell Signaling; 1 : 1000), and rabbit anti-p44/42 MAP kinase polyclonal antibody (9102, Cell Signaling; 1 : 1000), all from Eliot Spindel (Oregon National Primate Research Center). Blots were washed and probed with HRP-conjugated secondary antibodies (170-6515, 170-6516; BioRad; 1 : 1000), (sc-2020, Santa Cruz; 1 : 1000) for 90 min, washed, and developed with chemiluminescent substrates for 5 min (34080, 34095; Pierce).

For immunoprecipitations, equal concentrations of lysates were precleared for 30 min at 4°C with Protein G Plus/Protein A Agarose (IP10, Oncogene) or protein A Sepharose beads (170-0780-01, Amersham). Lysates were then cleared and incubated with the following antibodies overnight at 4°C: mouse anti-EGFR monoclonal antibody (05-101, Upstate; 1 : 50), mouse anti-erbB2 monoclonal antibody (c-neu Ab-3, OP15, Calbiochem; 1 : 50), rabbit anti-erbB3 (C-17) polyclonal antibody (sc-285, Santa Cruz; 1 : 200), and mouse anti-CD44 monoclonal antibodies, which were generated from the Hermes-3 hybridoma (HB-9480, ATCC; 1 : 10). The protein A/G agarose or protein A Sepharose beads, as described above, were washed and incubated with the lysates for 90 min at 4°C. The beads were then collected and washed five times in lysis buffer. Laemmli buffer was added to the lysates, boiled for 5 min, and loaded in equal concentrations onto a 5 or 7.5% SDS–polyacrylamide gel.

Construction of pEGFP-4.1B

The stop codon of 4.1B within the pcDNA3-4.1B vector was mutated and a *Bam*HI site created by mutagenesis using the following primers: forward (5′-CCA GAA GAT GGA GAG GAT GGA TCC GAG GAA TAA CTT AGC TTG CAC-3′) and reverse (5′-GTG CAA GCT AAG TTA TTC CTC GGA TCC ATC CTC TCC ATC TTC TGG-3′). In addition, a *Bam*HI site was created upstream of the 4.1B start site by an additional mutagenesis step using the following primers: forward (5′-GGC GCG CCC GGG ATC CCT GCT GAT C-3′) and reverse (5′-GAT CAG CAG GGA TCC CGG GCG CGC C-3′). The resulting pcDNA3-4.1B vector contained 4.1B flanked by *Bam*HI sites and a mutated stop codon. The mutated pcDNA3-4.1B and the pEGFP-N3 (BD Biosciences) vectors were both digested with *Bam*HI. The resulting DNA fragments were separated on an agarose gel, and the resulting 4.1B fragment as well as the linearized pEGFP vector was purified and then ligated. The resulting pEGFP-4.1B clones were verified to express the 4.1B-GFP fusion protein by transfection into MCF-10A cells, followed by immunolabeling for 4.1B and GFP.

BrdU incorporation assays and immunofluorescence

Cells were plated on coverslips and transfected with pEGFP or pEGFP-4.1B (described below) using Lipofectatime 2000 (Invitrogen) or induced to express DAL-1 with Muristerone A as described above. The cells were incubated for the indicated times, and the media were changed every 24–48 h. For the BrdU incorporation assays, BrdU (10 μM; Sigma) was added to cell media for 2 h prior to fixation. All cells were then washed in PBS and fixed in 4% paraformaldehyde for 15 min. After washing again in PBS, the cells for the BrdU assay were denatured with 2 N HCl for 20 min, and then washed extensively in PBS (4×20 min). For all immunofluorescence procedures, cells were blocked in 10% normal goat serum in PBS with 0.005% Triton X-100, and then probed with the indicated antibodies overnight. Antibodies used were rabbit anti-4.1B polyclonal antibody (Tran *et al*., 1999), mouse anti-BrdU (Ab-2) monoclonal antibody (Oncogene Research Products; 1 : 50), mouse anti-Ki67 monoclonal antibody (NCL-L-Ki67-MMI, Novocastra; 1 : 50), rabbit anti-GFP polyclonal antibody (sc-8334, Santa Cruz; 1 : 200), and Hoechst 33342 (Molecular Probes; 1 : 2000). The coverslips were then washed and probed with Alexa-Fluor-conjugated secondary antibodies (A-11029, A-11030, A-11034, A-11035, Molecular Probes; 1 : 500) and Hoechst 33342 (Molecular Probes; 1 : 2000) for 90 min before being washed and mounted. For the BrdU and Ki67 assays, MCF7-DAL-1 cells $\pm$ muristerone were assessed for BrdU or Ki67 labeling; GFP-positive MCF-10 and SKBR3 cells transfected with pEGFP or pEGFP-4.1B were assessed for BrdU or Ki67 labeling and compared to untransfected control cells.

TUNEL assay

MCF7-DAL1 cells were plated on coverslips and induced to express DAL-1 with 2 μM Muristerone A (Invitrogen). The cells were incubated for the indicated times, and the media were changed every 24–48 h. The coverslips were washed briefly in PBS and fixed in 4% paraformaldehyde for 1 h at room temperature. They were washed again in PBS and then permeabilized in 0.1% Triton X-100 in 0.1% sodium citrate and PBS for 2 min on ice. TUNEL labeling was performed using the *In situ* Cell Death Detection Kit, TMR red (Roche) according to the manufacturer's instructions. Both positive and negative controls were included with each experiment. Nuclei were labeled with Hoechst 33342 (Molecular Probes) briefly before the final washes. TUNEL-positive nuclei were counted and compared to total nuclei. Images were obtained with a Zeiss microscope using the $\times 63$ oil-immersion objective (Axioskop 40, Carl Zeiss Inc.).

Acknowledgements
We thank Sue Heffelfinger, Wallace Ip, and Nancy Ratner for helpful comments, Erik Knudsen, Eliot Spindel, and Mihael Iordanov for helpful comments and reagents. This work was supported in part by funding from the National Institutes of Health (NS39550 to LSS and NS41520 to DHG), a University of Cincinnati Distinguished Graduate Student Award (to RK), a Department of Defense grant (DAMD17-04-0266 to DHG), and an NIH grant supporting the Oregon National Primate Research Center (RR00163).

References

Akisawa N, Nishimori I, Iwamura T, Onishi S and Hollingsworth MA. (1999). *Biochem. Biophys. Res. Commun.*, **258,** 395–400.

Allred DC and Mohsin SK. (2000). *J. Mammary Gland Biol. Neoplasia*, **5,** 351–364.

Batchelor CL, Woodward AM and Crouch DH. (2004). *Exp. Cell Res.*, **296,** 208–222.
Charboneau AL, Singh V, Yu T and Newsham IF. (2002). *Int. J. Cancer*, **100,** 181–188.
Chau BN and Wang JY. (2003). *Nat. Rev. Cancer*, **3,** 130–138.
Chishti AH, Kim AC, Marfatia SM, Lutchman M, Hanspal M, Jindal H, Liu SC, Low PS, Rouleau GA, Mohandas N, Chasis JA, Conboy JG, Gascard P, Takakuwa Y, Huang SC, Benz Jr EJ, Bretscher A, Fehon RG, Gusella JF, Ramesh V, Solomon F, Marchesi VT, Tsukita S, Arpin A, Louvard D, Tonks NK, Anderson JM, Fanning AS, Bryant PJ, Woods DF and Hoover KB. (1998). *Trends Biochem. Sci.*, **23,** 281–282.
Chu I, Blackwell K, Chen S and Slingerland J. (2005). *Cancer Res.*, **65,** 18–25.
Cuppen E, Wijers M, Schepens J, Fransen J, Wieringa B and Hendriks W. (1999). *J. Cell Sci.*, **112,** 3299–3308.
Daniel CW and Smith GH. (1999). *J. Mammary Gland Biol. Neoplasia*, **4,** 3–8.
Faltus T, Yuan J, Zimmer B, Kramer A, Loibl S, Kaufmann M and Strebhardt K. (2004). *Neoplasia*, **6,** 786–795.
Fraenzer JT, Pan H, Minimo Jr L, Smith GM, Knauer D and Hung G. (2003). *Int. J. Oncol.*, **23,** 1493–1500.
Gascard P, Parra MK, Zhao Z, Calinisan VR, Nunomura W, Rivkees SA, Mohandas N and Conboy JG. (2004). *Biochim. Biophys. Acta*, **1680,** 71–82.
Gautreau A, Poullet P, Louvard D and Arpin M. (1999). *Proc. Natl. Acad. Sci. USA*, **96,** 7300–7305.
Gerdes J, Lemke H, Baisch H, Wacker HH, Schwab U and Stein H. (1984). *J. Immunol.*, **133,** 1710–1715.
Ghatak S, Misra S and Toole BP. (2005). *J. Biol. Chem.*, **280,** 8875–8883.
Gimm JA, An X, Nunomura W and Mohandas N. (2002). *Biochemistry*, **41,** 7275–7282.
Gutmann DH, Donahoe J, Perry A, Lemke N, Gorse K, Kittiniyom K, Rempel SA, Gutierrez JA and Newsham IF. (2000). *Hum. Mol. Genet.*, **9,** 1495–1500.
Gutmann DH, Hirbe AC, Huang ZY and Haipek CA. (2001). *Neurobiol. Dis.*, **8,** 266–278.
Hall IJ, Moorman PG, Millikan RC and Newman B. (2005). *Am. J. Epidemiol.*, **161,** 40–51.
Hunter KW. (2004). *Trends Mol. Med.*, **10,** 201–204.
Jhabvala-Romero F, Evans A, Guo S, Denton M and Clinton GM. (2003). *Oncogene*, **22,** 8178–8186.
Khanna C, Wan X, Bose S, Cassaday R, Olomu O, Mendoza A, Yeung C, Gorlick R, Hewitt SM and Helman LJ. (2004). *Nat. Med.*, **10,** 182–186.
Kissil JATJ. (2005).
Kittiniyom K, Gorse KM, Dalbegue F, Lichy JH, Taubenberger JK and Newsham IF. (2001). *Breast Cancer Res.*, **3,** 192–198.
Kittiniyom K, Mastronardi M, Roemer M, Wells WA, Greenberg ER, Titus-Ernstoff L and Newsham IF. (2004). *Genes Chromosomes Cancer*, **40,** 190–203.
Lutchman M and Rouleau GA. (1995). *Cancer Res.*, **55,** 2270–2274.
Mattagajasingh SN, Huang SC, Hartenstein JS, Snyder M, Marchesi VT and Benz EJ. (1999). *J. Cell Biol.*, **145,** 29–43.
McClatchey AI, Saotome I, Mercer K, Crowley D, Gusella JF, Bronson RT and Jacks T. (1998). *Genes Dev.*, **12,** 1121–1133.
Muranen T, Gronholm M, Renkema GH and Carpen O. (2005). *Oncogene*, **24,** 1150–1158.
Parra M, Gascard P, Walensky LD, Gimm JA, Blackshaw S, Chan N, Takakuwa Y, Berger T, Lee G, Chasis JA, Snyder SH, Mohandas N and Conboy JG. (2000). *J. Biol. Chem.*, **275,** 3247–3255.
Peters LL, Weier HU, Walensky LD, Snyder SH, Parra M, Mohandas N and Conboy JG. (1998). *Genomics*, **54,** 348–350.
Ponta H, Sherman L and Herrlich PA. (2003). *Nat. Rev. Mol. Cell Biol.*, **4,** 33–45.
Richert MM, Schwertfeger KL, Ryder JW and Anderson SM. (2000). *J. Mammary Gland Biol. Neoplasia*, **5,** 227–241.
Robb VA, Gerber MA, Hart-Mahon EK and Gutmann DH. (2005). *Oncogene*, **24,** 1946–1957.
Robb VA, Li W, Gascard P, Perry A, Mohandas N and Gutmann DH. (2003). *Neurobiol. Dis.*, **13,** 191–202.
Rouleau GA, Merel P, Lutchman M, Sanson M, Zucman J, Marineau C, Hoang-Xuan K, Demczuk S, Desmaze C, Plougastel B, Pulst SM, Lenoir G, Bijlsma E, Fashold R, Dumanski J, de Jong P, Parry D, Eldrige R, Aurias A, Delattre O and Thomas G. (1993). *Nature*, **363,** 515–521.
Scholzen T and Gerdes J. (2000). *J. Cell Physiol.*, **182,** 311–322.
Sebastian J, Richards RG, Walker MP, Wiesen JF, Werb Z, Derynck R, Hom YK, Cunha GR and DiAugustine RP. (1998). *Cell Growth Differ.*, **9,** 777–785.
Singh PK, Gutmann DH, Fuller CE, Newsham IF and Perry A. (2002). *Mod. Pathol.*, **15,** 526–531.
Singh V, Miranda TB, Jiang W, Frankel A, Roemer ME, Robb VA, Gutmann DH, Herschman HR, Clarke S and Newsham IF. (2004). *Oncogene*, **23,** 7761–7771.
Stern DF. (2003). *Exp. Cell Res.*, **284,** 89–98.
Stull MA, Rowzee AM, Loladze AV and Wood TL. (2004). *J. Mammary Gland Biol. Neoplasia*, **9,** 15–26.
Surace EI, Lusis E, Murakami Y, Scheithauer BW, Perry A and Gutmann DH. (2004). *J. Neuropathol. Exp. Neurol.*, **63,** 1015–1027.
Tran Y, Benbatoul K, Gorse K, Rempel S, Futreal A, Green M and Newsham I. (1998). *Oncogene*, **17,** 3499–3505.
Tran YK, Bogler O, Gorse KM, Wieland I, Green MR and Newsham IF. (1999). *Cancer Res.*, **59,** 35–43.
Trofatter JA, MacCollin MM, Rutter JL, Murrell JR, Duyao MP, Parry DM, Eldridge R, Kley N, Menon AG, Pulaski K, Haase VH, Ambrose CM, Munroe D, Bove C, Haines JL, Martuza RL, MacDonald ME, Seizinger BR, Short MP, Buckler AJ and Gusella JF. (1993). *Cell*, **72,** 791–800.
Tsukita S, Oishi K, Sato N, Sagara J and Kawai A. (1994). *J. Cell Biol.*, **126,** 391–401.
Tyler JM, Hargreaves WR and Branton D. (1979). *Proc. Natl. Acad. Sci. USA*, **76,** 5192–5196.
Tzahar E, Waterman H, Chen X, Levkowitz G, Karunagaran D, Lavi S, Ratzkin BJ and Yarden Y. (1996). *Mol. Cell. Biol.*, **16,** 5276–5287.
Whiteman MK, Hillis SD, Curtis KM, McDonald JA, Wingo PA and Marchbanks PA. (2004). *Obstet. Gynecol.*, **104,** 146–154.
Wobus M, Rangwala R, Sheyn I, Hennigan R, Coila B, Lower EE, Yassin RS and Sherman LS. (2002). *Appl. Immunohistochem. Mol. Morphol.*, **10,** 34–39.
Yageta M, Kuramochi M, Masuda M, Fukami T, Fukuhara H, Maruyama T, Shibuya M and Murakami Y. (2002). *Cancer Res.*, **62,** 5129–5133.
Yarden Y and Sliwkowski MX. (2001). *Nat. Rev. Mol. Cell Biol.*, **2,** 127–137.
Yu Y, Khan J, Khanna C, Helman L, Meltzer PS and Merlino G. (2004). *Nat. Med.*, **10,** 175–181.

Somatic inactivation of *Nf1* in hematopoietic cells results in a progressive myeloproliferative disorder

Doan T. Le, Namie Kong, Yuan Zhu, Jennifer O. Lauchle, Abigail Aiyigari, Benjamin S. Braun, Endi Wang, Scott C. Kogan, Michelle M. Le Beau, Luis Parada, and Kevin M. Shannon

The *NF1* tumor suppressor gene encodes a guanosine triphosphotase (GTPase)–activating protein that negatively regulates Ras signaling and is inactivated in a subset of juvenile myelomonocytic leukemias (JMMLs). Adoptive transfer of fetal liver cells from *Nf1* mutant mice models JMML; however, this system has important limitations as a platform for performing biologic and preclinical studies. We have exploited the interferon-inducible *Mx1-Cre* transgene to ablate a conditional mutant *Nf1* allele in hematopoietic cells. Somatic inactivation of *Nf1* induces a myeloproliferative disorder with 100% penetrance that is associated with a subacute clinical course, tissue infiltration by myeloid cells, hypersensitivity to granulocyte-macrophage colony stimulating factor, hyperproliferation, and resistance to apoptosis. These *Mx1-Cre, Nf1$^{flox/flox}$* mice establish a tractable experimental model for testing therapeutics and for identifying mutations that cooperate with hyperactive Ras in myeloid leukemogenesis. (Blood. 2004;103:4243-4250)

Introduction

Juvenile myelomonocytic leukemia (JMML) is an aggressive myeloproliferative disease (MPD) characterized by monocytosis, thrombocytopenia, splenomegaly, and malignant infiltration of the skin, lymph nodes, lungs, liver, and other organs (reviewed in Emanuel et al[1] and Arico et al[2]). The clinical course is relentless, and bone marrow transplantation is the only treatment that cures more than 10% of patients. Selective hypersensitivity of granulocyte-macrophage colony-forming unit (CFU-GM) progenitors to granulocyte-macrophage colony-stimulating factor (GM-CSF) is an in vitro hallmark of JMML.[3,4] The incidence of JMML is increased more than 200-fold in children with neurofibromatosis type 1 (NF1)[5,6]; this observation provided a starting point for elucidating the molecular basis of aberrant myeloid growth in this disorder. The *NF1* gene encodes neurofibromin, a guanosine triphosphotase (GTPase)–activating protein (GAP) that negatively regulates p21^{ras} (Ras) output by accelerating GTP hydrolysis (reviewed in Boguski and McCormick,[7] Bernards,[8] and Donovan et al[9]). Analysis of JMML cells from children with NF1 revealed homozygous *NF1* inactivation because of somatic loss of the normal allele, which is associated with hyperactive Ras.[10-13]

Two groups used homologous recombination in embryonic stem cells to disrupt *Nf1,* the murine homolog of *NF1*.[14,15] Approximately 10% of heterozygous (*Nf1*$^{+/-}$) mutant mice spontaneously develop a MPD that resembles JMML during the second year of life.[14] Homozygous mutant (*Nf1*$^{-/-}$) embryos fail around embryonic day 13 (E13) with cardiovascular defects[14,15]; however, CFU-GM colonies derived from mutant fetal livers show hypersensitive growth in response to GM-CSF that is similar to human JMML cells.[11,16] Importantly, adoptive transfer of *Nf1*$^{-/-}$ fetal liver cells consistently induces a JMML-like MPD in irradiated recipient mice.[16] *Nf1* inactivation leads to deregulated growth in multiple hematopoietic compartments and confers a durable proliferative advantage in competitive repopulation assays.[17,18] In addition, a cross between *Nf1* and *Gmcsf* mutant mice demonstrated that aberrant GM-CSF signaling plays a central role in initiating and maintaining the JMML-like MPD in vivo.[19]

In a previous study, irradiated recipient mice that received transplants with *Nf1*$^{-/-}$ fetal liver cells were harnessed to evaluate the efficacy of an inhibitor of the Ras processing enzyme farnesyltransferase, which included pharmacodynamic monitoring in primary hematopoietic cells.[20] However, this model is both expensive and cumbersome because it requires maintaining a large breeding colony, performing multiple timed matings followed by embryo dissections around E13, and injecting fetal liver cells into irradiated hosts. A "second-generation" mutant strain was recently engineered by introducing loxP sites into the *Nf1* locus by homologous recombination.[21] Somatic inactivation of this *Nf1^{flox}* allele, which is functionally wild type in the basal state, can be achieved by expressing Cre recombinase in specific cell types.[21,22] We have exploited the interferon-inducible *Mx1-Cre* strain[23] to ablate *Nf1* in hematopoietic cells, and we find that this consistently results in an MPD that is associated with leukocytosis, splenomegaly, hyperproliferation, impaired apoptosis, and in vitro hypersensitivity to GM-CSF. We further describe the consequences of *Nf1* inactivation on proliferation, survival, and Ras signaling in these mice.

From the Department of Pediatrics, University of California, San Francisco, California; the Department of Laboratory Medicine, University of California, San Francisco, California; University of Texas Southwestern, Dallas, Texas; Section of Hematology/Oncology, Department of Medicine, and The Cancer Research Center, University of Chicago, Chicago, Illinois.

Submitted August 7, 2003; accepted December 4, 2003. Prepublished online as *Blood* First Edition Paper, February 24, 2004; DOI 10.1182/blood-2003-08-2650.

Supported by the U.S. Army Neurofibromatosis Research Program (Project DAMD 17-02-1-0638), the National Institutes of Health (grants CA84221and CA72614), the Jeffrey and Karen Peterson Family Foundation, and the Frank A. Campini Foundation.

Reprints: Kevin M. Shannon, University of California, San Francisco, 513 Parnassus Ave, HSE 302, San Francisco, CA 94143; e-mail: kevins@itsa.ucsf.edu.

The publication costs of this article were defrayed in part by page charge payment. Therefore, and solely to indicate this fact, this article is hereby marked "advertisement" in accordance with 18 U.S.C. section 1734.

Materials and methods

Breeding and treatment with polyinosinic-polycytidylic acid (pI-pC)

Nf1^{flox} and *Mx1-Cre* mice were produced and characterized as described elsewhere.[21,23] Compound mutant (*Mx1-Cre*, *Nf1*$^{flox/flox}$) animals were generated on a mixed 129/Sv × C57BL/6 background. Pups received a single intraperitoneal injection at 3 to 5 days of age with 50 μL pI-pC (Sigma, St Louis, MO) at a concentration of 10 μg/μL diluted in sterile phosphate-buffered saline (PBS). Mice were maintained in the sterile animal care facility at the University of California, San Francisco (UCSF) and were fed pelleted chow and acidified water ad libitum. The experimental procedures were approved by the UCSF Committee on Animal Research.

Genotyping

We isolated DNA from blood samples using the GFX Genomic Blood DNA Purification Kit (Amersham, Arlington Heights, IL). Genotyping of the *Nf1*^{flox} and recombined allele was carried out by using the primer sequence and polymerase chain reaction (PCR) conditions as described by Zhu et al.[21] Genotyping for the *Mx1-Cre* allele was performed by using primers Cre1 (5′-CTG CAT TAC CGG TCG ATG CAA C-3′) and Cre2 (5′-GCA TTG CTG TCA CTT GGT CGT G-3′). Thermal cycle conditions were 94°C for 5 minutes and then 32 cycles of 94°C for 30 seconds and 70°C for 1 minute. The presence of a 300-bp band is indicative of the *Mx1-Cre* transgene.

Monitoring and isolation of hematopoietic cells

Mice were bled at 1.5, 3, and 5 months of age by nicking the dorsal tail veins with a surgical blade. Tail-vein blood samples (50-100 μL) were obtained for complete blood counts (CBCs). Samples were analyzed by using a Hemavet 850FS (DREW Scientific, Oxford, CT). Automated differential cell counts were used to monitor differentiated leukocyte populations over time. Criteria for killing mice by CO_2 inhalation included a disheveled appearance, hunching, abnormal gait, and pallor. Bone marrow cells were collected by removing tibias and femurs and flushing out the marrow cavity with Iscove modified Dulbecco medium (IMDM; GIBCO-BRL, Gaithersburg, MD) supplemented with 20% fetal calf serum (FCS; Hyclone Laboratories, Logan, UT). Single cell suspensions were prepared by gently drawing the cells through a 25-gauge needle. Cell viabilities were ascertained by trypan blue exclusion.

Pathologic analysis and flow cytometry

Blood smears and cytospins were stained with Wright Giemsa (Sigma). Spleens and sternums were collected and sent for sectioning to the Mouse Pathology Shared Resource at the UCSF Comprehensive Cancer Center. CBCs were measured in peripheral blood, and manual differential counts (100-400 cells) were determined from Wright Giemsa–stained smears (blood) or cytospins (bone marrow or spleen) by using published recommendations.[24] Fluorescence activated cell sorting (FACS) analysis was performed on peripheral blood, bone marrow, and splenocytes. Peripheral blood cells were incubated in red blood cell lysis buffer (0.16 M NH_4Cl, 0.1 M $KHCO_3$, 0.1 mM EDTA [ethylenediaminetetraacetic acid]) for 10 minutes at room temperature. The cells were washed twice in PBS and resuspended in PBS/0.1% bovine serum albumin (BSA), divided into aliquots, and placed in tubes; antibodies were added on ice to prevent capping. Isotype control antibodies conjugated to the fluorochromes fluorescein isothiocyanate (FITC) or phycoerythrin (PE) were used to determine background fluorescence, and a panel of lineage-specific antibodies was used, including CD3, B220, Gr-1, Mac1, c-kit, and Sca-1 (all antibodies from Pharmingen). Analysis was performed using FlowJo (Tree Star, San Carlos, CA), and data were collected using CellQuest software (Becton Dickinson, San Jose, CA).

Spectral karyotyping (SKY) analysis

Cytogenetic analysis was performed on spleen cells from mice with MPD. The initiation of short-term (24 hours) cultures, metaphase cell preparation, and spectral karyotyping were performed as described previously.[25] A minimum of 10 metaphase cells were analyzed per case.

Adoptive transfer protocol

Recipient mice were lethally irradiated with a single fraction of 900 cGy by using a cesium source that delivered irradiation at 227 rad/min. Sublethal irradiation was administered at a dose of 450 cGy. Recipient mice (8 weeks old) were injected with donor cells immediately after irradiation. Mice were warmed for 5 minutes under a heat lamp to induce tail-vein dilation. Hematopoietic cells (2×10^6 per recipient) were suspended in 500 μL IMDM with 20% FCS and injected through a 28-gauge needle into the dorsal tail vein. Recipients received prophylactic oral antibiotics, consisting of polymyxin sulfate and neomycin sulfate for 2 weeks after irradiation. CBCs were measured serially between 7 and 24 weeks after transplantation.

Progenitor growth

CFU-GM colonies were grown from bone marrow cells and splenocytes. These assays were performed in methylcellulose medium (Stem Cell Technologies, Vancouver, BC, Canada) containing glutamine, penicillin/streptomycin, β-mercaptoethanol (BME), and varying doses of recombinant murine GM-CSF. Bone marrow and spleen cells were cultured at 5×10^4 and 1×10^5 cells/mL, respectively. Duplicate plates containing 1 mL medium were established and incubated at 37°C in 5% CO_2 for 8 days. The colonies were scored through a binocular light microscope under 4 × magnification. To assess the effects of 13 *cis* retinoic acid (13*c*RA) on CFU-GM growth, various concentrations of the drug (10^{-4} M to 10^{-6} M) diluted in dimethyl sulfoxide (DMSO) were added to the medium immediately before plating.

Proliferation assay

The incorporation of 5-bromo-2-deoxyuridine (BrdU; Sigma) was measured in vivo in mice that were injected intraperitoneally with 1 mg BrdU/6 g body weight. The mice were killed 6 hours later, and marrow cells and splenocytes were collected and resuspended in IMDM supplemented with 20% FCS. Red cell lysis was performed as described in "Monitoring and isolation of hematopoietic cells," and the cells were washed with PBS. Cells were incubated overnight with 1% paraformaldehyde and 0.01% Tween-20 at 4°C, washed twice with PBS, and resuspended in DNAse (Sigma) for 30 minutes at 37°C. After 2 additional washes with PBS, cells were stained with BrdU-FITC (Pharmingen) for 20 minutes. The cells were washed twice with PBS and then analyzed by flow cytometry.

Apoptosis assay

Bone marrow cells were harvested in IMDM supplemented with 20% FCS, and the red cells were lysed as described in "Proliferation assay." The cells were resuspended in PBS with 2% FCS and 1.5 mM calcium chloride before staining with Annexin-GFP (a gift from Dr Joel Ernst, University of California, San Francisco) for 15 minutes at 4°C. The labeled cells were washed once in PBS and then analyzed by flow cytometry.

Isolation of Mac1-positive bone marrow cells

Bone marrow cells were harvested from tibias and femurs in 0.1% serum without growth factors and were labeled with an antimouse CD11b (Mac1)–PE antibody (1:50; Pharmingen) after red cell lysis. The stained cells were incubated with paramagnetic anti-PE microbeads (Miltenyi Biotech, Bergisch Gladbach, Germany) for 15 minutes at 4°C. The cells were passed through a 40-μ filter and were separated on an AutoMACS instrument using program Possel (Miltenyi Biotech). This procedure consistently yields more than 98% Mac1-positive cells.

Western blotting and Ras-GTP assay

Unfractionated bone marrow or Mac1-positive cells were incubated in 0.1% serum without growth factors for 4 hours, then stimulated with 0 or 10 ng/mL GM-CSF for 5 minutes. The cells were washed once with PBS containing 1 mM sodium orthovanadate and lysed in 25 mM HEPES (*N*-2-hydroxyethylpiperazine-*N*′-2-ethanesulfonic acid), pH 7.5, 150 mM

NaCl, 1% NP-40, 0.25% Na deoxycholate, 10% glycerol, 10 mM $MgCl_2$, 25 mM NaF, 1 mM Na orthovanadate, and COMPLETE protease inhibitors (Amersham). Protein concentrations were quantitated and equalized for loading by using the Bio-Rad protein assay (Bio-Rad, Hercules, CA). Samples were boiled for 5 minutes in 1 × Laemli buffer, run on a 10% Tris (tris(hydroxymethyl)aminomethane)–HCl Criterion Precast Gel (Bio-Rad), and transferred onto a nitrocellulose membrane. The membranes were blocked for 1 hour in TBS-Tween containing 5% milk prior to overnight incubation at 4°C with antiphospho-MEK 1/2 (mitogen-activated protein kinase kinase 1 and 2; 1:500; Cell Signaling Technologies, Beverly, MA), antiphospho-Akt (1:5000; a gift from Dr David Stokoe, University of California, San Francisco), anti-MEK 1/2 (1:5000; Cell Signaling Technologies), and anti-Akt (1:1000; Cell Signaling Technologies). The blots were developed with a horseradish peroxidase–conjugated secondary antirabbit antibody (Amersham). Proteins were visualized by enhanced chemiluminescence (Amersham). Ras-GTP levels were measured as described elsewhere by precipitating GTP-bound Ras with a fusion protein that includes the Ras binding domain of Raf.[26]

Results

Mx1-Cre, Nf1$^{flox/flox}$, and *Nf1*$^{flox/flox}$ littermates received a single injection of pI-pC (500 μg in 50 μL) at 3 to 5 days of age and were genotyped at weaning by analyzing DNA prepared from tail clips. As an additional control, some litters that were not treated with pI-pC were observed for signs of systemic illness. PCR analysis of DNA extracted from peripheral blood leukocytes at 6 weeks of age demonstrated complete excision of exons 31 and 32 in *Mx1-Cre, Nf1*$^{flox/flox}$ mice that received pI-pC (Figure 1A). Somatic inactivation of *Nf1* was dependent on inheritance of the *Mx1-Cre* transgene (Figure 1A). Consistent with previous data, the *Mx1-Cre* transgene was active in other tissues, and we detected partial inactivation of *Nf1* in kidney, lung, and other tissues (data not shown).

Cohorts of mice were observed for evidence of disease and by performing serial blood counts. Leukocyte counts and the numbers of differentiated myeloid and lymphoid cells were significantly elevated in the *Mx1-Cre, Nf1*$^{flox/flox}$ animals by 3 months of age (Figure 1B). Blood smears revealed increased numbers of morphologically normal lymphocytes, monocytes, and neutrophils. Animals with marked leukocytosis showed occasional intermediate myeloid forms (Figure 1C). Hemoglobin concentrations as well as red blood cell and platelet counts remained within the normal range (data not shown). *Mx1-Cre, Nf1*$^{flox/flox}$ mice developed overt signs of disease beginning between 5 and 6 months of age, which was characterized by hunching, abnormal gait, and a disheveled appearance, and 50% of the animals succumbed by 7.5 months (Figure 1D). This clinical syndrome was generally not accompanied by dramatic changes in peripheral blood counts, and transformation to acute leukemia did not occur. The development of MPD in *Nf1*$^{flox/flox}$ mice was dependent on the presence of the *Mx1-Cre* transgene. Interestingly, *Mx1-Cre, Nf1*$^{flox/flox}$ mice that were not injected with pI-pC occasionally developed MPD. These animals showed somatic inactivation of *Nf1* in blood and bone marrow, which was likely because of endogenous interferon production in response to a subclinical infection or another stimulus (data not shown).

Pathologic analysis of sick *Mx1-Cre, Nf1*$^{flox/flox}$ mice revealed progressive splenomegaly with extensive infiltration of myeloid cells at various stages of maturation (Figure 2A-C). There was periportal invasion within the liver (Figure 2B) but not in other tissues. The bone marrow was highly cellular and comprised myeloid cells at various stages of differentiation (Figure 2C-D). FACS analysis confirmed the presence of a high percentage of myeloid cells (Mac1$^+$ and Gr1$^+$ cells) (Figure 2E). Increased numbers of Mac-1$^+$, Gr-1^{lo} cells, which are likely to represent immature monocytic cells, were identified consistently. Cytogenetic and spectral karyotype analysis of spleen samples from 6 diseased mice did not reveal clonal karyotypic abnormalities. According to guidelines published by the Hematopathology Subcommittee of the Mouse Models of Human Cancer Consortium (MMHCC),[24] this disorder is classified as a myeloproliferative disease. This MPD models many features of human JMML, including increased numbers of differentiated granulocytic and monocytic cells, hypersensitivity to GM-CSF (see later in this section), and a subacute course. It is similar to the MPD that arises in lethally irradiated mice that are repopulated with homozygous *Nf1*-deficient fetal liver cells[16,19]; however, the course is somewhat more indolent. A complete histologic and FACS panel on the model has been posted on the MMHCC website (http://emice.nci.nih.gov/emice/mouse_models/organ_models/hema_models/hema_mouse_class/myelopro_disease/mpd).

A recent study in which a *Krox20-Cre* transgene was used to ablate *Nf1* in Schwann cells found that the incidence and penetrance of benign neurofibromas was markedly increased in a heterozygous mutant background (ie, in *Krox20-Cre, Nf1*$^{flox/-}$ versus *Krox20-Cre, Nf1*$^{flox/flox}$ mice).[22] On the basis of these data, we generated *Mx1-Cre, Nf1*$^{flox/-}$ mice to determine whether heterozygous inactivation of *Nf1* in nonhematopoietic cells present in the bone marrow microenvironment might modulate the subacute course of the MPD. In this experiment, *Mx1-Cre, Nf1*$^{flox/-}$ pups that were injected with pI-pC at 3 to 5 days of age developed MPD with similar blood counts, disease latency, and survival as *Mx1-Cre, Nf1*$^{flox/flox}$ mice (data not shown).

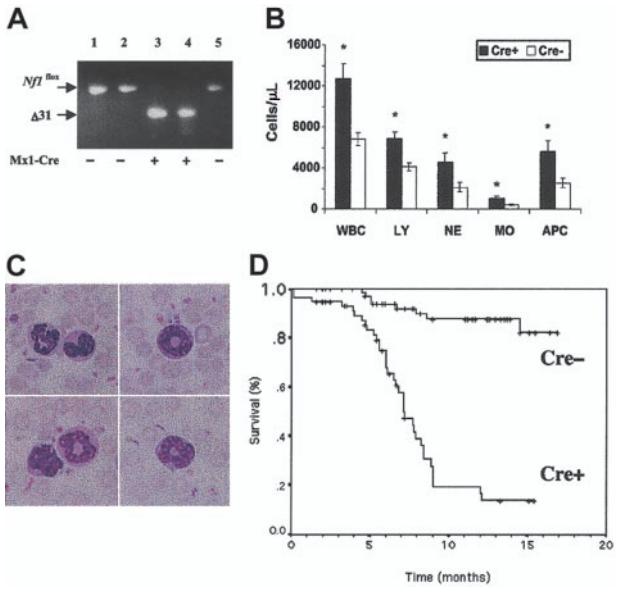

Figure 1. Blood leukocyte values and survival in *Mx1-Cre, Nf1*$^{flox/flox}$ and *Nf1*$^{flox/flox}$ mice. (A) PCR analysis of leukocyte DNA from 6-week-old pups that received a single injection of pI-pC shortly after birth. PCR amplification of the unrearranged *Nf1*^{flox} allele yields a 350-bp product. A 280-bp fragment corresponding to a deletion of exon 31 (Δ31) is visible in 2 pups that inherited the *Mx1-Cre* transgene (+) but not in 3 pups that did not (−). Absence of the unrearranged allele in lanes 3 and 4 confirms a high efficiency of somatic recombination. (B) White blood cell counts (WBCs) in 3-month-old pI-pC–treated *Mx1-Cre, Nf1*$^{flox/flox}$ (Cre$^+$) (n = 21) and control *Nf1*$^{flox/flox}$ littermates that did not inherit the *Mx1-Cre* transgene (Cre$^-$) (n = 18). The abbreviations are LY, lymphocytes; NE, neutrophils; MO, monocytes; APC, absolute phagocyte count (neutrophils + monocytes). Leukocyte counts are expressed as ± SEM. Asterisks indicate significant differences ($P < .05$ by Student *t* test) between the Cre$^+$ and Cre$^-$ animals. (C) A composite photomicrograph (original magnification × 400) of peripheral blood from a Cre$^+$ mouse shows mature neutrophils (top left), intermediate forms (top right), a monocyte and a mature neutrophil (bottom left), and an intermediate form, which is likely in the monocytic lineage (bottom right). (D) Kaplan-Meier analysis demonstrates a significant reduction in survival in Cre$^+$ (n = 59) versus Cre$^-$ (n = 72) littermates ($P < .0001$).

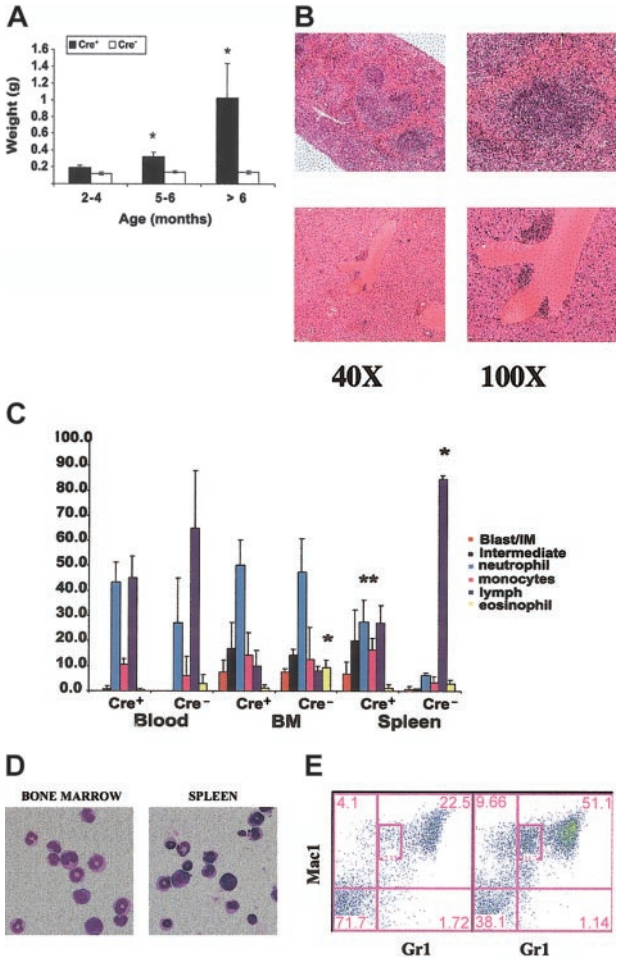

Figure 2. Pathologic analysis of tissues from *Mx1-Cre, Nf1 flox/flox* mice. (A) Cre$^+$ mice demonstrate progressive splenomegaly. Data are presented as the mean ± SEM. (A,C) Asterisks indicate significant differences ($P < .05$) between the Cre$^+$ and Cre$^-$ animals. (B) Spleen (top) sections from Cre$^+$ mice demonstrate expansion of the red pulp with myeloid infiltration. Liver sections (bottom) show periportal infiltration. (C) Manual differential counts of the percentage of nonerythroid cells in blood, bone marrow (BM), and spleen from Cre$^+$ and Cre$^-$ mice. Note that the bone marrow myeloid cells show a normal pattern of differentiation and that the spleen shows a massive increase in myelopoiesis. The data are shown as the mean ± SD. (D) Cytospins of bone marrow and spleen in a Cre$^+$ mouse with MPD show maturing neutrophilic and monocytic elements (original magnification × 200). (E) Representative FACS data from Cre$^-$ (left) and Cre$^+$ (right) bone marrows. Cre$^+$ mice with MPD demonstrate an increased percentage of Gr1$^+$/Mac1$^+$ cells (51% versus 22%). There is marked expansion in the Mac-1$^+$/Gr-1^{lo} subset (11.5% in Cre$^+$ versus 2.13% in Cre$^-$ mice), which is consistent with an increase in monocytic cells. The numbers shown indicate the percentage of cells within each quadrant.

JMML bone marrows and *Nf1*$^{-/-}$ fetal liver cells form increased numbers of CFU-GM colonies in the presence of nonsaturating concentrations of recombinant murine GM-CSF.[3,11,16,17] We detected elevated numbers of CFU-GM in the bone marrows of *Mx1-Cre, Nf1*$^{flox/flox}$ mice that were hypersensitive to GM-CSF (Figure 3A-B). In addition, mutant CFU-GM colonies were larger than normal and showed an abnormal spreading morphology (Figure 3C-D). Increased proliferation of myeloid progenitors from *Mx1-Cre, Nf1*$^{flox/flox}$ mice was also reflected by a 2- to 3-fold expansion in the number of cells recovered from methylcellulose cultures stimulated with 10 ng/mL recombinant murine GM-CSF. Wright-Giemsa staining revealed a higher percentage of monocyte-macrophage cells in *Mx1-Cre, Nf1*$^{flox/flox}$ cultures than in the control cultures (Figure 3E-F). Consistent with the myeloid infiltration visible in pathologic sections, the spleens of *Mx1-Cre, Nf1*$^{flox/flox}$ mice contained large numbers of CFU-GM, which formed colonies that were similar in size and morphology to those found in the bone marrow. By contrast, no CFU-GM colonies were obtained from the spleens of control mice (data not shown).

Retinoids partially correct the abnormal pattern of CFU-GM colony growth that is a hallmark of JMML,[1,27] and 13*c*RA induces transient clinical and hematologic improvement in some patients.[28] We, therefore, compared the effects of 13*c*RA on CFU-GM growth from *Mx1-Cre, Nf1*$^{flox/flox}$ and control bone marrows. As shown in Figure 3, *Mx1-Cre, Nf1*$^{flox/flox}$ marrows contained elevated numbers of CFU-GM, which were larger than wild-type colonies. Addition of 10^{-6} to 10^{-4} M 13*c*RA to methylcellulose cultures stimulated with 10 ng/mL GM-CSF induced proliferation of background cells as well as a dose-dependent reduction in the size of CFU-GM colonies. These effects were not selective but were observed in both mutant and wild-type cultures. Furthermore, 13*c*RA treatment was not associated with a reduction in the abnormally high percentage of monocyte-macrophage cells in CFU-GM grown from *Mx1-Cre, Nf1*$^{flox/flox}$ mice (data not shown).

Bone marrow mononuclear cells from *Mx1-Cre, Nf1*$^{flox/flox}$ mice that had been treated with pI-pC were injected into lethally (n = 10) or sublethally (n = 10) irradiated recipients to ascertain whether the MPD could be transferred to secondary hosts. Each lethally irradiated recipient was repopulated with mutant cells and developed MPD (Figure 4A). By contrast, the leukocyte counts of mice that received a sublethal dose of irradiation remained normal over 6 months of observation (Figure 4A). Analysis of DNA extracted from blood leukocytes 2 to 4 months after transplantation revealed both host and donor-derived cells in all recipients (data not shown). *Nf1*-deficient cells made a sustained contribution to hematopoiesis in many animals, including some in which the wild-type band disappeared from the blood after 6 months (Figure 4B). Interestingly, pathologic evaluation of sublethally irradiated mice that were killed 8 months after injection of *Nf1*$^{-/-}$ cells revealed normal spleen size and architecture and no splenic CFU-GM despite a substantial contribution of mutant cells to the peripheral blood (data not shown).

We measured BrdU incorporation and performed annexin V staining to ascertain the effects of *Nf1* inactivation on the proliferation and survival of primary hematopoietic cells. *Mx1-Cre, Nf1*$^{flox/flox}$ mice with MPD and controls were killed 6 hours after a single injection of BrdU, and the percentages of bone marrow and spleen cells that had incorporated the label were determined by flow cytometry. Whereas the fraction of BrdU-positive cells was similar in the bone marrows of diseased and control animals, proliferation was substantially greater within the spleens of *Mx1-Cre, Nf1*$^{flox/flox}$ mice (Figure 5A). Because the percentages of erythroid and myeloid cells in bone marrow and spleen differ markedly between *Mx1-Cre, Nf1*$^{flox/flox}$ and control mice, we also assessed BrdU incorporation in Mac1$^+$ cells. Interestingly, proliferation was comparable in bone marrow–derived cells; however, a higher percentage of splenic Mac1$^+$ cells was labeled in the *Mx1-Cre, Nf1*$^{flox/flox}$ mice (Figure 5B). Apoptosis was assessed by performing flow cytometry on bone marrow cells that had been labeled with an annexin V–green fluorescent protein (GFP). The percentage of freshly isolated cells stained by annexin-V was similar in *Mx1-Cre, Nf1*$^{flox/flox}$ and normal mice (data not shown); however, the mutant cells displayed greatly enhanced survival after 24 hours in culture without exogenous growth factors (Figure 5C).

We compared the percentage of Ras in the active GTP-bound conformation and assayed activation of the Ras effectors Akt and MEK in bone marrow mononuclear cells isolated from *Mx1-Cre, Nf1*$^{flox/flox}$ and normal mice. Unstimulated mutant cells showed a modest increase in baseline Ras-GTP levels (Figure 6A,C), but phosphorylation of the downstream effectors MEK and Akt were similar in unfractionated mutant and control bone marrows (Figure 6B-C). Exposure to GM-CSF induced robust Ras-GTP, MEK, and

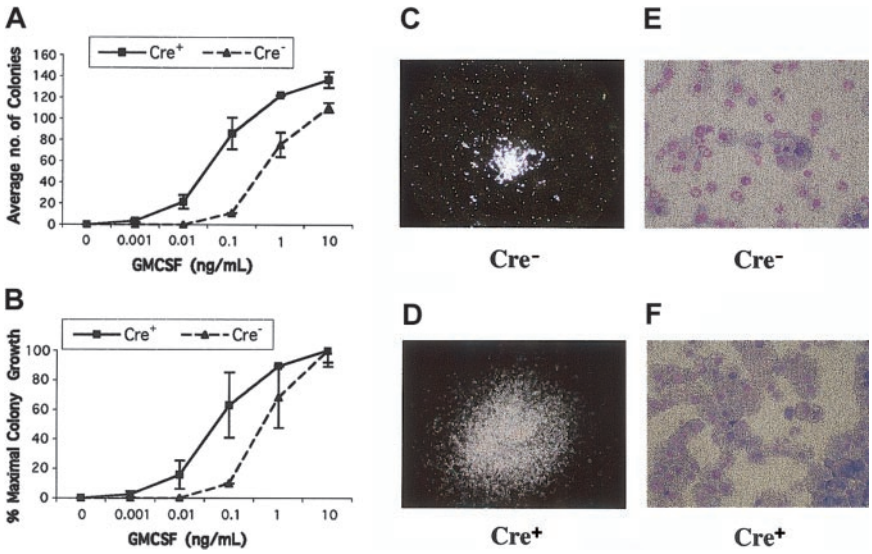

Figure 3. CFU-GM colony growth from *Mx1-Cre, Nf1*$^{flox/flox}$ and Cre$^-$ mice. (A-B) CFU-GM colony growth at various concentrations of GM-CSF. Bone marrow mononuclear cells were plated in duplicate in methylcellulose. Cre$^+$ bone marrow from mice with MPD show a left shift in the GM-CSF dose-response curve when expressed in terms of total numbers of colonies (A) or the calculated percentage of maximal colony growth (B). Colony numbers in duplicate 1-mL plates are shown with ranges from a representative experiment. (C-D) CFU-GM colonies grown from *Mx1-Cre, Nf1* $^{flox/flox}$ and control mice photographed at 40 × magnification. A typical CFU-GM morphology from a normal mouse is shown in panel C at 40 × magnification. The colonies grown from Cre$^+$ mice with MPD are larger and show abnormal spreading (D). (E-F) Cytospins of CFU-GM colonies stained with Wright-Giemsa from a wild-type mouse (E) contain approximately 70% neutrophils compared with 93% monocyte-macrophage cells in Cre$^+$ mice. Original magnification, × 500 for panels E and F.

Akt activation from baseline levels that was equivalent in both genotypes (Figure 6B-C). Because *Nf1*$^{-/-}$ and wild-type bone marrows showed marked differences with respect to the relative proportions of different cell types, we isolated Mac1-positive cells and compared MEK activation in this myeloid subpopulation. In these experiments, *Nf1*$^{-/-}$ cells showed sustained activation of MEK after exposure to GM-CSF (Figure 6D).

Discussion

We have developed a robust and tractable model of MPD by harnessing the *Mx1-Cre* transgene to induce somatic inactivation of the *Nf1* tumor suppressor and have used these *Mx1-Cre, Nf1*$^{flox/flox}$ mice to investigate how loss of *Nf1* perturbs the in vivo growth of primary hematopoietic cells. This work extends previous studies of cultured *Nf1*-deficient fetal liver cells and of recipient mice repopulated with these cells.[11,16-19]

We selected the *Mx1-Cre* strain on the basis of data from other laboratories that imply that this Cre recombinase is active in both hematopoietic stem cells and in differentiated progeny.[29-31] By inducing biallelic excision of a targeted locus, we could readily monitor the relative levels of recombined and unrearranged *Nf1* in blood and bone marrow. We found that a single injection of pI-pC resulted in highly efficient *Nf1* inactivation in all lineages. These results and our data showing that bone marrow from *Mx1-Cre, Nf1*$^{flox/flox}$ mice mediate long-term reconstitution in lethally irradiated recipients provide strong evidence that *Nf1* is inactivated in the stem-cell compartment. Furthermore, although the ultimate contribution of cells that have undergone somatic recombination to hematopoiesis will be influenced by both the structure of the loxP-targeted allele and by how rearranging the locus modulates cell survival and proliferation, our data underscore the value of the *Mx1-Cre* strain for modifying conditional mutant alleles in hematopoietic cells. Importantly, although we detected significant levels of somatic *Nf1* inactivation in some nonhematopoietic tissues, this was not associated with any overt phenotypes in mice observed for 9 to 12 months. However, this lack of specificity could be problematic for analyzing other conditional mutations.

Somatic inactivation of *Nf1* results in progressive splenomegaly with a shift in hematopoiesis from the marrow to the spleen, and we identified proliferating myeloid cells within the spleens of *Mx1-Cre, Nf1*$^{flox/flox}$ mice. Splenomegaly is a prominent feature of JMML, and many centers perform splenectomies before transplantation. Although the benefits of this procedure are unclear, our data suggest that the spleen is an important site of disease that contributes to the evolution of the murine MPD. We also found that bone marrow cells from *Mx1-Cre, Nf1*$^{flox/flox}$ mice are resistant to apoptosis, which is consistent with data from *Myb*-transformed myeloid cell lines.[26]

Previous studies of mice repopulated with *Nf1*$^{-/-}$ cells have emphasized the effects of *Nf1* inactivation on stem cells and myeloid lineage progenitors.[16,17,19] However, limited attention has been paid to lymphopoiesis. In addition to uniformly developing MPD, *Mx1-Cre,*

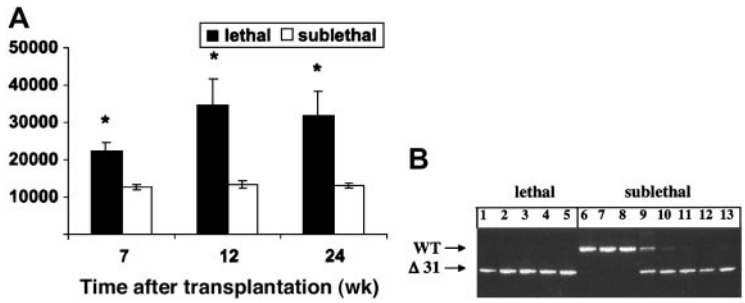

Figure 4. Adoptive transfer of marrow cells from *Mx1-Cre, Nf1* $^{flox/flox}$ mice with MPD. (A) WBCs in recipient mice that received a lethal or sublethal dose of radiation over time. Cells from 2 Cre$^+$ mice were injected into equal numbers of lethally and sublethally irradiated mice. Data represent the mean ± SEM. Asterisks indicate significant differences between recipients that received lethal versus sublethal radiation ($P < .05$). (B) PCR analysis of blood leukocytes from lethally irradiated recipients demonstrates reconstitution with mutant (Δ31) cells with absence of a signal from the wild-type host (lanes 1-5). By contrast, some sublethally irradiated recipients that were analyzed 6 months after adoptive transfer showed absence of mutant Δ31 cells (lanes 6-8), some showed repopulation with donor cells (lanes 11-13), and others demonstrated the presence of both wild-type and mutant cells (lanes 9,10). None of these sublethally irradiated recipients had developed evidence of MPD by 8 months after adoptive transfer.

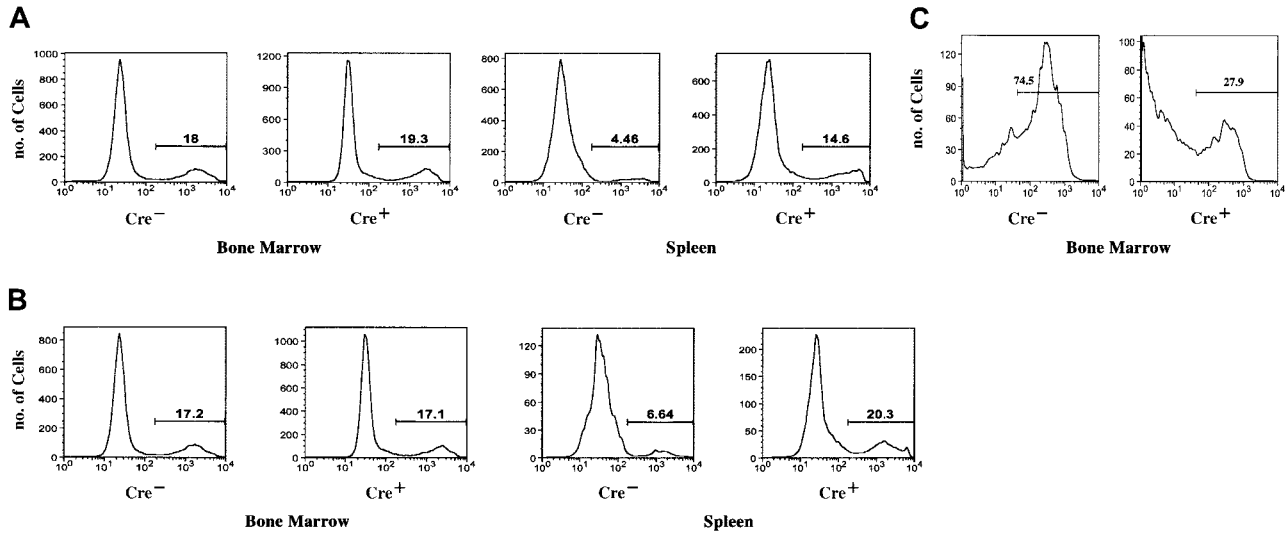

Figure 5. Proliferation and apoptosis in *Mx1-Cre, Nf1 flox/flox* and Cre⁻ mice. (A) BrdU incorporation in vivo by Cre⁺ and Cre⁻ bone marrow cells and splenocytes. Increased proliferation is seen in the spleens of Cre⁺ mice (14.6% versus 4.5% labeled cells). (B) BrdU labeling of Mac1⁺ cells from Cre⁺ and Cre⁻ mice. A higher percentage of splenic Mac1⁺ cells were labeled (20% versus 6.6%). (C) Annexin V staining of bone marrow mononuclear cells from Cre⁻ and Cre⁺ mice showing greatly reduced apoptosis of Cre⁺ cells after 24 hours in culture without exogenous growth factors (27.9% versus 74.5% in the controls). The histograms present representative data from an analysis of 3 mice of each genotype. The numbers shown in each panel indicate the percentage of positive cells.

Nf1$^{flox/flox}$ mice demonstrate lymphocytosis with increased numbers of differentiated T and B cells. These data are consistent with competitive repopulation studies, which revealed that loss of *Nf1* is associated with a proliferative advantage in both myeloid and lymphoid compartments.[18] The risk of lymphoid malignancies has been examined in large population-based studies of pediatric cancer registries in Japan and the United Kingdom. Whereas one group identified no significant increase,[32] the other report found a 5- to 10-fold higher incidence of acute lymphoblastic leukemia and non-Hodgkin lymphoma in children with NF1.[6] A child with NF1 has been described who presented with JMML and subsequently developed a T-cell lymphoma, both of which showed loss of the normal *NF1* allele.[33] Ingram et al[34] recently reported greater thymic cellularity and a modest increase in Ras-GTP levels in RAG2-deficient mice that received transplants with *Nf1*$^{-/-}$ fetal liver cells. Paradoxically, *Nf1*$^{-/-}$ T cells showed impaired proliferation in response to T-cell mitogens. *Mx1-Cre, Nf1*$^{flox/flox}$ mice provide a model that can be used to dissect the functional consequences of ablating *Nf1* in lymphoid cells.

Consistent with previous studies of primary fetal livers and of irradiated recipients reconstituted with these cells,[11,16,17] we found that

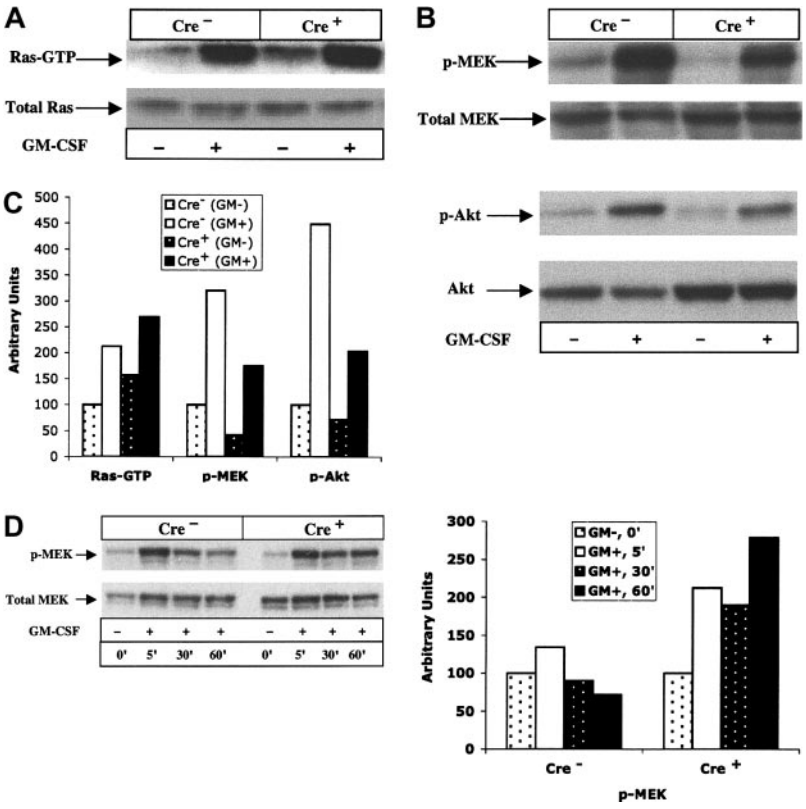

Figure 6. Signal transduction in bone marrow cells from *Mx1-Cre, Nf1 flox/flox* and Cre⁻ mice. (A) Bone marrow cells from mutant and control mice showing Ras-GTP levels in unstimulated cells and 5 minutes after GM-CSF. (B) Bone marrow cells from mutant and control mice showing basal and growth factor–induced levels of phosphorylated (p)–Akt and p-MEK in response to GM-CSF (at 5 minutes). (C) Ras-GTP, p-MEK, and p-Akt from panels A and B were quantified by densitometry. (D) Mac1-positive bone marrow cells from mutant and control mice showing basal and growth factor–induced activation of p-MEK in response to GM-CSF. The time course is shown from 5 to 60 minutes. Relative p-MEK activity is shown in the right panel. Levels in mutant and control cells were normalized for background and loading, with the unstimulated sample assigned arbitrary units of 100.

Mx1-Cre, Nf1$^{flox/flox}$ bone marrow cells model the hypersensitive pattern of CFU-GM colony growth that is a hallmark of JMML. These data establish a link between *Nf1* inactivation and this distinctive cellular phenotype. On the basis of this precedent, we exposed *Mx1-Cre, Nf1*$^{flox/flox}$ bone marrow cells to retinoids, but we did not observe selective effects on the growth of mutant CFU-GM colonies. These data imply that the therapeutic effects of 13*c*RA in JMML are not mediated though the GM-CSF/Ras/neurofibromin pathway.

Our adoptive transfer data are consistent with a previous report in which bone marrow from recipient mice repopulated with *Nf1*$^{-/-}$ fetal liver cells induced MPD in secondary hosts that received a myeloablative dose of radiation.[19] In addition, serial studies of sublethally irradiated mice demonstrated engraftment of mutant cells in most of the recipients without overt evidence of MPD after 8 months of observation. Furthermore, we did not detect splenomegaly or myeloid infiltration even in mice in which 100% of the peripheral blood leukocytes were derived from mutant cells. These data are remarkably consistent with the results of competitive repopulation experiments in which *Nf1*$^{-/-}$ fetal liver cells out-competed wild-type cells in the stem-cell compartment and in the lymphoid and myeloid lineages but failed to induce MPD in the absence of a high degree of chimerism.[18] In another study in which heterozygous *Nf1* inactivation cooperated with exposure to cyclophosphamide in leukemogenesis, some *Nf1*$^{+/-}$ mice showed loss of the wild-type allele without evidence of MPD when the experiment was terminated.[20] Together with these data, our results in sublethally irradiated recipients suggest that the presence of wild-type bone marrow cells can retard the development of MPD in vivo. These observations also support a model in which loss of *Nf1* in a susceptible bone marrow precursor confers a subtle growth advantage that progresses to *Nf1*-deficient hematopoiesis, followed by splenic invasion by myeloid precursors and, finally, by overt MPD. An unsettled question involves whether the MPD induced by *Nf1* inactivation is caused by progressive overgrowth of a stable population of mutant cells or involves clonal selection of a subpopulation that has acquired one or more cooperating mutations. Although the absence of acquired cytogenetic aberrations in the spleens of diseased mice is consistent with the former model, additional studies are required to resolve this issue.

We and others have detected hyperactive Ras signaling in JMML bone marrows,[11] in cell lines from *Nf1* mutant mice,[16,26] in c-kit–positive bone marrow cells isolated from the recipients of *Nf1*$^{-/-}$ fetal liver cells,[17] and in heterozygous *Nf1* mutant mast cells.[35] We were, therefore, surprised that bone marrow mononuclear cells from *Mx1-Cre, Nf1*$^{flox/flox}$ mice demonstrated a small increase in the percentage of Ras-GTP in unstimulated cells but similar levels of phosphorylated Akt and MEK compared with control cells. However, bone marrow–derived Mac1-positive cells from *Mx1-Cre, Nf1*$^{flox/flox}$ mice that were stimulated with GM-CSF showed sustained phosphorylation of MEK. Similarly, prolonged activation of extracellular-regulated kinase (ERK) was recently reported in *Nf1*-deficient mouse embryonic fibroblasts in response to 1% serum.[36] Our data support a mechanism whereby *Nf1* inactivation deregulates Ras signaling in a subset of hematopoietic cells, which may be difficult to detect in whole bone marrow. The CFU-GM fraction comprises approximately 0.1% of the nucleated cells in *Mx1-Cre, Nf1*$^{flox/flox}$ marrow, and we speculate that these cells are especially sensitive to loss of *Nf1*. Measuring the activation status of signaling cascades in rare subsets of primary cells is a challenging problem that will likely require adapting new methodologies such as the flow cytometry–based approach recently described by Perez and Nolan.[37] Our data also raise the possibility that some types of hematopoietic cells compensate for loss of *Nf1* by attenuating signaling networks, which may further complicate ascertaining the biochemical consequences of leukemia-associated mutations in vivo.

In addition to facilitating studies that directly address the role of *Nf1* in signal transduction and myeloid growth control, *Mx1-Cre, Nf1*$^{flox/flox}$ mice are a tractable experimental system for identifying molecular events that contribute to acute myeloid leukemia (AML). The classic studies of Land et al[38] demonstrated the principle of oncogene cooperativity in cellular transformation. Kelly et al[39] have applied this concept to AML and proposed that transcription factor fusion proteins cooperate with mutations that constitutively activate growth-promoting signal transduction pathways in leukemogenesis. Indeed, data from mice generally support the idea that neither type of leukemia-associated genetic lesion is sufficient to induce AML. For example, transgenic or knock-in models of transcription factor fusions such as *AML1-ETO*, *PML-RARA*, and *MLL-AF9* either do not spontaneously develop AML or show incomplete penetrance and prolonged latency.[29,40,41] By contrast, although inactivating *Nf1* or expressing either *BCR-ABL* or a mutant *FLT3* allele induces MPD,[16,39,42,43] additional events are required for AML. We envision 2 general strategies for harnessing *Mx1-Cre, Nf1*$^{flox/flox}$ mice to discover genes that cooperate with *Nf1* inactivation in leukemogenesis. The first strategy involves either performing genetic crosses with transgenic or knock-in strains that express fusion oncoproteins such as *PML-RARA*, *AML1-ETO*, or *MLL-AF9*, or transducing *Nf1*-deficient bone marrow with retroviruses that encode these or other leukemia-associated fusions followed by adoptive transfer into irradiated recipients. The second approach is to harness retroviral insertional mutagenesis to identify novel genes that cooperate with loss of *Nf1* in leukemogenesis.[44,45] In an important "proof of principle" experiment, Largaespada et al[16] found that *Nf1*$^{+/-}$ mice that were infected with the BXH-2 retrovirus developed AML with increased penetrance and reduced latency compared with wild-type littermates. These investigators identified inactivation of the normal *Nf1* allele in approximately 85% of BXH-2/*Nf1*$^{+/-}$ AMLs. Because both *Nf1* alleles are already mutated in *Mx1-Cre, Nf1*$^{flox/flox}$ animals that have been treated with pI-pC, this strain is theoretically superior to *Nf1*$^{+/-}$ mice for performing forward genetic screens. The predictable onset of MPD and the prolonged survival of *Mx1-Cre, Nf1*$^{flox/flox}$ mice may prove advantageous for uncovering genes that cooperate in the development of AML.

Finally, *Mx1-Cre, Nf1*$^{flox/flox}$ mice and cells from these animals can be used to test molecularly targeted agents with pharmacodynamic monitoring of relevant biochemical end points in primary target cells. Potential therapeutic strategies for treating JMML include developing GM-CSF receptor antagonists (reviewed in Iversen et al[46,47] and Frankel et al[48]), inhibitors of Ras processing enzymes (reviewed in Le and Shannon[49]), and agents that interfere with the activation of downstream effectors such as MEK.[50] Given the important role of hyperactive Ras in myeloid malignancies (reviewed in Lee and Shannon[49] and Sawyers and Denny[51]) and other cancers (reviewed in Bos[52] and Hingorani and Tuveson[53]), studies in this tractable disease model might identify agents that have therapeutic potential that extend beyond hematopoietic malignancies.

Acknowledgments

We thank Bhumi Patel and Elizabeth Davis for assistance in spectral karyotyping analysis, Sara Jew-Lim for assistance in genotyping, Jacob Rozmus for assistance with the Ras-GTP assay, Andrew Kim for assisting with adoptive transfer experiments, and Philip Chan for preparing pathologic specimens and downloading images to the MMHCC website.

References

1. Emanuel PD, Shannon KM, Castleberry RP. Juvenile myelomonocytic leukemia: molecular understanding and prospects for therapy. Mol Med Today. 1996;2:468-475.
2. Arico M, Biondi A, Pui C-H. Juvenile myelomonocytic leukemia. Blood. 1997;90:479-488.
3. Emanuel PD, Bates LJ, Castleberry RP, Gualtieri RJ, Zuckerman KS. Selective hypersensitivity to granulocyte-macrophage colony-stimulating factor by juvenile chronic myeloid leukemia hematopoietic progenitors. Blood. 1991;77:925-929.
4. Schiro R, Longoni D, Rossi V, et al. Suppression of juvenile chronic myelogenous leukemia colony growth by interleukin-1 receptor antagonist. Blood. 1994;83:460-465.
5. Bader JL, Miller RW. Neurofibromatosis and childhood leukemia. J Pediatr. 1978;92:925-929.
6. Stiller CA, Chessells JM, Fitchett M. Neurofibromatosis and childhood leukemia/lymphoma: a population-based UKCCSG study. Br J Cancer. 1994;70:969-972.
7. Boguski M, McCormick F. Proteins regulating Ras and its relatives. Nature. 1993;366:643-653.
8. Bernards A. Neurofibromatosis type 1 and Ras-mediated signaling: filling in the GAPs. Biochim Biophys Acta. 1995;1242:43-59.
9. Donovan S, Shannon KM, Bollag G. GTPase activating proteins: critical regulators of intracellular signaling. Biochim Biophys Acta. 2002;1602: 23-45.
10. Shannon KM, O'Connell P, Martin GA, et al. Loss of the normal NF1 allele from the bone marrow of children with type 1 neurofibromatosis and malignant myeloid disorders. N Engl J Med. 1994;330: 597-601.
11. Bollag G, Clapp DW, Shih S, et al. Loss of NF1 results in activation of the Ras signaling pathway and leads to aberrant growth in murine and human hematopoietic cells. Nat Genet. 1996;12: 144-148.
12. Miles DK, Freedman MH, Stephens K, et al. Patterns of hematopoietic lineage involvement in children with neurofibromatosis, type 1, and malignant myeloid disorders. Blood. 1996;88:4314-4320.
13. Side L, Taylor B, Cayouette M, et al. Homozygous inactivation of the NF1 gene in bone marrow cells from children with neurofibromatosis type 1 and malignant myeloid disorders. N Engl J Med. 1997;336:1713-1720.
14. Jacks T, Shih S, Schmitt EM, Bronson RT, Bernards A, Weinberg RA. Tumorigenic and developmental consequences of a targeted Nf1 mutation in the mouse. Nat Genet. 1994;7:353-361.
15. Brannan CI, Perkins AS, Vogel KS, et al. Targeted disruption of the neurofibromatosis type 1 gene leads to developmental abnormalities in heart and various neural crest-derived tissues. Genes Dev. 1994;8:1019-1029.
16. Largaespada DA, Brannan CI, Jenkins NA, Copeland NG. Nf1 deficiency causes Ras-mediated granulocyte-macrophage colony stimulating factor hypersensitivity and chronic myeloid leukemia. Nat Genet. 1996;12:137-143.
17. Zhang Y, Vik TA, Ryder JW, et al. Nf1 regulates hematopoietic progenitor cell growth and Ras signaling in response to multiple cytokines. J Exp Med. 1998;187:1893-1902.
18. Zhang Y, Taylor BR, Shannon K, Clapp DW. Quantitative effects of Nf1 inactivation on in vivo hematopoiesis. J Clin Invest. 2001;108:709-715.
19. Birnbaum RA, O'Marcaigh A, Wardak Z, et al. Nf1 and Gmcsf interact in myeloid leukemogenesis. Mol Cell. 2000;5:189-195.
20. Mahgoub N, Taylor BR, Gratiot M, et al. In vitro and in vivo effects of a farnesyltransferase inhibitor on Nf1-deficient hematopoietic cells. Blood. 1999;94:2469-2476.
21. Zhu Y, Romero MI, Ghosh P, et al. Ablation of NF1 function in neurons induces abnormal development of cerebral cortex and reactive gliosis in the brain. Genes Dev. 2001;15:859-876.
22. Zhu Y, Ghosh P, Charnay P, Burns DK, Parada LF. Neurofibromas in NF1: Schwann cell origin and role of tumor environment. Science. 2002; 296:920-922.
23. Kuhn R, Schwenk F, Aguet M, Rajewsky K. Inducible gene targeting in mice. Science. 1995;269: 1427-1429.
24. Kogan SC, Ward JM, Anver MR, et al. Bethesda proposals for classification of nonlymphoid hematopoietic neoplasms in mice. Blood. 2002;100: 238-245.
25. Le Beau MM, Bitts S, Davis EM, Kogan SC. Recurring chromosomal abnormalities in leukemia in PML-RARA transgenic mice parallel human acute promyelocytic leukemia. Blood. 2002;99:2985-2991.
26. Donovan S, See W, Bonifas J, Stokoe D, Shannon KM. Hyperactivation of protein kinase B and ERK have discrete effects on survival, proliferation, and cytokine expression in Nf1-deficient myeloid cells. Cancer Cell. 2002;2:507-514.
27. Emanuel PD, Zuckerman KS, Wimmer R, Cohn S, Chaffee S, Castleberry RP. In vivo 13-cis retinoic acid therapy decreased the in vitro GM-CSF hypersensitivity in JCML [abstract]. Blood. 1991; 78(suppl 1):170a.
28. Castleberry RP, Emanuel PD, Zuckerman KS, et al. A pilot study of isotretinoin in the treatment of juvenile chronic myelogenous leukemia. N Engl J Med. 1994;331:1680-1685.
29. Higuchi M, O'Brien D, Kumaravelu P, Lenney N, Yeoh E, Downing JR. Expression of a conditional AML1-ETO oncogene bypasses embryonic lethality and establishes a murine model of human t(8;21) acute myeloid leukemia. Cancer Cell. 2002;1:63-74.
30. Roberts CW, Leroux MM, Fleming MD, Orkin SH. Highly penetrant, rapid tumorigenesis through conditional inversion of the tumor suppressor gene Snf5. Cancer Cell. 2002;2:415-425.
31. Gerber HP, Malik AK, Solar GP, et al. VEGF regulates haematopoietic stem cell survival by an internal autocrine loop mechanism. Nature. 2002; 417:954-958.
32. Matsui I, Tanimura M, Kobayashi N, Sawada T, Nagahara N, Akatsuka J. Neurofibromatosis type 1 and childhood cancer. Cancer. 1993;72:2746-2754.
33. Cooper LJ, Shannon KM, Loken MR, Weaver M, Stephens K, Sievers EL. Evidence that juvenile myelomonocytic leukemia can arise from a pluripotential stem cell. Blood. 2000;96:2310-2313.
34. Ingram DA, Zhang L, McCarthy J, et al. Lymphoproliferative defects in mice lacking the expression of neurofibromin: functional and biochemical consequences of Nf1 deficiency in T-cell development and function. Blood. 2002; 100:3656-3662.
35. Ingram DA, Yang FC, Travers JB, et al. Genetic and biochemical evidence that haploinsufficiency of the Nf1 tumor suppressor gene modulates melanocyte and mast cell fates in vivo. J Exp Med. 2000;191:181-188.
36. Cichowski K, Santiago S, Jardim M, Johnson BW, Jacks T. Dynamic regulation of the Ras pathway via proteolysis of the NF1 tumor suppressor. Genes Dev. 2003;17:449-454.
37. Perez OD, Nolan GP. Simultaneous measurement of multiple active kinase states using polychromatic flow cytometry. Nat Biotechnol. 2002; 20:155-162.
38. Land H, Parada LF, Weinberg RA. Tumorigenic conversion of primary embryo fibroblasts requires at least two cooperating oncogenes. Nature. 1983;304:596-602.
39. Kelly L, Clark J, Gilliland DG. Comprehensive genotypic analysis of leukemia: clinical and therapeutic implications. Curr Opin Oncol. 2002;14: 10-18.
40. Corral J, Lavenir I, Impey H, et al. An Mll-AF9 fusion gene made by homologous recombination causes acute leukemia in chimeric mice: a method to create fusion oncogenes. Cell. 1996; 85:853-861.
41. Brown D, Kogan S, Lagasse E, et al. A PML-RARalpha transgene initiates murine acute promyelocytic leukemia. Proc Natl Acad Sci U S A. 1997;94:2551-2556.
42. Daley GQ, Van Etten RA, Baltimore D. Induction of chronic myelogenous leukemia in mice by the P210bcr/abl gene of the Philadelphia chromosome. Science. 1990;247:824-830.
43. Kelly LM, Liu Q, Kutok JL, Williams IR, Boulton CL, Gilliland DG. FLT3 internal tandem duplication mutations associated with human acute myeloid leukemias induce myeloproliferative disease in a murine bone marrow transplant model. Blood. 2002;99:310-318.
44. Li J, Shen H, Himmel KL, et al. Leukaemia disease genes: large-scale cloning and pathway predictions. Nat Genet. 1999;23:348-353.
45. Wolff L, Koller R, Hu X, Anver MR. A Moloney murine leukemia virus-based retrovirus with 4070A long terminal repeat sequences induces a high incidence of myeloid as well as lymphoid neoplasms. J Virol. 2003;77:4965-4971.
46. Iversen P, Rodwell RL, Pitcher L, Taylor KM, Lopez AF. Inhibition of proliferation and induction of apoptosis in JMML cells by the granulocyte-macrophage colony-stimulating factor analogue E21R. Blood. 1996;88:2634-2639.
47. Iversen PO, Lewis ID, Turczynowicz S, et al. Inhibition of granulocyte-macrophage colony-stimulating factor prevents dissemination and induces remission of juvenile myelomonocytic leukemia in engrafted immunodeficient mice. Blood. 1997;90: 4910-4917.
48. Frankel AE, Lilly M, Kreitman R, et al. Diphtheria toxin fused to granulocyte-macrophage colony-stimulating factor is toxic to blasts from patients with juvenile myelomonocytic leukemia and chronic myelomonocytic leukemia. Blood. 1998; 92:4279-4286.
49. Le DT, Shannon KM. Ras processing as a therapeutic target in hematologic malignancies. Curr Opin Hematol. 2002;9:308-315.
50. Sebolt-Leopold JS, Dudley DT, Herrera R, et al. Blockade of the MAP kinase pathway suppresses growth of colon tumors in vivo. Nat Med. 1999;5: 810-816.
51. Sawyers CL, Denny CT. Chronic myelomonocytic leukemia: tel-a-kinase what ets all about. Cell. 1994;77:171-173.
52. Bos JL. ras oncogenes in human cancer: a review. Cancer Res. 1989;49:4682-4689.
53. Hingorani SR, Tuveson DA. Ras redux: rethinking how and where Ras acts. Curr Opin Genet Dev. 2003;13:6-13.

REVIEW

Membrane organization and tumorigenesis—the NF2 tumor suppressor, Merlin

Andrea I. McClatchey[1,3] and Marco Giovannini[2]

[1]Massachusetts General Hospital, Center for Cancer Research and Harvard Medical School, Department of Pathology, Charlestown, Massachusetts 02129, USA; [2]Inserm U674, Fondation Jean Dausset-CEPH et Institut Universitaire d'Hématologie, Paris, France

The *NF2* tumor-suppressor gene was cloned more than a decade ago, but the function of its encoded protein, Merlin, remains elusive. Merlin, like the closely related ERM proteins, appears to provide regulated linkage between membrane-associated proteins and the actin cytoskeleton and is therefore poised to function in receiving and interpreting signals from the extracellular milieu. Recent studies suggest that Merlin may coordinate the processes of growth-factor receptor signaling and cell adhesion. Varying use of this organizing activity by different types of cells could provide an explanation for the unique spectrum of tumors associated with *NF2* deficiency in mammals.

The identification of the genetic defect responsible for the familial cancer syndrome Neurofibromatosis type 2 (NF2) nearly 15 years ago yielded the unexpected prospect that the encoded tumor suppressor was a cytoskeleton-associated protein (Rouleau et al. 1993; Trofatter et al. 1993). This was in marked contrast to the known and now "classic" tumor suppressors p53, Rb, and NF1 that function either to directly control the cell cycle machinery in the nucleus, or in the case of NF1, to directly negatively regulate mitogenic Ras signaling (Sherr 2004). Several factors have rendered progress in defining the molecular basis of NF2-associated tumorigenesis slow, including the rare incidence of NF2 in humans, the paucity of *NF2*$^{-/-}$ cell lines and technical challenges in studying the *NF2*-encoded protein, Merlin, which is a novel type of tumor suppressor. However, recent advances, highlighted by the study of NF2 function in several different model organisms have begun to yield a model of Merlin function that offers important lessons about the origins and progression of cancer and provides novel insight into some basic biological principles. In this review we have highlighted recent advances in understanding the pathology and molecular biology of NF2 with particular emphasis on the broader impact that the study of NF2 may have on the fields of tumor, cellular, and molecular biology.

The incidence of NF2 in humans is rare (fewer than one in 25,000 individuals) and the symptoms and phenotypes associated with NF2 are unusual and restricted (Evans et al. 2005). The hallmark of the disease is the development of Schwann cell tumors (schwannomas) on or around the vestibular branch of both eighth cranial nerves. Most NF2 patients go on to develop multiple schwannomas that are associated with other cranial nerves and spinal nerve roots, cranial and spinal meningiomas and, less frequently, intraspinal ependymomas. In contrast to other major human malignancies, these are benign, slow-growing tumors that respond poorly to chemotherapeutic intervention and cause significant morbidity. Indeed, the current standard of treatment remains local tumor control by repeated surgeries and radiation, which are often accompanied by damage of nerves and CNS structures (Evans et al. 1992).

Biallelic inactivation of the *NF2* gene can also be identified in most sporadically occurring schwannomas (Stemmer-Rachamimov et al. 1997) and a large fraction of sporadically occurring meningiomas (Ruttledge et al. 1994; Lomas et al. 2005). In addition to tumors that are associated with familial NF2, *NF2* mutations are frequently found in sporadic mesotheliomas of the lung lining that are associated with asbestos exposure (Bianchi et al. 1995; Sekido et al. 1995). More recently, *NF2* mutations have been reported in some sporadic thyroid carcinomas, hepatocellular carcinoma cell lines, and perineurial tumors, revealing additional cell types affected by *NF2* loss (Lasota et al. 2001; Pineau et al. 2003; Sheikh et al. 2004). The generation and study of *Nf2*-mutant strains of mice has further expanded the range of cancers associated with *NF2* mutation and cell types affected by *NF2* deficiency (see below). However, *NF2* mutations have not yet been reported in many common/prevalent human cancers. As discussed below, these data raise the important question of whether there is a biological and/

[*Keywords*: ERM proteins; Merlin/NF2; Schwann cells; ependyma; membrane organization; meninges]
[3]Corresponding author.
E-MAIL mcclatch@helix.mgh.harvard.edu; FAX (617) 726-7808.
Article and publication are at http://www.genesdev.org/cgi/doi/10.1101/gad.1335605.

or genetic basis for the unique spectrum of spontaneous tumors associated with *NF2* mutation in humans and mice.

A novel type of tumor suppressor

Initial studies of the function of the *NF2*-encoded tumor suppressor, Merlin (also known as Schwannomin), were modeled after studies of other tumor suppressors and of the closely related ERM proteins (Ezrin, Radixin, and Moesin). Early studies confirmed, as for other tumor suppressors, that overexpression of Merlin can block both cell proliferation and oncogene-induced transformation (Tikoo et al. 1994; Lutchman and Rouleau 1995). Indeed, Merlin can negatively regulate cyclin D1 levels, consistent with the cell cycle arrest observed when Merlin is overexpressed (Xiao et al. 2002). However, given its predominant localization to the membrane:cytoskeleton interface, Merlin is not likely to directly control the cell cycle machinery. Instead, Merlin, like the ERM proteins, appears to provide regulated linkage between membrane-associated proteins and the actin cytoskeleton and thereby to function in membrane organization. Merlin is therefore a novel type of tumor suppressor poised to function in receiving and interpreting signals from the extracellular milieu.

Model organisms

The identification of *NF2* homologs from other species and the functional characterization of their encoded proteins in other model organisms provides a valuable complement to the functional characterization of the mammalian NF2 protein. Genes similar to the human *NF2* gene can be identified in many other metazoans, including invertebrates (*Drosophila melanogaster*, *Anopheles gambiae*, *Caenorhabditis elegans*, *Xenopus laevis*), fish (*Danio rerio*, *Oryzias latipes*), and birds (*Gallus gallus*). No *NF2* homolog has been identified in *Saccharomyces cerevisiae* (yeast), suggesting that Merlin function is specific to the evolutionary branching of metazoans. The high degree of homology among metazoan *NF2* gene products is complemented by the fact that they can be used interchangeably in functional studies, i.e., the human protein can function reliably in mouse and *Drosophila* model systems (LaJeunesse et al. 1998; Giovannini et al. 1999).

Several *Nf2* mutant alleles that mimic naturally occurring human *NF2* mutations have been engineered in the mouse, allowing a comparison of the phenotypic effects of these mutations in an animal model. Three different targeting approaches resulted in germline *Nf2* homozygous mutants that were not viable (McClatchey et al. 1997; Giovannini et al. 2000). *Nf2* null embryos fail early during embryonic development without initiating gastrulation (McClatchey et al. 1997). The underlying defect in $Nf2^{-/-}$ embryos is not due to cell proliferation abnormalities in the embryo itself, but rather, the absence of extra-embryonic structures that are required to generate a mesoderm-inducing signal. Notably, Merlin function is also required for normal development in the fruitfly, *D. melanogaster* and in the flatworm *C. elegans* (Fehon et al. 1997; J. Gervais , J. Satterlee, and A.I. McClatchey, unpubl.).

In the mouse, heterozygosity for any of the three mutant *Nf2* alleles leads to a high incidence of bone tumors that exhibit loss of the wild-type *Nf2* allele (McClatchey et al. 1998; Giovannini et al. 2000). Differences in the grade of malignancy observed in these tumors might be explained by the use of different genetic backgrounds. Indeed, some studies have indicated that *Nf2* loss contributes to tumor metastasis (see below; McClatchey et al. 1997). Notably, $Nf2^{+/-}$ mice are collectively predisposed to developing a variety of other tumor types at lower frequency, suggesting a broader role for *Nf2* loss in tumorigenesis. None of the three strains of *Nf2* heterozygous mutant mice spontaneously develop the classic clinical features of human NF2. However, consistent with the identification of *NF2* mutations in asbestos-induced mesotheliomas in humans, $Nf2^{+/-}$ mice do show increased sensitivity to the carcinogenic effects of asbestos fibers. Intraperitoneal injection of asbestos fibers induces the formation of malignant mesotheliomas at a higher frequency in $Nf2^{+/-}$ mice than in wild-type mice (Fleury-Feith et al. 2003). Importantly, asbestos-induced tumors in $Nf2^{+/-}$ mice exhibit loss of the wild-type *Nf2* allele. These mice should be useful for further studies of the molecular pathogenesis, genetic modification, and environmental initiation of mesothelioma development.

Although *Nf2* heterozygous mutant mice that genetically mimic human NF2 patients do not spontaneously develop schwannomas, inactivation of both *Nf2* alleles specifically in Schwann cells (SCs) does yield manifestations of human NF2. Upon mating with transgenic *P0-Cre* mice, in which the Cre recombinase is expressed specifically in SCs and in a subset of neural crest cells, *Nf2* conditional mutant (*P0-Cre*;$Nf2^{flox2/flox2}$) mice develop SC hyperplasia, SC tumors, cataracts, and cerebral calcifications (Fig. 1A,B; Giovannini et al. 2000). Moreover, mice with biallelic inactivation of *Nf2* specifically in arachnoid cells develop a range of meningioma subtypes that are histologically similar to the human tumors (Kalamarides et al. 2002). Therefore, the lack of spontaneous schwannoma and meningioma development in $Nf2^{+/-}$ mice is not due to a fundamental difference in the function of mouse Merlin or in the biology of mouse Schwann and arachnoid cells, but instead to differences in the probability of loss of the wild-type allele in the cells from which schwannomas and meningiomas originate.

The growth-suppressing function of Merlin is conserved in other species. For example, somatic mosaic analysis reveals that clones of *Mer* homozygous mutant epithelial cells in the *Drosophila* eye hyperproliferate, providing a powerful system for carrying out genetic screens to identify modifiers of *Nf2* deficiency (LaJeunesse et al. 2001). Recent analyses of the chicken Merlin

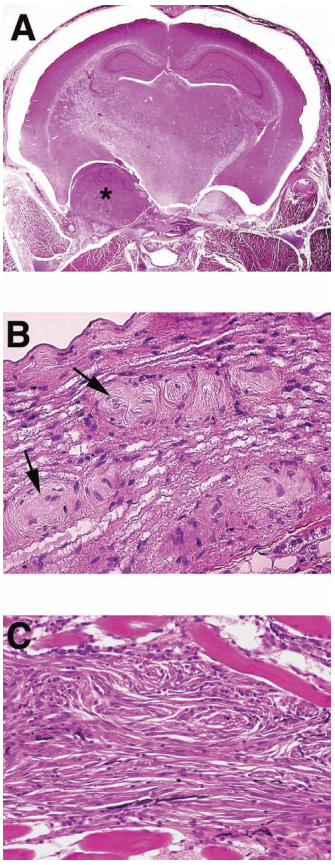

Figure 1. Loss of Merlin leads to SC hyperproliferation and tumorigenesis in animal models. (*A*) Hematoxylin and eosin (H&E)-stained section of frank schwannoma emanating from the trigeminal nerve of a *P0-Cre;Nf2*$^{flox2/flox2}$ mouse (*). (*B*) H&E-stained section depicting SC hyperplasia in the sciatic nerve of a *P0-Cre;Nf2*$^{flox2/flox2}$ mouse. (*C*) Malignant peripheral nerve sheath tumor in *Nf2a*-mutant zebrafish. Zebrafish bearing a germline mutation in one allele of the *NF2a* gene develop spindle cell tumors that have features in common with nerve sheath tumors from other species (image kindly provided by K. Edepli) (Amsterdam et al. 2004).

homolog also confirm its function as a negative regulator of proliferation in vitro and in vivo (Chen et al. 2004a,b). The study of the *Drosophila* Merlin protein has also provided key insight into the regions of Merlin that are required for its localization and function (LaJeunesse et al. 1998). This also led to the identification and analysis of the so-called "Blue Box" mutant, Mer$^{\Delta BB}$, which is known to act in a dominant-negative manner and therefore to interfere with the activity of the wild-type protein. Ectopic expression of Mer$^{\Delta BB}$ in the wing results in increased proliferation (LaJeunesse et al. 1998). Expression of the murine analog of Mer$^{\Delta BB}$ induces transformation of cultured NIH3T3 fibroblasts (Johnson et al. 2002). Interestingly, SC hyperplasia and tumors were observed in transgenic mice that express a patient-derived mutant version of Merlin lacking amino acids 39–121 in SCs, indicating that this isoform, when overexpressed, may also have dominant-negative properties (Giovannini et al. 1999). Therefore, when overexpressed, certain mutant versions of Merlin exhibit oncogenic properties. However, in human tumors, where expression of mutant *NF2* alleles is controlled by endogenous regulatory sequences, the same mutant Merlin isoforms must be unstable, resulting in a loss of function rather than a dominant oncogenic effect (Gautreau et al. 2002). Delineation of the regions of Merlin that are necessary for the dominant negative activity of overexpressed Merlin may provide novel mechanistic insight into Merlin function.

The different strains of *Nf2* mutant mice also provide powerful tools for investigating genetic cooperativity in tumorigenesis. The identification of tumor suppressor or other gene mutations that cooperate with *Nf2* loss can provide important mechanistic insight into Nf2-associated pathways. Dramatic cooperativity between the *Nf2* and *p53* tumor suppressor gene mutations is displayed by *Nf2*$^{+/-}$;*p53*$^{+/-}$ *cis* mice that carry heterozygous *Nf2* and *p53* mutations on the same chromosome; these mice develop multiple osteosarcomas early in life (McClatchey et al. 1998). Notably, *Nf2*$^{+/-}$;*p53*$^{+/-}$ *trans* mice develop fewer tumors with longer latency; therefore genetic linkage of cancer predisposing mutations can profoundly influence tumorigenesis. In conditional *Nf2* mutant mice, *p53* heterozygosity can also markedly increase the incidence of SC-derived malignant peripheral nerve sheath tumors (MPNSTs) (Robanus-Maandag et al. 2004). Importantly, the timing of *Nf2* inactivation seems to determine in which neural crest-derived cell type the growth advantage occurs since, in contrast to *P0-Cre;Nf2*$^{flox2/flox2}$;*p53*$^{+/-}$ mice, *P0-Cre;Nf2*$^{flox2/+}$;*p53*$^{+/-}$ *cis* mice develop osteogenic but not SC tumors. This difference in tumor spectrum could be simply explained by the fact that *P0-Cre;Nf2*$^{flox2/flox2}$;*p53*$^{+/-}$ mice do not require an additional event for biallelic inactivation of *Nf2* and SC hyperproliferation; in the *P0-Cre;Nf2*$^{flox2/+}$;*p53*$^{+/-}$ *cis* mice, spontaneous loss of the wild-type *Nf2* allele may occur more rapidly in osteoblasts than in SCs. Alternatively, this difference could reflect cell-type-specific consequences of sequential versus simultaneous loss of Nf2 and p53 function. Perhaps *Nf2* deficiency leads to p53-dependent growth arrest or apoptosis in OBs but not SCs. Finally, early biallelic *Nf2* loss in *P0-Cre;Nf2*$^{flox2/flox2}$;*p53*$^{+/-}$ mice could specifically target a population of SC progenitors that are particularly sensitive to loss of Merlin function.

More recently, the role of *NF2* and *p53* mutations in SC tumorigenesis has been emphasized by the observation of MPNST development in *NF2* (Amsterdam et al. 2004) and *p53* (Berghmans et al. 2005) mutant zebrafish (Fig. 1C). Although *p53* mutations are found in human MPNSTs, it is interesting to note that in NF2 patients, benign SC tumors initiated by biallelic *NF2* gene inactivation do not progress into MPNSTs (see below). Indeed, malignant transformation of a schwannoma is an exceedingly rare event and analysis of the few cases reported in the literature show that none of the patients had NF2 (Woodruff et al. 1994; McMenamin and Fletcher 2001).

Regulation of Merlin

Structure

Many studies have established parallels between Merlin and the ERMs. Central to Merlin function is the fact that like the ERM proteins, Merlin can undergo regulated intramolecular self-association (Gonzalez-Agosti et al. 1996; Sherman et al. 1997; Gronholm et al. 1999; Nguyen et al. 2001). Several recent structural studies have yielded complementary models of Merlin and ERM tertiary conformation. The 1.9 Å crystal structure of the complexed N-terminal FERM (Four-point-one, Ezrin, Moesin, Radixin) and C-terminal tail domains of mammalian Moesin reveals that the C-terminal tail adopts an extended conformation to interact with the trilobed FERM domain, masking potential binding sites of other proteins (Pearson et al. 2000). Most (~81%) of the residues that are conserved between Merlin and the ERM proteins map to this interface, indicating that Merlin likely adopts a similar conformation. Indeed, the structure of the isolated Merlin FERM domain is very similar to that of the ERMs (Shimizu et al. 2002). Although most human *NF2* mutations identified are deletions or truncating mutations that effect complete loss of function, missense mutations do occur and are distributed throughout the FERM domain and C-terminal tail, suggesting that Merlin function is highly dependent upon the tertiary configuration of the entire protein (Pearson et al. 2000). Mutations that disrupt self-association likely also alter Merlin localization and protein interactions. Like the ERMs, Merlin self-association is regulated, at least in part, by phosphorylation (see below).

Post-translational modification

An increasing number of studies have examined the regulation of Merlin by phosphorylation. It was recognized early on that the two major isoforms of Merlin visualized by SDS-PAGE and immunoblotting represent differentially phosphorylated species (Shaw et al. 1998). Although Merlin is phosphorylated on multiple residues, phosphorylation of a single serine residue, S518, causes the mobility shift and has therefore been best studied (Shaw et al. 2001; Kissil et al. 2002; Xiao et al. 2002; Rong et al. 2004). Available data suggest that S518 phosphorylation weakens self-association and inactivates the growth-suppressing function of Merlin. Phosphorylation of Merlin at S518 is regulated by specific cell culture conditions, including cell density, cell:substrate attachment, and growth factor availability (Shaw et al. 1998). The best-studied stimulus for Merlin S518 phosphorylation is activation of the small GTPase Rac1 (Shaw et al. 2001). Rac-induced phosphorylation of Merlin S518 appears to be mediated by the major Rac effector p21-activated kinase (Pak) (Kissil et al. 2002; Xiao et al. 2002). Interestingly, S518 can also be phosphorylated in a Pak-independent manner by protein kinase A (PKA) (Alfthan et al. 2004), suggesting that disparate stimuli regulate Merlin. Similarly, multiple signals appear to induce phosphorylation of a conserved C-terminal threonine residue in the ERM C-terminal tail (Matsui et al. 1998, 1999; Pietromonaco et al. 1998; Hipfner et al. 2004). Virtually nothing is known about the regulation or functional consequences of phosphorylation of other Merlin residues. Finally, phosphatidylinositol 4,5-bisphosphate (PIP_2) binding to the FERM domain is thought to cooperate with phosphorylation in weakening self-association during ERM activation; the mapped ERM PIP_2-binding sites are conserved in Merlin, suggesting that PIP_2 binding may also play an important role in regulating Merlin function (Barret et al. 2000). Collectively, these studies suggest that the cell may integrate multiple strategies to fine-tune the localization and activity of Merlin.

Subcellular localization

If Merlin's ability to organize membrane domains is central to its function as a tumor suppressor, then it is critical to define where Merlin is localized within the cell. This has been particularly challenging due to the low levels of endogenous Merlin in most cell types and to the insolubility of a substantial pool of Merlin. As a consequence, many studies have examined the localization of exogenous (overexpressed), often epitope-tagged Merlin, which may not fully mirror the endogenous protein. In *Drosophila* epithelia, endogenous Merlin is concentrated in the subapical junctional region, where it overlaps with the more apically localized Moesin (Bretscher et al. 2002). Similarly, in the *C. elegans* intestinal epithelium, exogenous nfm-1, the Merlin paralog, localizes basolaterally relative to erm-1 (Gobel et al. 2004). In cultured mammalian cells, endogenous and exogenous Merlin is concentrated in actin-rich structures such as membrane ruffles in isolated cells and along cell:cell boundaries as they form, consistent with its role in mediating contact-dependent inhibition of proliferation (see below; Gonzalez-Agosti et al. 1996; Maeda et al. 1999; Lallemand et al. 2003). Although the localization of Merlin in polarized mammalian epithelial cells has not been reported, Merlin localizes to synaptic junctions in cultured polarized neurons (Gronholm et al. 2005). In addition to concentrated localization to cell protrusions and cell:cell boundaries, some Merlin also exhibits diffuse localization throughout the membrane or cytoplasm and sometimes a punctate distribution that has been attributed to localization to intracellular vesicles or membrane lipid rafts (McCartney and Fehon 1996; Stickney et al. 2004). Indeed, vesicular and/or lipid raft localization would be consistent with a number of lines of recent evidence suggesting a role for Merlin in the endocytic trafficking of membrane receptors (see below). Finally, Merlin has recently been reported to localize to the nucleus in cultured cells under certain conditions (Kressel and Schmucker 2002; Muranen et al. 2005). It is not yet clear whether Merlin has an activity in the nucleus. However, the sum of the available data are consistent with the notion that Merlin normally carries out its growth-suppressing activity from the cell periphery; perhaps Merlin is removed from the periphery and sequestered in the

nucleus during conditions of exponential proliferation. Conversely, Merlin could help to sequester growth-promoting factors outside of the nucleus during conditions of growth arrest.

Pathways/activities

The NF2 field is at a critical juncture, passage of which will require innovative approaches to delineating the molecular basis of Merlin's function as a tumor suppressor. Many Merlin-interacting proteins have been reported—most of which also interact with the ERM proteins—and many cellular and molecular activities have been attributed to Merlin. However, follow-up functional studies of many of these putative interactors have not been forthcoming, perhaps due to the aforementioned technical challenges associated with isolating and localizing Merlin. The fact that a substantial fraction of Merlin is insoluble and that Merlin solubility is regulated, present biochemical challenges to ascribing functional significance to specific Merlin-associated proteins. Nevertheless, the Merlin-interacting proteins and phenotypic consequences of Merlin overexpression can be organized into several pathways that appear to be controlled by Merlin. Indeed, a key question is whether Merlin performs multiple independent functions, one of which is critical in tumor suppression, or whether Merlin controls a specific combination of pathways that collectively impart tumor suppression.

Rho GTPases

The function of Merlin and the ERM proteins has been linked to that of the Rho family of small GTPases that control actin cytoskeleton remodeling (for review, see Bretscher et al. 2002; McClatchey 2003). Central to the functional relationships between Merlin/ERMs and Rho GTPases are reciprocal modes of regulation. Thus, in addition to the role of Rac in regulating Merlin phosphorylation described above, overexpression of Merlin negatively regulates Rac-dependent signaling and $Nf2^{-/-}$ cells display phenotypes that are observed in cells expressing activated Rac alleles (Shaw et al. 2001). Similarly, in addition to Rho-dependent ERM phosphorylation, loss of the single *Drosophila* ERM protein Moesin, leads to elevated Rho signaling (Speck et al. 2003). Although the mechanism whereby Merlin/ERMs control Rho/Rac activity is not yet clear, Merlin/ERMs have been shown to physically interact with Rho guanine-dissociation inhibitor (RhoGDI) (Takahashi et al. 1997; Maeda et al. 1999). Like the ERMs, Merlin interaction with RhoGDI could counteract RhoGDI-mediated inhibition and sequestration of Rho or Rac in the cytosol, thereby effecting activation of Rho or Rac signaling. Alternatively, recent evidence suggests that Merlin can bind to and directly negatively regulate Pak itself (Kissil et al. 2003). This latter model predicts that Merlin does not regulate Rac–effector pathways that are Pak independent.

Actin remodeling

A key aspect of Merlin function that must be delineated is its functional association with the actin cytoskeleton. Merlin, like the ERMs, localizes to specific regions of cortical actin remodeling (den Bakker et al. 1995; Gonzalez-Agosti et al. 1996; Sainio et al. 1997). In contrast to the ERMs, Merlin does not have an actin-binding domain at the C terminus, but instead may bind actin directly via an N-terminal domain (Brault et al. 2001; James et al. 2001). Alternatively, interaction of Merlin with the actin cytoskeleton may occur indirectly via the cytoskeletal proteins βII spectrin, paxillin or the ERM proteins themselves (Scoles et al. 1998; Gronholm et al. 1999; Meng et al. 2000; Nguyen et al. 2001; Fernandez-Valle et al. 2002). Loss of Merlin function in SCs and keratinocytes yields marked changes in the morphology of the actin cytoskeleton (Pelton et al. 1998; Lallemand et al. 2003; A. Chan, D. Lallemand, A.I. McClatchey, and M. Giovannini, unpubl.). Similarly, loss of ERM function can lead to dramatic alterations in the cortical actin cytoskeleton (Speck et al. 2003). Although these phenotypes could be an indirect consequence of altered RhoGTPase activity as described above, Merlin may also directly control actin cytoskeleton remodeling. In fact, it has recently been reported that Merlin and the ERMs can directly interact with and inhibit the function of N-WASP, which normally controls activation of the actin nucleator Arp2/3 (Manchanda et al. 2005). The Arp2/3 complex nucleates actin subunits and drives actin filament branching in specialized cortical domains such as the membrane ruffle and adherens junction (AJ) where Merlin is concentrated (Bershadsky 2004).

Contact inhibition/cell:cell adhesion

Several studies suggest that Merlin can control contact-dependent inhibition of proliferation (Morrison et al. 2001; Johnson et al. 2002; Lallemand et al. 2003). Indeed, the key consequence of Merlin deficiency in cultured primary cells of several types is their failure to undergo contact-dependent inhibition of proliferation (Lallemand et al. 2003). Merlin phosphorylation and levels are regulated by cell density and Merlin localizes to nascent boundaries between cells as they form, suggesting a role in cell:cell communication (Shaw et al. 1998; Lallemand et al. 2003). Merlin may regulate contact-dependent inhibition of proliferation through interaction with the hyaluronic acid receptor CD44 in some cell types (Morrison et al. 2001). Alternatively, Merlin associates with and is required for the formation of stable cadherin-containing AJs between cells of several types (Lallemand et al. 2003). In this setting, Merlin appears to stabilize the final AJ structure in association with the actin cytoskeleton. The mechanistic basis of contact-dependent inhibition of proliferation of any cell type is poorly understood and the study of Merlin may provide novel insight into this important biological phenomenon. Moreover, it is well established that defective cell:cell communication can contribute to both tumor initiation and metas-

tasis, providing an explanation for the tumorigenic and metastatic consequences of *Nf2* deficiency in humans and mice.

Growth-factor/membrane-receptor signaling

Several lines of evidence suggest that Merlin can regulate receptor tyrosine kinase activity and perhaps trafficking. For example, genetic interactions between a *Mer* mutation and EGFR pathway mutations have been documented in *Drosophila* (LaJeunesse et al. 2001). In addition, Merlin has been reported to physically interact with several proteins with established roles in growth-factor receptor signaling. Thus, Merlin can form a ternary complex with a novel protein dubbed Magicin and Grb2, an adaptor that coordinates receptor tyrosine kinase and Ras signaling (Wiederhold et al. 2004). Merlin can also interact with EBP50/NHE-RF1, which can, in turn, interact with Erbin; both proteins are PDZ-domain containing adaptors that have been implicated in the membrane distribution of receptor tyrosine kinases (Murthy et al. 1998; Kolch 2003; Lazar et al. 2004; Rangwala et al. 2005). Similarly, Ezrin has been reported to interact with Lin-7/Pals1, which controls ErbB2 membrane distribution in *C. elegans* (Shelly et al. 2003; Cao et al. 2005). Moreover, Merlin can inhibit EGFR internalization and signaling upon cell:cell contact (M. Curto and A.I. McClatchey, unpubl.). A role for Merlin in later stages of endocytosis is suggested by its reported ability to interact with Hepatocyte Growth-Factor Receptor Substrate (HRS), which controls lysosomal trafficking of membrane receptors including the EGFR (Scoles et al. 2000). The localization of Merlin to vesicular structures under some conditions in *Drosophila* and mammalian cells together with its reported localization to lipid rafts further supports a role in membrane receptor trafficking (McCartney and Fehon 1996; Stickney et al. 2004). Regulation of growth-factor receptor surface availability and endocytosis would be a plausible mechanism whereby Merlin could control cell proliferation. The study of Merlin function could thus provide a novel insight into growth-factor receptor signaling and trafficking in normal cells and suggest novel avenues of growth-factor receptor deregulation in tumors.

Different complexes for different purposes or coordination of signaling from multiple membrane complexes?

If endogenous Merlin does control multiple different pathways as described above, this could reflect independent functions or a role for Merlin in coordinating signaling from multiple membrane complexes. Perhaps the accumulation of growth inhibitory signals from multiple Merlin-associated membrane complexes ultimately reaches a threshold that halts proliferation (Fig. 2). This threshold could vary in different cell types or contexts. For example, Merlin could stabilize large, actin-cytoskeleton-associated membrane-signaling complexes such as

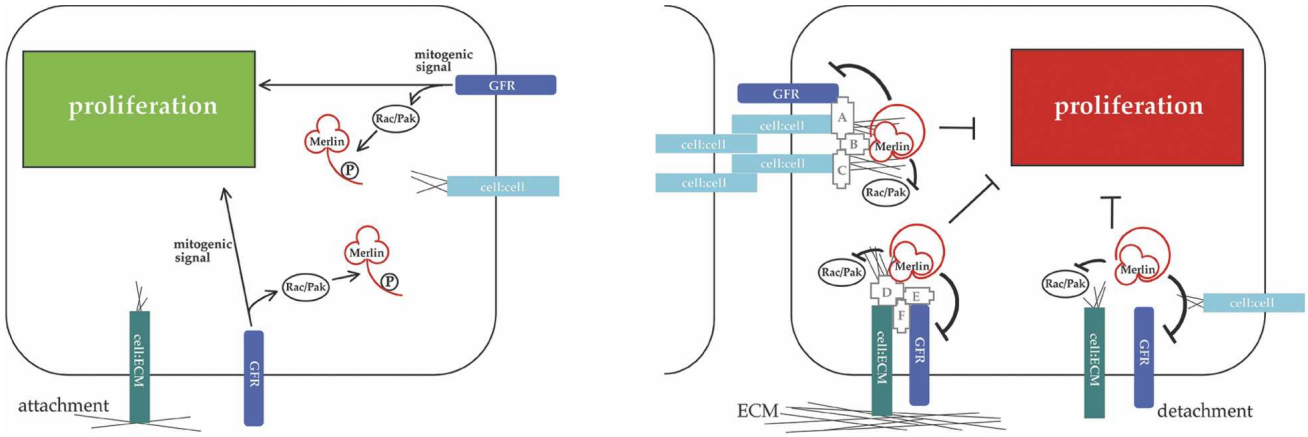

Figure 2. Merlin-organized complexes prevent mitogenic signaling and contact-dependent inhibition of proliferation. (*Left*) At low cell density in cell culture, Merlin is predominantly hyperphosphorylated and inactive and mitogenic signaling proceeds. Similarly, upon cell reattachment to certain ECM substrates, a pool of Merlin is rapidly phosphorylated. (*Right*) At high cell density in cell culture, Merlin is hypophosphorylated, self-associated, and active in mediating contact-dependent inhibition of proliferation. Merlin is recruited to nascent cell:cell boundaries where it appears to stabilize AJs between cells, perhaps by inhibiting Rac/Pak signaling and/or stabilizing the actin cytoskeleton. Under these conditions, Merlin may inhibit signaling from AJ-associated growth-factor receptors. Hypophosphorylated Merlin can also interact with cell:ECM receptors such as CD44, which binds to hyaluronic acid (HA); increased CD44:HA interaction with increased cell density leads to high levels of active Merlin, which may inhibit associated growth-factor receptors. Notably, complete cell detachment also leads to hypophosphorylation and activation of Merlin. Perhaps inhibited mitogenic signaling from multiple complexes accumulates, reaching a threshold that halts proliferation. The study and manipulation of cell:cell contact in two dimensions in cell culture is nonphysiological; in vivo cells in a tissue are contacting other cells and can override contact-dependent inhibition of proliferation under certain normal conditions or in the context of a tumor. Merlin may coordinate the receipt of physical information from the extracellular milieu with the receipt and processing of mitogenic stimuli.

the AJ by locally inhibiting Rac–Pak signaling and/or WASP-mediated actin filament protrusion. Increasing evidence suggests that growth-factor receptors physically associate with and are regulated by AJs (Takahashi and Suzuki 1996; Lampugnani et al. 2003; Qian et al. 2004). Merlin could also organize CD44-containing complexes that coordinate cell:ECM attachment and proliferation control; in addition to Merlin and Ezrin, CD44 can be found in complexes containing growth-factor receptors (Morrison et al. 2001; Cavallaro and Christofori 2004). A fundamental mechanism by which growth-factor receptors are regulated is via endocytosis. Both cell:ECM and cell:cell junctions are dynamic structures that also undergo regulated endocytic turnover. Perhaps by combining the turnover of adhesion structures with growth-factor receptors, the cell can coordinate cell adhesion stability with inhibition of mitogenic signaling—Merlin could function to integrate the two. This would be consistent with the observation that Merlin both controls AJ stability and prevents EGFR internalization (M. Curto and A.I. McClatchey, unpubl.) and with the reported role for Erbin in controlling both AJ formation and proliferation in SCs (Rangwala et al. 2005). Indeed, the study of Merlin could provide novel insight into the poorly understood mechanism whereby cells coordinate growth-factor receptor signaling and AJ turnover.

Schwann, arachnoid, ependymal, and mesothelial cells—unique properties?

Most tumor-suppressor genes including *NF2* are expressed broadly, providing little explanation for the restricted tumor spectrum exhibited by heterozygous mutant carriers. The predisposition of humans and mice that carry heterozygous tumor-suppressor gene mutations to certain types of tumors could be due to (1) cell-type-specific differences in the temporal occurrence of obligatory genetic events such as loss of the wild-type *Nf2* allele or cooperating mutations; (2) cell-autonomous differences in dependence of various cell types upon Merlin for proliferation control, perhaps due to differential expression of key components of a particular tumor-suppressor pathway such as associated proteins, regulators, downstream targets or proteins with partially or fully redundant functions; or (3) non-cell-autonomous differences in the contribution of surrounding heterozygous mutant tissue to tumorigenesis as has been demonstrated for NF1-associated tumors (Zhu et al. 2002).

Indeed, there is ample evidence for cell-type-specific consequences of *Nf2* deficiency. For example, although several types of $Nf2^{-/-}$ cells hyperproliferate in vivo, hyperproliferation is not a consequence of *Nf2* deficiency in *Nf2*-null mouse embryos as described above (McClatchey et al. 1997). Similarly, in the fly and in mosaic $Nf2^{-/-} \leftrightarrow$ wild-type mouse embryos *Nf2* deficiency leads to defects in many tissues, but hyperproliferation in only certain contexts in vivo (Fehon et al. 1997; LaJeunnesse et al. 1998; MacDougall et al. 2001; A.I. McClatchey, unpubl.). In some types of cultured cells (i.e., keratinocytes and SCs), but not others (fibroblasts, osteoblasts), loss of Merlin yields dramatic alterations in actin cytoskeleton morphology (Pelton et al. 1998; Lallemand et al. 2003; A. Chan, D. Lallemand, A.I. McClatchey, and M. Giovannini, unpubl.). Finally, stable AJs do not form at all in cultured $Nf2^{-/-}$ fibroblasts, osteoblasts, SCs, and keratinocytes, while more subtle defects in AJ stability and cell:cell communication are apparent in other $Nf2^{-/-}$ epithelial cells (A.I. McClatchey and M. Curto, unpubl.). Defective cell:cell communication is a consequence of *Nf2* deficiency in many different cell types. Are Schwann, arachnoid, ependymal, and mesothelial cells particularly dependent upon Merlin for integrating cell:cell communication with inhibition of cell proliferation?

SCs are neural crest-derived cells that undergo a sophisticated program of movement and differentiation as they associate with and insulate peripheral axons. Neural crest cells that migrate from the dorsal neural tube to the sensory ganglia and to positions along emerging peripheral axon bundles become immature SCs (for review, see Garratt et al. 2000). Both immature and mature SCs assume an exquisite degree of compartmentalization that is coordinated by intra- and intercellular junctions (Salzer 2003). Dividing immature SCs first loosely ensheath and then progressively segregate clusters of axons from one another with extensive cytoplasmic processes. The initial extension of SC processes along axons and communication between adjacent SCs appear to be mediated by N-cadherin; this association is required for contact-dependent signaling in SC proliferation and differentiation (Salzer et al. 1980a,b; Garratt et al. 2000). The mature peripheral nervous system contains both myelinating and nonmyelinating SCs. Nonmyelinating SCs continue to invest multiple unmyelinated axons. In contrast, myelinating SCs stretch to wrap a single axon multiple times, forming intracellular AJs between adjacent loops of membrane at the paranode and between internodal layers at Schmidt-Lanterman incisures (Fig. 3A; Salzer 2003). At the paranode, the terminal loops are attached to the axonal membrane via septate-like junctions that compartmentalize the axonal surface (for review, see Peles and Salzer 2000; Denisenko-Nehrbass et al. 2002). Merlin has been reported to localize to both the paranode and Schmidt-Lanterman incisures of myelinating SCs (Scherer and Gutmann 1996). Ultrastructural examination of sciatic nerves in *P0-Cre;* $Nf2^{flox2/flox2}$ mice revealed markedly abnormal myelination, although it is not clear whether these abnormally myelinating cells are the precursors of schwannoma development (Giovannini et al. 2000). In fact, human schwannomas do not commonly contain compact myelin (Erlandson and Woodruff 1982). As discussed below, a key issue for the study of NF2-associated tumorigenesis is defining the type of SC that gives rise to a schwannoma.

SCs are critically dependent upon signaling via the ErbB (EGFR) family of receptors for their survival, proliferation, and differentiation (for review, see Garratt et al. 2000). In general, ErbB-expressing SCs and their precursors respond to axonally derived neuregulin, the major functional ErbB ligand in the peripheral nervous sys-

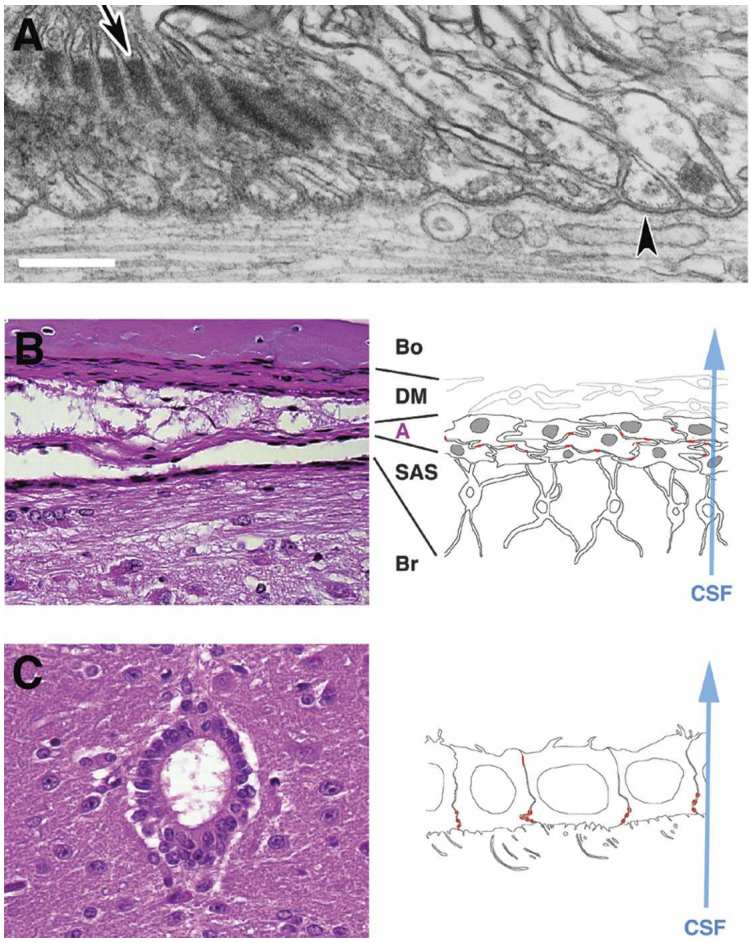

Figure 3. Specialized architecture of Schwann, arachnoid, and ependymal cells. (*A*) Myelinated fiber sectioned through the paranodal region of a node of Ranvier. Septate-like junctions form between each paranodal loop and the axon (arrowhead), while tight junctions and AJs form between adjacent loops (arrow). Bar, 500 nm. (Image kindly provided by Carmen Diaz.) (*B*, *left*) H&E-stained section depicting the arachnoid epithelium in the context of the three meningeal layers. (Bo) Bone; (DM) dura mater; (A) arachnoid; (SAS) subarachnoid space; (PM) pia mater; (Br) brain parenchyma (cerebral cortex). The arachnoid normally adheres to the inner surface of the dura, the space between them is a tissue-processing artifact. (*Right*) Schematic depicting the loosely interdigiting processes of the arachnoid epithelium that are connected by tight junctions and AJs (red). The direction of cerebrospinal fluid (CSF) transit through the arachnoid is shown (arrow). (*C*, *left*) The central canal of the spinal cord is lined by intraspinal ependymal cells (H&E staining). (*Right*) Schematic depicting the cellular architecture of the ependyma. Ependymal epithelial cells are connected by a complex series of apical AJs (red) (Peters et al. 1991). Tight junctions can be identified between cells in some regions of the ependyma, where they are often situated at the basal end of the cell (red). Tight junctions are also found in association with tanycytes, specialized bipolar cells that are inserted into the ependyma in certain regions. CSF transits from the spinal canal across the ciliated apical (*lower* in this figure) surface of the ependyma.

tem. In fact, ErbB signaling regulates myelin thickness by controlling the number of successive wraps made by individual SCs (Garratt et al. 2000; Michailov et al. 2004). Reduced ErbB signaling effects hypomyelination (fewer wraps) and excess ErbB signaling effects hypermyelination (more wraps). In this unique setting, intracellular communication between wraps and growth-factor receptor signaling must be coordinated and may be particularly sensitive to Merlin loss.

Much less is known about the molecular control of proliferation and cell:cell communication in the developing and mature meninges and ependyma. The arachnoid membrane lies between the outer dura and inner pia mater, collectively forming the meningeal layers that cover the brain and spinal cord (Fig. 3B; Yamashima 1996). Meningiomas tend to arise from arachnoid cells (also termed meningothelial cells) located within arachnoid villi, specialized projections that have an important role in the transport of cerebrospinal fluid (Louis et al. 2000). It has been reported that the number of E-cadherin-containing AJs is decreased in many meningiomas (Tohma et al. 1992; Yamashima et al. 1992). In fact, NF2 patients predominantly develop a particular type of meningioma known as the fibroblastic meningioma that lacks strong epithelial characteristics (Heinrich et al. 2003).

The ependymal epithelium lines the ventricles of the brain and central canal of the spinal cord and is a remnant of the proliferative ventricular zone that gives rise to most neurons and glia of the central nervous system during development (Fig. 3C; Peters et al. 1991). Together with the choroid plexus, these cells form the brain:cerebrospinal fluid (CSF) interface; in contrast to the major function of the adjacent choroid plexus in CSF secretion, the ependyma plays an important role in CSF transport (Del Bigio 1995). *NF2* mutations are associated with intraspinal ependymomas rather than intracranial ependymomas (Ebert et al. 1999). Notably, the spinal, but not cranial ependyma is capable of proliferative regeneration following injury (Nag 1997).

Both the arachnoid and ependyma are simple epithelia that are in contact with and involved in transport of CSF, which is a source of certain growth factors (Redzic and Segal 2004). The arachnoid is often described as a "delicate" epithelium. Ultrastructurally, normal arachnoid cells are characterized by loosely interdigitating cellular processes connected by junctional complexes; between the cellular processes are tunnels of extracellular space (Fig. 3B; Peters et al. 1991; Yamashima 1996). Ependymal cells form a simple ciliated cuboidal epithelium connected by apical adherens and gap junctions (Fig. 3C; Lagunowich et al. 1992; Lippoldt et al. 2000). Notably,

some studies have concluded that the ependyma is a "leaky" epithelium, perhaps due to the lack of tight junctions between cells in some regions of the ependyma (Gotow and Hashimoto 1982). Interestingly, the mesothelial lining also performs a critical active function in fluid transport across the peritoneal and pleural cavities. Therefore, like the arachnoid and ependyma, the mesothelia are designed to allow the passage of fluid. All three epithelia must both delimit a fluid-filled space and allow active transit of fluid. Could the histoarchitectural requirements of such epithelia be particularly sensitive to loss of Merlin? Could Merlin be particularly important for preventing signaling from growth-factor receptors that are exposed to a constant source of ligand in cells with loose or permeable intercellular junctions?

The most consistent phenotype associated with *Nf2* deficiency in cultured cells is loss of contact-dependent inhibition of proliferation. In a developing organism, cells in the context of a tissue are all in contact with other cells, but can divide and, therefore, override contact-dependent inhibition of proliferation at certain times. It is likely that cells in most adult tissues integrate multiple inhibitory signals to maintain contact-dependent inhibition of proliferation; perhaps certain cell types rely more heavily upon Merlin for this function. In mice and perhaps in humans, loss of *Nf2* is sufficient for hyperproliferation of SCs and arachnoid cells in vivo, although at least one additional mutation is likely required for frank tumor formation. Animal models of *Nf2* deficiency in the ependyma have not yet been described. Notably, *Nf2*-associated shwannomas, meningiomas, and ependymomas are benign tumors that do not progress to malignancy, perhaps reflecting physiological loss of contact-dependent inhibition of proliferation in vivo. In contrast, osteosarcomas and other tumors that spontaneously develop with longer latency in $Nf2^{+/-}$ mice are malignant and metastatic, likely reflecting the cooperative loss of Nf2 function and that of other growth inhibitory signals. Benign, slow-growing tumors represent a special therapeutic challenge, as standard chemotherapeutic strategies target rapidly dividing cells. In addition, it is well established that cells from malignant tumors are often particularly sensitive to the induction of apoptosis, a feature that is exploited by many chemotherapeutic agents (Johnstone et al. 2002).

Future directions/perspectives

There are many exciting directions and challenges ahead for the study of Nf2-associated tumorigenesis and the molecular function of Merlin. The study of *Nf2* function in animal models has extended our view of Merlin beyond its role in tumor suppression and revealed that Merlin function is essential in many different types of cells. In fact, functional studies of Merlin have already provided new insight into fundamental biological processes such as contact-dependent inhibition of proliferation, cell:cell communication, receptor trafficking, actin cytoskeleton remodeling, and membrane organization.

The study of *Nf2*-mutant mice suggests that loss of Merlin function could play an unexpectedly broad role in tumorigenesis and metastasis. Studies of tumorigenesis in these mice have revealed that both genetic and biological parameters can dictate the spectrum of spontaneous tumors associated with heterozygous *Nf2* mutation. Thus, linkage of cancer-predisposing mutations, temporal control of *Nf2* loss, and cell-type-specific phenotypic consequences of *Nf2* deficiency can each profoundly impact spontaneous tumor development in $Nf2^{+/-}$ mice. These principles are broadly applicable to the study of tumorigenesis initiated by other cancer-predisposing mutations.

A key goal for the study of NF2-associated tumorigenesis will be the determination of what cell type gives rise to the schwannoma. It has been suggested that schwannomas express key markers of immature SCs (Hung et al. 2002). However, some studies have indicated a surprising capacity of differentiated (myelinating) SCs to dedifferentiate (Harrisingh et al. 2004). So, does loss of Merlin cause progressive dedifferentiation of a mature SC or proliferation of a SC progenitor? A detailed histological and ultrastructural analysis of the initiation and progression of schwannomas in *Nf2*-mutant mice and parallel comparison to human *NF2*-mutant schwannomas should help to answer this question. Similarly, comparative analyses of the development of meningiomas in *NF2*-mutant mice and humans together with the development and analysis of models of ependymoma will provide valuable insight into the pathogenesis of these tumors.

The identification of additional genetic mutations that supplant cooperate with *Nf2* loss may provide important insight into the signaling pathways that are deregulated by *Nf2* loss. For example, while the vast majority of sporadic schwannomas exhibit biallelic *Nf2* inactivation, *Nf2* mutations have been identified in only a subset of sporadic meningiomas (Ruttledge et al. 1994; Lomas et al. 2005). This suggests the existence of another locus, which, when mutated somatically, can cause meningioma development. Mathematical modeling of vestibular schwannoma development in NF2 patients suggests that in addition to loss of the wild-type *Nf2* allele, one other mutational event may be necessary for the development of this tumor (Woods et al. 2003). In addition, the low incidence and late onset of schwannomas, in contrast to the high incidence of SC hyperplasia in *P0-Cre*;$Nf2^{flox2/flox2}$ mice strongly suggest that an additional mutation is required for the progression of SC hyperplasia to tumor formation (Giovannini et al. 1999, 2000; Stemmer-Rachamimov et al. 2004). Documentation of biallelic *NF2* inactivation in preneoplastic lesions (hyperplastic SCs and tumorlets) of NF2 patients also supports this hypothesis (Stemmer-Rachamimov et al. 1998).

Many strategies will be exploited to continue the investigation of the molecular mechanism of Merlin function. It will be critical to precisely define the subcellular localization of Merlin in different cell types under different conditions and to functionally validate each candidate Merlin-interacting protein. The identification of

higher order Merlin-containing complexes and examination of how such complexes respond to the loss of Merlin will provide important insight into how Merlin coordinates the physical and signaling properties of membrane complexes. In addition to further genetic analyses in *Drosophila* and investigation of *Nf2*$^{-/-}$ cells from mutant mice, new studies of Merlin orthologs in other species that exploit the unique strengths of each model system will provide powerful, complementary strategies for mechanistic studies of Merlin function. Collectively, the study of NF2-associated tumorigenesis in mammals, together with basic cellular and molecular studies in other model systems and in cell culture will facilitate the identification of potential therapeutic targets and the development of therapeutic strategies for NF2. Further molecular investigation of this novel tumor suppressor will continue to provide new insight into how cells organize their interface with the extracellular environment to coordinate positional information and proliferation control and how disorganization of this interface contributes to tumorigenesis and metastasis.

Acknowledgments

It was very difficult to maintain the focus of this review given all of the interesting studies of NF2—we apologize to those whose work we have not cited or have only mentioned briefly due to space limitations. We are particularly grateful to Marcello Curto for much valuable input, and to Michel Kalamarides, Dominique Lallemand, and Angeliki Louvi for thoughtful discussions and valuable comments on the manuscript. M.G. is supported by the Department of Defense Neurofibromatosis Research Program, James S. McDonnell Foundation, Association Neurofibromatoses et Recklinghausen, Association pour la Recherche sur le Cancer (ARECA), Canceropôle Ile-de France, and Inserm. A.I.M. is supported by the Department of Defense Neurofibromatosis Research Program and National Institutes of Health.

References

Alfthan, K., Heiska, L., Gronholm, M., Renkema, G.H., and Carpen, O. 2004. Cyclic AMP-dependent protein kinase phosphorylates merlin at serine 518 independently of p21-activated kinase and promotes merlin–ezrin heterodimerization. *J. Biol. Chem.* **279:** 18559–18566.

Amsterdam, A., Sadler, K.C., Lai, K., Farrington, S., Bronson, R.T., Lees, J.A., and Hopkins, N. 2004. Many ribosomal protein genes are cancer genes in zebrafish. *PLoS Biol.* **2:** E139.

Barret, C., Roy, C., Montcourrier, P., Mangeat, P., and Niggli, V. 2000. Mutagenesis of the phosphatidylinositol 4,5-bisphosphate (PIP(2)) binding site in the NH(2)-terminal domain of ezrin correlates with its altered cellular distribution. *J. Cell. Biol.* **151:** 1067–1080.

Berghmans, S., Murphey, R.D., Wienholds, E., Neuberg, D., Kutok, J.L., Fletcher, C.D., Morris, J.P., Liu, T.X., Schulte-Merker, S., Kanki, J.P., et al. 2005. tp53 mutant zebrafish develop malignant peripheral nerve sheath tumors. *Proc. Natl. Acad. Sci.* **102:** 407–412.

Bershadsky, A. 2004. Magic touch: How does cell-cell adhesion trigger actin assembly? *Trends Cell. Biol.* **14:** 589–593.

Bianchi, A.B., Mitsunaga, S.I., Cheng, J.Q., Klein, W.M., Jhanwar, S.C., Seizinger, B., Kley, N., Klein-Szanto, A.J., and Testa, J.R. 1995. High frequency of inactivating mutations in the neurofibromatosis type 2 gene (NF2) in primary malignant mesotheliomas. *Proc. Natl. Acad. Sci.* **92:** 10854–10858.

Brault, E., Gautreau, A., Lamarine, M., Callebaut, I., Thomas, G., and Goutebroze, L. 2001. Normal membrane localization and actin association of the NF2 tumor suppressor protein are dependent on folding of its N-terminal domain. *J. Cell. Sci.* **114:** 1901–1912.

Bretscher, A., Edwards, K., and Fehon, R.G. 2002. ERM proteins and merlin: Integrators at the cell cortex. *Nat. Rev. Mol. Cell. Biol.* **3:** 586–599.

Cao, X., Ding, X., Guo, Z., Zhou, R., Wang, F., Long, F., Wu, F., Bi, F., Wang, Q., Fan, D., et al. 2005. PALS1 specifies the localization of ezrin to the apical membrane of gastric parietal cells. *J. Biol. Chem.* **280:** 13584–13592.

Cavallaro, U. and Christofori, G. 2004. Multitasking in tumor progression: Signaling functions of cell adhesion molecules. *Ann. N.Y. Acad. Sci.* **1014:** 58–66.

Chen, Y., Gutmann, D.H., Haipek, C.A., Martinsen, B.J., Bronner-Fraser, M., and Krull, C.E. 2004a. Characterization of chicken Nf2/merlin indicates regulatory roles in cell proliferation and migration. *Dev. Dyn.* **229:** 541–554.

Chen, Y.X., Krull, C.E., and Reneker, L.W. 2004b. Targeted gene expression in the chicken eye by in ovo electroporation. *Mol. Vis.* **10:** 874–883.

Del Bigio, M.R. 1995. The ependyma: A protective barrier between brain and cerebrospinal fluid. *Glia* **14:** 1–13.

den Bakker, M.A., Tascilar, M., Riegman, P.H., Hekman, A.C., Boersma, W., Janssen, P.J., de Jong, T.A., Hendriks, W., van der Kwast, T.H., and Zwarthoff, E.C. 1995. Neurofibromatosis type 2 protein co-localizes with elements of the cytoskeleton. *Am. J. Pathol.* **147:** 1339–1349.

Denisenko-Nehrbass, N., Faivre-Sarrailh, C., Goutebroze, L., and Girault, J.A. 2002. A molecular view on paranodal junctions of myelinated fibers. *J. Physiol. Paris* **96:** 99–103.

Ebert, C., von Haken, M., Meyer-Puttlitz, B., Wiestler, O.D., Reifenberger, G., Pietsch, T., and von Deimling, A. 1999. Molecular genetic analysis of ependymal tumors. NF2 mutations and chromosome 22q loss occur preferentially in intramedullary spinal ependymomas. *Am. J. Pathol.* **155:** 627–632.

Erlandson, R.A. and Woodruff, J.M. 1982. Peripheral nerve sheath tumors: An electron microscopic study of 43 cases. *Cancer* **49:** 273–287.

Evans, D.G., Huson, S.M., Donnai, D., Neary, W., Blair, V., Newton, V., and Harris, R. 1992. A clinical study of type 2 neurofibromatosis. *Q. J. Med.* **84:** 603–618.

Evans, D.G., Moran, A., King, A., Saeed, S., Gurusinghe, N., and Ramsden, R. 2005. Incidence of vestibular schwannoma and neurofibromatosis 2 in the North West of England over a 10-year period: Higher incidence than previously thought. *Otol. Neurotol.* **26:** 93–97.

Fehon, R.G., Oren, T., LaJeunesse, D.R., Melby, T.E., and McCartney, B.M. 1997. Isolation of mutations in the *Drosophila* homologues of the human Neurofibromatosis 2 and yeast CDC42 genes using a simple and efficient reverse-genetic method. *Genetics* **146:** 245–252.

Fernandez-Valle, C., Tang, Y., Ricard, J., Rodenas-Ruano, A., Taylor, A., Hackler, E., Biggerstaff, J., and Iacovelli, J. 2002. Paxillin binds schwannomin and regulates its density-dependent localization and effect on cell morphology. *Nat. Genet.* **31:** 354–362.

Fleury-Feith, J., Lecomte, C., Renier, A., Matrat, M., Kheuang, L., Abramowski, V., Levy, F., Janin, A., Giovannini, M., and

Jaurand, M.C. 2003. Hemizygosity of Nf2 is associated with increased susceptibility to asbestos-induced peritoneal tumours. *Oncogene* **22:** 3799–3805.

Garratt, A.N., Britsch, S., and Birchmeier, C. 2000. Neuregulin, a factor with many functions in the life of a schwann cell. *Bioessays* **22:** 987–996.

Gautreau, A., Manent, J., Fievet, B., Louvard, D., Giovannini, M., and Arpin, M. 2002. Mutant products of the NF2 tumor suppressor gene are degraded by the ubiquitin–proteasome pathway. *J. Biol. Chem.* **277:** 31279–31282.

Giovannini, M., Robanus-Maandag, E., Niwa-Kawakita, M., van der Valk, M., Woodruff, J.M., Goutebroze, L., Merel, P., Berns, A., and Thomas, G. 1999. Schwann cell hyperplasia and tumors in transgenic mice expressing a naturally occurring mutant NF2 protein. *Genes & Dev.* **13:** 978–986.

Giovannini, M., Robanus-Maandag, E., van der Valk, M., Niwa-Kawakita, M., Abramowski, V., Goutebroze, L., Woodruff, J.M., Berns, A., and Thomas, G. 2000. Conditional biallelic Nf2 mutation in the mouse promotes manifestations of human neurofibromatosis type 2. *Genes & Dev.* **14:** 1617–1630.

Gobel, V., Barrett, P.L., Hall, D.H., and Fleming, J.T. 2004. Lumen morphogenesis in *C. elegans* requires the membrane-cytoskeleton linker erm-1. *Dev. Cell* **6:** 865–873.

Gonzalez-Agosti, C., Xu, L., Pinney, D., Beauchamp, R., Hobbs, W., Gusella, J., and Ramesh, V. 1996. The merlin tumor suppressor localizes preferentially in membrane ruffles. *Oncogene* **13:** 1239–1247.

Gotow, T. and Hashimoto, P.H. 1982. Intercellular junctions between specialized ependymal cells in the subcommissural organ of the rat. *J. Neurocytol.* **11:** 363–379.

Gronholm, M., Sainio, M., Zhao, F., Heiska, L., Vaheri, A., and Carpen, O. 1999. Homotypic and heterotypic interaction of the neurofibromatosis 2 tumor suppressor protein merlin and the ERM protein ezrin. *J. Cell. Sci.* **112:** 895–904.

Gronholm, M., Teesalu, T., Tyynela, J., Piltti, K., Bohling, T., Wartiovaara, K., Vaheri, A., and Carpen, O. 2005. Characterization of the NF2 protein merlin and the ERM protein ezrin in human, rat, and mouse central nervous system. *Mol. Cell. Neurosci.* **28:** 683–693.

Harrisingh, M.C., Perez-Nadales, E., Parkinson, D.B., Malcolm, D.S., Mudge, A.W., and Lloyd, A.C. 2004. The Ras/Raf/ERK signalling pathway drives Schwann cell dedifferentiation. *EMBO J.* **23:** 3061–3071.

Heinrich, B., Hartmann, C., Stemmer-Rachamimov, A.O., Louis, D.N., and MacCollin, M. 2003. Multiple meningiomas: Investigating the molecular basis of sporadic and familial forms. *Int. J. Cancer* **103:** 483–488.

Hipfner, D.R., Keller, N., and Cohen, S.M. 2004. Slik Sterile-20 kinase regulates Moesin activity to promote epithelial integrity during tissue growth. *Genes & Dev.* **18:** 2243–2248.

Hung, G., Colton, J., Fisher, L., Oppenheimer, M., Faudoa, R., Slattery, W., and Linthicum, F. 2002. Immunohistochemistry study of human vestibular nerve schwannoma differentiation. *Glia* **38:** 363–370.

James, M.F., Manchanda, N., Gonzalez-Agosti, C., Hartwig, J.H., and Ramesh, V. 2001. The neurofibromatosis 2 protein product merlin selectively binds F-actin but not G-actin, and stabilizes the filaments through a lateral association. *Biochem. J.* **356:** 377–386.

Johnson, K.C., Kissil, J.L., Fry, J.L., and Jacks, T. 2002. Cellular transformation by a FERM domain mutant of the Nf2 tumor suppressor gene. *Oncogene* **21:** 5990–5997.

Johnstone, R.W., Ruefli, A.A., and Lowe, S.W. 2002. Apoptosis: A link between cancer genetics and chemotherapy. *Cell* **108:** 153–164.

Kalamarides, M., Niwa-Kawakita, M., Leblois, H., Abramowski, V., Perricaudet, M., Janin, A., Thomas, G., Gutmann, D.H., and Giovannini, M. 2002. Nf2 gene inactivation in arachnoidal cells is rate-limiting for meningioma development in the mouse. *Genes & Dev.* **16:** 1060–1065.

Kissil, J.L., Johnson, K.C., Eckman, M.S., and Jacks, T. 2002. Merlin phosphorylation by p21-activated kinase 2 and effects of phosphorylation on merlin localization. *J. Biol. Chem.* **277:** 10394–10399.

Kissil, J.L., Wilker, E.W., Johnson, K.C., Eckman, M.S., Yaffe, M.B., and Jacks, T. 2003. Merlin, the product of the Nf2 tumor suppressor gene, is an inhibitor of the p21-activated kinase, Pak1. *Mol. Cell* **12:** 841–849.

Kolch, W. 2003. Erbin: Sorting out ErbB2 receptors or giving Ras a break? *Sci. STKE* **2003:** pe37.

Kressel, M. and Schmucker, B. 2002. Nucleocytoplasmic transfer of the NF2 tumor suppressor protein merlin is regulated by exon 2 and a CRM1-dependent nuclear export signal in exon 15. *Hum. Mol. Genet.* **11:** 2269–2278.

Lagunowich, L.A., Schneider, J.C., Chasen, S., and Grunwald, G.B. 1992. Immunohistochemical and biochemical analysis of N-cadherin expression during CNS development. *J. Neurosci. Res.* **32:** 202–208.

LaJeunesse, D.R., McCartney, B.M., and Fehon, R.G. 1998. Structural analysis of *Drosophila* merlin reveals functional domains important for growth control and subcellular localization. *J. Cell. Biol.* **141:** 1589–1599.

LaJeunesse, D.R., McCartney, B.M., and Fehon, R.G. 2001. A systematic screen for dominant second-site modifiers of Merlin/NF2 phenotypes reveals an interaction with blistered/DSRF and scribbler. *Genetics* **158:** 667–679.

Lallemand, D., Curto, M., Saotome, I., Giovannini, M., and McClatchey, A.I. 2003. NF2 deficiency promotes tumorigenesis and metastasis by destabilizing adherens junctions. *Genes & Dev.* **17:** 1090–1100.

Lampugnani, M.G., Zanetti, A., Corada, M., Takahashi, T., Balconi, G., Breviario, F., Orsenigo, F., Cattelino, A., Kemler, R., Daniel, T.O., et al. 2003. Contact inhibition of VEGF-induced proliferation requires vascular endothelial cadherin, β-catenin, and the phosphatase DEP-1/CD148. *J. Cell Biol.* **161:** 793–804.

Lasota, J., Fetsch, J.F., Wozniak, A., Wasag, B., Sciot, R., and Miettinen, M. 2001. The neurofibromatosis type 2 gene is mutated in perineurial cell tumors: A molecular genetic study of eight cases. *Am. J. Pathol.* **158:** 1223–1229.

Lazar, C.S., Cresson, C.M., Lauffenburger, D.A., and Gill, G.N. 2004. The Na+/H+ exchanger regulatory factor stabilizes epidermal growth factor receptors at the cell surface. *Mol. Biol. Cell* **15:** 5470–5480.

Lippoldt, A., Jansson, A., Kniesel, U., Andbjer, B., Andersson, A., Wolburg, H., Fuxe, K., and Haller, H. 2000. Phorbol ester induced changes in tight and adherens junctions in the choroid plexus epithelium and in the ependyma. *Brain Res.* **854:** 197–206.

Lomas, J., Bello, M.J., Arjona, D., Alonso, M.E., Martinez-Glez, V., Lopez-Marin, I., Aminoso, C., de Campos, J.M., Isla, A., Vaquero, J., et al. 2005. Genetic and epigenetic alteration of the NF2 gene in sporadic meningiomas. *Genes Chrom. Cancer* **42:** 314–319.

Louis, D.N., Scheithauer, B.W., Budka, H., von Deimling, A., and Kepes, J.J. 2000. *Meningiomas*. IARC Press, Lyon, France.

Lutchman, M. and Rouleau, G.A. 1995. The neurofibromatosis type 2 gene product, schwannomin, suppresses growth of NIH 3T3 cells. *Cancer Res.* **55:** 2270–2274.

MacDougall, N., Lad, L., Wilkie, G.S., Francis-Lang, H., Sullivan, W., and Davis, I. 2001. Merlin, the *Drosophila* homologue of neurofibromatosis-2, is specifically required in pos-

terior follicle cells for axis formation in the oocyte. *Development* **128:** 665–673.
Maeda, M., Matsui, T., Imamura, M., Tsukita, S., and Tsukita, S. 1999. Expression level, subcellular distribution and rho-GDI binding affinity of merlin in comparison with Ezrin/Radixin/Moesin proteins. *Oncogene* **18:** 4788–4797.
Manchanda, N., Lyubimova, A., Ho, H.Y., James, M.F., Gusella, J.F., Ramesh, N., Snapper, S.B., and Ramesh, V. 2005. The NF2 tumor suppressor Merlin and the ERM proteins interact with N-WASP and regulate its actin polymerization function. *J. Biol. Chem.* **280:** 12517–12522.
Matsui, T., Maeda, M., Doi, Y., Yonemura, S., Amano, M., Kaibuchi, K., Tsukita, S., and Tsukita, S. 1998. Rho-kinase phosphorylates COOH-terminal threonines of ezrin/radixin/moesin (ERM) proteins and regulates their head-to-tail association. *J. Cell. Biol.* **140:** 647–657.
Matsui, T., Yonemura, S., Tsukita, S., and Tsukita, S. 1999. Activation of ERM proteins in vivo by Rho involves phosphatidyl-inositol 4-phosphate 5-kinase and not ROCK kinases. *Curr. Biol.* **9:** 1259–1262.
McCartney, B.M. and Fehon, R.G. 1996. Distinct cellular and subcellular patterns of expression imply distinct functions for the *Drosophila* homologues of moesin and the neurofibromatosis 2 tumor suppressor, merlin. *J. Cell. Biol.* **133:** 843–852.
McClatchey, A.I. 2003. Merlin and ERM proteins: Unappreciated roles in cancer development? *Nat. Rev. Cancer* **3:** 877–883.
McClatchey, A.I., Saotome, I., Ramesh, V., Gusella, J.F., and Jacks, T. 1997. The Nf2 tumor suppressor gene product is essential for extraembryonic development immediately prior to gastrulation. *Genes & Dev.* **11:** 1253–1265.
McClatchey, A.I., Saotome, I., Mercer, K., Crowley, D., Gusella, J.F., Bronson, R.T., and Jacks, T. 1998. Mice heterozygous for a mutation at the Nf2 tumor suppressor locus develop a range of highly metastatic tumors. *Genes & Dev.* **12:** 1121–1133.
McMenamin, M.E. and Fletcher, C.D. 2001. Expanding the spectrum of malignant change in schwannomas: Epithelioid malignant change, epithelioid malignant peripheral nerve sheath tumor, and epithelioid angiosarcoma: A study of 17 cases. *Am. J. Surg. Pathol.* **25:** 13–25.
Meng, J.J., Lowrie, D.J., Sun, H., Dorsey, E., Pelton, P.D., Bashour, A.M., Groden, J., Ratner, N., and Ip, W. 2000. Interaction between two isoforms of the NF2 tumor suppressor protein, merlin, and between merlin and ezrin, suggests modulation of ERM proteins by merlin. *J. Neurosci. Res.* **62:** 491–502.
Michailov, G.V., Sereda, M.W., Brinkmann, B.G., Fischer, T.M., Haug, B., Birchmeier, C., Role, L., Lai, C., Schwab, M.H., and Nave, K.A. 2004. Axonal neuregulin-1 regulates myelin sheath thickness. *Science* **304:** 700–703.
Morrison, H., Sherman, L.S., Legg, J., Banine, F., Isacke, C., Haipek, C.A., Gutmann, D.H., Ponta, H., and Herrlich, P. 2001. The NF2 tumor suppressor gene product, merlin, mediates contact inhibition of growth through interactions with CD44. *Genes & Dev.* **15:** 968–980.
Muranen, T., Gronholm, M., Renkema, G.H., and Carpen, O. 2005. Cell cycle-dependent nucleocytoplasmic shuttling of the neurofibromatosis 2 tumour suppressor merlin. *Oncogene* **24:** 1150–1158.
Murthy, A., Gonzalez-Agosti, C., Cordero, E., Pinney, D., Candia, C., Solomon, F., Gusella, J., and Ramesh, V. 1998. NHE-RF, a regulatory cofactor for Na(+)–H+ exchange, is a common interactor for merlin and ERM (MERM) proteins. *J. Biol. Chem.* **273:** 1273–1276.
Nag, S. 1997. Ependyma. In *Textbook of neuropathology* (eds. R.L. Davis and D.M. Robertson), pp 111–136. Williams & Wilkins, Baltimore, MD.
Nguyen, R., Reczek, D., and Bretscher, A. 2001. Hierarchy of merlin and ezrin N- and C-terminal domain interactions in homo- and heterotypic associations and their relationship to binding of scaffolding proteins EBP50 and E3KARP. *J. Biol. Chem.* **276:** 7621–7629.
Pearson, M.A., Reczek, D., Bretscher, A., and Karplus, P.A. 2000. Structure of the ERM protein moesin reveals the FERM domain fold masked by an extended actin binding tail domain. *Cell* **101:** 259–270.
Peles, E. and Salzer, J.L. 2000. Molecular domains of myelinated axons. *Curr. Opin. Neurobiol.* **10:** 558–565.
Pelton, P.D., Sherman, L.S., Rizvi, T.A., Marchionni, M.A., Wood, P., Friedman, R.A., and Ratner, N. 1998. Ruffling membrane, stress fiber, cell spreading and proliferation abnormalities in human Schwannoma cells. *Oncogene* **17:** 2195–2209.
Peters, A., Palay, S.L., and Webster, H.D. 1991. *The fine structure of the nervous system. Neurons and their supporting cells*. Oxford University Press, New York.
Pietromonaco, S.F., Simons, P.C., Altman, A., and Elias, L. 1998. Protein kinase C-θ phosphorylation of moesin in the actin-binding sequence. *J. Biol. Chem.* **273:** 7594–7603.
Pineau, P., Marchio, A., Nagamori, S., Seki, S., Tiollais, P., and Dejean, A. 2003. Homozygous deletion scanning in hepatobiliary tumor cell lines reveals alternative pathways for liver carcinogenesis. *Hepatology* **37:** 852–861.
Qian, X., Karpova, T., Sheppard, A.M., McNally, J., and Lowy, D.R. 2004. E-cadherin-mediated adhesion inhibits ligand-dependent activation of diverse receptor tyrosine kinases. *EMBO J.* **23:** 1739–1784.
Rangwala, R., Banine, F., Borg, J.P., and Sherman, L.S. 2005. Erbin regulates mitogen-activated protein (MAP) kinase activation and MAP kinase-dependent interactions between Merlin and adherens junction protein complexes in Schwann cells. *J. Biol. Chem.* **280:** 11790–11797.
Redzic, Z.B. and Segal, M.B. 2004. The structure of the choroid plexus and the physiology of the choroid plexus epithelium. *Adv. Drug Deliv. Rev.* **56:** 1695–1716.
Robanus-Maandag, E., Giovannini, M., van der Valk, M., Niwa-Kawakita, M., Abramowski, V., Antonescu, C., Thomas, G., and Berns, A. 2004. Synergy of Nf2 and p53 mutations in development of malignant tumours of neural crest origin. *Oncogene* **23:** 6541–6547.
Rong, R., Surace, E.I., Haipek, C.A., Gutmann, D.H., and Ye, K. 2004. Serine 518 phosphorylation modulates merlin intramolecular association and binding to critical effectors important for NF2 growth suppression. *Oncogene* **23:** 8447–8454.
Rouleau, G.A., Merel, P., Lutchman, M., Sanson, M., Zucman, J., Marineau, C., Hoang-Xuan, K., Demczuk, S., Desmaze, C., Plougastel, B., et al. 1993. Alteration in a new gene encoding a putative membrane-organizing protein causes neuro-fibromatosis type 2. *Nature* **363:** 515–521.
Ruttledge, M.H., Sarrazin, J., Rangaratnam, S., Phelan, C.M., Twist, E., Merel, P., Delattre, O., Thomas, G., Nordenskjold, M., Collins, V.P., et al. 1994. Evidence for the complete inactivation of the NF2 gene in the majority of sporadic meningiomas. *Nat. Genet.* **6:** 180–184.
Sainio, M., Zhao, F., Heiska, L., Turunen, O., den Bakker, M., Zwarthoff, E., Lutchman, M., Rouleau, G.A., Jaaskelainen, J., Vaheri, A., et al. 1997. Neurofibromatosis 2 tumor suppressor protein colocalizes with ezrin and CD44 and associates with actin-containing cytoskeleton. *J. Cell. Sci.* **110:** 2249–2260.

Salzer, J.L. 2003. Polarized domains of myelinated axons. *Neuron* **40:** 297–318.

Salzer, J.L., Bunge, R.P., and Glaser, L. 1980a. Studies of Schwann cell proliferation. III. Evidence for the surface localization of the neurite mitogen. *J. Cell. Biol.* **84:** 767–778.

Salzer, J.L., Williams, A.K., Glaser, L., and Bunge, R.P. 1980b. Studies of Schwann cell proliferation. II. Characterization of the stimulation and specificity of the response to a neurite membrane fraction. *J. Cell. Biol.* **84:** 753–766.

Scherer, S.S. and Gutmann, D.H. 1996. Expression of the neurofibromatosis 2 tumor suppressor gene product, merlin, in Schwann cells. *J. Neurosci. Res.* **46:** 595–605.

Scoles, D.R., Huynh, D.P., Morcos, P.A., Coulsell, E.R., Robinson, N.G., Tamanoi, F., and Pulst, S.M. 1998. Neurofibromatosis 2 tumour suppressor schwannomin interacts with βII-spectrin. *Nat. Genet.* **18:** 354–359.

Scoles, D.R., Huynh, D.P., Chen, M.S., Burke, S.P., Gutmann, D.H., and Pulst, S.M. 2000. The neurofibromatosis 2 tumor suppressor protein interacts with hepatocyte growth factor-regulated tyrosine kinase substrate. *Hum. Mol. Genet.* **9:** 1567–1574.

Sekido, Y., Pass, H.I., Bader, S., Mew, D.J., Christman, M.F., Gazdar, A.F., and Minna, J.D. 1995. Neurofibromatosis type 2 (NF2) gene is somatically mutated in mesothelioma but not in lung cancer. *Cancer Res.* **55:** 1227–1231.

Shaw, R.J., McClatchey, A.I., and Jacks, T. 1998. Regulation of the neurofibromatosis type 2 tumor suppressor protein, merlin, by adhesion and growth arrest stimuli. *J. Biol. Chem.* **273:** 7757–7764.

Shaw, R.J., Paez, J.G., Curto, M., Yaktine, A., Pruitt, W.M., Saotome, I., O'Bryan, J.P., Gupta, V., Ratner, N., Der, C.J., et al. 2001. The Nf2 tumor suppressor, merlin, functions in Rac-dependent signaling. *Dev. Cell* **1:** 63–72.

Sheikh, H.A., Tometsko, M., Niehouse, L., Aldeeb, D., Swalsky, P., Finkelstein, S., Barnes, E.L., and Hunt, J.L. 2004. Molecular genotyping of medullary thyroid carcinoma can predict tumor recurrence. *Am. J. Surg. Pathol.* **28:** 101–106.

Shelly, M., Mosesson, Y., Citri, A., Lavi, S., Zwang, Y., Melamed-Book, N., Aroeti, B., and Yarden, Y. 2003. Polar expression of ErbB-2/HER2 in epithelia. Bimodal regulation by Lin-7. *Dev. Cell* **5:** 475–486.

Sherman, L., Xu, H.M., Geist, R.T., Saporito-Irwin, S., Howells, N., Ponta, H., Herrlich, P., and Gutmann, D.H. 1997. Interdomain binding mediates tumor growth suppression by the NF2 gene product. *Oncogene* **15:** 2505–2509.

Sherr, C.J. 2004. Principles of tumor suppression. *Cell* **116:** 235–246.

Shimizu, T., Seto, A., Maita, N., Hamada, K., Tsukita, S., Tsukita, S., and Hakoshima, T. 2002. Structural basis for neurofibromatosis type 2. Crystal structure of the merlin FERM domain. *J. Biol. Chem.* **277:** 10332–10336.

Speck, O., Hughes, S.C., Noren, N.K., Kulikauskas, R.M., and Fehon, R.G. 2003. Moesin functions antagonistically to the Rho pathway to maintain epithelial integrity. *Nature* **421:** 83–87.

Stemmer-Rachamimov, A.O., Xu, L., Gonzalez-Agosti, C., Burwick, J.A., Pinney, D., Beauchamp, R., Jacoby, L.B., Gusella, J.F., Ramesh, V., and Louis, D.N. 1997. Universal absence of merlin, but not other ERM family members, in schwannomas. *Am. J. Pathol.* **151:** 1649–1654.

Stemmer-Rachamimov, A.O., Nielsen, G.P., Rosenberg, A.E., Louis, D.N., Jones, D., Ramesh, V., Gusella, J.F., and Jacoby, L.B. 1998. The NF2 gene and merlin protein in human osteosarcomas. *Neurogenetics* **2:** 73–74.

Stemmer-Rachamimov, A.O., Louis, D.N., Nielsen, G.P., Antonescu, C.R., Borowsky, A.D., Bronson, R.T., Burns, D.K., Cervera, P., McLaughlin, M.E., Reifenberger, G., et al. 2004. Comparative pathology of nerve sheath tumors in mouse models and humans. *Cancer Res.* **64:** 3718–3724.

Stickney, J.T., Bacon, W.C., Rojas, M., Ratner, N., and Ip, W. 2004. Activation of the tumor suppressor merlin modulates its interaction with lipid rafts. *Cancer Res.* **64:** 2717–2724.

Takahashi, K. and Suzuki, K. 1996. Density-dependent inhibition of growth involves prevention of EGF receptor activation by E-cadherin-mediated cell-cell adhesion. *Exp. Cell Res.* **226:** 214–222.

Takahashi, K., Sasaki, T., Mammoto, A., Takaishi, K., Kameyama, T., Tsukita, S., and Takai, Y. 1997. Direct interaction of the Rho GDP dissociation inhibitor with ezrin/radixin/moesin initiates the activation of the Rho small G protein. *J. Biol. Chem.* **272:** 23371–23375.

Tikoo, A., Varga, M., Ramesh, V., Gusella, J., and Maruta, H. 1994. An anti-Ras function of neurofibromatosis type 2 gene product (NF2/Merlin). *J. Biol. Chem.* **269:** 23387–23390.

Tohma, Y., Yamashima, T., and Yamashita, J. 1992. Immunohistochemical localization of cell adhesion molecule epithelial cadherin in human arachnoid villi and meningiomas. *Cancer Res.* **52:** 1981–1987.

Trofatter, J.A., MacCollin, M.M., Rutter, J.L., Murrell, J.R., Duyao, M.P., Parry, D.M., Eldridge, R., Kley, N., Menon, A.G., Pulaski, K., et al. 1993. A novel moesin-, ezrin-, radixin-like gene is a candidate for the neurofibromatosis 2 tumor suppressor. *Cell* **72:** 791–800.

Wiederhold, T., Lee, M.F., James, M., Neujahr, R., Smith, N., Murthy, A., Hartwig, J., Gusella, J.F., and Ramesh, V. 2004. Magicin, a novel cytoskeletal protein associates with the NF2 tumor suppressor merlin and Grb2. *Oncogene* **23:** 8815–8825.

Woodruff, J.M., Selig, A.M., Crowley, K., and Allen, P.W. 1994. Schwannoma (neurilemoma) with malignant transformation. A rare, distinctive peripheral nerve tumor. *Am. J. Surg. Pathol.* **18:** 882–895.

Woods, R., Friedman, J.M., Evans, D.G., Baser, M.E., and Joe, H. 2003. Exploring the 'two-hit hypothesis' in NF2: Tests of two-hit and three-hit models of vestibular schwannoma development. *Genet. Epidemiol.* **24:** 265–272.

Xiao, G.H., Beeser, A., Chernoff, J., and Testa, J.R. 2002. p21-activated kinase links Rac/Cdc42 signaling to merlin. *J. Biol. Chem.* **277:** 883–886.

Yamashima, T. 1996. On arachnoid villi and meningiomas: Functional implication of ultrastructure, cell adhesion mechanisms, and extracellular matrix composition. *Pathol. Oncol. Res.* **2:** 144–149.

Yamashima, T., Tohma, Y., and Yamashita, J. 1992. Expression of cell adhesion molecule E-cadherin in human arachnoid villi. *J. Neurosurg.* **77:** 749–756.

Zhu, Y., Ghosh, P., Charnay, P., Burns, D.K., and Parada, L.F. 2002. Neurofibromas in NF1: Schwann cell origin and role of tumor environment. *Science* **296:** 920–922.

Susceptibility to astrocytoma in mice mutant for *Nf1* and *Trp53* is linked to chromosome 11 and subject to epigenetic effects

Karlyne M. Reilly*†, Robert G. Tuskan*, Emily Christy‡§, Dagan A. Loisel‡§, Jeremy Ledger‡, Roderick T. Bronson¶, C. Dahlem Smith‖, Shirley Tsang, David J. Munroe**, and Tyler Jacks‡§**

*Mouse Cancer Genetics Program, National Cancer Institute, Frederick, MD 21702; ‡Department of Biology and Center for Cancer Research and §Howard Hughes Medical Institute, Massachusetts Institute of Technology, Cambridge, MA 02169; ¶Department of Pathology, Harvard Medical School, Boston, MA 02115; and Laboratories of ‖Animal Sciences Program and **Molecular Technology, Science Applications International Corporation, Frederick, MD 21702

Edited by Bert Vogelstein, The Sidney Kimmel Comprehensive Cancer Center at Johns Hopkins, Baltimore, MD, and approved July 9, 2004 (received for review February 21, 2004)

Astrocytoma is the most common malignant brain tumor in humans. Loss of the p53 signaling pathway and up-regulation of the ras signaling pathway are common during tumor progression. We have shown previously that mice mutant for *Trp53* and *Nf1* develop astrocytoma, progressing to glioblastoma, on a C57BL/6J strain background. In contrast, here we present data that mice mutant for *Trp53* and *Nf1* on a 129S4/SvJae background are highly resistant to developing astrocytoma. Through analysis of F_1 progeny, we demonstrate that susceptibility to astrocytoma is linked to chromosome 11, and that the modifier gene(s) responsible for differences in susceptibility is closely linked to *Nf1* and *Trp53*. Furthermore, this modifier of astrocytoma susceptibility is itself epigenetically modified. These data demonstrate that epigenetic effects can have a strong effect on whether cancer develops in the context of mutant ras signaling and mutant p53, and that this mouse model of astrocytoma can be used to identify modifier phenotypes with complex inheritance patterns that would be unidentifiable in humans. Because analysis of gene function in the mouse is often performed on a mixed C57BL/6,129 strain background, these data also provide a powerful example of the potential of these strains to mask interesting gene functions.

Astrocytoma is a characteristically diffuse tumor of the central nervous system (CNS). Because of its diffuse infiltration, it often cannot be completely resected, leading to a very poor prognosis for patients. Astrocytoma, together with glioblastoma (the highest grade of astrocytoma), accounts for more than three-quarters of all gliomas, making it the most common malignant brain tumor (1). The 5-year survival rate for glioblastoma is <3%. A better understanding of the genetic risk factors associated with astrocytoma will give insight into the mechanism of astrocytoma initiation and progression and will lead to better screening methods and new targets for therapy.

Data from human populations pointing to genetic risk factors for astrocytoma are sparse. Malmer *et al.* (2) have examined the increased family risk of developing low- vs. high-grade glioma and favor the view that autosomal recessive genes affect astrocytoma risk, although the role of a common environment in familial risk cannot be excluded. Several familial cancer syndromes show an increased risk for astrocytoma, including neurofibromatosis type 1 (NF1) (3, 4) and Li–Fraumeni syndrome (LFS) (5). NF1 patients have a mutation in the *NF1* gene (6) (*Nf1* in the mouse) and are predisposed to neurofibromas and optic gliomas, with an increased risk for malignant peripheral nerve sheath tumors and diffuse astrocytoma/glioblastoma (3, 4). Studies of NF1 families have demonstrated a role for modifier genes unlinked to *NF1* in the severity of the disease with respect to the numbers of neurofibromas and the presence or absence of optic gliomas (7). Studies of NF1 patients have also shown that patients with optic glioma are more likely to develop CNS tumors such as astrocytoma (8, 9), although this observation is as likely due to the particular mutant allele of *NF1* (10) as to genetic or environmental risk factors. Astrocytomas are also frequently associated with mutations in *Tp53* in sporadic cases (11, 12) or in LFS patients carrying germline mutations in the *Tp53* gene (5) (*Trp53* in the mouse). Although there are no clear data in patients that genetic background affects the risk of particular tumors in LFS patients, data from the mouse show that the strain background can affect the incidence of teratomas and mammary tumors in *Trp53* mutant mice (13, 14). The relatively low penetrance of astrocytoma in the population makes association studies to look at genetic risk factors difficult. The identification of these risk factors is best accomplished in inbred animal models and the results then tested in human populations.

Because of the difficulty of identifying genetic risk factors in humans with astrocytoma, we have used a mouse model of the disease to examine the genetic basis of astrocytoma susceptibility. Although several mouse models now exist that recapitulate the pathology of astrocytoma (15), we have chosen the *Nf1;Trp53cis* (*NPcis*) mutant mouse model, because it can be propagated by a simple breeding strategy and is maintained on an inbred strain background to facilitate the dissection of modifier genetics. In this model, *Nf1* and *Trp53* are mutated on the same chromosome (chr) 11 of the mouse and are tightly linked so that they are inherited as a single mutation in genetic crosses. The mice on a C57BL/6J (B6) inbred strain background develop astrocytomas spontaneously with an average latency of 6 months and show loss of the WT copies of *Nf1* and *Trp53* (16). Because astrocytomas were not observed in the original characterization of *NPcis* mice on a C57BL/6J,129S4/SvJae mixed background (17, 18), we hypothesized that modifier genes affect susceptibility to astrocytoma between the B6 and 129S4/SvJae (129) strains. To address this possibility directly, we have generated this model on an inbred 129 background and examined the genetics of susceptibility to astrocytoma.

Materials and Methods

Generation of *NPcis* Mice on Different Genetic Backgrounds. *NPcis* mice on a B6 background were generated as described (16) and

This paper was submitted directly (Track II) to the PNAS office.

Abbreviations: NF1, neurofibromatosis type 1; SSLP, simple sequence length polymorphism; *NPcis*, *Nf1;Trp53cis*; B6, C57BL/6J; 129, 129S4/SvJae; A, A/J; DB, DBA/2J; CB, CBA/J; 129S1, 129S1/SvImJ; 129X1, 129X1/SvJ; SNP, single nucleotide polymorphism; chr, chromosome; WHO, World Health Organization; NCBI, National Center for Biotechnology Information; dbSNP, Single Nucleotide Polymorphism Database.

Data deposition: The SNP data reported in this paper have been deposited in the NCBI Single Nucleotide Polymorphism Database (dbSNP) (dbSNP ID nos. 28476647-28476655; see also Table 4, which is published as supporting information on the PNAS web site).

†To whom correspondence should be addressed. E-mail: kreilly@ncifcrf.gov.

www.pnas.org/cgi/doi/10.1073/pnas.0401236101

maintained by crossing to WT B6 purchased from The Jackson Laboratory. The *NPcis*-B6 mice described here are backcross generation 8–11 onto B6. The *NPcis*-129 mice were generated by crossing *Nf1*+/− 129 mice (19) to *Trp53*+/− 129 mice (20) to generate *Nf1;Trp53trans* 129 mice that were then crossed to WT 129 mice, maintained as a colony at Massachusetts Institute of Technology (MIT) to generate the *NPcis* mice. F_1 progeny between *NPcis*-B6 and A/J (A), DBA/2J (DB), and CBA/J (CB) were generated by crossing *NPcis*-B6 mice to inbred strains purchased from The Jackson Laboratory. *NPcis*-B6 × 129 F_1 progeny were generated from an *NPcis*-B6 male inbred 16 generations onto B6 crossed to WT 129 females (Fig. 3, cross A). *NPcis*-129XB6 F_1 progeny were generated by crossing either male or female *NPcis*-129 mice to WT B6 (Fig. 3, cross B and C). All mice were maintained on a 9% fat diet. Twelve of the mice in this study (all F_1s between B6 and 129) were moved from MIT to National Cancer Institute–Frederick (NCI–Frederick) at ≈6 months of age to complete the aging study. We have not observed any change in phenotype of these strains at NCI–Frederick, so these mice were pooled with the mice aged entirely at MIT. All mice in this study were cared for according to the policies of the Animal Care and Use Committees of MIT and NCI–Frederick.

Genotyping of *NPcis* Mice. Mice were genotyped for *Trp53* mutations by PCR on tail-clip DNA as described (20). Mutations in *Nf1* were assayed by PCR as described (19) or by using the primers Nf1 WT 5′-TTCTGGCCTTATTGGACACC-3′, Nf1 common 5′-GCACAAAAGAGGCACTGGAT-3′, Nf1 mutant 5′-GGAGAGGCTTTTTGCTTCCT-3′, with an annealing temperature of 60°C. We added 0.1% BSA and 1% polyvinylpyrrolidone (catalogue no. PVP-40, Sigma–Aldrich) to improve specificity of the PCR reaction (21). For analysis of simple sequence length polymorphisms (SSLPs), tail DNA was amplified with ResGen MapPairs primer sets (Invitrogen) for 35 cycles and run on a 3% Metaphor agarose (Cambrex, East Rutherford, NJ), 1× Tris-borate-EDTA-buffered gel. The markers used were D11Mit20, D11Mit271, D11Mit140, D11Mit349, D11Mit5, D11Mit341, D11Mit285, and D11Mit258. Chromosomal locations of SSLP markers, *Trp53*, and *Nf1* were taken from National Center for Biotechnology Information (NCBI) Mouse Build 32, version 1 (www.ncbi.nlm.nih.gov/genome/guide/mouse).

Phenotyping of *NPcis* Mice. Mice were aged until tumors developed as described (16) and processed for hematoxylin and eosin-stained sections. The midline sagittal section and a parasagittal section through the eye were examined independently by K.M.R. and by two veterinary neuropathologists, R.T.B. and C.D.S. A consensus diagnosis was determined by K.M.R. based on the World Health Organization (WHO) grading criteria for diffuse astrocytoma (22) and given the prefix GEM to indicate that the tumors arise in genetically engineered mouse models.

Statistical Analysis of Tumor Spectrum. Statistical analysis was performed as described (16). Differences in astrocytoma incidence were compared pairwise between strains by χ^2 test in Microsoft EXCEL X.

Single Nucleotide Polymorphism (SNP) Analysis. Chr 11 SNPs with a B6 genotype were downloaded from the NCBI Single Nucleotide Polymorphism Database (dbSNP) (Build 120) (www.ncbi.nlm.nih.gov/SNP). We selected 597 SNPs located between D11Mit271 (45.4 Mb, NCBI Build 32) and D11Mit285 (82.6 Mb, NCBI Build 32) polymorphic for B6 and 129. PCR primers were designed for 161 DNA fragments containing the 597 SNPs. REVEAL ANALYSIS (Spectrumedix, State College, PA) was used to identify PCR fragments that were polymorphic between B6 and 129. Of the 89 DNA fragments found to be polymorphic or uninterpretable by REVEAL ANALYSIS, 48 fragments were chosen for sequencing. SNPs were confirmed by sequencing in both directions along the DNA strand and genotyped on the B6, 129, A, CB, and DB strains. Sequencing primers used are reported in Table 4. The Celera SNP database (www.celeradiscoverysystems.com) was searched for SNPs between D11Mit271 (44.2 Mb, release R3.6) and D11Mit285 (96.5 Mb, release R3.6). Two search criteria were used: (*i*) 129S1/SvImJ (129S1) ≠ B6 and 129S1 ≠ A and 129S1 ≠ DB and (*ii*) 129X1/SvJ (129X1) ≠ B6 and 129X1 ≠ A and 129X1 ≠ DB. Results were manually checked for genotyping ambiguities. The genotype with the higher count number was taken as the more accurate genotype. Results of the search are reported in Table 5, which is published as supporting information on the PNAS web site.

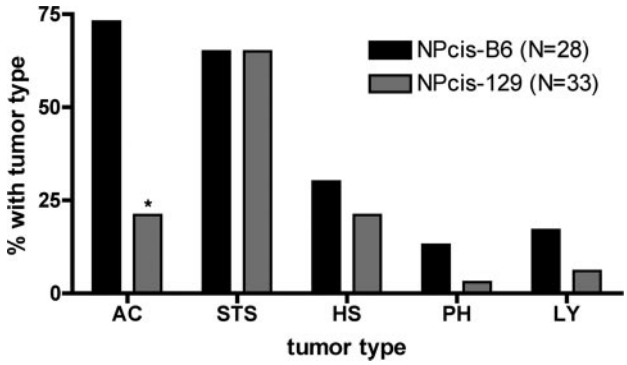

Fig. 1. Tumor spectrum of *NPcis*-B6 and *NPcis*-129 mice. The graph shows the major tumor types observed. The difference in astrocytoma incidence in the two strains is statistically significant ($P = 0.001$, indicated by asterisk). Tumor types are astrocytoma (AC), soft-tissue sarcoma (STS), histiocytic sarcoma (HS), pheochromocytoma (PH), and lymphoma (LY).

Results

To test the difference in susceptibility to astrocytoma between the B6 and 129 strains, we have regenerated the *NPcis* mice on an inbred 129 background by crossing *Nf1*+/− 129 and *Trp53*+/− 129 mice to regenerate the *cis* mutant chr (16–18). *NPcis* mice on a 129 background develop significantly fewer astrocytomas compared with *NPcis*-B6 mice (Fig. 1). Soft-tissue sarcomas were seen frequently on both the B6 and 129 backgrounds, as observed on the B6,129 mixed background (17, 18). We did not observe significant differences in the incidence of other common tumor types, lymphoma, histiocytic sarcoma, or pheochromocytoma. *NPcis*-129 mice developed fewer astrocytomas in the population than *NPcis*-B6 mice, and the astrocytomas were lower grade in *NPcis*-129 mice. On the B6 background, 89% of astrocytomas were classified as GEM WHO III, whereas 29% of astrocytomas on the 129S4/SvJae background were classified as GEM WHO III, with the remainder classified as GEM WHO II (Fig. 2). We have generated cell lines from *NPcis-129* astrocytomas that show loss of the WT copies of *Trp53* and *Nf1* (data not shown).

To determine whether the genes modifying astrocytoma formation in *NPcis* mice act dominantly in the B6 or 129 strain, we generated F_1 progeny between the B6 and 129 strains carrying the *NPcis* mutation. We found upon analyzing these F_1 progeny that susceptibility to astrocytoma does not follow simple Mendelian inheritance, in that some F_1 progeny were resistant to astrocytoma and others were susceptible (Fig. 3, Table 1). We have examined the data to look for epigenetic effects with respect to inheritance of the strain background from the mother or father, inheritance of the *NPcis* mutant chr from the B6 or 129 strain, and inheritance of the *NPcis* mutant chr from the mother or father.

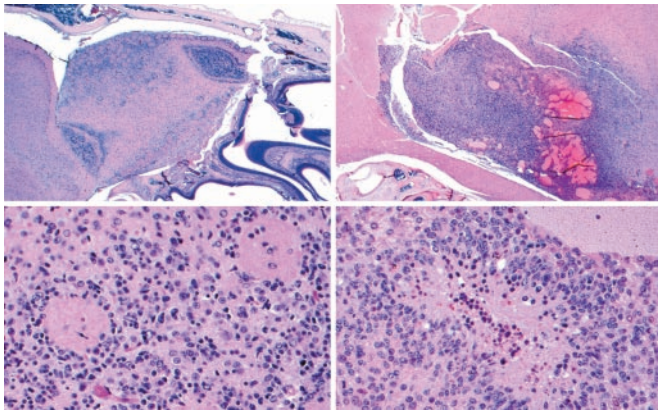

Fig. 2. Histology of astrocytoma in the resistant *NPcis*-129 strain compared with the susceptible F_1 progeny of *NPcis*-129 crossed to WT B6. (*Left*) One of the two GEM WHO III tumors found in *NPcis*-129 mice ($n = 33$). The tumor is confined to a focal area of the ventral olfactory bulb (*Upper Left*). Atypical nuclei diffusely infiltrate the olfactory bulb (*Lower Left*) and mitotic figures are rare (not shown). (*Right*) One of three GEM WHO IV tumors found in F_1 *NPcis*-129XB6 progeny ($n = 22$). This tumor is characterized by infiltrative boundaries (*Upper Right*), a high mitotic index, and pseudopallisading tumor cells around areas of necrosis (*Lower Right*).

Maternal or paternal imprinting of a modifier from B6 or 129 could alter the expression pattern of the modifier gene(s) and affect its ability to act on astrocytoma susceptibility. Similarly, strain differences inherited specifically from the mother, such as mitochondria or other cytoplasmic maternal factors, could potentially affect developmental pathways leading to indirect effects on astrocytoma susceptibility. We examined whether astrocytoma susceptibility changed when B6 alleles were inherited from the mother or father. Table 1 shows that astrocytoma susceptibility is not affected by imprinting of strain-specific genes or by strain-specific maternal factors. Mice that inherit B6 from either the maternal (Fig. 3, cross C) or the paternal side (Fig. 3, crosses A and B) show a similar incidence of astrocytoma. In both cases, F_1 progeny were significantly more susceptible than the *NPcis* 129 parental strain ($P = 0.03$ for B6 coming from the mother, and $P = 0.01$ for B6 coming from the father).

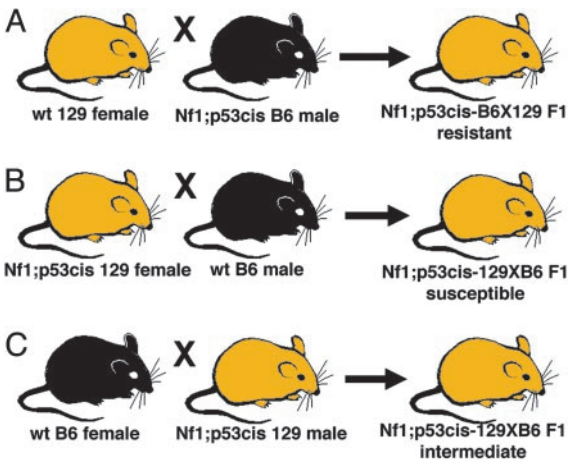

Fig. 3. F_1 crosses between B6 and 129. F_1 progeny were generated in three different crosses. (*A*) An *NPcis*–B6 male was bred to a WT 129 female to give *NPcis*-B6X129 F_1 progeny that were resistant to astrocytoma. (*B*) *NPcis*-129 females were bred to WT B6 males to give *NPcis*-129XB6 F_1 progeny that were susceptible to astrocytoma. (*C*) An *NPcis*-129 male was bred to a WT B6 female to give *NPcis*-129XB6 F_1 progeny that developed an intermediate astrocytoma phenotype.

Table 1. Inheritance of mutant chr 11 affects astrocytoma susceptibility

Cross (Fig. 3)	Cross	*n*	With astrocytoma	Without astrocytoma	*P*, χ^2
A	WT 129 female × *NPcis* B6 male	19	6 (32%)	13 (68%)	
B	*NPcis* 129 female × WT B6 male	22	16 (73%)	6 (27%)	
C	WT B6 female × *NPcis* 129 male	23	12 (52%)	11 (48%)	
A+B	129 female × B6 male	41	22 (54%)	19 (46%)	
C	B6 female × 129 male	23	12 (52%)	11 (48%)	0.9
B+C	*NPcis* 129 × WT B6	45	28 (62%)	17 (38%)	
A	*NPcis* B6 × WT 129	19	6 (32%)	13 (68%)	0.03
A+C	WT female × *NPcis* male	42	18 (43%)	24 (57%)	
B	*NPcis* female × WT male	22	16 (73%)	6 (27%)	0.02

The *Nf1* and *Trp53* mutant chr, or conversely WT chr 11, could affect tumorigenesis differently, depending on whether it is inherited from B6 or 129. For example, particular alleles of *Nf1* or *Trp53* could be less effective at blocking tumorigenesis in the heterozygous state, or the WT chr from one strain might be lost more easily than the other strain to initiate tumorigenesis, as has been shown for strain effects on $APC^{Min/+}$ mice (23). Additionally, genes tightly linked to *Nf1* and *Trp53* on chr 11 might affect tumorigenesis differently when inherited from B6 or 129. We examined the effect of inheriting the mutant chr from either 129 or B6. Table 1 shows that F_1 progeny inheriting the *NPcis* mutant chr from 129 (Fig. 3, crosses B and C) are significantly more

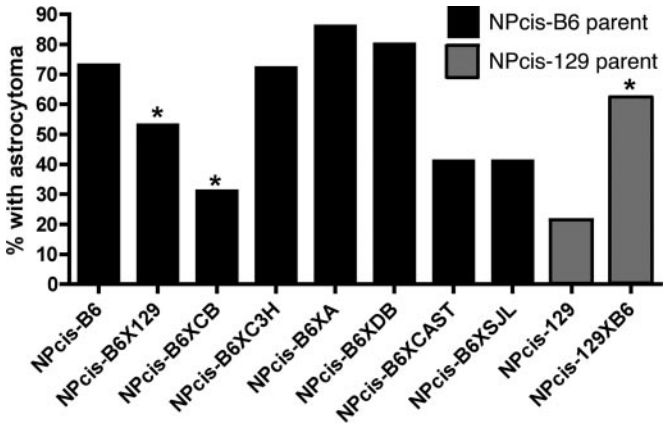

Fig. 4. Astrocytoma incidence in F_1 progeny of different inbred strains. *NPcis*–B6X129 F_1 progeny (cross A, Fig. 3) show reduction in astrocytoma incidence compared to the *NPcis*-B6 parental strain ($P = 0.02$). *NPcis*-129XB6 F_1 progeny (cross B and C, Fig. 3), show increase in astrocytoma incidence compared to the *NPcis*-129 parental strain ($P = 0.0009$). *NPcis*–B6XCB F_1 progeny show reduction in astrocytoma incidence compared to the *NPcis*–B6 parental strain ($P = 0.04$). Previously published data (16) from B6XC3H/HeJ, B6XCAST/EiJ, and B6XSJL/J are shown for comparison. Of the seven strains tested, only 129 and CB show significant resistance to astrocytoma compared to B6. Statistically significant changes relative to the parental strain are indicated by asterisks. NPcis-B6 $n = 28$, NPcis-B6X129 $n = 19$, NPcis-B6XCB $n = 26$, NPcis-B6XC3H $n = 25$, NPcis-B6XA $n = 20$, NPcis-B6XDB $n = 20$, NPcis-B6XCAST $n = 22$, NPcis-B6XSJL $n = 34$, NPcis-129 $n = 33$, and NPcis-129XB6 $n = 45$. (Adapted from ref. 16.)

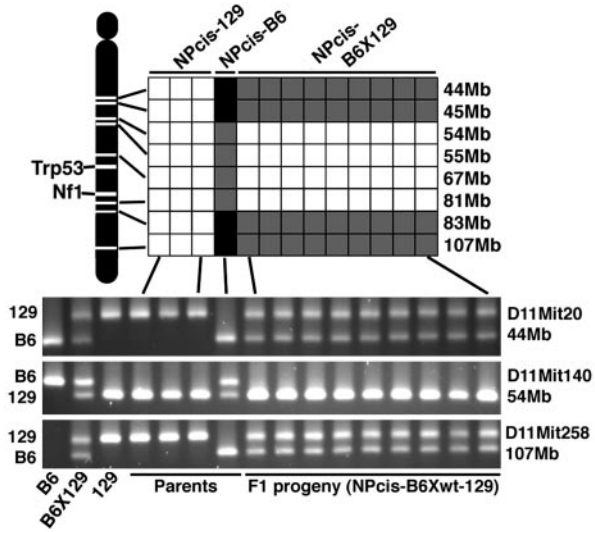

Fig. 5. SSLP characterization of chr 11 in *NPcis* parents and F_1 progeny. SSLP markers spanning the region around *Trp53* and *Nf1* were genotyped for differences between B6 and 129. (*Upper*) A summary of the results indicating homozygous 129 (white), homozygous B6 (black), and heterozygous B6X129 (gray). (*Lower*) Three SSLP examples. *Trp53* is located at 69 Mb and *Nf1* is located at 73 Mb. In the congenic region the *NPcis*-B6 parent is heterozygous for 129 and B6 sequences, and the F_1 progeny are homozygous for 129. Outside the congenic region the *NPcis*-B6 parent is homozygous for B6 sequences, and the F_1 progeny are heterozygous for 129 and B6 sequences. The first three lanes of the gel (*Lower*) are inbred and F_1 control DNA samples to show the size of the SSLP fragments for each strain.

susceptible to developing astrocytoma than F_1 progeny inheriting the mutant chr from the B6 strain (Fig. 3, cross A) ($P = 0.03$). F_1 progeny inheriting the mutant chr from 129 and the WT chr 11 from B6 are significantly more susceptible to astrocytoma than the *NPcis*-129 parental strain (Fig. 4) ($P = 0.0009$), demonstrating a dominant effect of the WT B6 chr 11 on astrocytoma susceptibility. The F_1 progeny inheriting the mutant chr from B6 and the WT chr 11 from 129 are significantly more resistant to astrocytoma than the *NPcis*-B6 parent (Fig. 4) ($P = 0.02$), demonstrating a dominant effect of the WT 129 chr 11 on astrocytoma resistance. These data suggest that the WT copy of chr 11 acts dominantly to modify susceptibility to astrocytoma.

Because the data in Table 1 point to a role of chr 11 in modifying astrocytoma susceptibility, we determined whether imprinting on this chr affects astrocytoma formation, given that one copy of chr 11 is lost during tumor initiation, leaving only the maternal or paternal copy. This is distinct from the analysis described above, in that it does not require the modifier to be polymorphic between B6 and 129, but only that it be linked to *Nf1* and *Trp53*. Table 1 shows that F_1 progeny inheriting the *NPcis* chr from the mother (Fig. 3, cross B) are more susceptible to astrocytoma than F_1 progeny inheriting the mutant chr from the father (Fig. 3, cross A and C) ($P = 0.02$). We found no significant differences in the incidence of astrocytoma between male and female F_1 progeny. It is not clear from this analysis whether the imprinting effect is at the same gene locus as the B6 or 129 modifying locus, but both loci are linked to chr 11.

To further analyze the differences on chr 11 between the different F_1 progeny, we genotyped SSLP markers along the length of chr 11. The original *Nf1* and *Trp53* mutations used to generate the *NPcis*-B6 animals were made on a 129 strain background (19, 20). During the inbreeding of mutations onto B6, the region around *Nf1* and *Trp53* is continually selected and retains 129 sequence. The *NPcis*-B6 male founder used to generate the F_1 progeny in cross A of Fig. 3 retains 129 sequence from 54 through 81 Mb on chr 11 (Fig. 5). The *NPcis* F_1 progeny in cross A inherit this congenic region and are homozygous for 129 sequence around *Trp53* and *Nf1*.

We performed a survey of six additional inbred strains to look at the effects on astrocytoma susceptibility in F_1 progeny. Three of these F_1 strain combinations (B6XC3H/HeJ, B6XCAST/EiJ, and B6XSJL/J) have been published (16) and are included in Fig. 4 for comparison. As we described previously, *NPcis*-B6XCAST/EiJ and *NPcis*-B6XSJL/J F_1 progeny develop fewer astrocytomas overall but develop astrocytomas at the same age as *NPcis*-B6 mice and show accelerated tumor latency, developing other tumors before they live long enough to develop astrocytoma. Therefore, the reduction of astrocytoma in these two F_1 groups is not necessarily due to resistance to astrocytoma. We found that the CB strain had a similar effect to the 129 strain when crossed to *NPcis*-B6 mice. In both cases, the F_1 progeny are significantly more resistant to astrocytoma than the *NPcis* parental strain. The *NPcis*-B6XCB F_1 progeny showed no significant differences in any other tumor type, developing soft-tissue sarcomas, pheochromocytomas, histiocytic sarcomas, and lymphomas similarly to the *NPcis*-B6 parental line, and there was no significant change in the survival curves between the F_1 and the B6 parental strain. Furthermore, the astrocytomas that developed in *NPcis*-B6XCB mice were delayed relative to *NPcis*-B6 mice. Thus, similar to the modifying effect observed in the 129 strain, the CB strain modifier effect is limited to increasing resistance to astrocytoma and is not seen in five other strains examined.

Because both 129 and CB can dominantly repress astrocytomas in *NPcis*-B6 mice, whereas A and DB cannot, the polymorphisms responsible for this effect are expected to be polymorphic between 129 and B6, 129 and A, and 129 and DB. If the dominant effects of 129 and CB are due to the same locus, the polymorphisms may also have a common haplotype in 129 and CB. We analyzed SNPs from both the NCBI dbSNP database and the Celera SNP database to determine whether there are SNPs within the region shown in Fig. 5 that fit these criteria. We selected 597 SNPs from the congenic region between D11Mit271 and D11Mit285 in NCBI dbSNP, contained on 161 PCR frag-

Table 2. NCBI, sequenced SNPs polymorphic for B6 and 129

ss#	Gene	N Mb*	C Mb*	B6	A	DB	129	CB
12733678	Vamp2	68.7	73.0	G	G	G	A	G
12733665	Vamp2	68.7	73.0	A	A	A	G	A
12733667	Vamp2	68.7	73.0	G	G	G	A	G
12732038	Chrnb1	69.4		C		C	T	T
5069192	Trpv1†	72.8	77.8	C	C	C	G	G

ss#, NCBI dbSNP submitted sequence identification no.
*N Mb, physical location in NCBI; C Mb, location in Celera.
†The Trpv1 SNP and one of the SNPs in Trpv3 in Table 3 are the same SNP.

Table 3. Celera, genes with >10 candidate SNPs

Gene ID	Gene	N Mb*	C Mb*	No. SNPs
mCG140133	Trim11	58.6	60.7	11
mCG23374	NcoR1	61.9	66.3	41
mCG14821	1700019I23Rik	62.5	66.9	15
mCG11237	Vamp2	68.7	73.0	11
mCG21169	Rabep1	70.4	75.4	31
mCG6663	Ankfy1	72.3	77.3	12
mCG140764	Trpv3†	72.8	77.8	11
mCG48633	Msi2h	87.9	95.0	28

*N Mb, physical location in NCBI; C Mb, location in Celera.
†The Trpv1 SNP in Table 2 and one of the SNPs in Trpv3 are the same SNP.

MEDICAL SCIENCES

ments. Of these 161 PCR fragments, 72 were found to not contain polymorphisms between B6 and 129 by REVEAL ANALYSIS of hybrid stability. Of the remaining 89, 48 were sequenced, and of 159 SNPs represented, 13 were found to be polymorphic for B6 and 129. Of the 13 SNPs, 8 were polymorphic for 129 and A, and 6 were polymorphic for 129 and DB. Two SNPs were found that met all criteria, in that they were polymorphic for 129 and B6, 129 and A, and 129 and DB, and were not polymorphic for 129 and CB (Table 2)

The Celera database was searched directly for SNPs that are polymorphic for 129 and B6, 129 and A, and 129 and DB. There are two 129 substrains represented in the Celera database, 129X1 and 129S1. Of the 46,736 SNPs within the congenic region between D11Mit271 and D11Mit285, 16,220 SNPs were polymorphic between either B6 and 129X1 or B6 and 129S1. Of the 16,220 SNPs, 854 were polymorphic for A and DB. The SNPs covered intergenic regions and 117 gene products. Identified genes varied between those with a single candidate SNP and those with as many as 41 candidate SNPs. The genes with many SNPs fitting the candidate criteria likely represent regions of common haplotypes between B6, A, and DB, polymorphic with 129. Because of potential differences between our 129 strain and 129X1 and 129S1, these 854 candidate SNPs will need to be confirmed by direct sequencing of 129 and CB. The candidate genes with >10 candidate SNPs are listed in Table 3. The complete summary of the candidate SNPs identified from NCBI dbSNP and Celera are included as Tables 4 and 5.

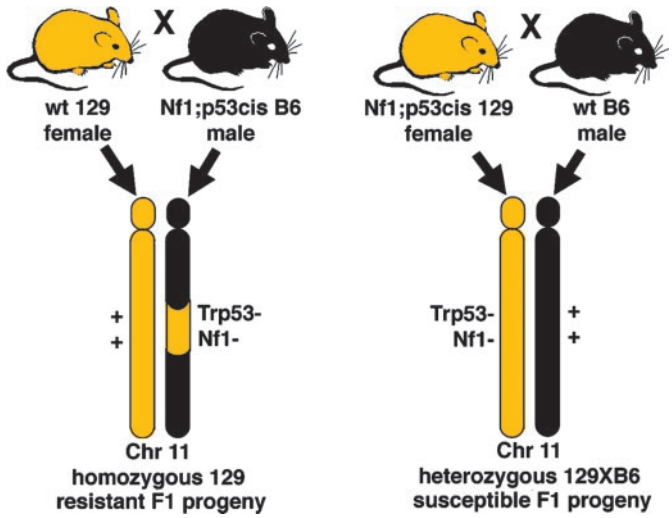

Fig. 6. Model for inheritance of resistance to astrocytoma. The F_1 progeny showing different susceptibility to astrocytoma differ in the strain background around the *Trp53* and *Nf1* loci. *NPcis*-B6 mice are inbred from 129 and carry a 129 congenic region on chr 11 (*Left*), whereas *NPcis*-129 mice are inbred 129 along the entire length of chr 11 (*Right*). F_1 progeny differ in whether they are homozygous for 129 around *Nf1* and *Trp53* or heterozygous for B6 and 129. According to this model, the B6 alleles on chr 11 confer susceptibility to astrocytoma in a dominant manner.

Discussion

The identification of modifier genes or susceptibility and resistance genes in human cancer is difficult, particularly in the case of less common cancers such as astrocytoma, where familial clustering is more difficult to find. We demonstrate here that modifier genes on mouse chr 11 affect susceptibility to astrocytoma in the presence of mutations in the ras and p53 signaling pathways, two of the major pathways mutated in human astrocytoma. Furthermore, these modifier genes show complex inheritance patterns in mice, suggesting that their identification in humans would be especially difficult. We use phenotype data from several inbred strains to identify potential candidate genes on chr 11. By identifying the genes responsible for these effects and understanding their mechanism, it may be possible to implicate them in human astrocytoma.

The data presented here show that susceptibility to astrocytoma depends on the mode of inheritance of the *NPcis* mutant chr. Because *NPcis*-B6 mice were inbred from a B6,129 background and the original mutations were engineered on a 129 background (19, 20), the *NPcis* mice inbred onto B6 carry regions of 129 sequence surrounding the two mutations on chr 11. Our data suggest that a major modifier affecting resistance to astrocytoma lies within these 129-retained regions in the *NPcis* B6 inbred mice. We have mapped the region of 129 sequence in the *NPcis*-B6 parent of our F_1 crosses and found that the region is >27 and <38 Mb in length surrounding *Nf1* and *Trp53* (Fig. 5). According to our model (Fig. 6), *NPcis*-129 mice are homozygous for 129 alleles at all loci, whereas *NPcis*-B6 mice are heterozygous for B6 and 129 at a small number of loci, including the region around *Nf1* and *Trp53* on chr 11. The B6 modifier allele(s) acts dominantly in this model to increase susceptibility to astrocytoma. In the case of the F_1 progeny inheriting the *NPcis* chr from the 129 line, the progeny inherit the modifier allele from the WT B6 parent and are susceptible (Table 1). In the case of the F_1 progeny inheriting the *NPcis* chr from the B6 line, the progeny do not inherit the dominant modifier allele and are resistant. The model predicts that B6, A, and DB all carry similar dominant susceptibility alleles at the modifier locus, whereas 129 and CB carry recessive resistance alleles. The dominant effect seen in *NPcis* B6XCB mice is due to loss of the B6 susceptibility allele and maintenance of two recessive resistance alleles at the modifier locus. Alternatively, the modifier in the CB background may be unlinked to the modifier on chr 11 but acts dominantly to suppress astrocytoma in the F_1 progeny.

We have tested whether candidate SNPs exist within the congenic region that are consistent with our phenotype data, using in silico haplotype mapping (24, 25) and sequencing. Importantly, no candidate SNPs were identified in *Trp53* or *Nf1*. Many of the candidates identified are expressed in the brain, and several are implicated in CNS stem cell biology or astrocytoma. *NcoR1* has been shown to inhibit the differentiation of neural stem cells into astrocytes (26). The *Msi2h* gene product has been implicated in the proliferation and maintenance of neural stem cells (27). Changes in neural stem cells could favor the development of astrocytoma by increasing the number of cells available to become tumorigenic. Alternatively, genes affecting neural stem cell differentiation could affect how well astrocytes maintain their differentiated state and resist transformation. *Sparc* is up-regulated in diffuse astrocytomas (28); however, because the 129, A, and DB share a common genotype, *Sparc* is not the best candidate for the astrocytoma modifier.

In addition to the observed strain-origin effect in F_1s, we have also observed a parent-origin effect of *NPcis* inheritance in F_1s (Table 1). Because the parent-origin effect is specific to chr 11 and not to the inheritance of B6 or 129, we argue that strain-specific differences in mitochondria from the mother or other cytoplasmic maternal factors are not responsible for this effect. This suggests that imprinting of genes on chr 11 modulates the susceptibility to astrocytoma. Imprinted genes have been identified on chr 11 in the mouse, supporting this possibility (29, 30). The F_1 data suggest that inheritance of the WT chr 11 from the father increases susceptibility, whereas inheritance of the WT chr 11 from the mother decreases susceptibility. It remains to be seen whether this effect is due to silencing of a maternal susceptibility allele or to silencing of a paternal resistance allele, and whether this effect acts on the same locus as the strain-origin effect. Whereas the strain-origin effect points to a locus linked to *Nf1* and *Trp53*, due to 129 sequences found in *NPcis*-B6 mice, the imprinted modifier could be anywhere on chr 11, affecting

tumorigenesis through loss or reduplication of monoallelic expression. Interestingly, Grb10 is a tyrosine kinase receptor adaptor protein imprinted on chr 11 and paternally expressed in the mouse brain (31, 32). It is likely that many imprinted genes exist along chr 11, and our experiments do not localize the imprinted modifier because large regions of WT chr 11 are likely lost during tumor initiation. It remains to be seen whether Grb10 or another monoallelically expressed gene on chr 11 can specifically alter tumor progression.

The modifier genes acting on astrocytoma susceptibility in this mouse model do not affect the development of other tumor types or tumor latency. This suggests that the modifiers act not on the overall tumor suppressor function of *Nf1* and/or *Trp53* but rather on the effect of one or both of these genes on the CNS. The modifier genes could be acting within the precursor cell to the astrocytoma, the tumor cell as it progresses, or in the surrounding normal tissue to support tumor growth and survival. Because the WT copies of *Nf1* and *Trp53* are lost during the initiation of tumorigenesis in *NPcis* mice (16, 17), modifier alleles linked to these genes on the WT copy of chr 11 may be affecting tumorigenesis during initiation steps or by acting in surrounding normal tissue to alter tumor progression. We observe that the tumors in *NPcis* 129 mice are lower grade in addition to being fewer in number; therefore, we favor an effect of the modifier on tumor progression as well as tumor initiation.

Much of the characterization of mutant phenotypes in the mouse occurs on 129 substrains or B6,129 mixed strain backgrounds. This is due to the predominant use of 129 embryonic stem cells for gene targeting. These data demonstrate the importance of examining phenotypes on multiple strain backgrounds. The role of mutations in the ras and p53 pathways in astrocytoma is well established; however, mouse models generated by mutation in these pathways fail to develop astrocytoma on the 129 inbred and B6,129 mixed backgrounds. It is only when the mutations are moved to B6 that the importance of these pathways in murine astrocytoma is appreciated.

We thank M. Perella, D. Crowley, A. Caron, and K. Mercer for technical assistance; E. Frazier for assistance with figures; and M. McLaughlin, N. Copeland, and K. Hunter for helpful discussions. This work was supported in part by grants from the Leukemia and Lymphoma Society, the American Association for Cancer Research, the American Cancer Society, the Department of the Army, and the Ludwig Foundation, and by federal funds from the National Cancer Institute under contract NO1-CO-12400 to Science Applications International Corporation–Frederick. T.J. is an Investigator of the Howard Hughes Medical Institute.

1. Central Brain Tumor Registry of the United States (2002) *CBTRUS: 2002–2003 Primary Brain Tumors in the United States–Statistical Report* (Central Brain Tumor Registry of the United States, Chicago).
2. Malmer, B., Henriksson, R. & Gronberg, H. (2002) *Neuroepidemiology* **21,** 279–286.
3. Blatt, J., Jaffe, R., Deutsch, M. & Adkins, J. C. (1986) *Cancer* **57,** 1225–1229.
4. Sorensen, S. A., Mulvihill, J. J. & Nielsen, A. (1986) *N. Engl. J. Med.* **314,** 1010–1015.
5. Malkin, D. (1994) *Biochem. Biophys. Acta* **1198,** 197–213.
6. Gutmann, D., Wood, D. & Collins, F. (1991) *Proc. Natl. Acad. Sci. USA* **88,** 9658–9662.
7. Easton, D., Ponder, M., Huson, S. & Ponder, B. (1993) *Am. J. Hum. Genet.* **53,** 305–313.
8. Friedman, J. M. & Birch, P. (1997) *Neuropediatrics* **28,** 131–132.
9. Szudek, J., Evans, D. G. & Friedman, J. M. (2003) *Hum. Genet.* **112,** 289–297.
10. Ars, E., Kruyer, H., Morell, M., Pros, E., Serra, E., Ravella, A., Estivill, X. & Lazaro, C. (2003) *J. Med. Genet.* **40,** e82.
11. von Deimling, A., Eibl, R. H., Ohgaki, H., Louis, D. N., von Ammon, K., Petersen, I., Kleihues, P., Chung, R. Y., Wiestler, O. D. & Seizinger, B. R. (1992) *Cancer Res.* **52,** 2987–2990.
12. Fults, D., Brockmeyer, D., Tullous, M. W., Pedone, C. A. & Cawthon, R. M. (1992) *Cancer Res.* **52,** 674–679.
13. Harvey, M., McArthur, M., Montgomery Jr., C., Bradley, A. & Donehower, L. (1993) *FASEB J.* **7,** 938–942.
14. Kuperwasser, C., Hurlbut, G. D., Kittrell, F. S., Dickinson, E. S., Laucirica, R., Medina, D., Naber, S. P. & Jerry, D. J. (2000) *Am. J. Pathol.* **157,** 2151–2159.
15. Weiss, W. A., Israel, M., Cobbs, C., Holland, E., James, C. D., Louis, D. N., Marks, C., McClatchey, A. I., Roberts, T., Van Dyke, T., *et al.* (2002) *Oncogene* **21,** 7453–7463.
16. Reilly, K. M., Loisel, D. A., Bronson, R. T., McLaughlin, M. E. & Jacks, T. (2000) *Nat. Genet.* **26,** 109–113.
17. Cichowski, K., Shih, T., Schmitt, E., Santiago, S., Reilly, K., McLaughlin, M., Bronson, R. & Jacks, T. (1999) *Science* **286,** 2172–2176.
18. Vogel, K., Klesse, L., Velasco-Miguel, S., Meyers, K., Rushing, E. & Parada, L. (1999) *Science* **286,** 2176–2179.
19. Jacks, T., Shih, T. S., Schmitt, E. M., Bronson, R. T., Bernards, A. & Weinberg, R. A. (1994) *Nat. Genet.* **7,** 353–361.
20. Jacks, T., Remington, L., Williams, B. O., Schmitt, E. M., Halachmi, S., Bronson, R. T. & Weinberg, R. A. (1994) *Curr. Biol.* **4,** 1–7.
21. Xin, Z., Velten, J. P., Oliver, M. J. & Burke, J. J. (2003) *BioTechniques* **34,** 820–824, 826.
22. Kleihues, P. & Cavenee, W. (2000) *Pathology and Genetics of Tumours of the Nervous System* (International Agency for Research on Cancer, Lyon, France).
23. Shoemaker, A. R., Moser, A. R., Midgley, C. A., Clipson, L., Newton, M. A. & Dove, W. F. (1998) *Proc. Natl. Acad. Sci. USA* **95,** 10826–10831.
24. Grupe, A., Germer, S., Usuka, J., Aud, D., Belknap, J. K., Klein, R. F., Ahluwalia, M. K., Higuchi, R. & Peltz, G. (2001) *Science* **292,** 1915–1918.
25. Park, Y. G., Clifford, R., Buetow, K. H. & Hunter, K. W. (2003) *Genome Res.* **13,** 118–121.
26. Hermanson, O., Jepsen, K. & Rosenfeld, M. G. (2002) *Nature* **419,** 934–939.
27. Sakakibara, S., Nakamura, Y., Yoshida, T., Shibata, S., Koike, M., Takano, H., Ueda, S., Uchiyama, Y., Noda, T. & Okano, H. (2002) *Proc. Natl. Acad. Sci. USA* **99,** 15194–15199.
28. Rempel, S. A., Golembieski, W. A., Ge, S., Lemke, N., Elisevich, K., Mikkelsen, T. & Gutierrez, J. A. (1998) *J. Neuropathol. Exp. Neurol.* **57,** 1112–1121.
29. Hatada, I., Sugama, T. & Mukai, T. (1993) *Nucleic Acids Res.* **21,** 5577–5582.
30. Miyoshi, N., Kuroiwa, Y., Kohda, T., Shitara, H., Yonekawa, H., Kawabe, T., Hasegawa, H., Barton, S. C., Surani, M. A., Kaneko-Ishino, T. & Ishino, F. (1998) *Proc. Natl. Acad. Sci. USA* **95,** 1102–1107.
31. Blagitko, N., Mergenthaler, S., Schulz, U., Wollmann, H. A., Craigen, W., Eggermann, T., Ropers, H. H. & Kalscheuer, V. M. (2000) *Hum. Mol. Genet.* **9,** 1587–1595.
32. Hikichi, T., Kohda, T., Kaneko-Ishino, T. & Ishino, F. (2003) *Nucleic Acids Res.* **31,** 1398–1406.

Developmental Cell, Vol. 6, 855–864, June, 2004, Copyright ©2004 by Cell Press

Ezrin Is Essential for Epithelial Organization and Villus Morphogenesis in the Developing Intestine

Ichiko Saotome, Marcello Curto, and Andrea I. McClatchey*
MGH Cancer Center and
Harvard Medical School Department of Pathology
149 13th Street
Charlestown, Massachusetts 02129

Summary

Ezrin, Radixin, and Moesin (the ERM proteins) supply regulated linkage between membrane proteins and the actin cytoskeleton. The study of mammalian ERM proteins has been hampered by presumed functional overlap. We have found that Ezrin, the only ERM detected in epithelial cells of the developing intestine, provides an essential role in configuring the mouse intestinal epithelium. Surprisingly, Ezrin is not absolutely required for the formation of brush border microvilli or for the establishment or maintenance of epithelial polarity. Instead, Ezrin organizes the apical terminal web region, which is critical for the poorly understood process of de novo lumen formation and expansion during villus morphogenesis. Our data also suggest that Ezrin controls the localization and/or function of certain apical membrane proteins that support normal intestinal function. These in vivo studies highlight the critical function of Ezrin in the formation of a multicellular epithelium rather than an individual epithelial cell.

Introduction

Cell polarization—the generation of cellular asymmetry—is critical for determining the functional properties of individual cells and for the morphogenesis of multicellular tissues during development (Nelson, 2003). Although cells establish asymmetry in many different ways, the generation of distinct apical and basolateral domains by epithelial cells is a paradigm for understanding how cells polarize. The formation of a polarized epithelium is governed by the organization of individual cell membrane domains and cell:cell junctions via interaction between membrane proteins and the cytoskeleton. The ERM proteins (Ezrin, Radixin, and Moesin) link membrane proteins to the actin cytoskeleton, and their function has been implicated in the formation of specialized membrane domains in nonepithelial cells such as the T cell uropod, podocyte foot process, and fibroblast membrane ruffle (Bretscher et al., 2002; McClatchey, 2003). ERM function has also been implicated in the formation of apical microvilli in epithelial cells, and recent studies suggest that the single *Drosophila* ERM protein plays a key role in maintaining epithelial integrity in vivo (Speck et al., 2003).

*Correspondence: mcclatch@helix.mgh.harvard.edu

The ERM proteins provide architectural and/or regulatory contribution to cell polarity (Bretscher et al., 2002; McClatchey, 2003). Membrane:cytoskeleton association of the ERMs is regulated by conformation-dependent changes in subcellular localization, suggesting an active and dynamic function. The ERMs are activated via phosphorylation-mediated disruption of intramolecular self-association and consequent translocation to the membrane:cytoskeleton interface. The small GTPase RhoA is the best-studied stimulus of ERM activation (Hirao et al., 1996; Shaw et al., 1998; Matsui et al., 1998). At the membrane, the ERMs can interact with several proteins including EBP50/NHE-RF (ERM-binding phosphoprotein of 50 kD/Na^+/H^+ exchanger regulatory factor) and the related E3KARP (Exchanger 3 kinase A regulatory protein), PDZ domain-containing adaptors that, in turn, interact with a variety of transmembrane proteins including the Na^+/H^+ exchanger (NHE3), cystic fibrosis transmembrane regulator (CFTR), and platelet-derived growth factor receptor (PDGFR; Reczek et al., 1997; Murthy et al., 1998; Yun et al., 1998; Short et al., 1998; Maudsley et al., 2000). This linkage is thought to facilitate proper receptor localization and/or regulation (Bretscher et al., 2000; Shenolikar and Weinman, 2001).

The study of mammalian ERMs has been impeded by presumed redundancy. Most cultured cells express multiple ERM proteins, prompting the use of dominant-negative ERM isoforms, although the mechanism by which they inactivate endogenous ERM function is unclear. Moreover, *moesin*-deficient mice are viable with no gross abnormalities, and *radixin*-deficient mice are viable but develop hyperbilirubinemia with defective localization of the Mrp2 transporter to bile canalicular membranes (Doi et al., 1999; Kikuchi et al., 2002). Among the ERM proteins, Ezrin exhibits the most restricted pattern of expression in vivo and is the only ERM detected in some polarized epithelia including the small intestinal epithelium (Figures 6A and 6B; Berryman et al., 1993; Ingraffea et al., 2002).

The lumen of the midgestational embryonic intestine is lined by a flat stratified epithelium supported by outer stromal tissue (Mathan et al., 1975; Babyatsky and Podolsky, 2003). In contrast, the mature small intestinal surface is covered with abundant finger-like villi that project into the luminal space. Villus morphogenesis is a remarkable process that features transformation of the stratified epithelium to a polarized columnar epithelial monolayer surrounding each villus. The apical surface of the mature intestinal epithelium is covered with dense brush border microvilli. We have found that in the absence of Ezrin, the only ERM protein detected in the developing small intestinal epithelium, the transition from a stratified to columnar epithelium is incomplete, resulting in abnormal villus morphogenesis. Specifically, Ezrin is required for proper apical membrane assembly, which is particularly important for the propagation of polarity during the formation and expansion of secondary lumina within the stratified epithelium, a key but poorly understood step in villus morphogenesis (Mathan et al., 1975; Madara et al., 1981; Toyota et al., 1989).

Our study indicates that Ezrin is not absolutely required for microvillus formation or for the establishment or maintenance of epithelial cell polarity. Instead, Ezrin performs a critical function in organizing the apical domain of the intestinal epithelial cell and its associated apical junctions that mediate communication between cells in the intestinal epithelium.

Results

Generation of Ez-Deficient Mice

To study Ezrin function in vivo, we engineered a conditional *Ez* allele with loxP sites flanking exons 3 to 5 of the *ezrin* gene by homologous recombination in mouse embryonic stem (ES) cells (Supplemental Figure S1 at http://www.developmentalcell.com/cgi/content/full/6/6/855/DC1). To identify cells that express *ezrin* in vivo, we introduced a cassette containing a promoterless β-galactosidase-neomycin (β-geo) fusion flanked by FRT sites into intron 5; this allele is designated $Ez^{loxP\text{-}\beta geo}$. Chimeric $Ez^{+/loxP\text{-}\beta geo}\leftrightarrow$wt mice generated using two independently targeted ES cell clones yielded germline transmission of the *Ez* mutant allele to F1 $Ez^{+/loxP\text{-}\beta geo}$ mice (Supplemental Figure S1B). Zygotic deletion of exons 3–5 was achieved by crossing to EIIa-*Cre* transgenic mice; the recombined allele is designated $Ez^{\Delta 345\text{-}\beta geo}$ (Supplemental Figure S1C; Lasko et al., 1996). Both immunoblotting of lysates from $Ez^{\Delta 345\text{-}\beta geo/\Delta 345\text{-}\beta geo}$ tissues using two different antibodies and immunohistochemical analysis of $Ez^{\Delta 345\text{-}\beta geo/\Delta 345\text{-}\beta geo}$ tissue revealed the complete absence of Ezrin protein (Supplemental Figure S1D, Figure 6C; not shown); we will refer to the $Ez^{\Delta 345\text{-}\beta geo}$ allele as "Ez^{-}."

Ezrin Expression in Embryonic and Adult Tissues

Ezrin is expressed by many types of cultured cells, but its expression is restricted in vivo (Bretscher et al., 2000). Although *ezrin* expression in the developing blastocyst and in several adult tissues has been documented (Louvet et al., 1996; Berryman et al., 1993), a systematic evaluation of *ezrin* expression during embryonic development has not been reported. In the developing embryo, expression of β-*geo* from the $Ez^{loxP\text{-}\beta geo}$ allele was primarily detected in secretory/absorptive epithelia, including the chorionic villus, kidney, bronchial, choroid plexus, and intestinal epithelia, mirroring endogenous *ezrin* expression (Figures 1A–1C and 6A; not shown). β-*geo* expression was also prominent in the lens and dorsal aspect of the neural tube (Figures 1D and 1E). This pattern of expression persisted in adult mouse tissues as has been described for *ezrin* expression in the adult rat (Berryman et al., 1993; Ingraffea et al., 2002; not shown). Thus, Ezrin function may be particularly important in cells with specialized apical surfaces.

$Ez^{-/-}$ Neonates Exhibit Defective Villus Architecture

Intercrossing of $Ez^{+/-}$ mice yielded submendelian ratios of homozygous $Ez^{-/-}$ neonates (~12%). Despite their normal appearance at birth, $Ez^{-/-}$ neonates failed to thrive postnatally and did not survive past weaning, despite normal respiratory and suckling behaviors. In light of these symptoms and the strong expression of *ezrin* in the intestine, we examined the digestive tracts of $Ez^{-/-}$ pups. Whole-mount preparations of wild-type small intestines revealed a luminal surface covered with abundant villi (Figure 2A). In contrast, the luminal surface of the $Ez^{-/-}$ intestine is covered with cauliflower-shaped villi that appear to reflect the aggregation of multiple individual villi (Figure 2B). Histological analysis confirmed this interpretation. Instead of a villus unit composed of a single layer of columnar epithelium surrounding a mesenchymal core as in the wild-type (Figure 2C), the unit of structure in the $Ez^{-/-}$ intestine is multilobed and composed of multiple villi that are fused or intertwined (Figure 2D). This structure is morphologically distinct from that of intestinal adenomas, multilobed structures that initially are anchored by a single stalk to the intestinal mucosa and develop via overgrowth of a single villus (Bienz and Clevers, 2000). The morphological complexity of the $Ez^{-/-}$ villi increased with postnatal age, leading to the formation of complex amalgamated structures (Figures 2E and 2F).

Although not yet fully developed, the neonatal rodent intestine exhibits features of mature intestinal architecture (Stappenbeck et al., 1998). Cell division is restricted to the intervillus epithelium and is followed by migration of immature epithelial cells up the villus axis. As precursors move out of the future crypt, they differentiate into mature polarized enterocytes, goblet cells, or enteroendocrine cells; Paneth cells arise from precursors that move down to the base of the crypt. Despite the abnormal morphology of $Ez^{-/-}$ villi, histochemical staining revealed normal numbers and distribution of goblet, enteroendocrine, and Paneth cells (Figures 2G and 2H; not shown). Moreover, short-term 5-bromo-deoxyuridine (BrdU) labeling indicated that cell division was appropriately restricted to the base of each $Ez^{-/-}$ villus (Figures 2I and 2J). At later times after labeling (2 days), BrdU-positive cells were distributed similarly throughout wild-type and $Ez^{-/-}$ villi, indicating similar rates of migration along the villus axis (not shown). The progressive complexity of the $Ez^{-/-}$ villus suggests that the normal extrusion of cells from the villus tip may not occur in regions where two $Ez^{-/-}$ villi are fused. Otherwise, the development and maintenance of the mature crypt-villus unit proceeds normally in the absence of Ezrin despite dramatically aberrant villus architecture.

Abnormal Villus Morphogenesis in Developing $Ez^{-/-}$ Intestines

Abnormal villus morphology was already apparent in the $Ez^{-/-}$ neonatal intestine, indicating that the defect arose during embryonic development. In mice, intestinal villi begin to form at 14.5 days of gestation (E14.5; Stappenbeck et al., 1998; Babyatsky and Podolsky, 2003). At that time, the intestinal lumen is surrounded by a multilayered stratified epithelium. During the next 24 hr, in proximal-to-distal fashion, the intestinal lining undergoes dramatic morphological change, resulting in the formation of abundant villi. During villus formation, the stratified epithelium is converted to a single layer of columnar epithelium as the underlying mesenchyme condenses and evaginates to form the villus core. By E16.5 the process is complete and mitosis becomes restricted to the intervillus epithelium, which matures

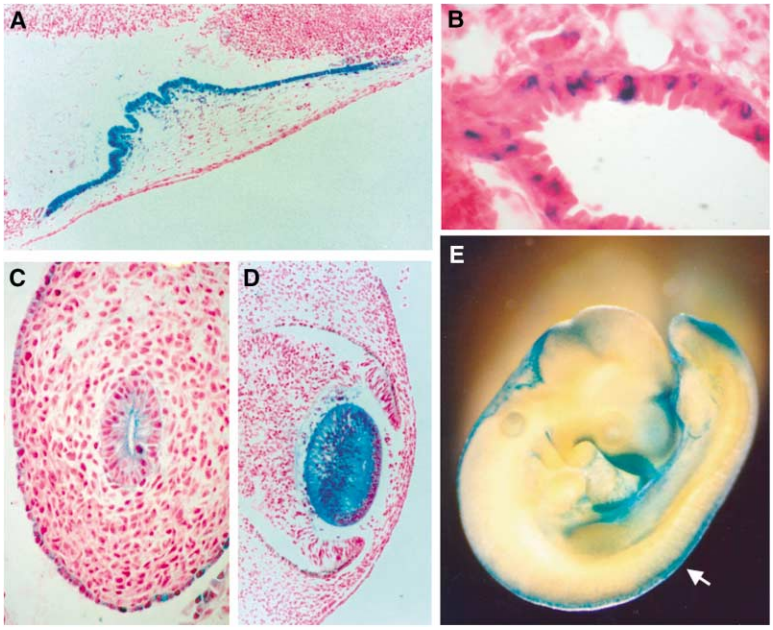

Figure 1. LacZ Staining Reveals β-*geo* Expression from the Targeted Allele under the Control of the Endogenous *ezrin* Promoter

(A–D) LacZ-stained, paraffin-embedded, and sectioned tissues. β-*geo* is expressed in the E12.5 choroid plexus ([A] 100×), adult alveolar epithelium ([B] 1000×), E12.5 intestinal epithelium ([C] 200×), and E12.5 lens ([D] 100×). (E) Whole-mount staining reveals β-*geo* expression in the dorsal neural tube (arrow) in an $Ez^{+/-}$ E9.5 embryo.

postnatally to become the stem cell-containing crypts of the adult intestine.

At E14.5, wild-type and $Ez^{-/-}$ intestines are grossly indistinguishable, with a small luminal space surrounded by stratified epithelium (Figures 3A and 3B). However, by E15.5 villus formation in $Ez^{-/-}$ embryos is clearly abnormal. Instead of the discrete, individual villus units apparent in the wild-type intestine, $Ez^{-/-}$ villi are fused together via regions of disorganized, stratified epithelial cells (Figures 3C and 3D). By E16.5, wild-type villi are separated by larger luminal spaces while most $Ez^{-/-}$ villi remain fused, exhibiting complex architecture (Figures 3E and 3F). Mucinous substance trapped in the luminal spaces between fused villi suggests that they are not continuous with the central lumen (see Figures 2D and 2H, arrows).

Polarization of $Ez^{-/-}$ Intestinal Epithelial Cells

Cells lining the central lumen of wild-type and $Ez^{-/-}$ E14.5 intestines display apical surface markers, junctional complexes, and small, irregular microvilli; cells embedded within the stratified epithelium are surrounded by patchy cell:cell junctions containing E-cadherin and β-catenin (Mathan et al., 1975; Toyota et al., 1989). By E15.5, polarization of cells surrounding each villus is evidenced by basolateral restriction of E-cadherin/β-catenin and an apical surface marked by a developing brush border and apical markers such as Crumbs3 (Figures 4A, 4C, and 4E; Makarova et al., 2003). Cells forming sites of fusion between $Ez^{-/-}$ villi remain stratified, but regions that are not fused contain cells that are polarized by these criteria (Figures 4B, 4D, and 4F). Although elongated (see below), apical junctions between polarized $Ez^{-/-}$ epithelial cells are present. Tight junctions and desmosomes are apparent ultrastructurally, and immunohistochemical localization of tight and adherens junction components is similar in polarized wild-type and $Ez^{-/-}$ intestinal epithelial cells (Supplemental Figure S2). These observations suggest that Ezrin is not required for intestinal epithelial cell polarization per se, but rather for completing the transition from stratified to columnar epithelium in all cells.

Microvillus Formation in $Ez^{-/-}$ Intestinal Epithelial Cells

Ezrin was originally identified as a component of brush border microvilli that cover the apical surface of polarized epithelial cells in several tissues including the kidney, placenta, and intestine (Bretscher, 1983; Berryman et al., 1993). Indeed, it has been suggested that Ezrin-mediated linkage between the lateral membrane and actin core is required for microvillus formation (Takeuchi et al., 1994; Berryman et al., 1995; Crepaldi et al., 1997; Bonhila et al., 1999). Surprisingly, ultrastructural examination of the apical surface of $Ez^{-/-}$ intestinal epithelial cells revealed a brush border with a microvillar density similar to wild-type (Figures 5A and 5B). However, $Ez^{-/-}$ microvilli are short, thick, and nonuniform relative to wild-type, resembling the immature microvilli of undifferentiated crypt cells prior to their migration and differentiation (Louvard et al., 1992). Instead, the actin-rich terminal web region that also contains Ezrin and provides a platform into which brush border microvilli are anchored is markedly thickened and undulating in contrast to the flat, compact terminal web of wild-type cells (Figures 5A and 5B, brackets; Supplemental Figure S2; Berryman et al., 1993). Actin is concentrated at the $Ez^{-/-}$ apical surface as in wild-type, indicating that a terminal web structure is present (not shown). Apical cell junctions that are continuous with the terminal web region are also elongated and wavy in the absence of Ezrin (Figure 5B, asterisks; Supplemental Figure S2). In fact, the distance from microvillus tip to the base of the terminal web region is comparable in wild-type and $Ez^{-/-}$ intestinal epithelial cells. Villin, a major brush border component, localizes apically in both wild-type and $Ez^{-/-}$ intestinal

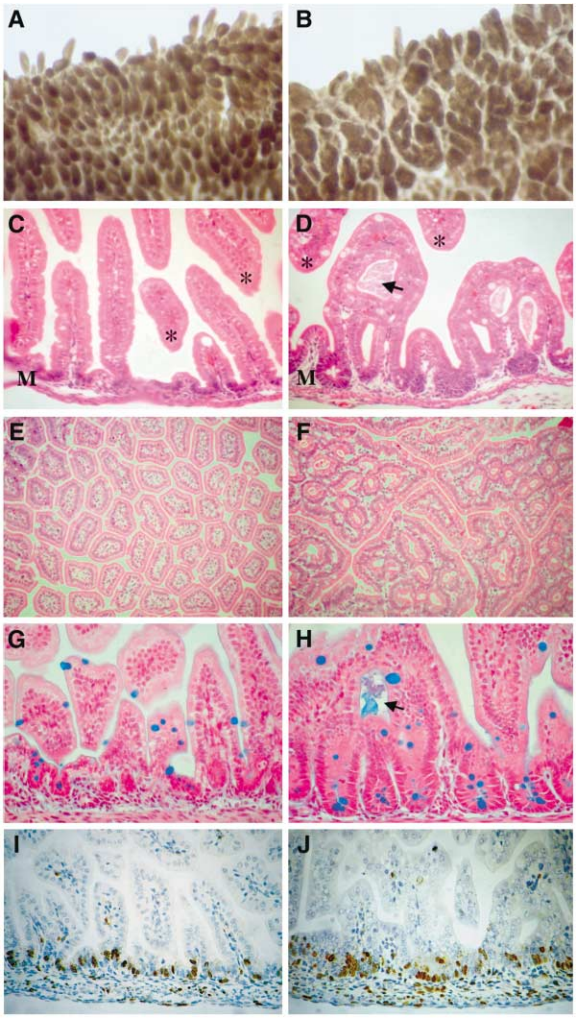

Figure 2. Abnormal Intestinal Villus Morphology in $Ez^{-/-}$ Neonates

(A and B) Whole-mount preparations reveal aberrant, multilobed villi in the neonatal $Ez^{-/-}$ small intestine (B) in contrast to the dense uniform villi covering the surface of the neonatal wild-type intestinal lumen (A).

(C and D) Hematoxylin- and eosin-stained sections reveal single villus units in the wild-type intestine (C); instead, $Ez^{-/-}$ villi are composed of multiple individual units that are fused together (D). Luminal spaces between "fused" villi often contain trapped mucinous substance (arrow). Developing crypts are located at the villus base adjacent to the supporting mucosa (M). Transverse sections of villi originating outside the plane of section are marked by an asterisk. Images at 400×.

(E and F) By P19, the complexity of the $Ez^{-/-}$ villus structure is markedly increased (F), compared with the single villi apparent in the wild-type (E); transverse villus sections are shown. Images at 200×.

(G–J) Proliferation and differentiation proceed normally in $Ez^{-/-}$ intestinal villi.

(G and H) Alcian blue staining of paraffin sections identifies a similar number and distribution of goblet cells in wild-type (G) and $Ez^{-/-}$ (H) intestinal villi. Images at 600×.

(I and J) BrdU incorporation is restricted to the base of each villus in both wild-type (I) and $Ez^{-/-}$ (J) small intestines. Images at 400×.

epithelial cells (not shown). Thus, Ezrin is not required for the formation of brush border microvilli per se, but rather for the organization of the underlying terminal web from which microvilli project.

Localization of Apical Membrane Proteins in the Absence of Ezrin

Although Crumbs3 localizes apically in $Ez^{-/-}$ intestinal epithelial cells in regions where villi are not fused (Figures 4E and 4F), the ERM binding partner EBP50/NHE-RF, which is apically concentrated in wild-type intestinal epithelial cells, remains diffusely localized in $Ez^{-/-}$ cells, whether they are polarized or not (Figures 5C and 5D). Moreover, despite normal expression levels, EBP50/NHE-RF is not phosphorylated in the $Ez^{-/-}$ intestine (Figure 5E). Thus, EBP50/NHE-RF phosphorylation and apical localization is dependent upon the ERM proteins. In contrast, the Na^+/H^+ exchanger 3 (NHE3), a key membrane target of EBP50/NHE-RF, does localize apically in polarized $Ez^{-/-}$ intestinal epithelial cells (Supplemental Figure S3). Indeed, EBP50/NHE-RF has been shown to regulate rather than localize NHE3 (Weinman et al., 2003). Other unidentified apical membrane proteins that interact with EBP50/NHE-RF may also be misregulated or mislocalized in the absence of Ezrin (Shenolikar and Weinman, 2001). However, the normal apical localization of GPI-linked alkaline phosphatase and integral membrane sucrase isomaltase together with the glycocalyx displayed by $Ez^{-/-}$ microvilli (indicative of the presence of glycosylated proteins) suggests that gross defects in apical membrane sorting do not occur in the absence of Ezrin (Supplemental Figure S3).

Secondary Lumen Formation

The fusion of portions of $Ez^{-/-}$ villi could be due to either aberrant attachment or incomplete segregation during morphogenesis. Central to the process of villus morphogenesis is the resolution of the stratified epithelium to a columnar epithelial monolayer lining each villus. An important but poorly understood feature of this transition is the development of multiple secondary lumina that form within the stratified epithelium, expand, and eventually fuse with the central lumen, effecting the resolution of individual villi (Mathan et al., 1975; Madara et al., 1981; Toyota et al., 1989).

To determine whether Ezrin plays a role in secondary lumen formation, we examined Ezrin expression and localization in wild-type intestinal epithelial cells during this transition. Ezrin is expressed by the intestinal epithelium beginning as early as E12.5 (see Figures 1C and 6A). In contrast, Moesin and Radixin are expressed exclusively in the surrounding stromal tissue (Figure 6B; Berryman et al., 1993; Ingraffea et al., 2002). In the stratified epithelium prior to E14.5, Ezrin is localized throughout the cell; shortly thereafter, discrete streaks of concentrated Ezrin become apparent between epithelial cells embedded in the stratified layers or extending from the central lumen (Figures 6D and 6E, arrows). Crumbs3 also localizes to these streaks, which mark the nascent apical membrane of secondary lumina (see Figure 7A). By E15.5, most wild-type villi are discrete units covered by a single layer of columnar epithelial cells with Ezrin concentrated across their apical surfaces (Figures 6A, 6F, and 6G). Some wild-type villi are still separating, with Ezrin-positive apical surfaces moving toward each other as the cells "unzip" (Figures 6F and 6G). Thus, Ezrin is a marker of nascent apical surface during the formation and expansion of secondary lumina within the stratified intestinal epithelium.

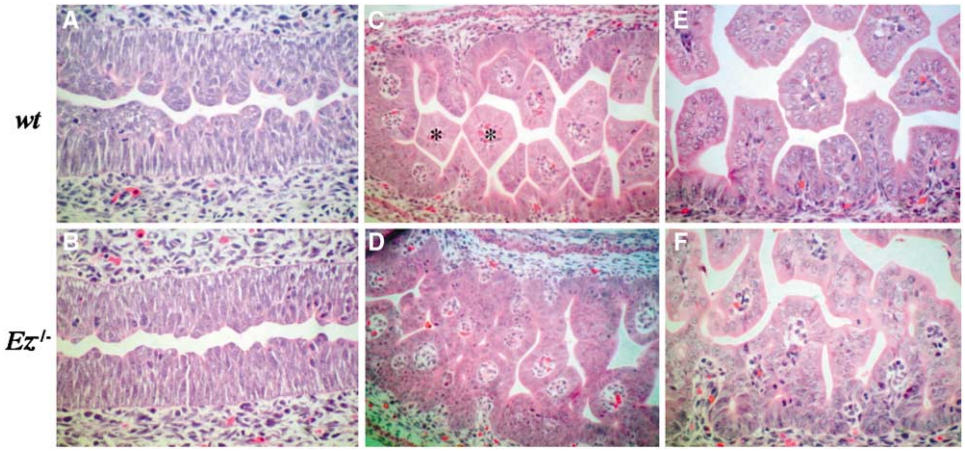

Figure 3. Abnormal Villus Morphogenesis in $Ez^{-/-}$ Embryos

Hematoxylin- and eosin-stained sections of wild-type (A, C, and E) and $Ez^{-/-}$ (B, D, and F) embryonic intestines.

(A and B) The stratified epithelium lining the developing gut in wild-type (A) and $Ez^{-/-}$ (B) E14.5 embryos is comparable. Images at 600×.

(C and D) However, as villus morphogenesis proceeds at E15.5, $Ez^{-/-}$ villi (D) are abnormally shaped and often fused together in contrast to the individual villus units apparent in the wild-type ([C] asterisks, transverse sections).

(E and F) By E16.5, wild-type villi are larger and completely segregated (E) but $Ez^{-/-}$ villi remain fused (F). Images at 400×.

The fusion of villi in $Ez^{-/-}$ intestines suggests that unzipping of stratified epithelial cells occurs abnormally during villus morphogenesis. Immunostaining for Crumbs3 revealed a similar distribution of secondary lumina throughout the stratified epithelium in wild-type and $Ez^{-/-}$ E14.5 intestines (Figures 7A and 7B). Similarly, electron microscopy revealed the presence of secondary lumina lined with microvilli in both the wild-type and *Ez* mutant (Figures 7C and 7D). However, as in the neonatal intestine (Figure 5B), the microvilli and apical surfaces lining new lumina at E14.5 are already disorganized in the *Ez* mutant. In the wild-type, secondary lumina expand and fuse, forming a network that is continuous with the central lumen. Lumen expansion is driven both by reorientation of the plane of cell division so that it is perpendicular to the new lumen and by propagation of polarity from cell to cell. In contrast, many $Ez^{-/-}$ secondary lumina failed to expand appreciably and bordering cells often formed pseudocysts around the new luminal space, suggesting that they reoriented their plane of division and continued to divide without inducing the polarization of adjacent cells (see Figures 3D, 3F, and 4B, arrows). Thus, Ezrin appears to be required for the propagation of polarity from cell to cell during secondary lumen expansion. Together with the obvious disorganization of the terminal web region and elongated apical junctions, these data are consistent with a model whereby Ezrin normally functions to organize the apical

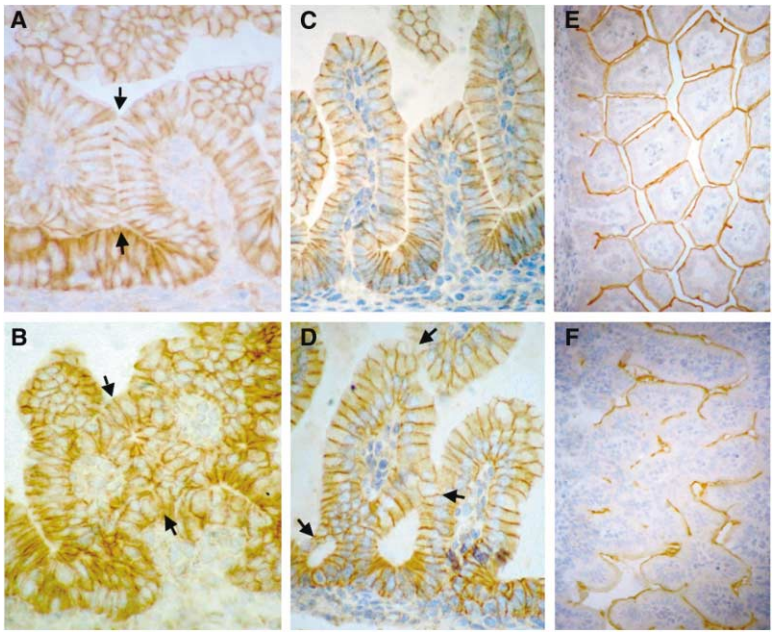

Figure 4. Incomplete Polarization of the $Ez^{-/-}$ Intestinal Epithelium

(A–D) Immunohistochemical localization of β-catenin to lateral boundaries between epithelial cells in wild-type (A and C) and $Ez^{-/-}$ (B and D) E15.5 (A and B) and E16.5 (C and D) intestines. Note the boundary between wild-type E15.5 villi where β-catenin is excluded (arrows in [A]). In the *Ez* mutant, the boundary between two villi is not well demarcated and contains bridges of nonpolarized cells (arrows in [B]). By E16.5, larger spaces between wild-type villi are evident and apical surfaces lack β-catenin staining (C), while $Ez^{-/-}$ villi have enlarged but remain attached via β-catenin-positive boundaries (arrows in [D]). Images at 1000×.

(E) Crumbs3 marks the apical surface surrounding developing villi in wild-type E15.5 intestines. Image at 400×.

(F) In the $Ez^{-/-}$ intestine, Crumbs3 localizes to the apical surface of epithelial cells that line luminal surfaces but is not detectable where villi are fused. Image at 400×.

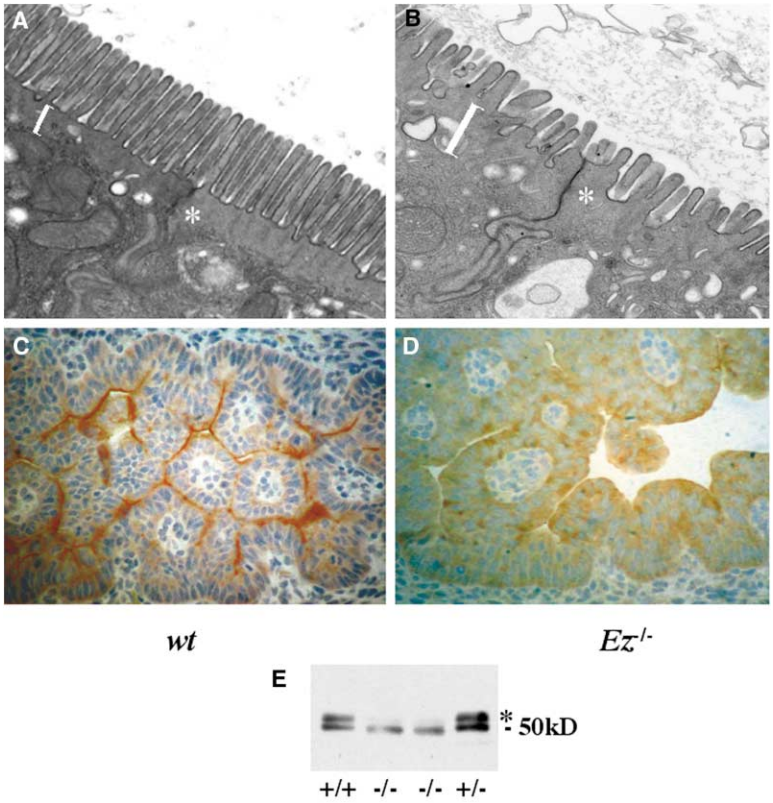

Figure 5. Apical Defects in $Ez^{-/-}$ Intestinal Epithelial Cells

(A and B) Transmission EM reveals densely packed, uniform, and rod-like brush border microvilli across the apical surface of wild-type intestinal epithelial cells (A). In contrast, $Ez^{-/-}$ brush border microvilli are numerous but thickened, nonuniform, and misoriented (B). The terminal web region immediately beneath the brush border is thickened and undulating in the *Ez* mutant in contrast to the wild-type (brackets). Electron-dense apical junctions at the terminal web boundaries are elongated in the *Ez* mutant (asterisks). Images at 11,000×.

(C) The ERM-interacting EBP50/NHE-RF is concentrated at the apical surface outlining each wild-type villus. Image at 400×.

(D) In contrast, EBP50/NHE-RF is diffusely localized in $Ez^{-/-}$ intestinal epithelial cells and does not apically concentrate, even in successfully polarized cells. Image at 400 ×.

(E) Western blot analysis reveals that EBP50/NHE-RF is phosphorylated in wild-type and $Ez^{+/-}$ but not $Ez^{-/-}$ neonatal intestinal tissue (upper species, asterisk).

terminal web and associated apical junctions that mediate cell:cell communication during secondary lumen expansion (Figure 7E).

Discussion

The apical surface of polarized epithelial cells is a highly specialized membrane domain whose integrity is dependent upon the actin cytoskeleton. The ERM proteins localize to the apical surface of epithelial cells, and several studies conclude that they are required for microvillus formation and/or epithelial cell polarity (Takeuchi et al., 1994; Berryman et al., 1995; Crepaldi et al., 1997; Bonhila et al., 1999; Speck et al., 2003). We have found that Ezrin, the only ERM protein detected in the developing intestinal epithelium, is not required for microvillus formation or epithelial polarization per se. Instead, our data suggest that Ezrin plays an essential role in configuring the apical terminal web region, which provides a platform for anchoring both brush border microvilli and apical cell:cell junctions in polarized intestinal epithelial cells. In the absence of Ezrin, the terminal web region is disorganized, microvilli project nonuniformly from its surface, and apical junctions are elongated and sinuous. This interpretation is consistent with the work of Karagiosis and Ready (2004), who recently described an essential role for Moesin in shaping the rhabdomere terminal web of the *Drosophila* photoreceptor.

Our studies indicate that Ezrin-mediated integrity of the terminal web region is critical for secondary lumen expansion during villus morphogenesis. This poorly understood phenomenon is central to the formation of discrete villi from a stratified epithelium. Originally described ultrastructurally, secondary lumina are thought to initiate via the delivery of vesicles containing apical membrane to specialized cell:cell junctions that form between cells in the stratified epithelium in response to unknown cues (Mathan et al., 1975; Madara et al., 1981; Toyota et al., 1989). As continued vesicle delivery expands the new apical surface, the junctional complex is propagated at its leading edge. The two apposing cells reorient their planes of division and divide parallel to the new lumen, contributing to its expansion. When the propagating cell:cell junction reaches an adjacent cell, apical junction components must be recruited and a new terminal web initiated within that adjacent cell. This step appears to be defective in the absence of Ezrin. The abnormal terminal web structure and contiguous apicolateral junctions in $Ez^{-/-}$ intestinal epithelial cells suggest that Ezrin function may be important for establishing a "polarizing" landmark in adjacent cells during secondary lumen expansion. Assembly of the apical junctional complex is known to provide such a landmark during epithelial polarization in other systems (Nelson, 2003). Despite the identification of tight/adherens junctions and desmosomes in the $Ez^{-/-}$ intestinal epithelium, these junctional complexes are markedly elongated and sinuous; a detailed analysis may reveal more subtle defects in their architecture or composition. Notably, the NF2 tumor suppressor, Merlin, the closest relative of the ERM proteins, plays an important role in organizing the cortical actin ring and associated junctional complexes in primary keratinocytes (Lallemand et al., 2003). It will be interesting to directly compare the roles of

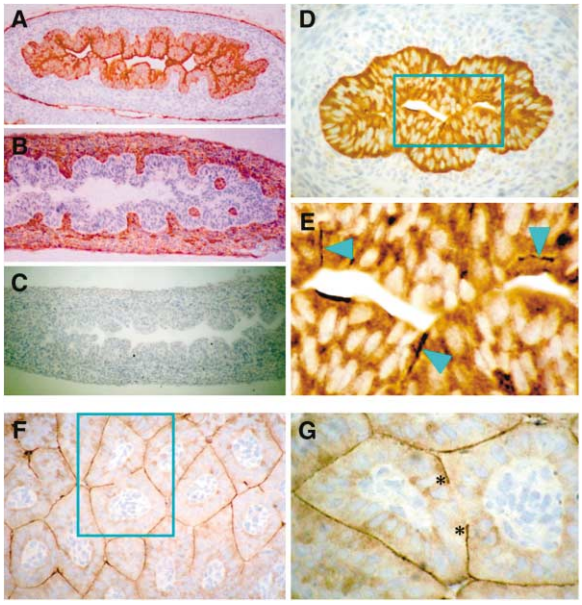

Figure 6. Ezrin Localization in the Developing Intestine

(A) At E15.5, Ezrin is expressed at high levels throughout the epithelial compartment but not in the stroma.

(B) Immunostaining using an antibody that detects both Moesin and Radixin reveals that their expression is restricted to the stromal compartment. This pattern was also seen using an antibody that detects only Radixin.

(C) Ezrin is not detected in the E15.5 $Ez^{-/-}$ intestine. Images in (A)–(C) at 400×.

(D and E) In the wild-type E14.5 intestine, in addition to diffuse localization throughout the cell, Ezrin becomes concentrated at apical surfaces, including nascent secondary lumina (arrowheads in E). Boxed area in (D) is enlarged in (E). Image in (D) at 600×; image in (E) at ~1000×.

(F and G) By E15.5, Ezrin is concentrated across the angular apical surfaces of nascent villi. Boxed area in (F) is enlarged in (G) depicting the unzipping of two Ezrin-positive apical surfaces moving toward each other (asterisks). Images at 600×.

Merlin and the ERM proteins in organizing the apical domain of fully polarized epithelial cells.

Visual comparison of E15.5 wild-type and $Ez^{-/-}$ intestines reveals that in addition to their obvious fusion, the overall geometry of $Ez^{-/-}$ villi is different (see Figures 3–6). Wild-type villi are angular—straight rows of apposed columnar cells are separated by thin spaces that meet at sharp angles, likely reflecting recent unzipping. In contrast, $Ez^{-/-}$ villi are markedly rounded. We speculate that this reflects differences in tension across the developing wild-type and $Ez^{-/-}$ epithelia. Nonuniform distribution of tension throughout the wild-type intestinal cylinder might govern secondary lumen expansion much like the three-dimensional transmission of cracks through thick ice. The continuity of the terminal web region and apical junctions may confer a level of tension across the developing epithelium that is critical for the propagation of apical junctions and secondary lumina from cell to cell; abnormal tension across the $Ez^{-/-}$ apical surface may blunt secondary lumen expansion. This could also explain the accordion-like appearance of the apical surface of polarized $Ez^{-/-}$ epithelial cells that is apparent upon electron microscopy (Figure 5B; Supplemental Figure S2).

The best-known mechanism of ERM activation is via Rho-induced phosphorylation (Hirao et al., 1996; Shaw et al., 1998; Matsui et al., 1998). Recent genetic studies in *Drosophila* suggest that the ERMs can also negatively regulate Rho activity (Speck et al., 2003). In the absence of the single *Drosophila* ERM protein Moesin, many cells in the imaginal disc lose polarity and are extruded from the epithelium, a phenotype that can be rescued by reducing Rho activity (Speck et al., 2003). Perhaps this phenotype also reflects altered tension across the apical surface of this simple epithelial monolayer. Although not well studied in intestinal epithelial cells, Rho is a key regulator of the cortical actin network and actomyosin contractility in other cell types and likely plays an important role in organizing the terminal web and associated apical junctions in these cells (Etienne-Manneville and Hall, 2002). The ERM proteins may function as rheostats of cytoskeletal tension, modulating Rho GTPase activity in response to changes in tension across an epithelial monolayer.

The wasting and eventual death of $Ez^{-/-}$ neonates may not be solely due to abnormal villus morphology. Instead, Ezrin may be required for the localization or function of apical membrane proteins that are critical for intestinal function. We found that EBP50/NHE-RF, which links the ERMs to certain apical membrane proteins, is neither apically concentrated nor phosphorylated in the $Ez^{-/-}$ intestine. Apparently Merlin, which also interacts with EBP50/NHE-RF and is expressed in the intestinal epithelium, cannot fulfill this function. NHE3 localizes apically in the absence of both Ezrin and EBP50/NHE-RF, but it is likely misregulated in the $Ez^{-/-}$ intestine, as EBP50/NHE-RF is required for NHE3 regulation in other tissues (Weinman et al., 2003). Although EBP50/NHE-RF may regulate or localize other unidentified apical membrane proteins in the intestine, the appropriate localization of several apical membrane proteins in the absence of Ezrin argues against a global role for Ezrin in apical membrane trafficking.

The intestinal phenotype described here is the most obvious defect apparent in $Ez^{-/-}$ neonates. Careful inspection may reveal additional phenotypes in tissues that express high levels of Ezrin and may explain the submendelian proportion of $Ez^{-/-}$ neonates. The conditional design of our *Ez* allele will allow us to examine the consequences of Ezrin deficiency in other tissues in vivo. Our results highlight the poorly understood phenomenon of de novo lumen formation, which also occurs during the development of other organs such as the colon, thyroid, and mammary gland (Luciano et al., 1979; Hogan and Kolodziej, 2002). De novo lumen formation occurs during tubulogenesis in other organs; however, in this case lumen formation within the center of a cord of cells is likely directed by the outer basal lamina rather than by cell:cell propagation (Hogan and Kolodziej, 2002; Lubarsky and Krasnow, 2003). On the other hand, apical surface formation serves distinct roles in other epithelial tissues. For example, apical constriction of neuroepithelial cells in the dorsal neural tube and stretching of lens epithelial cells play key roles in neural tube closure and lens formation, both of which feature active changes in tension across the tissue (Bush et al., 1990; Yamada et al., 2000); *ezrin* is highly expressed by both cell types (Figures 1D and 1E). Notably, the ERM

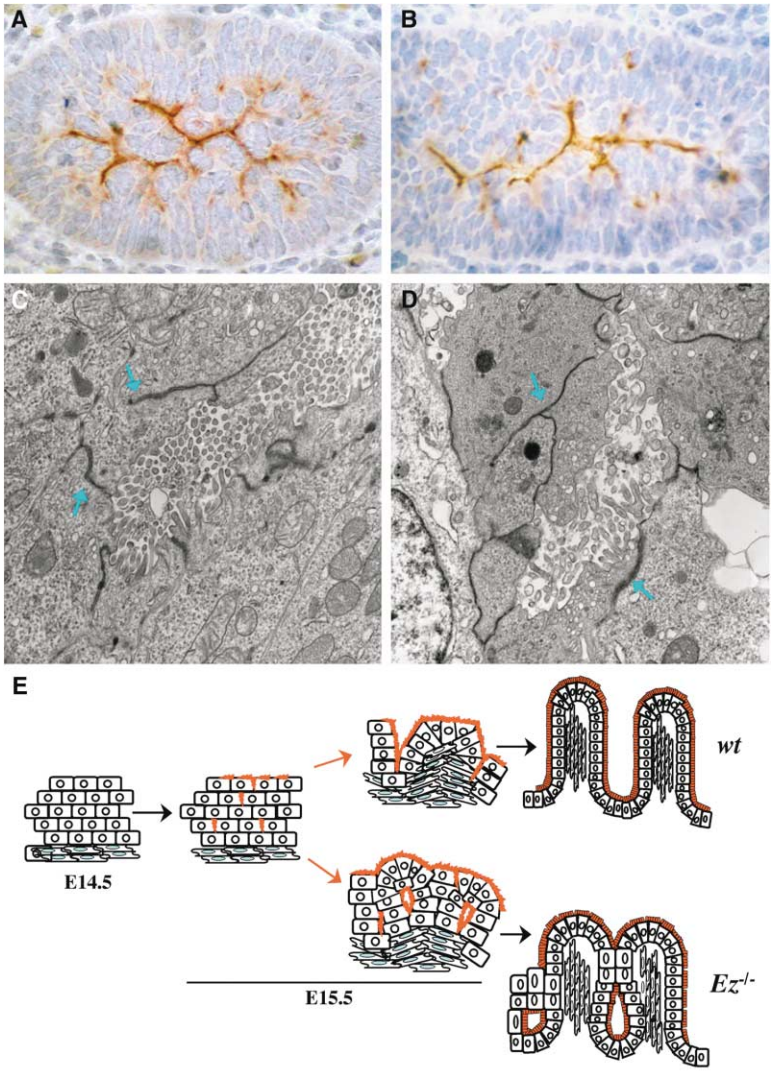

Figure 7. Secondary Lumen Initiation in the Developing $Ez^{-/-}$ Intestine

Crumbs3 staining (A and B) and electron microscopy (C and D) reveal similar numbers and distribution of secondary lumina in E15.0 wild-type and $Ez^{-/-}$ intestines. Unusually elongated apical junctions mark the boundaries between cells surrounding the developing lumen in both wild-type and *Ez* mutant (arrows). Images in (A) and (B) at 600×; images in (C) and (D) at 15,000×.

(E) Model of secondary lumen expansion in wild-type villus morphogenesis (top), leading to complete segregation of villi. In the $Ez^{-/-}$ intestine, secondary lumen form but their expansion stalls, leading to incomplete villus segregation and abnormal villus morphology (bottom).

proteins are unique to multicellular organisms, suggesting that they evolved in response to cell-cell communication. Many studies have examined the effects of perturbing ERM function in individual cultured cells. We have identified a specific role for Ezrin in the organization of the apical domain of individual cells and consequent morphogenesis of an epithelium—a role accentuated by the architecture of a three-dimensional tissue.

Experimental Procedures

Generation of Targeted Ez Allele

Screening of a mouse 129/Sv genomic library with a probe corresponding to base pairs −90 to 396 of the mouse *ezrin* cDNA yielded two 17 kb genomic clones encompassing exons 2–7 of *ezrin*. A promoterless β-geo-tk cassette was engineered by combining β-galactosidase-neomycin fusion and thymidine kinase coding regions from pSAβgeo (provided by Sheila Thomas; MacGregor et al., 1995) and pPNT (McClatchey et al., 1997) plasmids. After inserting frt-containing oligonucleotides at either end, the frt-β-geo-tk-frt cassette was introduced into intron 5. LoxP-containing oligonucleotides were introduced 5′ to this cassette and into intron 2 (Supplemental Figure S1A).

Screening of ES Cell Clones

Electroporation into J1 ES cells and subsequent drug selection was as described (McClatchey et al., 1997). Surviving clones were evaluated by Southern blotting of SpeI- or BamHI-digested DNA (Supplemental Figure S1B). 5′ and 3′ probes were generated by subcloning 0.8 kb KpnI and 0.5 kb ApaI fragments. Injection of two homologously targeted clones into blastocysts yielded chimeric animals that transmitted the *Ez* mutant allele to their offspring, which were bred to EIIa-*Cre* mice to remove *ezrin* exons 3–5 (Lasko et al., 1996). Zygotic EIIa-*Cre* expression yielded germline transmission of the recombined allele. Cre-mediated excision was confirmed by Southern blotting of SpeI-digested DNA using the 5′ probe. Phenotypes observed in $Ez^{-/-}$ pups derived from either ES cell clone were indistinguishable. All mice examined were on a mixed 129/SvJ;C57Bl/6J background. We also crossed F1 129/Sv;C57Bl/6J $Ez^{+/-}$ mice to hACTB::*Flpe*.9205 mice that express the Flp recombinase in the zygote (kindly provided by Sue Dymecki; Rodriguez et al., 2000). As expected, Flp expression effected deletion of the β-geo cassette generating a conditional allele; mice homozygous for the conditional allele are viable and normal.

Western Blot Analysis

Tissue extracts were prepared by homogenization in RIPA buffer (1% Triton X-100, 0.5% deoxycholate, 0.1% SDS, 50 mM Tris-Cl [pH 7.4], 150 mM NaCl, 1 mM EDTA, 1 mM EGTA, and a protease/

phosphatase inhibitor cocktail). Proteins (30–40 μg) were separated on 8% SDS-PAGE gels, transferred to Immobilon (Millipore), and probed with anti-Ezrin (1/1000, NeoMarkers #3C12; 1/2000, Babco) or anti-EBP50/NHE-RF (1/2000, Abcam #3452) antibodies. HRP-conjugated secondary antibodies were detected by chemiluminescence.

Detection of β-*geo* Expression in *Ez*$^{loxP\text{-}\beta\text{-}geo/+}$ Tissues

Detection of β-*geo* expression was performed as described (McClatchey et al., 1997). Briefly, embryos or tissues were rinsed in 0.1 M $NaPO_4$ buffer (pH 7.3), fixed (0.2% glutaraldehyde, 5 mM EGTA, 2 mM MgCl, 0.1 M $NaPO_4$ buffer [pH 7.3]), washed three times (2 mM MgCl, 0.02% NP-40, 0.01% deoxycholate, 0.1 M $NaPO_4$ buffer [pH 7.3]), and stained overnight in X-gal (1 mg/ml X-gal, 5 mM K-ferricyanide, 5 mM K-ferrocyanide) at room temperature. Stained embryos were photographed, dehydrated, paraffin-embedded, sectioned, and counterstained with nuclear Fast Red (PolyScientific).

Whole-Mount Preparation of Intestinal Villi

Whole-mount preparation of intestinal villi was performed as described (Stappenbeck and Gordon, 2000). Briefly, intestines were flushed with cold PBS, opened lengthwise and attached to filter paper, fixed in periodate-lysine-paraformaldehyde (PLP) for 1 hr at room temperature, washed three times in PBS, incubated in DTT buffer (20 mM DTT, 20% ethanol, 150 mM Tris-HCl [pH 8.0]) for 45 min at room temperature, and photographed.

Histochemistry and Immunohistochemistry

Dissected tissues were fixed in 10% neutral buffered-formalin, processed, and paraffin-embedded. Sections were stained with hematoxylin and eosin or subject to immunohistochemistry using the following primary antibodies: anti-Ezrin (1:200; NeoMarkers #3C12), anti-Moesin (1/400, NeoMarkers #38/87), anti-Radixin (1/18.5 a kind gift from Anthony Bretscher; Ingraffea et al., 2002), anti-EBP50/NHE-RF (1/250, ABCAM #3452), anti-Crumbs3 (1/200, a kind gift from Ben Margolis; Makarova et al., 2003), anti-sucrase isomaltase (1/100, a kind gift from Hans-Peter Hauri), anti-β-catenin (1/50, BD Biosciences clone 14), anti-NHE3 (1/200, Chemicon clone 19F5), anti-BrdU (1/200, Becton Dickinson), and anti-Z0-1 (1/60, Zymed). Antigen retrieval was achieved by boiling in 10 mM citrate buffer (20 min) for all antibodies except anti-BrdU and anti-ZO-1, which utilized treatment with 0.1% trypsin (20 min, 37°C) and 2 mg/ml protease (10 min, 37°C; Sigma), respectively. HRP-conjugated secondary antibodies were detected using the DAB peroxidase substrate kit (Vector Laboratories). For sucrase isomaltase detection, fresh tissues were embedded in OTC, snap-frozen, and sectioned by cryostat.

Histochemical identification of intestinal cell types was performed on paraffin sections using Periodic Acid Schiff, Alcian Blue, and Grimelius silver stain reagents as recommended by the manufacturer (PolyScientific). Alkaline phosphatase (AP) activity was detected using an AP substrate kit (Vector Laboratories).

Electron Microscopy

Tissues were fixed in 4% glutaraldehyde in PBS, embedded in 2% agar, and postfixed in 1.33% osmium tetroxide (Bunting et al., 1996). Samples were dehydrated in a graded series of ethanols, rinsed twice in propylene oxide, infiltrated with propylene oxide/epoxy mixtures, and rinsed three times in pure epoxy resin and polymerized overnight at 60°C. 1 μm sections were prepared and stained with toluidine blue. Representative areas were chosen, thin-sectioned, stained with lead citrate, and examined on a Philips 301 electron microscope. Images were captured by an Advanced Microscopy Techniques imaging system.

Acknowledgments

We are particularly grateful to Martin Selig for graciously providing time and expertise in electron microscopy. Antibodies were generously provided by Ben Margolis, Tony Bretscher, and Hans-Peter Hauri. We would like to thank Rick Fehon, Jeff Settleman, and Nick Dyson for critical reading of the manuscript and Dominique Lallemand and McClatchey lab members for stimulating discussions.

Received: December 16, 2003
Revised: April 7, 2004
Accepted: April 7, 2004
Published: June 7, 2004

References

Babyatsky, M.W., and Podolsky, D.K. (2003). Growth and development of the gastrointestinal tract. In Textbook of Gastroeneterology, T. Yamada, ed. (Philadelphia, PA: Lippincott Williams & Williams).

Berryman, M., Franck, Z., and Bretscher, A. (1993). Ezrin is concentrated in the apical microvilli of a wide variety of epithelial cells whereas moesin is found primarily in endothelial cells. J. Cell Sci. *105*, 1025–1043.

Berryman, M., Gary, R., and Bretscher, A. (1995). Ezrin oligomers are major cytoskeletal components of placental microvilli: a proposal for their involvement in cortical morphogenesis. J. Cell Biol. *131*, 1231–1242.

Bienz, M., and Clevers, H. (2000). Linking colorectal cancer to Wnt signaling. Cell *103*, 311–320.

Bonhila, V.L., Finneman, S.C., and Rodriguez-Boulan, E. (1999). Ezrin promotes morphogenesis of apical microvilli and basal infoldings in retinal pigment epithelium. J. Cell Biol. *147*, 1533–1547.

Bretscher, A. (1983). Purification of an 80,000-dalton protein that is a component of the isolated microvillus cytoskeleton, and its localization in nonmuscle cells. J. Cell Biol. *97*, 425–432.

Bretscher, A., Chambers, D., Bguyen, R., and Reczek, D. (2000). ERM-Merlin and EBP50 protein families in plasma membrane organization and function. Annu. Rev. Cell Biol. *16*, 113–143.

Bretscher, A., Edwards, K., and Fehon, R.G. (2002). ERM proteins and merlin: integrators at the cell cortex. Nat. Rev. Mol. Cell Biol. *3*, 586–599.

Bunting, R.W., Selig, M.K., and Dickersin, G.R. (1996). Ultrastructure of peripheral blood granulocytes from patients with low serum cobalamin. J. Submicrosc. Cytol. Pathol. *28*, 187–195.

Bush, K.T., Lynch, F.J., DeNittis, A.S., Steinberg, A.B., Lee, H.Y., and Nagele, R.G. (1990). Neural tube formation in the mouse: a morphometric and computerized three-dimensional reconstruction study of the relationship between apical constriction of neuroepithelial cells and the shape of the neuroepithelium. Anat. Embryol. *181*, 49–58.

Crepaldi, T., Gautreau, A., Comoglio, P.M., Louvard, D., and Arpin, M. (1997). Ezrin is an effector of hepatocyte growth factor-mediated migration and morphogenesis in epithelial cells. J. Cell Biol. *138*, 423–434.

Doi, Y., Itoh, M., Yonemura, S., Ishihara, S., Takano, H., Noda, T., Tsukita, S., and Tsukita, S. (1999). Normal development of mice with unimpaired cell adhesion/cell motility/actin-based cytoskeleton without compensatory up-regulation of Ezrin or Radixin in Moesin gene knockout. J. Biol. Chem. *274*, 2315–2321.

Etienne-Manneville, S., and Hall, A. (2002). Rho GTPases in cell biology. Nature *420*, 629–635.

Hirao, M., Sato, N., Kondo, T., Yonemura, S., Monden, M., Sasaki, T., Takai, Y., Tsukita, S., and Tsukita, S. (1996). Regulation mechanism of ERM (ezrin/radixin/moesin) protein/plasma membrane association: possible involvement of phosphatidylinotisol turnover and Rho-dependent signaling pathway. J. Cell Biol. *135*, 37–51.

Hogan, B.L.M., and Kolodziej, P.A. (2002). Molecular mechanisms of tubulogenesis. Nat. Rev. Genet. *3*, 513–523.

Ingraffea, J., Reczek, D., and Bretscher, A. (2002). Distinct cell-type specific expression of scaffolding proteins EBP50 and E3KARP: EBP50 is generally expressed with Ezrin in specific epithelia, whereas E3KARP is not. Eur. J. Cell Biol. *81*, 61–68.

Karagiosis, S.A., and Ready, D.F. (2004). Moesin contributes an essential structural role in *Drosophila* photoreceptor morphogenesis. Development *131*, 725–732.

Kikuchi, S., Hata, M., Fukumoto, K., Yamane, Y., Matsui, T., Tamura, A., Yonemura, S., Yamagishi, H., Keppler, D., Tsukita, S., and Tsukita, S. (2002). Radixin deficiency causes conjugated hyperbilirubinemia

with loss of Mrp2 from bile canalicular membranes. Nat. Genet. *31*, 320–325.

Lallemand, D., Curto, M., Saotome, I., Giovannini, M., and McClatchey, A.I. (2003). *Nf2*-deficiency promotes tumorigenesis and metastasis by destabilizing adherens junctions. Genes Dev. *17*, 1090–1100.

Lasko, M., Pichel, J.G., Gorman, J.R., Sauer, B., Okamoto, Y., Lee, E., Alt, F.W., and Westphal, H. (1996). Efficient *in vivo* manipulation of mouse genomic sequences at the zygote stage. Proc. Natl. Acad. Sci. USA *93*, 5860–5865.

Louvard, D., Kedinger, M., and Hauri, H.-P. (1992). The differentiating intestinal epithelial cell: establishment and maintenance of functions through interactions between cellular structures. Annu. Rev. Cell Biol. *8*, 157–195.

Louvet, S., Aghion, J., Santa-Maria, A., Mangeat, P., and Maro, B. (1996). Ezrin becomes restricted to outer cells following asymmetrical division in the preimplantation mouse embryo. Dev. Biol. *177*, 568–579.

Lubarsky, B., and Krasnow, M.A. (2003). Tube morphogenesis: making and shaping biological tubes. Cell *112*, 19–28.

Luciano, L., Thiele, J., and Reale, E. (1979). Development of follicles and of occluding junctions between the follicular cells of the thyroid gland. A thin-section and freeze-fracture study in the fetal rat. J. Ultrastruct. Res. *66*, 164–181.

MacGregor, G.R., Zambrowicz, B.P., and Soriano, P. (1995). Tissue non-specific alkaline phosphatase is expressed in both embryonic and extraembryonic lineages during mouse embryogenesis but is not required for migration of primordial germ cells. Development *121*, 1487–1496.

Madara, J.L., Neutra, M.R., and Trier, J.S. (1981). Junctional complexes in fetal rat small intestine during morphogenesis. Dev. Biol. *86*, 170–178.

Makarova, O., Roh, M.H., Liu, C.J., Laurinec, S., and Margolis, B. (2003). Mammalian Crumbs3 is a small transmembrane protein linked to protein associated with Lin-7 (Pals-1). Gene *302*, 21–29.

Mathan, M., Moxey, P., and Trier, J.S. (1975). Morphogenesis of fetal rat duodenal villi. Am. J. Anat. *146*, 73–92.

Matsui, T., Maeda, M., Doi, Y., Yonemura, S., Amano, M., Kaibuchi, K., Tsukita, S., and Tsukita, S. (1998). Rho-kinase phosphorylates COOH-terminal threonines of ezrin/radixin/moesin (ERM) proteins and regulates their head-to-tail association. J. Cell Biol. *140*, 647–657.

Maudsley, S., Zamah, A.M., Rahman, N., Blitzer, J.T., Luttrell, L.M., Lefkowitz, R.J., and Hall, R.A. (2000). Platelet-derived growth factor receptor assocation with Na^+/H^+ exchanger regulatory factor potentiates receptor activity. Mol. Cell. Biol. *20*, 8352–8363.

McClatchey, A.I. (2003). Merlin and the ERM proteins: unappreciated roles in cancer development? Nat. Rev. Cancer *3*, 877–883.

McClatchey, A.I., Saotome, I., Ramesh, V., Gusella, J.F., and Jacks, T. (1997). The *Nf2* tumor suppressor gene product is essential for extraembryonic development immediately prior to gastrulation. Genes Dev. *11*, 1253–1265.

Murthy, A., Gonzalez-Agosti, C., Cordero, E., Pinney, D., Candia, C., Solomon, F., Gusella, J., and Ramesh, V. (1998). NHE-RF, a regulatory cofactor for Na^+-H^+ exchange, is a common interactor for Merlin and ERM (MERM) proteins. J. Biol. Chem. *273*, 1273–1276.

Nelson, J.W. (2003). Adaptation of core mechanisms to generate cell polarity. Nature *422*, 766–774.

Reczek, D., Berryman, M., and Bretscher, A. (1997). Identification of EBP50: a PDZ-containing phosphoprotein that associates with members of the Ezrin-radixin-moesin family. J. Cell Biol. *139*, 169–179.

Rodriguez, C.I., Buchholz, F., Galloway, J., Sequerra, R., Kasper, J., Ayala, R., Stewart, A.F., and Dymecki, S.M. (2000). High-efficiency deleter mice show that FLPe is an alternative to Cre-*loxP*. Nat. Genet. *25*, 139–140.

Shaw, R.J., Henry, M., Solomon, F., and Jacks, T. (1998). RhoA-dependent phosphorylation and relocalization of ERM proteins into apical membrane/actin protrusions in fibroblasts. Mol. Biol. Cell *9*, 403–419.

Shenolikar, S., and Weinman, J. (2001). NHERF: targeting and trafficking membrane proteins. Am. J. Physiol. Renal Physiol. *280*, F389–F395.

Short, D.B., Trotter, K.W., Reczek, D., Kreda, S.M., Bretscher, A., Boucher, R.C., Stutts, M.J., and Milgram, S.L. (1998). An apical PDZ protein anchors the cystic fibrosis transmembrane conductance regulator to the cytoskeleton. J. Biol. Chem. *273*, 19797–19801.

Speck, O., Hughes, S.C., Noren, N.K., Kulikauskas, R.M., and Fehon, R.G. (2003). Moesin functions antagonistically to the Rho pathway to maintain epithelial integrity. Nature *421*, 83–87.

Stappenbeck, T.S., and Gordon, J.I. (2000). Rac1 mutations produce aberrant epithelial differentiation in the developing and adult mouse small intestine. Development *127*, 2629–2642.

Stappenbeck, T.S., Wong, M.H., Saam, J.R., Mysorekar, I.U., and Gordon, J.I. (1998). Notes from some crypt watchers: regulation of renewal in the mouse intestinal epithelium. Curr. Opin. Cell Biol. *10*, 702–709.

Takeuchi, K., Sato, N., Kasahara, H., Funayama, N., Nagafuchi, A., Yonemura, S., Tsukita, S., and Tsukita, S. (1994). Perturbation of cell adhesion and microvilli formation by antisense oligonucleotides to ERM family members. J. Cell Biol. *125*, 1371–1384.

Toyota, T., Yamamoto, M., and Kataoka, K. (1989). Light and electron microscope study on developing intestinal mucosa in rat fetuses with special reference to the obliteration of the intestinal lumen. Arch. Histol. Cytol. *52*, 51–60.

Weinman, E.J., Steplock, D., and Shenolikar, A. (2003). NHERF-1 uniquely transduces the camp signals that inhibit sodium-hydrogen exchange in mouse renal apical membranes. FEBS Lett. *536*, 141–144.

Yamada, T., Richiert, D., Tumminia, S.J., and Russell, P. (2000). The tensegrity model applied to the lens: a hypothesis for the presence of the fiber cell ball and sockets. Med. Hypotheses *55*, 36–39.

Yun, C.H., Lamprecht, G., Forster, D.V., and Sidor, A. (1998). NHE3 kinase A regulatory protein E3KARP binds to the epithelial brush border Na^+/H^+ exchanger NHE3 and the cytoskeletal protein ezrin. J. Biol. Chem. *273*, 25856–25863.

Early inactivation of p53 tumor suppressor gene cooperating with NF1 loss induces malignant astrocytoma

Yuan Zhu,[1,5] Frantz Guignard,[1] Dawen Zhao,[2] Li Liu,[5] Dennis K. Burns,[3] Ralph P. Mason,[2] Albee Messing,[4] and Luis F. Parada[1,*]

[1]Center for Developmental Biology and Kent Waldrep Foundation Center for Basic Research on Nerve Growth and Regeneration
[2]Cancer Imaging Program, Department of Radiology
[3]Department of Pathology, University of Texas Southwestern Medical Center, Dallas, Texas 75390
[4]Department of Pathobiological Sciences, Waisman Center and School of Veterinary Medicine, University of Wisconsin, Madison, Wisconsin 53705
[5]Division of Molecular Medicine and Genetics, Departments of Internal Medicine and Cell and Developmental Biology, University of Michigan Medical School, Ann Arbor, Michigan 48109
*Correspondence: luis.parada@utsouthwestern.edu

Summary

Malignant astrocytoma, the most prevalent primary brain tumor, is resistant to all known therapies and frequently harbors mutations that inactivate p53 and activate Ras signaling. We have generated mouse strains that lack p53 and harbor a conditional allele of the NF1 tumor suppressor that negatively regulates Ras signaling. The mice develop malignant astrocytomas with complete penetrance. The majority of tumors display characteristics of glioblastoma multiforme with concomitant alteration of signaling pathways previously described in the human counterparts of this neoplasm. We find that the sequence of tumor suppressor inactivation influences tumorigenicity and that earliest evidence of tumor formation localizes to regions of the brain that contain a multipotent stem cell population capable of in vivo differentiation into neurons and glia.

Introduction

Astrocytomas, composed predominantly of astrocyte-like cells, are the most common neoplasm in the central nervous system (CNS) (Kleihues and Cavenee, 2000). According to the World Health Organization (WHO) grading system, grade II–IV astrocytomas (collectively called malignant astrocytoma) are biologically malignant and diffusely infiltrate the brain. Grade IV astrocytoma, or glioblastoma multiforme (GBM), is one of the most aggressive human cancers, with a median survival of less than 1 year. Unfortunately, this prognosis has not changed significantly over the past two decades, despite advances in neurosurgery, radiation, and chemotherapy (Holland, 2001; Maher et al., 2001; Zhu and Parada, 2002).

There are two subtypes of GBMs. Primary GBMs arise rapidly or de novo without any evidence of prior clinical disease, whereas secondary GBMs derive from preexisting low-grade lesions after long latency ranging from 5 to 10 years (Kleihues and Cavenee, 2000; Maher et al., 2001). Human genetic studies indicate that two frequent molecular characteristics of low-grade astrocytomas are loss of p53 and elevated expression of platelet-derived growth factor (PDGF) and its receptor tyrosine kinase (RTK), PDGFR (Guha et al., 1995; Hermanson et al., 1992; Nister et al., 1988). These observations suggest that these pathways may participate in the initiation of astrocytoma. Individuals afflicted with neurofibromatosis type 1 (NF1) are predisposed to malignant astrocytoma in the brain with a greater than 5-fold increased incidence throughout their lives (Rasmussen et al., 2001). The NF1 tumor suppressor product neurofibromin is a functional Ras GTPase-activating protein (GAP) (Cichowski and Jacks, 2001; Zhu and Parada, 2001). Thus, loss of neurofibromin results in abnormal activation of Ras, a major mediator of RTK signaling.

Heterozygous mice carrying germline null mutations in both p53 and NF1 on the same chromosome (termed cisNF1/p53 mice) develop low- to intermediate-grade astrocytomas, with up to 75% penetrance depending on the genetic background (Reilly et al., 2000, 2004). We reasoned that the increased incidence of astrocytoma in NF1 patients might indicate a con-

SIGNIFICANCE

Recent studies indicate that brain tumors, including glioblastoma multiforme, contain a subpopulation of cancer cells that display stem cell characteristics, including self-renewal and multipotentiality, and are responsible for in vivo tumor growth. Whether these brain cancer stem cells are derived from neoplastic transformation of normal neural stem cells remains to be determined. Through analysis of mouse models with complete penetrance of malignant astrocytoma, we demonstrate that astrocytoma cells of all grades display stem cell characteristics and that early presymptomatic lesions reside within the subventricular zone (SVZ) of the lateral ventricle, one region of the CNS that contains neurogenic stem cells. These studies provide evidence that the SVZ cells may serve as a cell-of-origin for malignant astrocytoma.

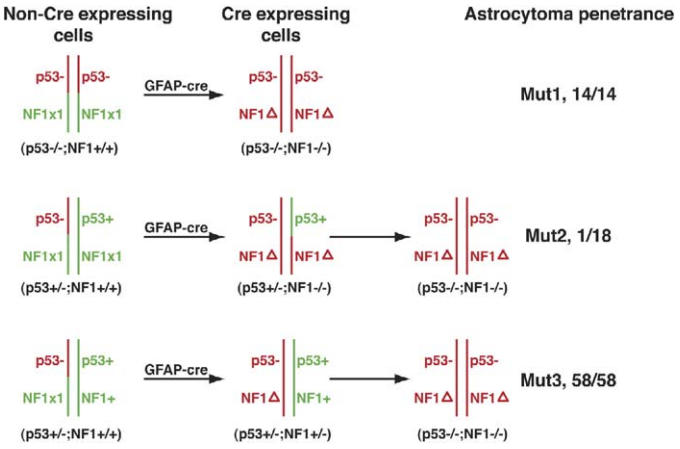

Figure 1. Schematic drawing of the genetic configurations of Mut1–3 mice

The green color is used to label the normal alleles, including the wild-type allele (+) and the floxed allele (x1); the red color is used to label the null alleles, including the recombined floxed allele (Δ) and the knockout allele (−). Genotypes for each cell type are indicated in parentheses.

vergence on the requirement for Ras signaling with sporadic astrocytomas via PDGFR activation. To refine our understanding of the target cell for p53 inactivation and Ras pathway activation in astrocytoma induction, we combined a germline p53 mutation (Jacks et al., 1994) with a neural-specific NF1 mutation (Zhu et al., 2001). The resultant mice develop malignant astrocytomas with 100% penetrance and provide evidence for the cell-of-origin in the subventricular zone (SVZ) of the adult brain and a requirement for p53 loss preceding or concomitant inactivation of NF1. The availability of an accurate mouse model for malignant astrocytoma initiation and progression will permit detailed investigation into the pathogenesis of, and novel therapeutic targets for, this incurable tumor.

Results

Mouse models for malignant astrocytoma

In mice, genetic p53 inactivation fails to induce astrocytomas. Instead, the predominant tumors are lymphomas or sarcomas (Donehower et al., 1992; Jacks et al., 1994). We generated three compound mutant mouse strains harboring mutations in the linked p53 and NF1 tumor suppressor genes (Mut1–3; Figure 1). Critical for this purpose was the genetic configuration of a floxed NF1 allele linked to a null p53 allele on mouse chromosome 11 (Figure 1) and the use of a Cre transgenic strain under the control of the human glial fibrillary acidic protein promoter (*hGFAP*-cre) (Malatesta et al., 2003; Zhu et al., submitted; Zhuo et al., 2001). Although GFAP is widely used as a mature glial-specific marker for normal and reactive astrocytes in the CNS (Ridet et al., 1997), more recent data indicate that the human GFAP promoter is also active in most embryonic radial glial cells that exhibit neural progenitor cell properties (Malatesta et al., 2000, 2003; Noctor et al., 2001; Zhuo et al., 2001). To determine the scope of *hGFAP*-cre transgene expression and activity, we crossed this mouse strain to the Rosa26-LacZ reporter strain (Soriano, 1999; Zhuo et al., 2001). Between embryonic day 10.5 (E10.5) and E12.5, Cre-mediated recombination, as revealed by LacZ expression, was evident in discrete neuroectodermal regions of the forebrain and hindbrain and in trigeminal ganglia (see Figures S1A–S1F in the Supplemental Data available with this article online). Consistent with previous reports (Malatesta et al., 2003; Zhuo et al., 2001), the consequence of early ventricular Cre expression in neural progenitor cells is that, at birth (P0.5), most cortical and hippocampal neurons express the LacZ reporter gene (Figures S1G–S1I). Thus, early onset of the human GFAP promoter in neural progenitor cells leads to Cre-mediated recombination in early CNS cells as well as their progeny, including adult neural stem/progenitor cells in the SVZ (Merkle et al., 2004; Tramontin et al., 2003) and neurons, astrocytes, and oligodendrocytes (Malatesta et al., 2003; Zhuo et al., 2001).

Mut1 (*p53$^{-/-}$;NF1$^{flox/flox}$;hGFAP-cre*+) mice lack p53 in the germline and NF1 function in CNS cells as a consequence of *hGFAP*-cre-mediated recombination in developing neural progenitor cells and mature astrocytes (Malatesta et al., 2003; Zhuo et al., 2001). As in Mut1, Mut2 (*p53$^{+/-}$;NF1$^{flox/flox}$;hGFAP-cre*+) mice lack NF1 in CNS cells but are heterozygous for p53. Mut3 (*cisp53$^{+/-}$;NF1$^{+/flox}$;hGFAP-cre*+) mice are compound heterozygotes for p53 and NF1 in CNS cells (Figure 1). All Mut1 (14/14; Figure 1) mice developed GFAP-positive astrocytomas ranging from infiltrative low-grade lesions (grade II; Figures 2A, 2D, and 2G); to higher-grade anaplastic astrocytomas (grade III; Figure 2B, 2E, and 2H); to GBMs (grade IV; Figures 2C, 2F, and 2I). As a consequence of germline p53 nullizygosity, these mice also developed lymphomas and sarcomas causing early mortality, likely explaining the reduced development of GBM (2/14) (Figures 2J and 2K). All Mut3 mice also developed CNS tumors (58/58; Figures 1 and 2K), and among the subset allowed to survive to end-stage of symptoms, approximately 70% had GBMs (14/21; Figure 2K) exhibiting every discernible feature of the human counterpart, including the presence of pseudopalisading tumor cells (Figures 3A and 3B), necrosis (Figures 3C and 3D), microvascular proliferation (Figures 3E and 3F), and secondary structures of Scherer (Figures 3G–3J). All symptomatic Mut3 mice had anaplastic astrocytomas or GBMs, while asymptomatic Mut3 mice had either low-grade tumors or no tumors (Figure 2K and Figure S2). Given the 100% incidence of tumor formation, these findings are most consistent with a model in which tumors arise as low-grade lesions that progress to higher-grade tumors with characteristics of GBM over time.

In contrast to the two genetic configurations described above, the Mut2 strain rarely developed CNS tumors (Figures 1 and 2K; see below). Immunohistochemical analysis showed that all Mut1 astrocytomas expressed Cre recombinase demonstrating NF1 deficiency (Figure 4A), while at the molecular level, astrocytomas from the Mut3 mice exhibited inactivation of both p53 and NF1 genes (Figures 4B and 4C). These data indicate that loss of p53 and NF1 is sufficient to initiate the development of a full spectrum of malignant astrocytomas in mice.

Molecular validation

Analysis of tumor tissues from human astrocytomas has demonstrated accrual of specific genetic lesions during progression from low-grade to high-grade astrocytoma (Holland, 2001; Maher et al., 2001; Zhu and Parada, 2002). These include

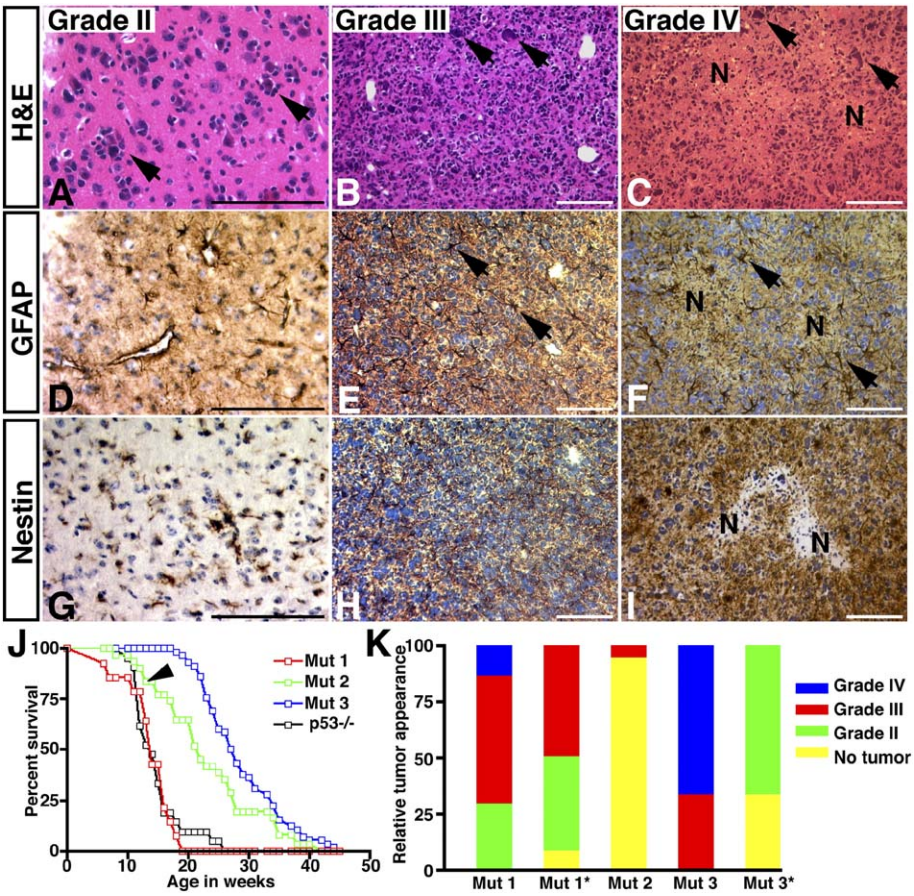

Figure 2. Mut1 mice develop a full spectrum of malignant astrocytoma

Sections from grade II, grade III, and grade IV astrocytomas of Mut1 brains were stained with hematoxylin and eosin (H&E) (**A–C**), an anti-GFAP antibody (**D–F**), and an anti-nestin antibody (**G–I**). Arrows in **A** point to abnormal tumor cells surrounding neurons (perineuronal satellitosis); arrows in **B** and **C** point to multinucleated giant cells; and arrows in **E** and **F** indicate reactive astrocytes. **J:** Survival curves of Mut1, Mut2, Mut3, and p53 null ($p53^{-/-}$) mice. The following numbers of mice were used for each group of mutant mice: Mut1, n = 14; Mut2, n = 21; Mut3, n = 58; $p53^{-/-}$, n = 20. The incidence of non-CNS tumors observed in Mut1–3 mice is as follows: Mut1, 9/14; Mut2, 4/21; and Mut3, 11/58. **K:** The graph shows astrocytoma frequency and grade observed in end-stage Mut1 mice (n = 14), asymptomatic Mut1* mice (n = 12; 6 to 10 weeks of age), end-stage Mut2 mice (n = 18), end-stage Mut3 mice (n = 21), and asymptomatic Mut3* mice (n = 3; 18 weeks of age). "N," necrosis. Scale bar, 50 μm.

deregulation of the Rb-mediated pathway and the PI-3K/AKT/PTEN pathway. We examined expression of two components of the Rb pathway, Cdk4 and cyclin D1, by immunohistochemistry (Figures 5A–5F; n = 5) and found that these high-grade tumors had intense nuclear expression of both Cdk4 (Figures 5A and 5D) and cyclin D1 proteins (Figures 5B and 5E), whereas normal CNS cells did not (Figure S3). To examine the status of the Ras pathway, activation of MAP kinase (MAPK) was assessed with phospho-specific antibodies. Consistent with loss of NF1 function, both low-grade (Figure 5G) and high-grade astrocytomas (Figures 5H and 5I) contain high levels of activated MAPK. In contrast, as in human tumors, activation of AKT was consistently found in higher-grade tumors (grade II, 0/5, Figure 5J; grade III, 1/5, Figures 5K and 5L; grade IV, 5/5, Figures 5M and 5P).

Two additional noteworthy molecular features of human astrocytoma are present in these mice. VEGF expression increases in the transition from lower-grade tumors to GBMs (Figures 5N and 5Q). In addition, although morphologically similar, high-grade tumors are molecularly heterogeneous, as evidenced by a regional downregulation of MAPK (Figure 5O) within tumors that retain activated AKT throughout (Figure 5R). These data are consistent with a causal role for loss of p53 and activation of Ras-MAPK in astrocytoma initiation followed by deregulation of the Rb-mediated pathway and the PI-3K/AKT/PTEN pathway in progression to GBM. These results provide experimental evidence that our tumor models resemble human malignant astrocytoma both at the pathologic and molecular levels.

Site of tumor origin and stem cell characteristics

The cell-of-origin of astrocytoma is a much investigated but unresolved question. While there has been increasing evidence that human astrocytoma cells resemble neural stem/progenitor cells (Hemmati et al., 2003; Ignatova et al., 2002; Singh et al., 2003), the existing evidence also supports the model that has evoked initial astrocyte dedifferentiation followed by malignant transformation (Bachoo et al., 2002). Consistent with the cancer stem cell model (Hemmati et al., 2003; Ignatova et al., 2002; Singh et al., 2003, 2004), astrocytomas of all grades (Mut1, n = 14; Mut3, n = 21) expressed a marker for neural stem cells, nestin (Figures 2G–2I; Figures S2E and S2F). In the adult brain, two areas have been identified as primary sources of multipotent neural stem cells (Gage, 2000). One is the SVZ of the lateral ventricle, and the other is the subgranular layer (SGL) in the dentate gyrus of the hippocampus (Alvarez-Buylla et al., 2001; Gage, 2000). Histological analysis of end-stage Mut1 and Mut3 brains showed that, as in human malignant astrocytoma, high-grade astrocytomas were dispersed throughout the brain (Figure S4A), and magnetic resonance imaging (MRI) provided radiographic images characteristic of human malignant astrocytoma (Figure S4B). To investigate whether tu-

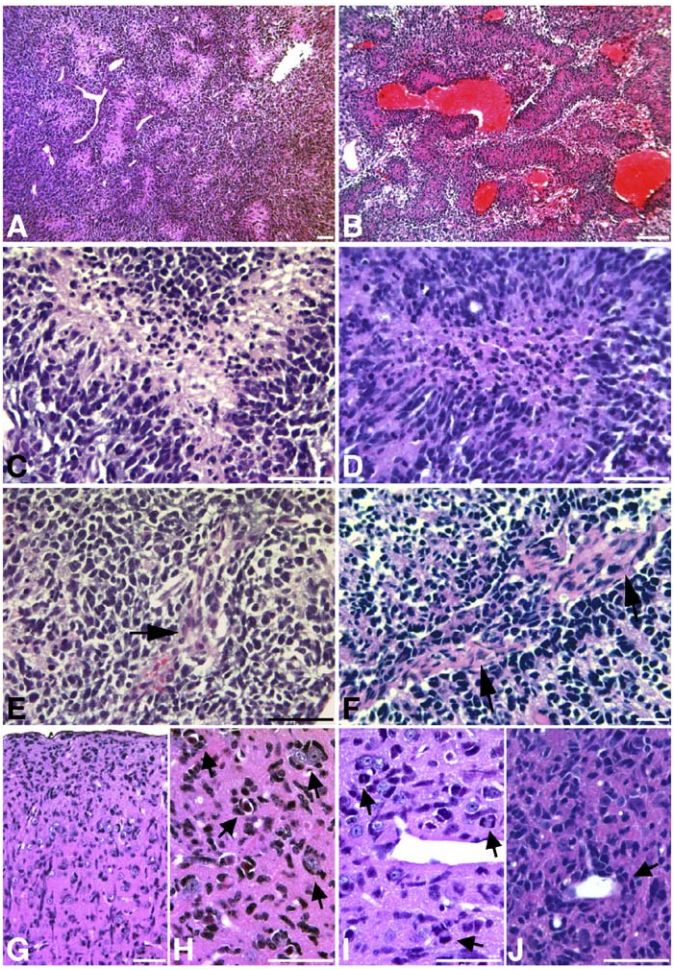

Figure 3. Histological hallmarks of GBM in Mut3 brains

Brain sections from the Mut3 brains were stained with H&E. GBMs from two independent Mut3 brains were characterized by the presence of multifocal pseudopalisading tumor cells (**A and B**), necrosis (**C and D**), microvascular proliferation (arrows in **E** and **F**), and secondary structures of Scherer, including accumulation of tumor cells in the subpial zone of the cerebral cortex (**G**), perineuronal satellitosis characterized by tumor cells surrounding neurons (arrows in **H**), and perivascular satellitosis characterized by tumor cells surrounding blood vessels (arrow in **J**). Arrows in **I** indicate mitotic figures amid the tumor cells. Scale bar, 50 μm.

mor origin was dispersed or confined to specific regions, we followed a cohort of seven asymptomatic 8-week-old Mut1 mice over a 3 week period (the last image was taken when mice were 11 weeks old). Detectable tumor growth occurred in five of these mice (Figure 6), always arising from the forebrain in association with the SVZ (Figures 6A–6C). However, tumor lesions that were barely detectable on the MRI scan (Figures 6D and 6E and Figures 6G and 6H) were of substantial size, precluding unambiguous identification of the specific site of tumor origin (Figures 6F and 6I), despite the fact that these tumors were also associated with the SVZ (Figure 6I, inset). We therefore next examined a cohort of 12 asymptomatic Mut1 mice at earlier time points between 6 and 10 weeks of age. Seven of the mutant mice showed one or two early lesions per brain. Among these seven mutant mice, five showed lesions

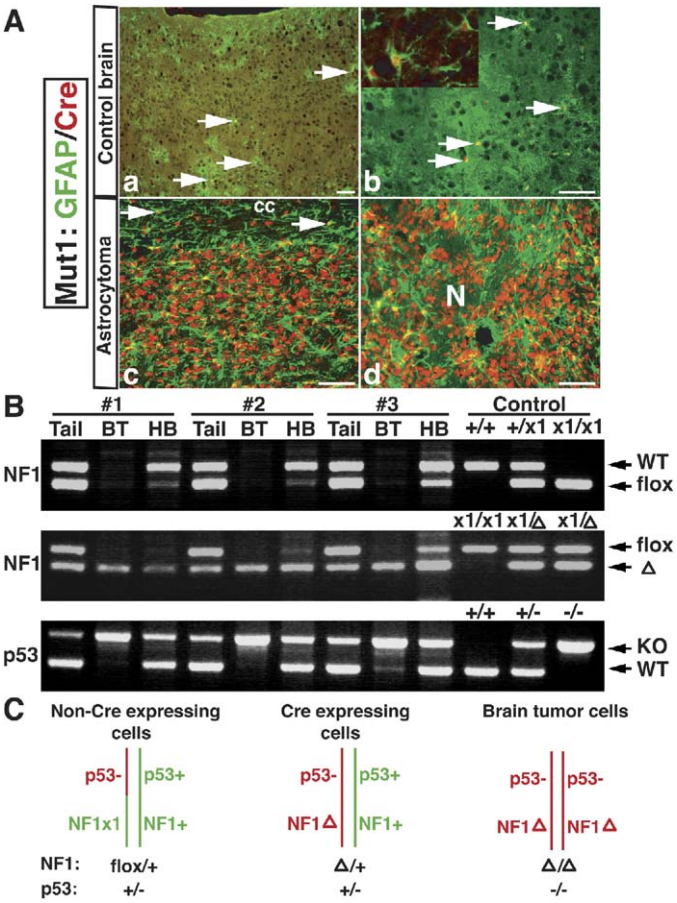

Figure 4. Inactivation of p53 and NF1 tumor suppressors in Mut1 and Mut3 astrocytomas

A: Sections from normal cerebral cortex (**Aa and Ab**), a grade III astrocytoma (**Ac**), and a GBM (**Ad**) of Mut1 brains were subjected to double-labeling immunofluorescence with anti-GFAP (green) and anti-Cre (red). In the normal adult brain, every Cre-positive astrocyte also expressed GFAP (arrows in **Aa** and **Ab**), indicating the specificity of the human GFAP promoter. The inset in **Ab** shows the morphology of the Cre-expressing GFAP-positive astrocytes. In astrocytomas and GBMs, every tumor cell expressed Cre recombinase indicative of NF1 deficiency in the Mut1 strain (**Ac and Ad**). Notably, a significant number of tumor cells downregulate GFAP expression in GBM (**Ad**). Arrows in **Ac** point to normal astrocytes adjacent to tumor tissues expressing both Cre and GFAP. CC, corpus callosum; N, necrosis. Scale bar, 50 μm.

B: Genomic DNAs isolated from tail tissues, brain tumors (BT), and hindbrain (HB) of three independent Mut3 mice (#1–#3) were subjected to PCR-based assays for genotyping the NF1 and p53 gene. Upper panel: a PCR assay that identifies the wild-type (WT) and the floxed (flox) NF1 allele showed that the tail tissues of the Mut3 mice contained one wild-type NF1 allele and one floxed NF1 allele; Cre-expressing tissues (e.g., hindbrain) retained the wild-type NF1 allele but lost most of the floxed allele as a result of Cre-mediated recombination; and brain tumors lost both the wild-type and the floxed NF1 alleles indicative of NF1 deficiency. Middle panel: a PCR assay identifying the floxed NF1 allele and recombined floxed allele (Δ) confirmed that the floxed NF1 allele in both hindbrain and brain tumors transformed into the recombined allele. Of note, a subpopulation of cells in tail tissues underwent recombination as well. Bottom panel: PCR assay identifying the wild-type and the null allele (KO) of the p53 gene showing that tail tissues and hindbrain of Mut3 mice are heterozygous for the p53 gene, while brain tumors lost the wild-type p53 allele.

C: Schematic drawing of allelic loss of NF1 and p53 in astrocytoma formation as described in **B**. The green color is used to label the normal alleles, including the wild-type allele (+) and the floxed allele (flox); the red color is used to label the null alleles, including the recombined floxed allele (Δ) and the knockout allele (−).

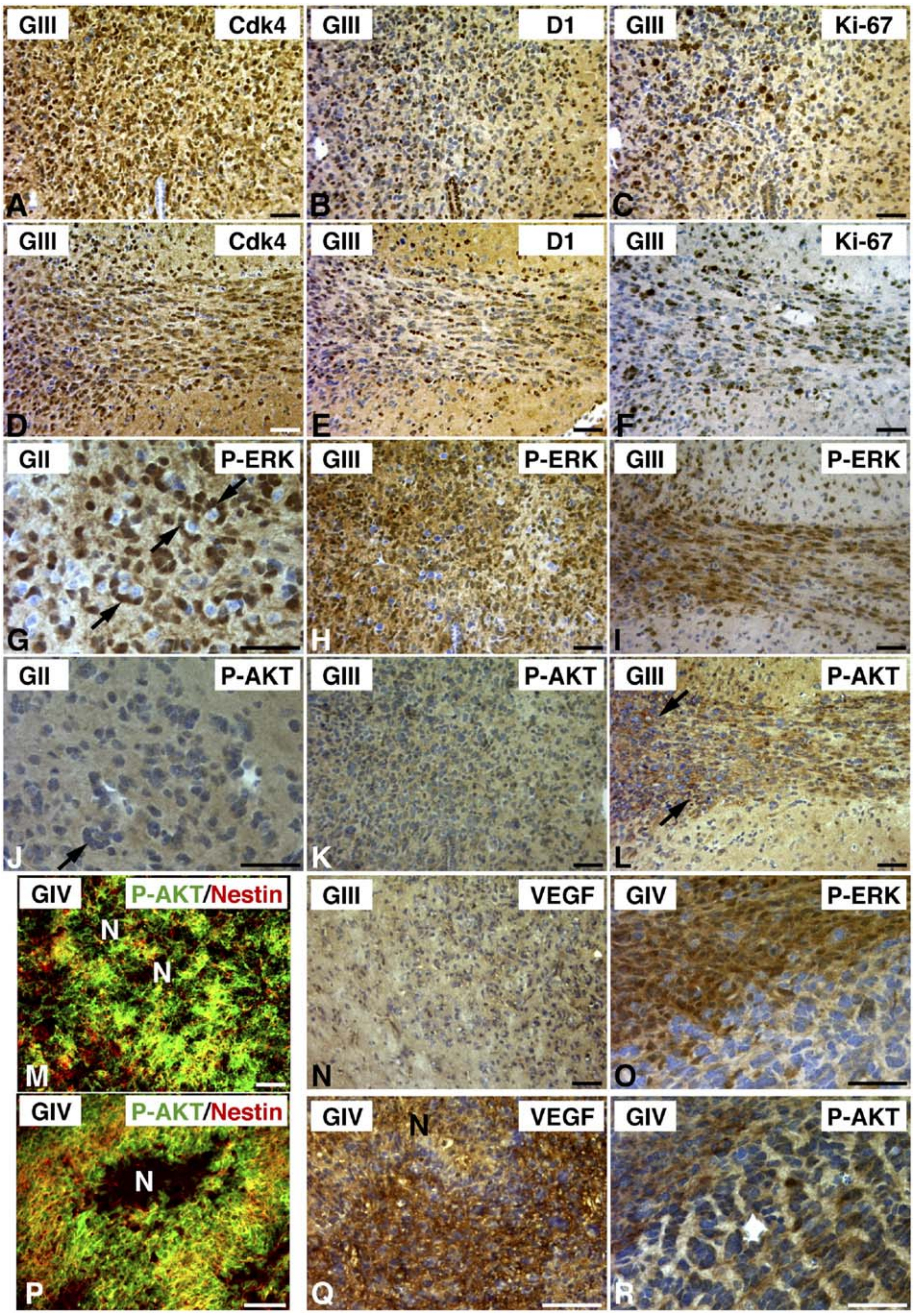

Figure 5. Molecular analysis of high-grade astrocytomas and GBMs

Adjacent sections from two grade III astrocytomas (GIII) were stained with anti-Cdk4 (**A and D**), anti-cyclin D1 (**B and E**), and a marker of proliferation, anti-Ki-67, to identify proliferating cells (**C and F**). In contrast to normal CNS cells that have little Cdk4 and cyclin D1 expression, high-grade tumors showed strong nuclear staining of Cdk4 and cyclin D1. Adjacent sections from a low-grade astrocytoma (GII) (**G and J**) and two grade III astrocytomas (GIII) (**H and K; I and L**) were stained with anti-phospho-erk (P-ERK) and anti-phospho-AKT (P-AKT), respectively. Arrows in **G** and **J** point to abnormal tumor cells surrounding neurons; arrows in **L** indicate P-AKT-positive tumor cells. Sections from a GBM were subjected to double-labeling immunofluorescence with anti-P-AKT (green) and anti-nestin (red) (**M and P**). "N," necrosis. Sections from a grade III astrocytoma (**N**) and a GBM (**Q**) were stained with anti-VEGF. Adjacent sections from a GBM were stained with anti-P-ERK (**O**) and anti-P-AKT (**R**). Scale bar, 50 μm.

directly associated with the SVZ (Figure 7), and the two others had a lesion in the hippocampus and the thalamus, respectively, but both contained abnormal cells within the SVZ (data not shown). Normally, adult neural stem cells are tightly organized in the SVZ (Figures 7A, 7D, and 7G). In contrast, early tumor cells were highly infiltrative. Early tumors showed infiltration into the white matter (Figures 7B, 7E, and 7H) and penetration into both the white matter and gray matter (Figures 7C, 7F, and 7I). Similar to normal neural stem cells (Figures 7D and 7G, arrows) (Doetsch et al., 1999), early tumor cells also expressed both nestin and GFAP (Figures 7E and 7F) and proliferated (Figures 7H and 7I). These early tumor cells were morphologically different from nestin/GFAP double-positive reactive astrocytes (Figure 7F, inset) that were identified within the high-grade tumors. The majority of Ki-67-positive cells expressed nestin (Figures 7H and 7I; 95% ± 2%; n = 96). These observations are most consistent with the interpretation that SVZ cells are most susceptible to p53/NF1-mediated astrocytoma formation and that incipient tumor cells share phenotypic characteristics with normal neural stem cells.

The infiltrative characteristics of malignant astrocytoma typically place the tumor cells within a milieu of nontumor endogenous neurons and glia. Among a total of 14 GBMs, we analyzed pure noninfiltrative tumor tissues in six GBMs. Two GBMs

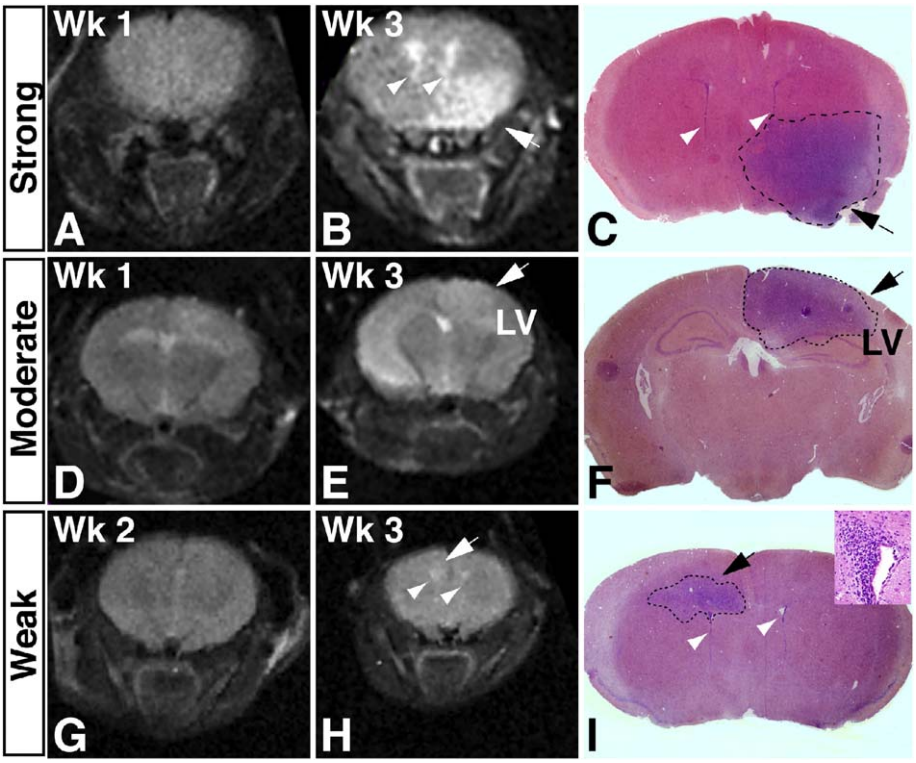

Figure 6. In vivo growth pattern of astrocytomas on the MRI scan

A cohort of asymptomatic Mut1 mice was subjected to MRI scan once a week over a 3 week period. Representative T2-weighted images of three Mut1 mice were scanned by MRI at week 1 (Wk1) (**A and D**), week 2 (**G**), and week 3 (Wk3) (**B, E, and H**). Following MRI, mice were subjected to histological analysis. Sections at similar levels of MRI images (**B, E, and H**) were stained with H&E (**C, F, and I**). No overt lesions were identified on the images scanned at early weeks (**A, D, and G**). Hyperintense T2 signals ranging from strong to moderate to weak were identified on the images at week 3 (**B, E, and H**). Arrows point to tumors, and arrowheads indicate the SVZ. The dashed lines in **C**, **F**, and **I** mark the tumor margin. The inset in **I** shows the abnormal tumor cells associated with the SVZ. LV, lateral ventricle.

contained tumor cells spreading on the surface of the brain (Figure 8A). We also obtained two GBM tumor samples that grew into the ventricular zone from the SVZ (Figure 8B). This rare direction of growth resulted in pure noninfiltrative tumor tissue. In addition, we analyzed two GBMs that formed multifocal pseudopalisading tumor cells (Figure 8C). The identity of these pure noninfiltrative tumor tissues was further confirmed by presence of a series of classic neuropathological characteristics including atypical nuclei. Immunohistochemical analysis revealed that these high-grade tumors contained cells from all neural lineages. Cells in the pure tumor tissues stained positive for the following: an astrocytic marker, GFAP (Figures 8D, 8E, and 8F); an oligodendrocytic marker, proteolipid protein (PLP), that is the most abundant myelin protein in the mammalian CNS (Figures 8G–8I) (Griffiths et al., 1998; Lu et al., 2000; Zhou et al., 2000); and neuronal markers including Tuj1 (Figures 8M–8O) and MAP2 (Figures 8P–8R). Of note, the expression of neuronal markers Tuj1 (Katsetos et al., 2001) and MAP2 (Singh et al., 2004) has previously been observed in human GBMs. Tumor cells expressed minimal or no myelin basic protein (MBP) (Figures 8J–8L), a marker for mature oligodendrocytes. The absence of MBP staining further confirmed that these tumor tissues contained minimal or no endogenous neurons or glia, as MBP is normally highly expressed in myelinating oligodendrocytes (Figure 8J, arrows). These data support the model that, in vivo, glioblastoma cells have the stem cell capacity to undergo multilineage differentiation (Singh et al., 2004).

Early p53 inactivation is critical for malignant astrocytoma formation

Genetic mutations in the p53 tumor suppressor gene are common hallmarks of progression in many solid tumors (Vogelstein et al., 2000; Vousden and Lu, 2002). In contrast, p53 mutations are among the earliest genetic lesions identified in malignant astrocytomas (Louis et al., 1993; Rasheed et al., 1994; van Meyel et al., 1994; von Deimling et al., 1992). The availability of the three Mut strains permitted us to examine whether the early timing of p53 loss affected tumorigenicity (Figure 1). Whereas the Mut1 strain harbors germline homozygous null p53 (resulting in p53 loss preceding NF1 loss); the Mut2 strain harbors a heterozygous germline p53 mutation such that, in the context of *hGFAP*-cre, NF1 loss is forced by recombination and precedes p53 loss of heterozygosity (LOH) in neural progenitors and derivatives. Finally, the Mut3 strain harbors a cisNF1flox/p53 mutant chromosome and a wild-type chromosome in CNS cells. LOH in this strain occurs by loss of the wild-type chromosome such that loss of both tumor suppressors occurs simultaneously (a process referred to as co-LOH) (Figure 1) (Cichowski et al., 1999; Reilly et al., 2000; Vogel et al., 1999). In contrast to the Mut1 and Mut3 strains, the majority of Mut2 mice analyzed (17/18) did not develop astrocytomas (Figures 1 and 2K). About 20% of Mut2 mice survived to the same age as tumorigenic Mut3 mice but did not develop astrocytomas (Figure 2J). Approximately 80% of Mut2 mice died at a significantly earlier age compared to Mut3 mice. Since the incidence of non-CNS tumors observed in Mut2 (4/21, 19%) and Mut3 (11/58, 19%) was almost identical, we cannot attribute the death of Mut2 mice to p53-associated tumors. We speculate that premature death of Mut2 mice may result from NF1 deficiency in developing CNS cells leading to abnormal CNS development (Zhu et al., submitted). To rule out the possibility that the premature death may preclude these Mut2 mice from developing astrocytomas, we studied three

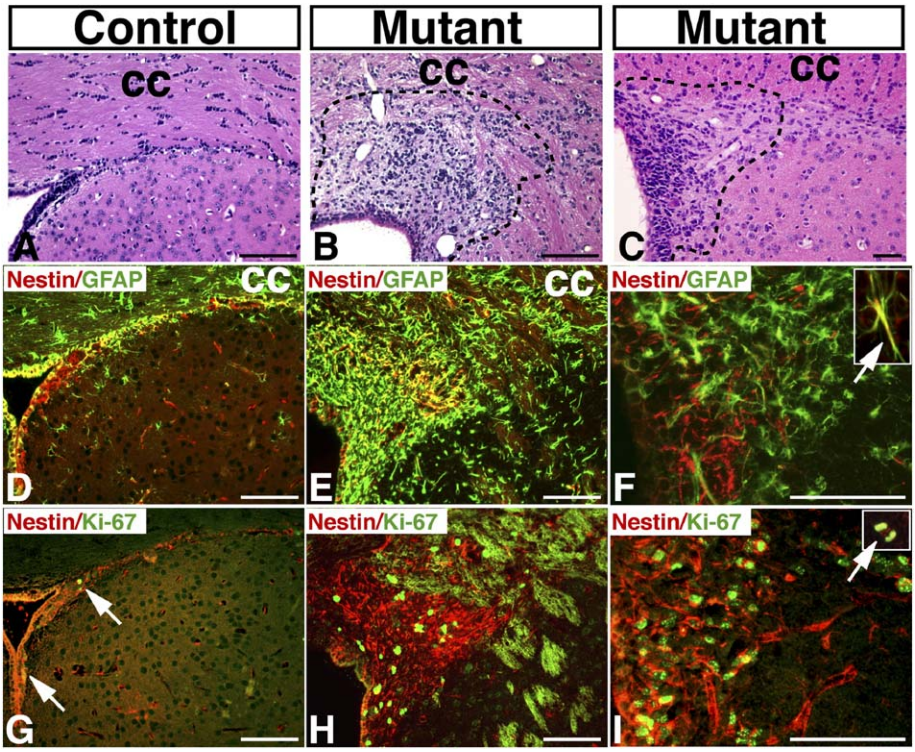

Figure 7. Astrocytomas are confined to the subventricular zone of the lateral ventricle

Adjacent sections from the SVZ of a control and two mutant brains were stained with H&E (**A–C**) and immunofluorescence by anti-nestin (red)/anti-GFAP (green) (**D–F**) and anti-nestin (red)/anti-Ki-67 (green) (**G–I**). Of note, mutant brains had nascent tumors associated with the SVZ. The tumor margin is marked by the dashed lines (**B and C**). The inset in **F** (arrow) shows a nestin/GFAP double-positive reactive astrocyte, and the inset in **I** (arrow) shows a nestin/Ki-67 double-positive (arrow) cell undergoing mitosis. CC, corpus callosum. Scale bar, 100 μm.

asymptomatic Mut3 mice at 18 weeks of age, a time point when over 85% of Mut2 mice were alive and tumor free (Figure 2J, arrowhead). Histological analysis revealed that two of three asymptomatic Mut3 mice already exhibited low-grade astrocytomas (Figure 2K and Figure S2). We therefore conclude that the target cells that give rise to malignant astrocytoma require p53 loss prior to or concomitant to NF1 loss (Ras activation). In the converse configuration, early loss of NF1 fails to provide selective advantage to the target cells for tumor initiation. These genetic data demonstrate that the early loss of p53 is essential for astrocytoma formation in these mouse models.

Discussion

Mouse models

Detailed molecular characterization of human astrocytoma has provided considerable insight into the many oncogenes, tumor suppressors, and signaling pathways that become altered in the processes of tumor initiation and progression (Holland, 2001; Maher et al., 2001; Zhu and Parada, 2002). The present study demonstrates that loss of p53 and activation of the Ras pathway via NF1 inactivation in CNS cells is sufficient to cause malignant astrocytoma formation with 100% penetrance. Although malignant astrocytomas of all grades were identified in both Mut1 and Mut3 models, exclusively low-grade lesions were found only in presymptomatic mice, except for two Mut1 mice with p53-associated lymphomas. As compared to well-differentiated low-grade astrocytomas in humans, tumors of similar grade in these models display greater degree of nuclear atypia. Along with these observations, rapid development of GBMs in both Mut1 (from 10 to 20 weeks) and Mut3 (from 20 to 45 weeks) mice suggests that these models may resemble primary GBM in humans. Consistently, a recent population-based study reported that p53 mutations were identified in about 28% of human primary GBMs, a subset of which (7.5%) also harbored amplification of epidermal growth factor receptor (EGFR) (Ohgaki et al., 2004).

The role of the NF1 tumor suppressor gene in malignant astrocytoma

Although benign astrocytoma in the optic pathway (optic pathway glioma) occurs in 15% to 20% of children with NF1, the NF1-associated risk of developing malignant astrocytomas has not been determined until recently. One study using U.S. death certificates from 1983 to 1997 reported that brain tumors occurred 5.5 times more frequently in NF1 patients than in the general population (Rasmussen et al., 2001). Particularly, the relative risk of brain tumors in NF1 patients older than 10 years was estimated to reach as much as 100 times greater than those without NF1. Many of the tumors from such patients were high-grade malignant astrocytomas (Gutmann et al., 2002). Furthermore, molecular analysis revealed that NF1-associated malignant astrocytomas harbored genetic alterations, including p53 mutations and p16INK4A/ARF deletions, that are commonly observed in sporadic counterparts (Gutmann et al., 2003). Together, these observations not only provide evidence that p53 inactivation can cooperate with NF1 loss in the development of human malignant astrocytomas, but also suggest that NF1-associated and sporadic malignant astrocytomas may share similar molecular mechanisms underlying tumor progression. Thus, our models may provide a useful tool to dissect the molecular basis of tumor progression

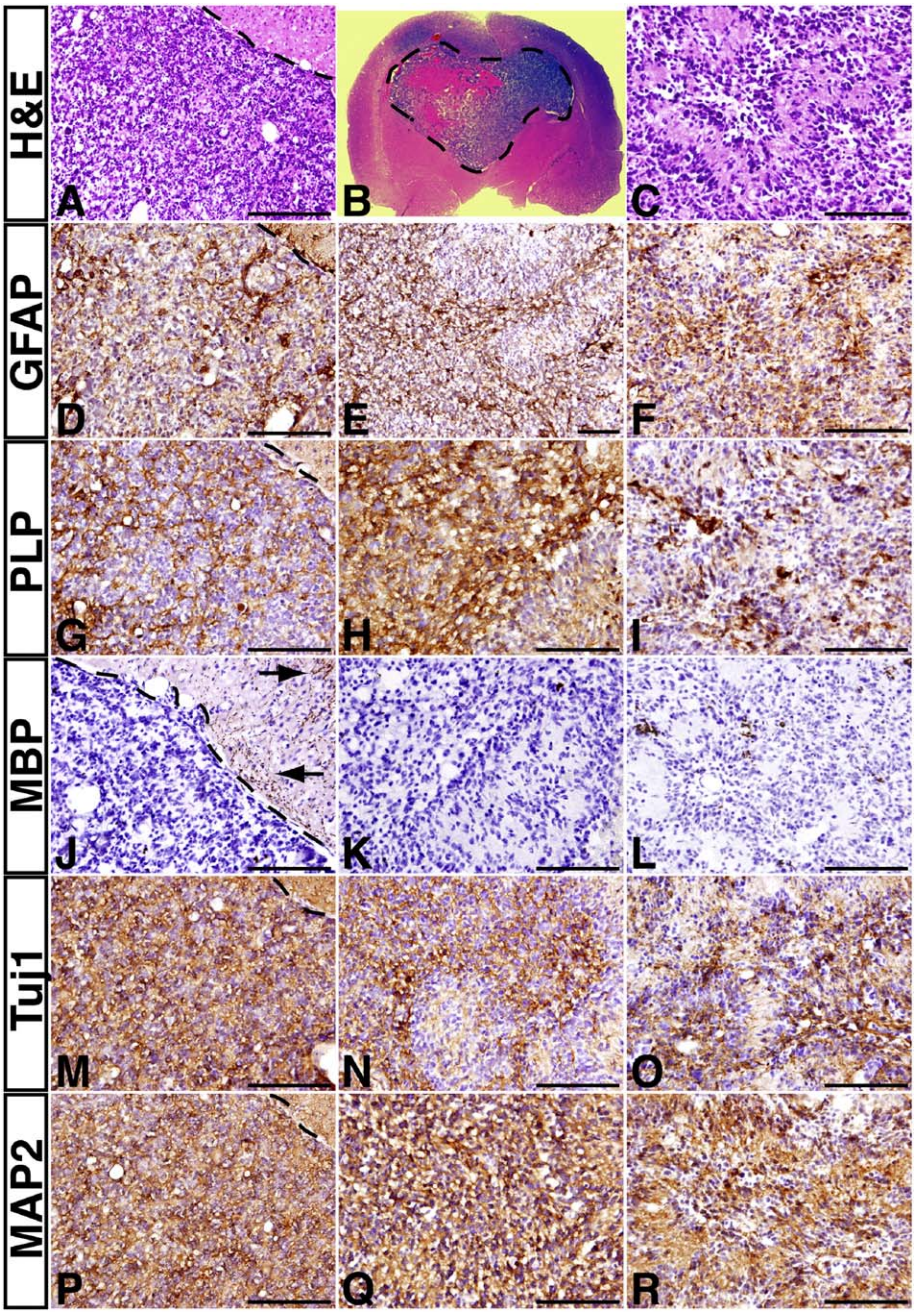

Figure 8. GBM cells have the stem cell capacity to undergo multilineage differentiation in vivo

A–C: Sections from three representative GBMs that contained pure noninfiltrative tumor tissues were stained with H&E. The dashed lines in **A** and **B** mark the border between the main tumor mass and surrounding brain tissues. Adjacent sections of **A**–**C** were stained with anti-GFAP (**D–F**), anti-PLP (**G–I**), anti-MBP (**J–L**), anti-Tuj1 (**M–O**), and MAP2 (**P–R**). Of note, in contrast to normal brain that contains extensive MBP staining (arrows in **J**), minimal or no staining was detected in these pure noninfiltrative tumor tissues (**J–L**). Scale bar, 100 μm.

underlying both NF1-associated and sporadic malignant astrocytomas.

Although one of the first characterized NF1 mutations in somatic cells was identified in a sporadic grade III malignant astrocytoma (Li et al., 1992), loss of NF1 mRNA or protein expression was not observed in sporadic astrocytomas in a subsequent study using a large number of human primary tumors and cell lines (Gutmann et al., 1996). Thus, it is generally believed that NF1 is not involved in sporadic malignant astrocytomas, which instead frequently activate Ras pathways via deregulated PDGFR or EGFR (Holland, 2001; Kleihues and Cavenee, 2000; Maher et al., 2001; Zhu and Parada, 2002). Particularly, p53 mutations and overexpression of PDGFR are often identified in the same tumors, suggesting a cooperative effect between these two pathways in the development of human malignant astrocytoma (Hermanson et al., 1996). Furthermore, the cooperative effect between p53 inactivation and PDGF overexpression has also been established in a mouse model using murine retroviral gene transfer (Hesselager et al., 2003). However, in a recent study using the replication-competent avian leukemia virus splice acceptor (RCAS)/tv-a system, targeted overexpression of a PDGF ligand (PDGF-B) into nestin- and GFAP-expressing cells in neonatal mouse brains induced oligodendrogliomas and oligoastrocytomas, respec-

tively (Dai et al., 2001). Furthermore, loss of p53 did not enhance the formation of these PDGF-induced tumors. Possible explanations for the discrepancy between experimentally induced tumors via p53/NF1 or PDGF alterations include potentially different cell-of-origin for these tumors, and differences in genetic backgrounds. The present studies demonstrate that the most likely location for the cell-of-origin for malignant astrocytoma in p53/NF1 mutant mice is in the SVZ of the adult brain (see below). The localization and origin of PDGF-induced tumors arising in neonatal brain cells remains unclear. The target cells in that model apparently have greater potential to undergo oligodendrocytic differentiation (Sauvageot and Stiles, 2002).

The site of tumor origin

Recent studies indicate that brain tumors, including GBM, contain a subpopulation of stem cell-like cells or cancer stem cells that display stem cell characteristics, including self-renewal and multipotentiality (Hemmati et al., 2003; Ignatova et al., 2002; Singh et al., 2003, 2004), and are responsible for in vivo tumor growth (Galli et al., 2004; Singh et al., 2004). Whether these brain cancer stem cells are derived from neoplastic transformation of normal neural stem cells remains to be determined. As compared to previously published mouse models for malignant astrocytoma (Ding et al., 2001; Hesselager et al., 2003; Holland et al., 1998, 2000; Reilly et al., 2000; Xiao et al., 2002), the complete penetrance of the tumor phenotype and rapid tumor development in Mut1 model allowed histological and noninvasive MRI analysis to investigate the site of tumor origin. The results indicate that, as in human GBM, mature tumors are dispersed throughout the CNS, and yet the earliest identifiable area of a tumor is confined to the SVZ. In the genetic setting of the Mut1 model, all GFAP-positive mature astrocytes or committed glial progenitor cells throughout the adult brain contain the same genetic mutations (inactivation of both p53 and NF1 tumor suppressors), as do the adult neural stem cells within the SVZ. Therefore, the observation that malignant astrocytomas specifically are located within the SVZ indicates that (1) there exists a specific cell type(s) in the SVZ that is more susceptible to p53/NF1-mediated astrocytoma formation as compared to those in other regions of the brain, or (2) the microenvironment in the SVZ provides a favorable niche for the growth of early tumor cells, which either arise within the SVZ or migrate there from the other regions of the brain. Based upon current knowledge, one fundamental difference between the SVZ and the other regions of the adult brain (except for the SGL of the hippocampal dentate gyrus) is the existence of specific GFAP-positive "astrocyte"-like cells, which possess the capacity of stem cells to undergo self-renewal and multilineage differentiation (Alvarez-Buylla et al., 2001; Gage, 2000; Temple and Alvarez-Buylla, 1999). It has been shown that these GFAP-positive neural stem cells are present in the SVZ of both human and rodent adult brains (Doetsch et al., 1999; Sanai et al., 2004). In light of these observations, our results suggest that the GFAP-positive neural stem cells in the SVZ of the adult brain are a likely candidate to be the cell-of-origin for malignant astrocytomas in our models.

A recent study demonstrated that neonatal astrocytes may serve as a cell-of-origin for malignant astrocytoma in response to deregulated EGFR signaling and INK4a/ARF deficiency. Thus, it is possible that different cell types in the CNS, including neural stem/progenitor cells, glial progenitor cells (e.g., NG2-positive glia), or even terminally differentiated astrocytes, may serve as a cell-of-origin for malignant astrocytoma. The combination of different glioma-associated genetic lesions may induce different CNS cell types to form malignant astrocytoma. Therefore, our models may mimic a subset of human malignant astrocytomas with p53 deficiency and activated Ras signaling, which may arise from the SVZ cells.

The timing of genetic mutations

We also provide genetic evidence that not only is inactivation of both p53 and NF1 sufficient for initiation of astrocytoma formation, but the timing of inactivation is critical. For astrocytoma induction, p53 inactivation must either precede or coincide with Ras activation via NF1 loss. This is consistent with the observation that mutations in the p53 gene are among the earliest genetic lesions identified in human malignant astrocytoma (Holland, 2001; Maher et al., 2001; Zhu and Parada, 2002). In many other solid tumors, including colon cancer and malignant peripheral sheath tumors (Kinzler and Vogelstein, 1996; Zhu and Parada, 2002), p53 inactivation occurs in later stages of tumor development when tumor cells already display invasive phenotypes. Thus, either early p53 inactivation provides a selective advantage for astrocytoma cells to acquire early onset invasive phenotype or activation of Ras signaling via NF1 loss leads to apoptosis or senescence of target cells, which can be attenuated by p53 inactivation.

Although activated Ras mutations have not been identified in human malignant astrocytoma, in mice, overexpression of an activated H-Ras transgene under the control of the hGFAP promoter leads to the development of malignant astrocytomas with high penetrance (Ding et al., 2001). This is in striking contrast to the observations that loss of NF1 alone (e.g., Mut2 mice in this study) is not sufficient to cause astrocytoma formation in the brain (Bajenaru et al., 2002). Apparently, oncogenic Ras signaling is not equivalent to NF1 inactivation. Given that human malignant astrocytoma typically arises during adulthood, it is unlikely that human patients contain a significant number of developing CNS cells with high levels of Ras signaling as the Ras transgenic model does. In contrast, mutant cells with p53/NF1 deficiency via co-LOH in the Mut3 model most likely arise during adulthood, as these mutant mice had normal development and did not develop tumors until 5 months of age. In this regard, the Mut3 mutant mice may provide a better model that mimics human malignant astrocytoma as an adult disease compared to the Ras transgenic mice.

Clinical implication

Our study cannot rule out alternative models for astrocytoma initiation such as cellular dedifferentiation and transformation (Bachoo et al., 2002; Galli et al., 2004; Singh et al., 2004). The expression of nestin and other lineage-specific markers in tumor cells can simply reflect deregulated gene expression. Whether these nestin-expressing cells within tumors represent the cancer stem cells remains to be determined. Nevertheless, identification of the SVZ as the site of tumor origin in our models may have implications on therapeutic strategies for preventing and treating a subset of human malignant astrocytomas (Recht et al., 2003). These observations challenge models of gliomagenesis, which assume tumor development from at large transformed glia or committed glial progenitors. As a con-

sequence, for a tumor that arises from the SVZ, current treatment focusing merely on local lesions will not be sufficient to eradicate tumor cells, as these cells may be eventually replenished from the cell pool within the SVZ. This may offer one explanation of why the current treatment for malignant astrocytoma ultimately fails.

Experimental procedures

Generation of Mut1–3 mutant mice

The mutant mice harboring the linked p53 null mutation and the floxed NF1 allele on the same chromosome (*cis* mice) were generated by crossing $NF1^{flox/+}$ mice to $p53^{+/-}$ mice to generate $p53^{+/-};NF1^{flox/+}$ *trans* mice that were then crossed to wild-type F1 129Svj/C57Bl6 mice (Jacks et al., 1994; Zhu et al., 2001). As for $NF1^{flox/+}$ mice and $p53^{+/-}$ mice, $p53^{+/-};NF1^{+/flox}$ *cis* mice were maintained on 129Svj/C57Bl6 hybrid background. The Mut3 strain was generated by crossing $p53^{+/-};NF1^{+/flox}$ *cis* mice to *hGFAP*-cre transgenic mice that were generated on the FVB background (Zhuo et al., 2001). The resultant Mut3 strain was crossed five generations onto 129Svj/C57Bl6 hybrid background. Mut1 and Mut2 strains were generated by crossing the Mut3 mice to $p53^{+/-};NF1^{flox/flox}$ *cis* mice. Therefore, Mut1–3 mice analyzed in this study were maintained on approximately 99% 129Svj/C57Bl6 (49.5%/49.5%) and 1% FVB hybrid background. Many Mut1–3 mice analyzed in this study were littermates. Mice with the floxed NF1 allele, p53 null allele, and Cre transgene were genotyped as described previously (Jacks et al., 1994; Zhu et al., 2001). All mice in this study were cared for according to the guidelines that were approved by the Animal Care and Use Committees of the University of Texas Southwestern Medical Center at Dallas and University of Michigan at Ann Arbor.

Histology and tumor analysis

Mice were aged until signs of distress appeared. Then, mice were perfused with 4% paraformaldehyde (PFA), and brains were dissected, followed by overnight postfixation in 4% PFA at 4°C. Brains were divided into three pieces along the rostral to caudal axis, and each piece was processed for either paraffin-embedded or cryostat sections. Serial sections were prepared at 5 μm for paraffin sections or 14 μm for cryostat sections. Every tenth slide was stained by H&E. Stained sections were examined under light microscope by Y.Z. and D.K.B. independently. Tumor grading was determined by Y.Z. and D.K.B. based upon the WHO grading system for malignant astrocytoma (Kleihues and Cavenee, 2000). Adjacent sections were subjected to immunohistochemistry (see below). For PCR analysis, tumor tissues were dissected in ice-cold PBS and digested with proteinase K as described (Zhu et al., 2002).

Immunohistochemistry

Paraffin sections were deparaffinized and rehydrated. Sections were subjected to immunohistochemistry as described previously (Zhu et al., 1998, 2001). The visualization of primary antibodies was performed with either a horseradish peroxidase system (Vectastain ABC kit, Vector) or immunofluorescence by using Cy3-conjugated anti-rabbit/mouse and Cy2-conjugated anti-mouse/rabbit secondary antibodies (Jackson lab) at 1:200 dilution. The dilutions of primary antibodies used in this study were as follows: GFAP (rabbit, 1:2000, DAKO), nestin (mouse, 1:200, Chemicon), Cre (mouse, 1:1000, BABCO), P-ERK (rabbit, 1:200, Cell Signaling), P-AKT (rabbit, 1:100, Cell Signaling), Cdk4 (rabbit, 1:200, Santa Cruz), cyclin D1 (mouse, 1:200, Zymed), Ki-67 (rabbit, 1:1000, Novocastra), VEGF (mouse, 1:50, Upstate Biotech), Olg2 (rabbit, 1:300, a gift of Dr. R. Lu), NeuN (mouse, 1:500, Chemicon), Tuj1 (mouse, 1:200, Covance), NF200 (rabbit, 1:200, Sigma). Sections were examined under either a light or a fluorescence microscope (Olympus). The colocalization of two antigens was further confirmed by confocal microscopy (Zeiss).

MRI analysis

Mutant mice were scanned when they exhibited signs of distress. In preparation for MRI, a mouse was given Avertin (0.4 ml, 20 mg/ml; i.p.) and maintained under general gaseous anesthesia (1 dm^3/min air and 0.8% isoflurane). A mouse tail vein was catheterized using a 27G butterfly (Abbott Laboratories, Abbott Park, IL) for contrast agent administration. MRI experiments were performed using a 4.7 T horizontal magnet equipped with a Varian Inova imaging system. The mouse was placed in a home-built eight-element birdcage coil (~2 cm in diameter). Fast scout images in a sagittal orientation indicated pertinent slices for high-resolution images. T1-weighted (TR = 250 ms; TE = 15 ms) and T2-weighted (TR = 1500 ms; TE = 80 ms) spin echo multislice (SEMS) axial images were acquired, and contrast-enhanced T1-weighted images were acquired immediately after i.v. bolus injection of Gd-DTPA-BMA (0.1 mmol/kg body weight; Omniscan). MRI parameters included a field of view (FOV) of 3–4 cm, a matrix size of 128 × 128, a slice thickness of 1 mm, and two acquisitions. Following MRI, the mouse was sacrificed, and a whole mouse brain was dissected and was subjected to histological analysis, as described above. Follow-up study examined asymptomatic mutant mice once a week over a 3 week period to detect tumor development.

Supplemental data

The Supplemental Data include four figures and can be found with this article online at http://www.cancercell.org/cgi/content/full/8/2/119/DC1/.

Acknowledgments

We thank A. DeShaw, P. Houston, and S. McKinnon for technical assistance; Dr. Q.R. Lu for an Olig2 antibody; members of the Parada lab for support; and Dr. S. Kernie for critically reading the manuscript. This work is supported by grants from the National Institute of Neurological Disorders and Stroke and the Department of Defense (L.F.P.). Y.Z. acknowledges support from the National Neurofibromatosis Foundation (Young Investigator Award), the Biological Sciences Scholars Program, and the Comprehensive Cancer Center (Munn Idea Award) of the University of Michigan Medical School, General Motors Cancer Research Scholar Program. D.Z. and R.P.M. thank Todd Soesbe for coil construction the National Cancer Institute for P20 Pre-ICMIC grant CA86354.

Received: April 15, 2005
Revised: June 13, 2005
Accepted: July 19, 2005
Published: August 15, 2005

References

Alvarez-Buylla, A., Garcia-Verdugo, J.M., and Tramontin, A.D. (2001). A unified hypothesis on the lineage of neural stem cells. Nat. Rev. Neurosci. *2*, 287–293.

Bachoo, R.M., Maher, E.A., Ligon, K.L., Sharpless, N.E., Chan, S.S., You, M.J., Tang, Y., DeFrances, J., Stover, E., Weissleder, R., et al. (2002). Epidermal growth factor receptor and Ink4a/Arf: convergent mechanisms governing terminal differentiation and transformation along the neural stem cell to astrocyte axis. Cancer Cell *1*, 269–277.

Bajenaru, M.L., Zhu, Y., Hedrick, N.M., Donahoe, J., Parada, L.F., and Gutmann, D.H. (2002). Astrocyte-specific inactivation of the neurofibromatosis 1 gene (NF1) is insufficient for astrocytoma formation. Mol. Cell. Biol. *22*, 5100–5113.

Cichowski, K., and Jacks, T. (2001). NF1 tumor suppressor gene function: narrowing the GAP. Cell *104*, 593–604.

Cichowski, K., Shih, T.S., Schmitt, E., Santiago, S., Reilly, K., McLaughlin, M.E., Bronson, R.T., and Jacks, T. (1999). Mouse models of tumor development in neurofibromatosis type 1. Science *286*, 2172–2176.

Dai, C., Celestino, J.C., Okada, Y., Louis, D.N., Fuller, G.N., and Holland, E.C. (2001). PDGF autocrine stimulation dedifferentiates cultured astrocytes and induces oligodendrogliomas and oligoastrocytomas from neural progenitors and astrocytes in vivo. Genes Dev. *15*, 1913–1925.

Ding, H., Roncari, L., Shannon, P., Wu, X., Lau, N., Karaskova, J., Gutmann, D.H., Squire, J.A., Nagy, A., and Guha, A. (2001). Astrocyte-specific expression of activated p21-ras results in malignant astrocytoma formation in a transgenic mouse model of human gliomas. Cancer Res. *61*, 3826–3836.

Doetsch, F., Caille, I., Lim, D.A., Garcia-Verdugo, J.M., and Alvarez-Buylla, A. (1999). Subventricular zone astrocytes are neural stem cells in the adult mammalian brain. Cell *97*, 703–716.

Donehower, L.A., Harvey, M., Slagle, B.L., McArthur, M.J., Montgomery, C.A., Jr., Butel, J.S., and Bradley, A. (1992). Mice deficient for p53 are developmentally normal but susceptible to spontaneous tumours. Nature *356*, 215–221.

Gage, F.H. (2000). Mammalian neural stem cells. Science *287*, 1433–1438.

Galli, R., Binda, E., Orfanelli, U., Cipelletti, B., Gritti, A., De Vitis, S., Fiocco, R., Foroni, C., Dimeco, F., and Vescovi, A. (2004). Isolation and characterization of tumorigenic, stem-like neural precursors from human glioblastoma. Cancer Res. *64*, 7011–7021.

Griffiths, I., Klugmann, M., Anderson, T., Thomson, C., Vouyiouklis, D., and Nave, K.A. (1998). Current concepts of PLP and its role in the nervous system. Microsc. Res. Tech. *41*, 344–358.

Guha, A., Dashner, K., Black, P.M., Wagner, J.A., and Stiles, C.D. (1995). Expression of PDGF and PDGF receptors in human astrocytoma operation specimens supports the existence of an autocrine loop. Int. J. Cancer *60*, 168–173.

Gutmann, D.H., Giordano, M.J., Mahadeo, D.K., Lau, N., Silbergeld, D., and Guha, A. (1996). Increased neurofibromatosis 1 gene expression in astrocytic tumors: positive regulation by p21-ras. Oncogene *12*, 2121–2127.

Gutmann, D.H., Rasmussen, S.A., Wolkenstein, P., MacCollin, M.M., Guha, A., Inskip, P.D., North, K.N., Poyhonen, M., Birch, P.H., and Friedman, J.M. (2002). Gliomas presenting after age 10 in individuals with neurofibromatosis type 1 (NF1). Neurology *59*, 759–761.

Gutmann, D.H., James, C.D., Poyhonen, M., Louis, D.N., Ferner, R., Guha, A., Hariharan, S., Viskochil, D., and Perry, A. (2003). Molecular analysis of astrocytomas presenting after age 10 in individuals with NF1. Neurology *61*, 1397–1400.

Hemmati, H.D., Nakano, I., Lazareff, J.A., Masterman-Smith, M., Geschwind, D.H., Bronner-Fraser, M., and Kornblum, H.I. (2003). Cancerous stem cells can arise from pediatric brain tumors. Proc. Natl. Acad. Sci. USA *100*, 15178–15183.

Hermanson, M., Funa, K., Hartman, M., Claesson-Welsh, L., Heldin, C.H., Westermark, B., and Nister, M. (1992). Platelet-derived growth factor and its receptors in human glioma tissue: expression of messenger RNA and protein suggests the presence of autocrine and paracrine loops. Cancer Res. *52*, 3213–3219.

Hermanson, M., Funa, K., Koopmann, J., Maintz, D., Waha, A., Westermark, B., Heldin, C.H., Wiestler, O.D., Louis, D.N., von Deimling, A., and Nister, M. (1996). Association of loss of heterozygosity on chromosome 17p with high platelet-derived growth factor α receptor expression in human malignant gliomas. Cancer Res. *56*, 164–171.

Hesselager, G., Uhrbom, L., Westermark, B., and Nister, M. (2003). Complementary effects of platelet-derived growth factor autocrine stimulation and p53 or Ink4a-Arf deletion in a mouse glioma model. Cancer Res. *63*, 4305–4309.

Holland, E.C. (2001). Gliomagenesis: genetic alterations and mouse models. Nat. Rev. Genet. *2*, 120–129.

Holland, E.C., Hively, W.P., DePinho, R.A., and Varmus, H.E. (1998). A constitutively active epidermal growth factor receptor cooperates with disruption of G1 cell-cycle arrest pathways to induce glioma-like lesions in mice. Genes Dev. *12*, 3675–3685.

Holland, E.C., Celestino, J., Dai, C., Schaefer, L., Sawaya, R.E., and Fuller, G.N. (2000). Combined activation of Ras and Akt in neural progenitors induces glioblastoma formation in mice. Nat. Genet. *25*, 55–57.

Ignatova, T.N., Kukekov, V.G., Laywell, E.D., Suslov, O.N., Vrionis, F.D., and Steindler, D.A. (2002). Human cortical glial tumors contain neural stem-like cells expressing astroglial and neuronal markers in vitro. Glia *39*, 193–206.

Jacks, T., Remington, L., Williams, B.O., Schmitt, E.M., Halachmi, S., Bronson, R.T., and Weinberg, R.A. (1994). Tumor spectrum analysis in p53-mutant mice. Curr. Biol. *4*, 1–7.

Katsetos, C.D., Del Valle, L., Geddes, J.F., Assimakopoulou, M., Legido, A., Boyd, J.C., Balin, B., Parikh, N.A., Maraziotis, T., de Chadarevian, J.P., et al. (2001). Aberrant localization of the neuronal class III β-tubulin in astrocytomas. Arch. Pathol. Lab. Med. *125*, 613–624.

Kinzler, K.W., and Vogelstein, B. (1996). Lessons from hereditary colorectal cancer. Cell *87*, 159–170.

Kleihues, P., and Cavenee, W.K. (2000). Pathology and Genetics of Tumors of the Nervous System (Lyon, France: IARC Press).

Li, Y., Bollag, G., Clark, R., Stevens, J., Conroy, L., Fults, D., Ward, K., Friedman, E., Samowitz, W., Robertson, M., et al. (1992). Somatic mutations in the neurofibromatosis 1 gene in human tumors. Cell *69*, 275–281.

Louis, D.N., von Deimling, A., Chung, R.Y., Rubio, M.P., Whaley, J.M., Eibl, R.H., Ohgaki, H., Wiestler, O.D., Thor, A.D., and Seizinger, B.R. (1993). Comparative study of p53 gene and protein alterations in human astrocytic tumors. J. Neuropathol. Exp. Neurol. *52*, 31–38.

Lu, Q.R., Yuk, D., Alberta, J.A., Zhu, Z., Pawlitzky, I., Chan, J., McMahon, A.P., Stiles, C.D., and Rowitch, D.H. (2000). Sonic hedgehog-regulated oligodendrocyte lineage genes encoding bHLH proteins in the mammalian central nervous system. Neuron *25*, 317–329.

Maher, E.A., Furnari, F.B., Bachoo, R.M., Rowitch, D.H., Louis, D.N., Cavenee, W.K., and DePinho, R.A. (2001). Malignant glioma: genetics and biology of a grave matter. Genes Dev. *15*, 1311–1333.

Malatesta, P., Hartfuss, E., and Gotz, M. (2000). Isolation of radial glial cells by fluorescent-activated cell sorting reveals a neuronal lineage. Development *127*, 5253–5263.

Malatesta, P., Hack, M.A., Hartfuss, E., Kettenmann, H., Klinkert, W., Kirchhoff, F., and Gotz, M. (2003). Neuronal or glial progeny: regional differences in radial glia fate. Neuron *37*, 751–764.

Merkle, F.T., Tramontin, A.D., Garcia-Verdugo, J.M., and Alvarez-Buylla, A. (2004). Radial glia give rise to adult neural stem cells in the subventricular zone. Proc. Natl. Acad. Sci. USA *101*, 17528–17532.

Nister, M., Libermann, T.A., Betsholtz, C., Pettersson, M., Claesson-Welsh, L., Heldin, C.H., Schlessinger, J., and Westermark, B. (1988). Expression of messenger RNAs for platelet-derived growth factor and transforming growth factor-α and their receptors in human malignant glioma cell lines. Cancer Res. *48*, 3910–3918.

Noctor, S.C., Flint, A.C., Weissman, T.A., Dammerman, R.S., and Kriegstein, A.R. (2001). Neurons derived from radial glial cells establish radial units in neocortex. Nature *409*, 714–720.

Ohgaki, H., Dessen, P., Jourde, B., Horstmann, S., Nishikawa, T., Di Patre, P.L., Burkhard, C., Schuler, D., Probst-Hensch, N.M., Maiorka, P.C., et al. (2004). Genetic pathways to glioblastoma: a population-based study. Cancer Res. *64*, 6892–6899.

Rasheed, B.K., McLendon, R.E., Herndon, J.E., Friedman, H.S., Friedman, A.H., Bigner, D.D., and Bigner, S.H. (1994). Alterations of the TP53 gene in human gliomas. Cancer Res. *54*, 1324–1330.

Rasmussen, S.A., Yang, Q., and Friedman, J.M. (2001). Mortality in neurofibromatosis 1: an analysis using U.S. death certificates. Am. J. Hum. Genet. *68*, 1110–1118.

Recht, L., Jang, T., Savarese, T., and Litofsky, N.S. (2003). Neural stem cells and neuro-oncology: quo vadis? J. Cell. Biochem. *88*, 11–19.

Reilly, K.M., Loisel, D.A., Bronson, R.T., McLaughlin, M.E., and Jacks, T. (2000). Nf1;Trp53 mutant mice develop glioblastoma with evidence of strain-specific effects. Nat. Genet. *26*, 109–113.

Reilly, K.M., Tuskan, R.G., Christy, E., Loisel, D.A., Ledger, J., Bronson, R.T., Smith, C.D., Tsang, S., Munroe, D.J., and Jacks, T. (2004). Susceptibility to astrocytoma in mice mutant for Nf1 and Trp53 is linked to chromosome 11 and subject to epigenetic effects. Proc. Natl. Acad. Sci. USA *101*, 13008–13013.

Ridet, J.L., Malhotra, S.K., Privat, A., and Gage, F.H. (1997). Reactive astrocytes: cellular and molecular cues to biological function. Trends Neurosci. *20*, 570–577.

Sanai, N., Tramontin, A.D., Quinones-Hinojosa, A., Barbaro, N.M., Gupta,

N., Kunwar, S., Lawton, M.T., McDermott, M.W., Parsa, A.T., Manuel-Garcia Verdugo, J., et al. (2004). Unique astrocyte ribbon in adult human brain contains neural stem cells but lacks chain migration. Nature *427*, 740–744.

Sauvageot, C.M., and Stiles, C.D. (2002). Molecular mechanisms controlling cortical gliogenesis. Curr. Opin. Neurobiol. *12*, 244–249.

Singh, S.K., Clarke, I.D., Terasaki, M., Bonn, V.E., Hawkins, C., Squire, J., and Dirks, P.B. (2003). Identification of a cancer stem cell in human brain tumors. Cancer Res. *63*, 5821–5828.

Singh, S.K., Hawkins, C., Clarke, I.D., Squire, J.A., Bayani, J., Hide, T., Henkelman, R.M., Cusimano, M.D., and Dirks, P.B. (2004). Identification of human brain tumour initiating cells. Nature *432*, 396–401.

Soriano, P. (1999). Generalized lacZ expression with the ROSA26 Cre reporter strain. Nat. Genet. *21*, 70–71.

Temple, S., and Alvarez-Buylla, A. (1999). Stem cells in the adult mammalian central nervous system. Curr. Opin. Neurobiol. *9*, 135–141.

Tramontin, A.D., Garcia-Verdugo, J.M., Lim, D.A., and Alvarez-Buylla, A. (2003). Postnatal development of radial glia and the ventricular zone (VZ): a continuum of the neural stem cell compartment. Cereb. Cortex *13*, 580–587.

van Meyel, D.J., Ramsay, D.A., Casson, A.G., Keeney, M., Chambers, A.F., and Cairncross, J.G. (1994). p53 mutation, expression, and DNA ploidy in evolving gliomas: evidence for two pathways of progression. J. Natl. Cancer Inst. *86*, 1011–1017.

Vogel, K.S., Klesse, L.J., Velasco-Miguel, S., Meyers, K., Rushing, E.J., and Parada, L.F. (1999). Mouse tumor model for neurofibromatosis type 1. Science *286*, 2176–2179.

Vogelstein, B., Lane, D., and Levine, A.J. (2000). Surfing the p53 network. Nature *408*, 307–310.

von Deimling, A., Eibl, R.H., Ohgaki, H., Louis, D.N., von Ammon, K., Petersen, I., Kleihues, P., Chung, R.Y., Wiestler, O.D., and Seizinger, B.R. (1992). p53 mutations are associated with 17p allelic loss in grade II and grade III astrocytoma. Cancer Res. *52*, 2987–2990.

Vousden, K.H., and Lu, X. (2002). Live or let die: the cell's response to p53. Nat. Rev. Cancer *2*, 594–604.

Xiao, A., Wu, H., Pandolfi, P.P., Louis, D.N., and Van Dyke, T. (2002). Astrocyte inactivation of the pRb pathway predisposes mice to malignant astrocytoma development that is accelerated by PTEN mutation. Cancer Cell *1*, 157–168.

Zhou, Q., Wang, S., and Anderson, D.J. (2000). Identification of a novel family of oligodendrocyte lineage-specific basic helix-loop-helix transcription factors. Neuron *25*, 331–343.

Zhu, Y., and Parada, L.F. (2001). Neurofibromin, a tumor suppressor in the nervous system. Exp. Cell Res. *264*, 19–28.

Zhu, Y., and Parada, L.F. (2002). The molecular and genetic basis of neurological tumours. Nat. Rev. Cancer *2*, 616–626.

Zhu, Y., Richardson, J.A., Parada, L.F., and Graff, J.M. (1998). Smad3 mutant mice develop metastatic colorectal cancer. Cell *94*, 703–714.

Zhu, Y., Romero, M.I., Ghosh, P., Ye, Z., Charnay, P., Rushing, E.J., Marth, J.D., and Parada, L.F. (2001). Ablation of NF1 function in neurons induces abnormal development of cerebral cortex and reactive gliosis in the brain. Genes Dev. *15*, 859–876.

Zhu, Y., Ghosh, P., Charnay, P., Burns, D.K., and Parada, L.F. (2002). Neurofibromas in NF1: Schwann cell origin and role of tumor environment. Science *296*, 920–922.

Zhuo, L., Theis, M., Alvarez-Maya, I., Brenner, M., Willecke, K., and Messing, A. (2001). hGFAP-cre transgenic mice for manipulation of glial and neuronal function in vivo. Genesis *31*, 85–94.

Inactivation of NF1 in CNS causes increased glial progenitor proliferation and optic glioma formation

Yuan Zhu[1,4,*], Takayuki Harada[1], Li Liu[4], Mark E. Lush[1], Frantz Guignard[1], Chikako Harada[1], Dennis K. Burns[2], M. Livia Bajenaru[3], David H. Gutmann[3] and Luis F. Parada[1]

[1]Center for Developmental Biology and Kent Waldrep Foundation Center for Basic Research on Nerve Growth and Regeneration, University of Texas Southwestern Medical Center, Dallas, TX 75390-9133, USA
[2]Department of Pathology, University of Texas Southwestern Medical Center, Dallas, TX 75390-9133, USA
[3]Department of Neurology, Washington University School of Medicine, St Louis, MO 63110, USA
[4]Division of Molecular Medicine and Genetics, Departments of Internal Medicine and Cell and Developmental Biology, University of Michigan Medical School, Ann Arbor, MI 48109, USA
*Author for correspondence (e-mail: yuanzhu@umich.edu)

Accepted 12 October 2005

Development 132, 5577-5588
Published by The Company of Biologists 2005
doi:10.1242/dev.02162

Summary

The gene responsible for neurofibromatosis type 1 (NF1) encodes a tumor suppressor that functions as a negative regulator of the Ras proto-oncogene. Individuals with germline mutations in NF1 are predisposed to the development of benign and malignant tumors of the peripheral and central nervous system (CNS). Children with this disease suffer a high incidence of optic gliomas, a benign but potentially debilitating tumor of the optic nerve; and an increased incidence of malignant astrocytoma, reactive astrogliosis and intellectual deficits. In the present study, we have sought insight into the molecular and cellular basis of NF1-associated CNS pathologies. We show that mice genetically engineered to lack NF1 in CNS exhibit a variety of defects in glial cells. Primary among these is a developmental defect resulting in global reactive astrogliosis in the adult brain and increased proliferation of glial progenitor cells leading to enlarged optic nerves. As a consequence, all of the mutant optic nerves develop hyperplastic lesions, some of which progress to optic pathway gliomas. These data point to hyperproliferative glial progenitors as the source of the optic tumors and provide a genetic model for NF1-associated astrogliosis and optic glioma.

Key words: Neurofibromatosis type 1, Optic glioma, Glial progenitor, Astrocyte, Tumor suppressor gene, Mouse

Introduction

Astrocytic tumors or astrocytomas account for a vast majority of primary central nervous system (CNS) tumors (Holland, 2001; Kleihues and Cavenee, 2000; Maher et al., 2001; Zhu and Parada, 2002). According to the World Health Organization (WHO) grading system, astrocytomas can be classified into four histopathological grades. Grade II-IV astrocytomas are malignant neoplasms that diffusely infiltrate surrounding brain structures. Such astrocytic neoplasms may occur at any age, but are more common in adults than in children. By contrast, pilocytic astrocytomas, classified as Grade I neoplasms in the WHO grading scheme, are generally benign and tend to be better circumscribed (Holland, 2001; Kleihues and Cavenee, 2000; Maher et al., 2001; Zhu and Parada, 2002). Although pilocytic astrocytoma is the most common glioma in children, the molecular and genetic basis is largely unknown.

Individuals afflicted with a familial cancer syndrome, neurofibromatosis type 1 (NF1), are predisposed to the development of astrocytomas (Listernick et al., 1999). Approximately 15 to 20% of children with NF1 develop pilocytic astrocytomas predominantly within the optic pathway, hypothalamus and, occasionally, in the other brain areas (Listernick et al., 1999; Listernick et al., 1997). Like their sporadic counterparts, most NF1-associated pilocytic astrocytomas are benign and can remain static for many years. However, despite histological benign features, a significant number of these tumors will endure and cause vision impairment and other neurological symptoms (Listernick et al., 1999). The *NF1* gene encodes the protein product, neurofibromin, which shares homology with members of the family of Ras GTPase activating proteins (GAPs) (Ballester et al., 1990; Viskochil, 1999; Xu et al., 1990). Like GAPs, neurofibromin attenuates the Ras-mediated signaling pathway by accelerating the conversion of activated Ras-GTP to inactive Ras-GDP. Consistent with the role of the *NF1* gene as a tumor suppressor gene, loss of heterozygosity at the NF1 locus and loss of neurofibromin expression have been observed in a variety of NF1-associated tumors, including astrocytomas (Gutmann et al., 2000; Kluwe et al., 2001). In one case report, loss of neurofibromin expression in an NF1-associated pilocytic astrocytoma correlated with the elevated Ras-GTP and activation of Ras downstream effectors such as mitogen-activated protein kinase (MAPK) and phosphatidylinositol 3-kinase (PI-3K) (Lau et al., 2000).

Functional activation of the Ras pathway through upregulation of receptor tyrosine kinases such as PDGF and

EGF receptors has been well documented in diffusely infiltrative malignant astrocytomas (Holland, 2001; Kleihues and Cavenee, 2000; Maher et al., 2001; Zhu and Parada, 2002). However, similar molecular alterations have not been observed in pilocytic astrocytomas (Gutmann et al., 2002; Li et al., 2001). It has been suggested that the *NF1* gene might be involved in regulating the proliferation of mature astrocytes (Bajenaru et al., 2002). Although neurofibromin is expressed below detection levels in normal astrocytes (Daston and Ratner, 1992; Daston et al., 1992; Huynh et al., 1994), it was reported that loss of *NF1* confers a growth advantage to neonatal astrocytes in vitro (Bajenaru et al., 2002). Conventional NF1 knockout mice ($Nf1^{-/-}$) are embryonic lethal (Brannan et al., 1994; Jacks et al., 1994) and although heterozygous mice ($Nf1^{+/-}$) are cancer prone, they do not develop astrocytomas (Jacks et al., 1994). Conditional mutant mice lacking NF1 specifically in neurons also fail to develop astrocytomas although increased number of non-neoplastic GFAP (glial fibrillary acidic protein) expressing reactive astrocytes was observed (Zhu et al., 2001). These results suggest that NF1 can regulate the growth of astrocytes both intrinsically and also indirectly through neurons.

During embryonic development, multipotent neural stem/progenitor cells progressively lose developmental potential and become lineage-restricted neuronal progenitor cells or glial progenitor cells (Gage, 2000; Temple, 2001). Gliogenesis occurs after neurogenesis and extends into postnatal stages. In the setting of NF1, the greatest risk for development of optic glioma is the first 6 years of life (Listernick et al., 1999). This observation suggests that the *NF1* gene might play a role in regulating the proliferation of progenitor cells. Furthermore, recent reports demonstrate that pilocytic astrocytomas express molecular markers reminiscent of glial progenitor cells (Gutmann et al., 2002; Li et al., 2001).

To determine the role of NF1 in the development of neural cell types and understand cellular and molecular basis of NF1-associated astrocytoma formation, we used a bacteriophage Cre/loxP system to target a *Nf1* mutation (Zhu et al., 2001) into multipotent neural stem/progenitor cells and their derivatives, including glia and neurons (Zhuo et al., 2001). We show that loss of NF1 promotes the proliferation of glial progenitor cells resulting in increased numbers of GFAP-expressing astrocytes in both developing and adult brains. Furthermore, NF1 also plays an indispensable role in the maintenance of the differentiation state of mature astrocytes. Finally, we describe a new mouse model for NF1-associated optic pathway glioma.

Materials and methods

Control and mutant mice

The control mice used in this study are the pool of phenotypically indistinguishable mice with genotypes $Nf1^{flox/flox}$, $Nf1^{flox/+}$ and $Nf1^{flox/+}$;*hGFAP*-cre+. The mutant mice designated $Nf1^{hGFAP}KO$ include both $Nf1^{flox/-}$;*hGFAP*-cre+ and $Nf1^{flox/flox}$;*hGFAP*-cre+, which have similar phenotypes. The genotyping procedures for the Nf1flox allele, *Nf1*-null allele and Cre transgene have been described previously (Zhu et al., 2001).

Size and weight analysis of mice

$Nf1^{hGFAP}KO$ and control littermates at the age of P0.5, P8 and 2 months were used to determine mass (g). Age-matched mutant and control mice were perfused with 4% paraformaldehyde (PFA). Brains were dissected and post-fixed in 4% PFA overnight, and separated into forebrain and hindbrain for analysis. Statistical analysis was carried out using Student's *t*-test. $P<0.05$ was considered to be significant.

lacZ staining and double immunofluorescence

E10.5, E12.5 embryos or cryostat sections from postnatal or adult tissues were prepared and subjected to X-gal analysis as described previously (Zhu et al., 1998). Adjacent sections were subjected to double immunofluorescence with anti-*lacZ* (rabbit, 1:200, 5′ and 3′) and anti-NeuN (mouse, 1:200, Chemicon) or anti-*lacZ* and anti-GFAP (mouse, 1:100, Pharmingen).

BrdU assay

P8 mutant and control littermates were pulsed with BrdU for 2 hours, and adult mice (4-6 months) were pulsed with BrdU five times a day at 2-hour intervals. The dose of BrdU was 50 μg/g (gram, body mass). Mice were perfused with 4% PFA 2 hours after the last pulse. Brains were dissected and processed for either paraffin-embedded or cryostat sections. BrdU immunohistochemistry was performed as described previously (Zhu et al., 1998). The dilution of BrdU antibody was 1:50 (Becton Dickinson). The number of BrdU-positive cells was counted in one out of each ten serially prepared sections. Statistical analysis was carried out using Student's *t*-test. $P<0.05$ was considered to be significant.

Immunohistochemistry

After post-fixed in 4% PFA overnight, tissues were prepared for free-floating vibratome sections at 50 μm, cryostat sections at 14 μm or paraffin wax-embedded sections at 5 μm. Paraffin sections were deparaffinized and rehydrated. Sections were subjected to immunohistochemical analysis as described previously (Zhu et al., 2001). The visualization of primary antibodies was performed with either a horseradish peroxidase system (Vectastain ABC kit, Vector) or immunofluorescence by using Cy3-conjugated anti-rabbit/mouse and Cy2-conjugated anti-mouse/rabbit secondary antibodies at 1:200 dilution (Jackson Laboratories). The dilution of primary antibodies used in this study were: GFAP (rabbit, 1:2000, DAKO), nestin (mouse, 1:200, Chemicon), BLBP (rabbit, 1:1000, a gift from N. Heintz), PAX2 (rabbit, 1:1000, a gift from G. Dressler), P-erk (rabbit, 1:200, Cell Signaling), Cre (mouse, 1:1000, BABCO), Ki-67 (Rabbit, 1:1000, Novocastra Labs). Sections were examined under either light or fluorescence microscope (Olympus). The co-localization of two antigens was further confirmed by confocal microscopy (Zeiss).

Results

Generation of neural-specific *Nf1* knockout mice

Previous studies have shown that the Cre transgenic strain under the control of human GFAP promoter (*hGFAP*-cre) expresses Cre recombinase not only in mature astrocytes, but also in multipotent radial glial cells that exhibit neural stem/progenitor cell properties and can give rise to both glia and neurons during development (Malatesta et al., 2003; Malatesta et al., 2000; Noctor et al., 2001; Zhu et al., 2005; Zhuo et al., 2001). To target the *Nf1* mutation into neural stem/progenitor cells during development, we crossed the *hGFAP*-cre transgene to $Nf1^{flox/-}$ and $Nf1^{flox/flox}$ mice (Zhu et al., 2001). Resultant double transgenic $Nf1^{flox/-}$;*hGFAP-cre*+ and $Nf1^{flox/flox}$;*hGFAP-cre*+ mice were phenotypically indistinguishable, termed $Nf1^{hGFAP}KO$. The $Nf1^{hGFAP}KO$ mice were born in appropriate Mendelian ratios although they exhibited growth retardation as early as P8 (see Fig. S1A in the supplementary material). In maturity, the weight differential between control littermates and $Nf1^{hGFAP}KO$ mice

approached 50% (see Fig. S1A in the supplementary material). The mutant pups exhibited a series of abnormal neurological behaviors (data not shown) and failed to thrive. As shown in Fig. S1B (see supplementary material), the half-life for mutant mice was ~26 weeks and all mutants perished by 47 weeks of age.

In contrast to the diminished body weight, the *Nf1^{hGFAP}KO* mutant brain mass was slightly larger than that of control brains, although this did not reach statistical significance (0.54±0.01 versus 0.52±0.02, P=0.43), except in the forebrain where the size of mutant tissues was significantly larger than that of controls (see Fig. S1C in the supplementary material, 1.08±0.02 versus 0.94±0.02, P=0.0003).

Increased GFAP-positive astrocytes in adult *Nf1^{hGFAP}KO* mutant brains

To determine whether *Nf1^{hGFAP}KO* mutant brains have developmental or cellular defects, we performed histological analysis. Although the mutant cerebellum has conspicuous developmental defects that may contribute to the neurological abnormalities observed in mutant mice (see Fig. S1C in the supplementary material, data not shown), all other anatomical regions of *Nf1^{hGFAP}KO* brains appear relatively normal, including neuronal lamination in the cerebral cortex and hippocampus (see Fig. S2 in the supplementary material and data not shown). Immunohistochemical analysis with an antibody against GFAP revealed that *Nf1^{hGFAP}KO* mutant brains exhibited astrogliosis (see Fig. S2 in the supplementary material), a CNS pathology that is characterized by increased expression of GFAP coupled with hypertrophy of astrocytes, including enlarged somata and thickened processes (Ridet et al., 1997). Staining of other astrocytic markers, including S100β, further confirmed that *Nf1^{hGFAP}KO* mutant brains had increased numbers of astrocytes (data not shown). In contrast to our previous observation that neuronal loss of NF1 leads to astrogliosis restricted to the gray matter (Zhu et al., 2001), *Nf1^{hGFAP}KO* brains have extensive astrogliosis throughout both the gray and white matter, including the corpus callosum and anterior commissure (see Fig. S2I,J,M,N in the supplementary material). We next performed BrdU analysis to label proliferating cells and TUNEL analysis to detect apoptotic cells. Both analyses failed to detect significant differences between adult mutant and control brains (Fig. 1A and data not shown). Thus, the excess number of GFAP-positive astrocytes present in adult *Nf1^{hGFAP}KO* mutant gray and white matter probably results from early events that affect proliferation, apoptosis, differentiation or any combination of these factors.

Increased proliferating glial progenitor cells during development

To examine the status of glial progenitors in *Nf1^{hGFAP}KO* mutant brains, we selected postnatal day 8 (P8) for analysis. At P8, neurogenesis is largely complete but glial development and proliferation is still active (Bayer and Altman, 1991; Jacobson, 1991; Qian et al., 2000). P8 also coincides with the first detectable morphological differences between mutant and wild-type pups (see Fig. S1A in the supplementary material). The results of BrdU incorporation and immunohistochemical studies indicated that during development, mutant brains contain excess proliferating cells (Fig. 1B,C) that express a neural stem/progenitor cell marker, nestin (Fig. 2A,B), and an early glial progenitor cell marker, brain lipid binding protein

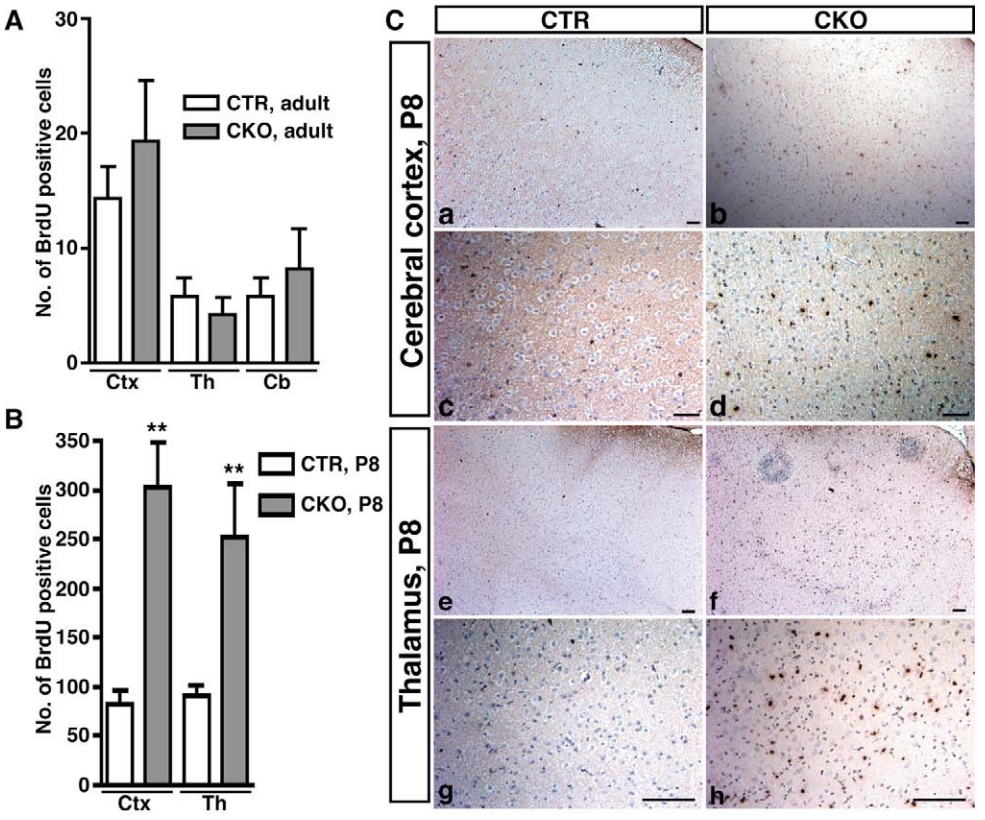

Fig. 1. Comparison of the number of BrdU-positive cells in adult and developing control and mutant brains. (A) The number of BrdU-positive cells in the cerebral cortex (Ctx), thalamus (Th) and cerebellum (Cb) of adult mutant brains (n=6) was not significantly different from those in adult control brains (n=6). The data plotted are mean±s.e.m. Cerebral cortex, P=0.42; thalamus, P=0.46; cerebellum, P=0.57. (B) The number of BrdU-positive cells in developing mutant brains (n=5) was significantly increased relative to those in controls (n=3). Cerebral cortex, P=0.001; thalamus, P=0.007. **P<0.01. (C) Sections from the P8 control cerebral cortex (a,c) and thalamus (e,g), and the P8 mutant cortex (b,d) and thalamus (f,h) were stained with an anti-BrdU antibody. In contrast to the control P8 brains, which have low proliferation, the mutant brains contain significantly more BrdU-positive cells. Scale bars: 100 μm.

(BLBP) (Fig. 2C,D) (Feng et al., 1994; Kurtz et al., 1994). Consistent with this, the majority of proliferating cells in both control (Fig. 2E,G) and mutant brains at P8 (Fig. 2F,H) do not express mature astrocyte markers, such as GFAP. We observed no difference in apoptosis between mutant and control brains that could contribute to the increased numbers of proliferating glial progenitors at this stage (data not shown).

To determine whether glial progenitor cells in P8 brains express the Cre transgene and hence are NF1 deficient, we performed immunohistochemical analysis. In both P8 control and mutant brains, most GFAP-positive astrocytes express the Cre transgene (Fig. 3; Fig. 4A), which is consistent with the previous observations in the adult brain (Malatesta et al., 2003; Zhu et al., 2005; Zhuo et al., 2001). However, not all of the Cre-positive cells expressed GFAP (Fig. 3A, parts a-d; 3B, parts a-d). Although these Cre-positive/GFAP-negative cells co-exist with Cre-positive/GFAP-positive astrocytes throughout the brain, they represent the major cell type in the thalamus (Fig. 3A) and in the periphery of the cerebellar white matter (Fig. 3B), where we determined that most of these GFAP-negative cells express both Cre and BLBP (Fig. 3A, parts e,f; 3B, parts e,f). These data indicate that the Cre transgene is expressed in the BLBP-positive glial progenitor cells in both P8 control and mutant brains. Thus, we conclude that NF1 deficiency as a consequence of Cre-mediated recombination leads to increased numbers of proliferating glial progenitor cells in P8 brains.

Nf1$^{-/-}$ glial progenitor cells differentiate

We also determined an increased number of GFAP-positive astrocytes in P8 mutant brains (Fig. 2F,H; Fig. 3A, part b; Fig. 3B, part b; Fig. 4A, parts b,d) as compared with controls (Fig. 2E,G; Fig. 3A, part a; Fig. 3B, part a; Fig. 4A, parts a,c). To verify that the GFAP-expressing astrocytes in mutant brains are NF1 deficient, we used a Cre antibody to label *Nf1*$^{-/-}$ cells. As shown in Fig. 4A, most of the GFAP-expressing cells in *Nf1*^{hGFAP}*KO* brains, including the cerebral cortex (Fig. 4A, part b) and the hippocampal dentate gyrus (DG) (Fig. 4A, parts d,f), co-express Cre and exhibit similar morphology to those astrocytes in control cortex (Fig. 4A, part a) and dentate gyrus (Fig. 4A, parts c,e). Furthermore, similar to normal counterparts (Fig. 4B, parts a,c), mutant astrocytes express GFAP but not nestin in most areas of P8 brains (Fig. 4B, parts b,d). A small number of cells expressing both GFAP and nestin were observed in both P8 control and mutant dentate gyrus (arrows in Fig. 4B, parts e,f) and the subventricular zone, which are probably neural stem/progenitor cells that persist into adulthood (Alvarez-Buylla et al., 2001). Thus, loss of NF1 promotes the proliferation of glial progenitor cells that retain the capacity to differentiate into GFAP-expressing astrocytes. We conclude that the tumor suppressor gene, NF1, is a negative regulator of the proliferation for glial progenitor cells but not for mature astrocytes.

A subset of *Nf1*$^{-/-}$ astrocytes express nestin in the adult brain

In normal adult brains, nestin immunoreactivity is mainly restricted to the well-characterized sites of stem cell residence: the subgranular layer of the dentate gyrus (DG; Fig. 5A) and the subventricular

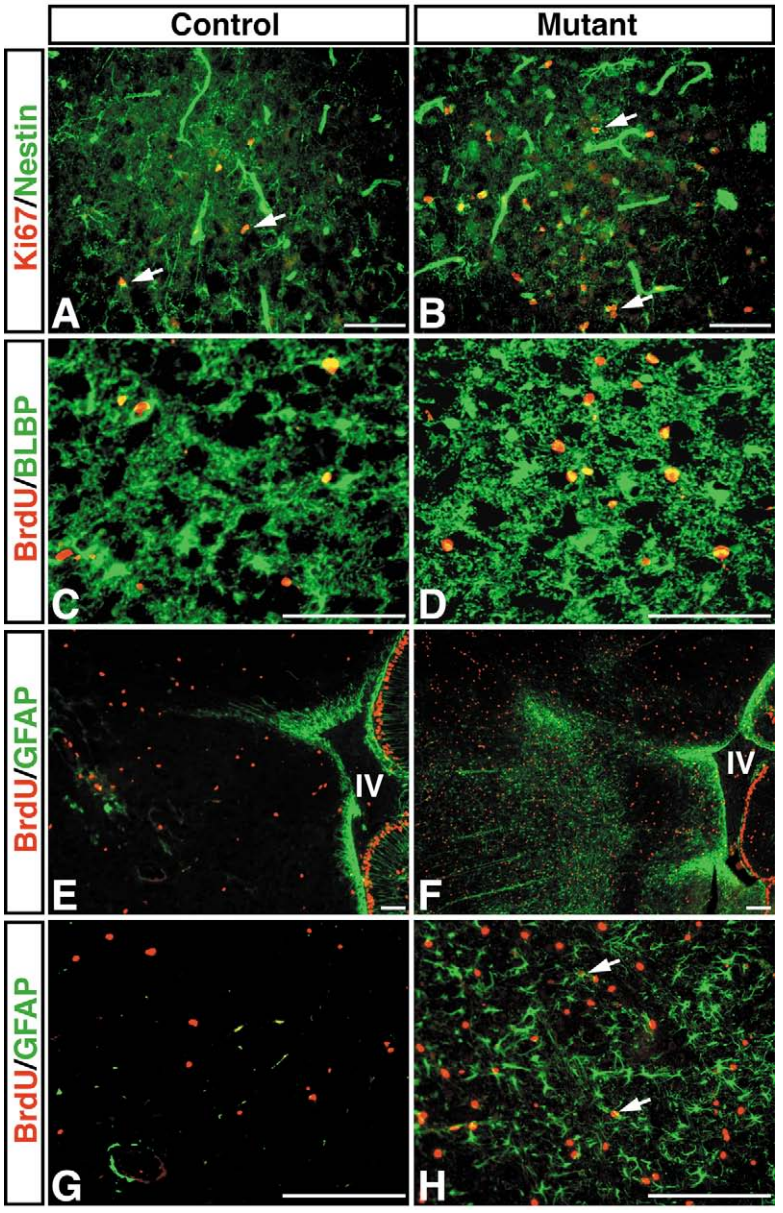

Fig. 2. Proliferating cells in P8 control and mutant brains express progenitor cell markers, not a mature astrocyte marker. Sections from P8 control and *Nf1*^{hGFAP}*KO* mutant brains were subjected to double-labeling immunofluorescence with anti-Ki67 (red) and anti-nestin (green) (A,B), with anti-BrdU (red) and anti-BLBP (green) (C,D), and with anti-BrdU (red) and anti-GFAP (green) (E,F). BrdU staining in the external granule cells in the P8 cerebella serves an internal positive control for this study (E,F). (G,H) Higher magnification of sections in E,F, showing that only a small number of BrdU-positive cells in the mutant brain but not in the control brain expressed GFAP (arrows in H). (A-D) Sections from the thalamus. (E-F) Sections from the brainstem. IV, the fourth ventricle. Scale bars: 100 μm.

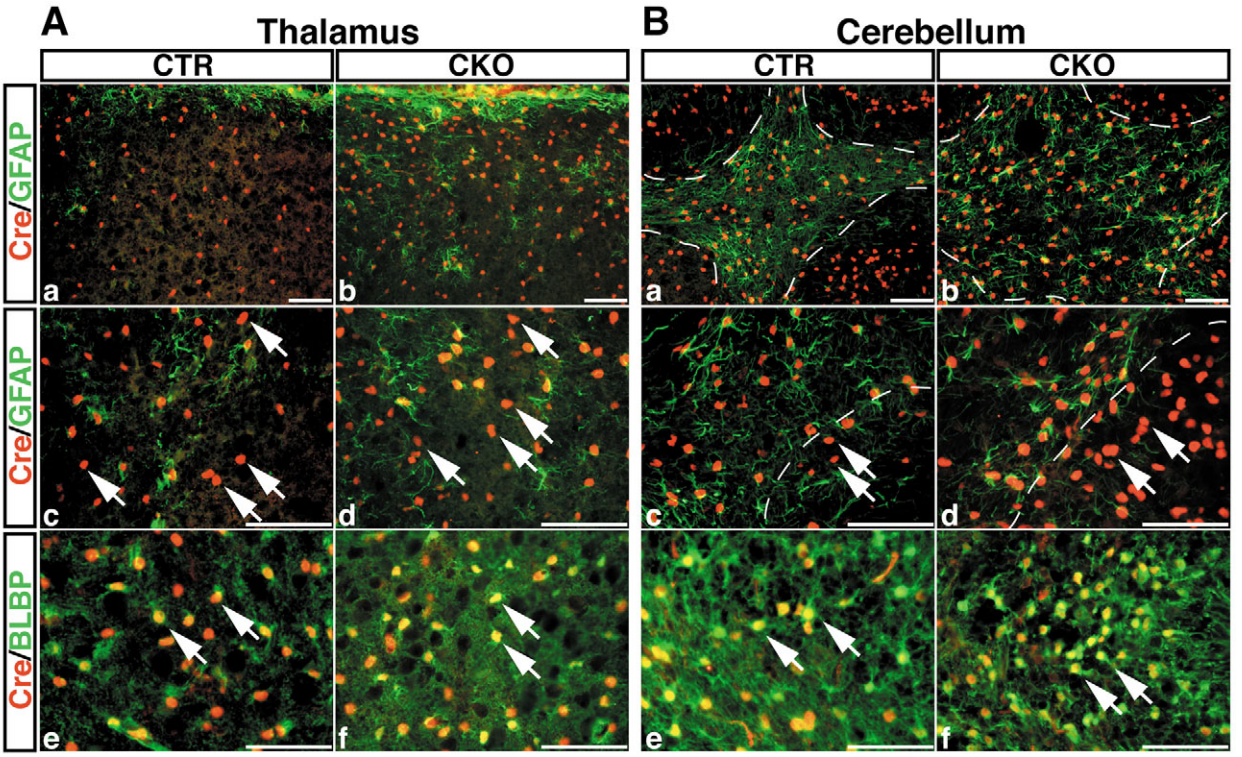

Fig. 3. *hGFAP-cre* is expressed in glial progenitor cells during postnatal development. (A) Sections from the thalamus of P8 control (a,c,e) and mutant (CKO) brains (b,d,f) were subjected to double-labeling immunofluorescence with anti-Cre (red) and anti-GFAP (green) (a-d), and anti-Cre (red) and anti-BLBP (green) (e,f). (B) Sections from the cerebellar white matter of P8 control (a,c,e) and mutant brains (b,d,f) were subjected to double-labeling immunofluorescence with anti-Cre/anti-GFAP (a-d) and anti-Cre/anti-BLBP (e,f). The mutant cerebellar white matter has significantly more GFAP-positive cells than control (marked by broken lines in a-d). Most of the Cre-positive/GFAP-negative glial progenitor cells are distributed in the periphery of the cerebellar white matter (outside the broken lines). Arrows indicate glial progenitor cells expressing Cre and BLBP, but not GFAP. Genotypes: control mice, $Nf1^{flox/+}$;*hGFAP*-cre+; mutant mice, $Nf1^{flox/-}$;*hGFAP*-cre+ or $Nf1^{flox/flox}$;*hGFAP*-cre+. Scale bars: 100 μm.

zone of the lateral ventricle (LV; Fig. 5C) (Gage, 2000). In brains of a subset of aged $Nf1^{hGFAP}KO$ mutant mice analyzed (8/14), nestin-positive cells were identified throughout the brain parenchyma, including the hippocampus (outside the subgranular layer, arrows in Fig. 5B) and cortex (Fig. 5D). All the nestin-positive cells had morphological features of mature astrocytes and co-expressed GFAP (Fig. 5B,D,H, inset), suggesting that these nestin/GFAP-positive cells represent abnormal astrocytes and that absence of NF1 results in abnormal co-expression of early and mature glial markers. In addition, consistent with NF1 inactivation, glial cells in $Nf1^{hGFAP}KO$ mutant brains have elevated levels of activated MAPK (Fig. 5E,F). As the aberrant expression of nestin in $Nf1^{hGFAP}KO$ mutant brains was only observed in a subset of aged (Fig. 5G,H), but not in P8 (Fig. 4B) or young adult (P30, data not shown) mutant mice, we suggest that NF1 may play a role in maintenance of the differentiated state of mature astrocytes in the adult brain.

We monitored a cohort of 45 $Nf1^{hGFAP}KO$ mutant mice, 10 of which survived more than 8 months. Detailed histological analysis of mutant brains (cerebral cortex, hippocampus, thalamus, hypothalamus and cerebellum) revealed no evidence of tumor formation. Thus, despite the induced early progenitor hyperproliferation during development, loss of NF1 alone is not sufficient to cause astrocytoma formation in the brain. This is consistent with the fact that while individuals with NF1 are reported to have a variety of brain abnormalities, including increased reactive astrogliosis (Nordlund et al., 1995), only a small percentage of these individuals develop astrocytomas in the brain (Listernick et al., 1999; Rubin and Gutmann, 2005).

Tumorigenic potential: a model for optic glioma

Approximately 15-20% of children with NF1 develop benign gliomas along the optic pathway with characteristics of pilocytic astrocytoma (Listernick et al., 1999). Using the Rosa26-*lacZ* reporter mouse strain (Soriano, 1999), we identified that *hGFAP*-cre-mediated recombination occurred in the optic nerve and the retina (Fig. 6A,B). The density of *lacZ*-positive cells appeared highest in the area of the optic nerve immediately adjacent to the retina (Fig. 6A-D). Double labeling with antibodies against *lacZ* and GFAP revealed that the majority of *lacZ*-positive cells in the optic nerve were GFAP-expressing astrocytes (Fig. 6C,D). Furthermore, *hGFAP*-cre-mediated recombination in the optic nerve was confirmed by PCR analysis (Fig. 6E) (Zhu et al., 2002; Zhu et al., 2005). We next examined the optic nerves from $Nf1^{hGFAP}KO$ mutant mice along with control littermates. Of optic nerves from twenty nine mutant mice analyzed, 18 were significantly enlarged in diameter (Fig. 6F-H; Fig. 7A,B) and reminiscent of similarly prepared optic nerves from individuals

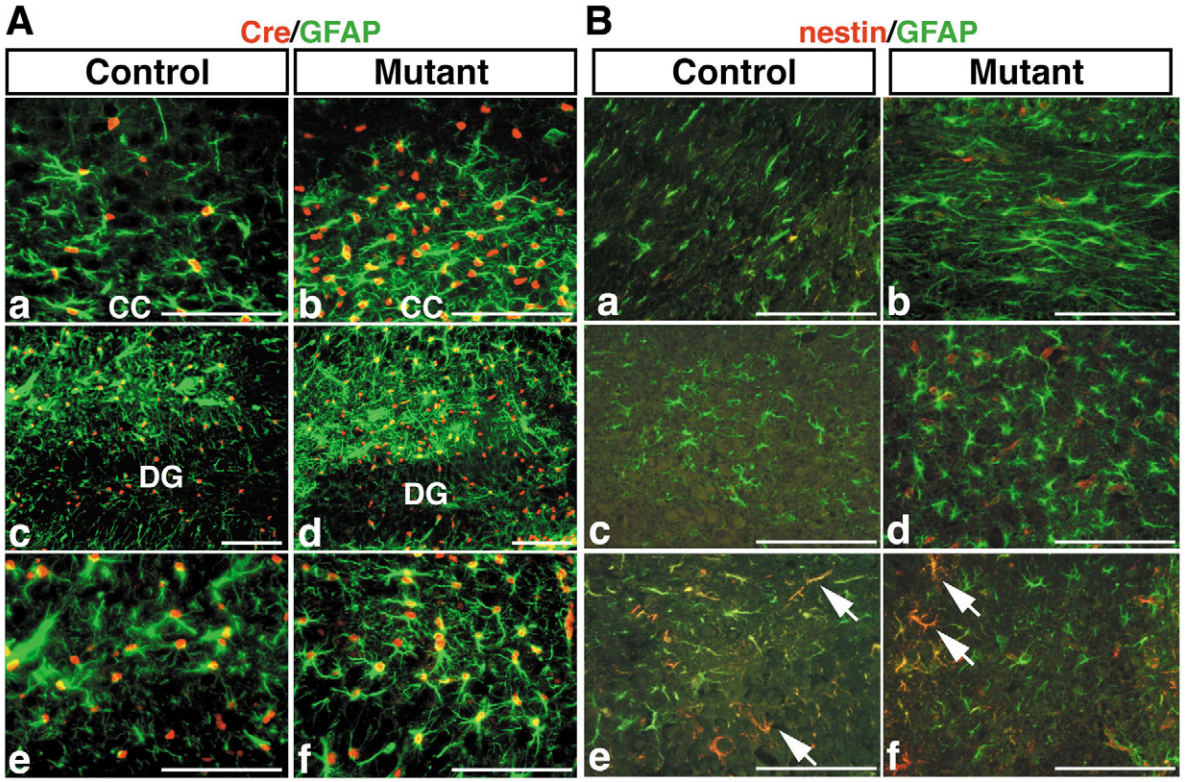

Fig. 4. *Nf1*$^{-/-}$ glial progenitor cells undergo astrocytic differentiation. (A) Sections from P8 control (a,c,e) and *Nf1*^{hGFAP}*KO* mutant (b,d,f) brains were subjected to double-labeling immunofluorescence with anti-Cre (red) and anti-GFAP (green). (a,b) Sections from the control and mutant cerebral cortex (CC); (c-f) low (c,d) and high (e,f) magnification of sections from control and mutant hippocampal dentate gyrus (DG). Most of the GFAP-positive cells also express the Cre transgene. (B) Sections from P8 control (a,c,e) and *Nf1*^{hGFAP}*KO* mutant (b,d,f) brains were subjected to double-labeling immunofluorescence with anti-nestin (red) and anti-GFAP (green). (a,b) Sections from the corpus callosum; (c,d) sections from the brainstem; (e,f) sections from the dentate gyrus. Most of the GFAP-positive astrocytes in both control and mutant P8 brains do not express nestin, except in the dentate gyrus (arrows in e,f), where a small number of cells express both GFAP and nestin. There are low levels of nestin expression in the endothelial cells. Genotypes: control mice, *Nf1*$^{flox/+}$;*hGFAP*-cre+; mutant mice, *Nf1*$^{flox/-}$;*hGFAP*-cre+ or *Nf1*$^{flox/flox}$;*hGFAP*-cre+. Scale bars: 100 μm.

with NF1 with optic gliomas (Kleihues and Cavenee, 2000). Histological analysis revealed evidence of disorganization and increased cellularity throughout the optic nerves from all of the 29 mutant mice (Fig. 7C,D). The dysplastic nature of the cells in the mutant optic nerves is illustrated by double labeling with nestin and GFAP (Fig. 7E-H). We found that mature optic nerve astrocytes retain low levels of nestin expression (Frisen et al., 1995). Furthermore, consistent with the pattern of *hGFAP*-cre-mediated recombination in the optic pathway, the most pronounced changes were found in the area immediately adjacent to the retina (Fig. 7I,J), which contained dense clusters of randomly oriented glial nuclei. Detailed pathological analysis revealed that six out of 29 mutant mice (6/29) developed conspicuous neoplastic lesions (Fig. 8A-C). In contrast to normal nerves, which are comprised of well-organized astrocytes expressing both nestin and GFAP (Fig. 8D), neoplastic cells are completely disorganized and downregulate nestin expression (Fig. 8E,F). Although the optic nerve lesions observed in this tumor model lack some common features of pilocytic astrocytomas, such as Rosenthal fibers and granular bodies, these lesions display pathological features similar to human tumors, which include the location in the anterior optic nerve, coarse fibrillary appearance and nuclear pleiomorphism with clustered atypical tumor nuclei (also see Fig. 9K,M).

BrdU analysis showed that mutant optic nerves contain five- to ten-fold increases in proliferating cells (Fig. 9A). In all cases, proliferating cells in both adult control (Fig. 9B,D) and mutant nerves (Fig. 9C,E) did not express GFAP, indicating that, as in the developing brain, loss of NF1 promotes the proliferation of progenitor cells in the optic nerve. By contrast, BrdU-positive cells in the optic nerve express nestin (arrows in Fig. 9F,G). These observations suggest that *Nf1*^{hGFAP}*KO* mutant optic nerves contain increased numbers of glial progenitor cells. When compared with adult control proximal (Fig. 9H,J) and distal (Fig. 9L) optic nerves that had few or no BLBP-expressing cells, adult mutant nerves contained numerous BLBP-positive cells that exhibited nuclear atypia indicative of neoplastic transformation (Fig. 9I, arrows in Fig. 9K,M). In addition, we also used an independent glial progenitor marker, Pax2 (Mi and Barres, 1999), to confirm that mutant optic nerves had increased numbers of glial progenitor cells (Fig. 9N,O).

We confirmed that the pathology observed in the optic nerves results from loss of NF1 by immunohistochemical analysis with a Cre antibody (data not shown). Consistently, mutant glial cells have high MAPK activity (Fig. 10A-D) with

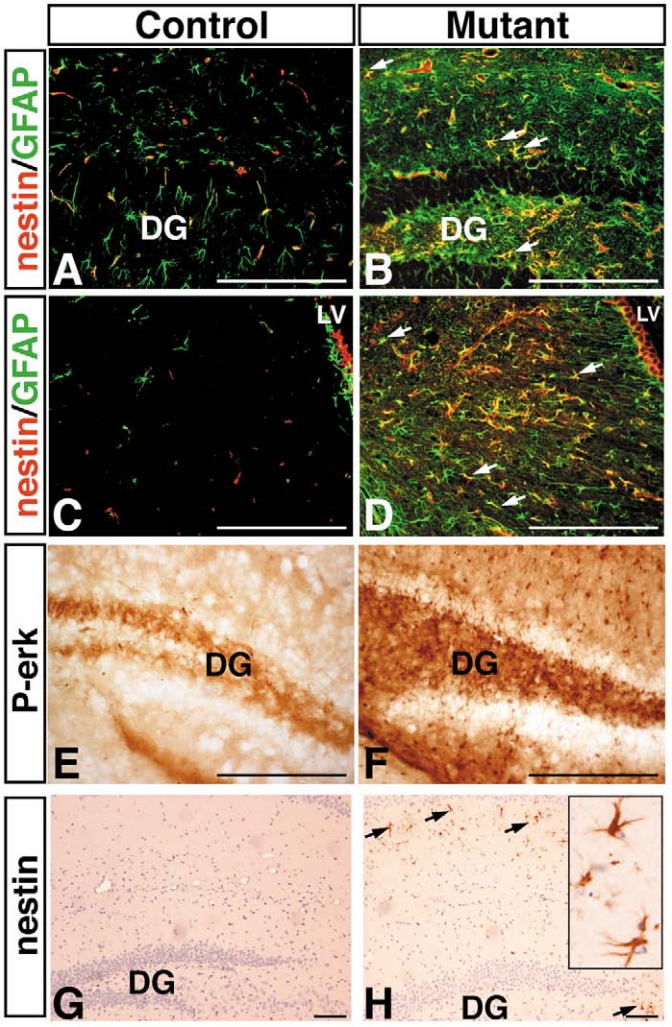

Fig. 5. A subset of *Nf1*$^{-/-}$ astrocytes in the adult brain express nestin. Sections from adult control (A) and mutant (B) dentate gyrus (DG), as well as control (C) and mutant (D) cerebral cortex were subjected to double-labeling fluorescence with anti-nestin (red) and anti-GFAP (green). LV, lateral ventricle. Reactive astrocytes expressing both GFAP and nestin were observed only in the mutant brain (arrows in B,D). Immunohistochemical analysis with anti-P-erk of the control (E) and mutant (F) dentate gyrus. A population of nestin-positive reactive astrocytes (arrows in H, see inset for high magnification) was identified only in a subset of aged mutant brains, but not in control or mutant mice at young age (G). Scale bars: 100 μm.

a subset of mutant glial cells showing activated MAPK but lacking GFAP. These results suggest that both glial progenitor cells (Fig. 10F, arrowheads) and astrocytes (Fig. 10F, arrows) in mutant optic nerves had activated MAPK. These observations suggest that activation of Ras/MAPK pathway as a consequence of NF1 inactivation may underlie hyperplasia and glioma formation in the mutant optic nerve.

To examine whether NF1 heterozygosity in surrounding cells contributes to the development of optic glioma, we crossed *Nf1*$^{flox/flox}$ mice into a different GFAP-cre* transgenic strain (Bajenaru et al., 2002) that targets Cre-mediated recombination only in astrocytes of the retina (see Fig. S3A,B in the supplementary material). When crossed to the Rosa26-*lacZ* reporter strain, the GFAP-cre* activity showed co-expression with astrocytic markers (GFAP), but not with neuronal markers in retina (NeuN; see Fig. S3E,F in the supplementary material). In some regions of the brain, GFAP-cre*-mediated recombination occurred in both glia and neurons (see Fig. S3C,D in the supplementary material) (Fraser et al., 2004). Detailed analysis of the optic nerve in these aged *Nf1*$^{flox/flox}$;*GFAP-cre**+ mutant mice (12 months old) revealed no evidence of hyperplasia compared with that observed for *Nf1*^{hGFAP}*KO*. These results support the notion that the

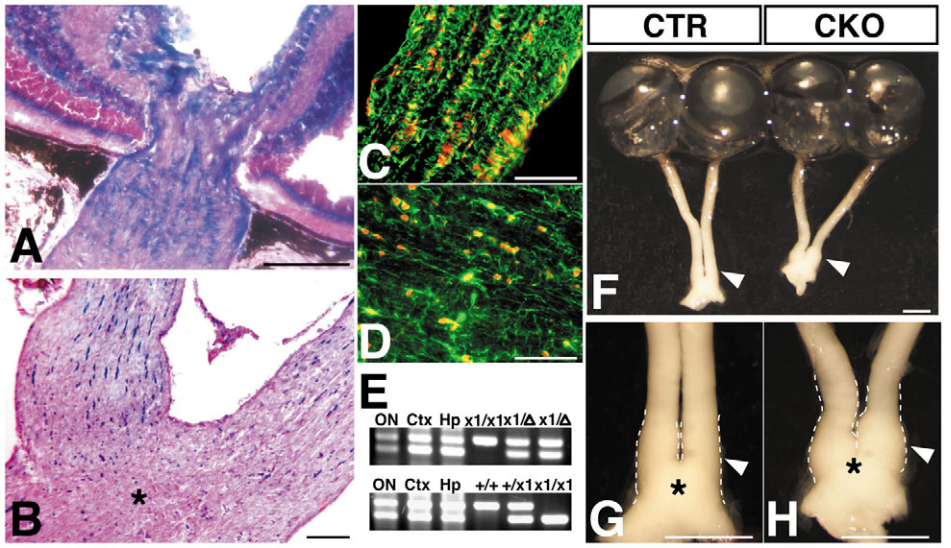

Fig. 6. Cre-mediated recombination leads to enlarged optic nerves. X-gal staining of the proximal optic nerve immediately adjacent to the retina (A) and distal optic nerve near the chiasm (asterisk) (B). Optic nerves were dissected from 2-month-old mice with the genotype of *hGFAP*-cre+; Rosa26-*lacZ*/+ (*n*=3). (C,D) Adjacent sections to A,B were subjected to double-labeling immunofluorescence with anti-*lacZ* (red) and anti-GFAP (green). Most of the *lacZ*-positive cells are GFAP-expressing astrocytes. (E) *hGFAP-cre*-mediated recombination in the optic nerve was revealed by PCR analysis. Upper panel: a PCR assay identifying the floxed NF1 allele (×1) and recombined floxed allele (Δ) indicated that a significant number of the floxed NF1 alleles in the optic nerve (ON), cerebral cortex (Ctx) and hippocampus (Hp) of the *Nf1*$^{flox/+}$;*hGFAP*-cre+ mice transformed into the recombined alleles. Bottom panel: a PCR assay that identifies the wild type (+) and the floxed (×1) NF1 allele confirmed the genotype of the tissues analyzed. (F) A representative of control (left) and mutant (right) eyes with the optic nerves and chiasm (arrowheads). High-magnification of view of control (G) and mutant (H) optic nerves with chiasms (asterisk). The mutant nerve has a conspicuous enlargement (indicated by broken lines and arrowheads). Scale bars: 100 μm in A-D; 1 mm in F-H.

heterozygous state of surrounding cells may contribute to NF1 nullizygous glial hyperplasia and neoplasia in the optic nerve (Bajenaru et al., 2003).

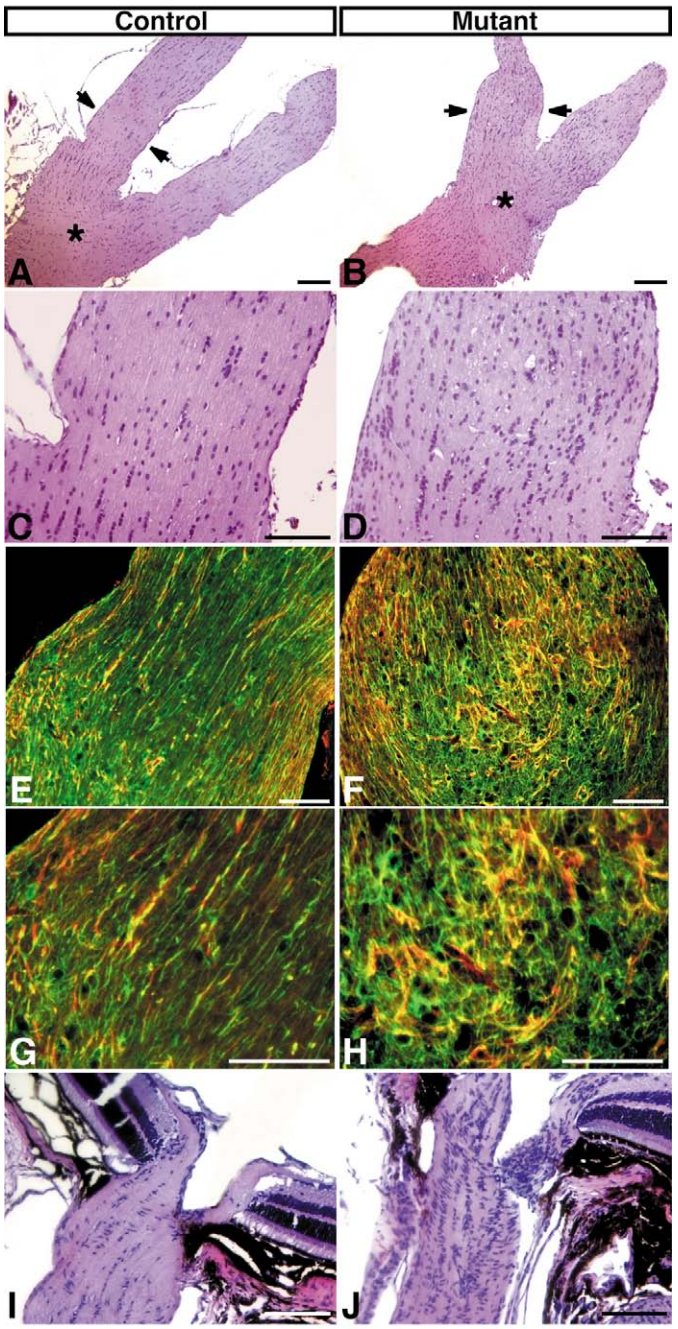

Fig. 7. *Nf1*^{hGFAP}*KO* optic nerves are hyperplastic. Sections from control (A,C) and mutant (B,D) distal optic nerves and chiasms (asterisk) were stained with Hematoxylin and Eosin. Arrows in A,B indicate the enlarged area of the nerves shown in C,D, respectively. Adjacent sections from control (E,G) and mutant (F,H) optic nerves were stained with anti-nestin (red) and anti-GFAP (green). Mutant optic nerves are enlarged (B), hyperplastic (D) and disorganized (F,H). Sections from control (I) and mutant (J) proximal optic nerves were stained with Hematoxylin and Eosin. The most pronounced hypercellularity was observed in the proximal optic nerves (J). Scale bars: 100 μm.

Discussion

Through analysis of neural-specific NF1 knockout mice, we demonstrate that the NF1 tumor suppressor gene has pivotal roles in the appropriate development of the CNS glial cell lineage and that sustained increased proliferation in glial progenitor cells may underlie tumor formation in the optic nerve.

NF1 and proliferation of glial progenitor cells

Consistent with the role of NF1 as a tumor suppressor gene, recent studies have demonstrated that loss of NF1 function confers a growth advantage to a variety of cell types in vitro, including neural stem/progenitor cells in the embryonic forebrain (Dasgupta and Gutmann, 2005), oligodendrocyte precursor cells from the embryonic spinal cord (Bennett et al., 2003), Schwann cells (Kim et al., 1997) and fibroblasts (Rosenbaum et al., 1995), etc. However, because of early embryonic lethality of NF1 homozygous mutants, insights into the function of NF1 during late developmental stages and adulthood remain limited (Bajenaru et al., 2003; Bajenaru et al., 2002; Zhu et al., 2002; Zhu et al., 2001). For example, despite the fact that several lines of evidence point to the *Nf1* gene as a negative regulator of astrocyte proliferation (Bajenaru et al., 2002), the in vivo role of the *Nf1* gene in mature astrocytes has not been fully addressed. Our studies indicate that NF1-deficient mature astrocytes in the adult brain do not show a significant increase in proliferation. Instead, we show significantly increased proliferation during postnatal CNS development. These proliferating cells express progenitor cell markers found in both multipotent neural stem/progenitor cells and glial progenitor cells (Anthony et al., 2004; Feng et al., 1994; Frisen et al., 1995; Kurtz et al., 1994; Lendahl et al., 1990). We conclude that these proliferative cells most probably represent glial progenitor cells, as neurogenesis is largely complete and gliogenesis persists in the P8 brain (Bayer and Altman, 1991; Jacobson, 1991; Qian et al., 2000). Thus, our studies demonstrate that the *Nf1* gene is a negative regulator of proliferation in glial progenitor cells and provide evidence that the NF1-associated pathology observed in the adult brain could result from developmental defects.

NF1 in differentiation of the astrocyte lineage

Increased numbers of NF1-deficient, GFAP-positive mature astrocytes were observed in both developing and adult *Nf1*^{hGFAP}*KO* mutant brains. Because *hGFAP*-cre is expressed in a majority of astrocyte precursors, radial glia in the embryonic brain (Malatesta et al., 2003) and glial progenitor cells in the postnatal brain (this study), it is reasonable to assume that the majority of mutant astrocytes arise from NF1 deficient progenitor cells. Thus, in vivo, NF1 is dispensable for astrocytic differentiation. As no increased proliferation or reduced apoptosis was observed in NF1-deficient mature astrocytes in both P8 and adult brains, the increased numbers of GFAP-positive astrocytes in adult mutant brains probably result from excess generation of glial progenitor cells, as observed during development. In brains of a subset of aged *Nf1*^{hGFAP}*KO* mutant mice, we identified an unusual population of cells that express both nestin and GFAP. These nestin/GFAP-positive cells morphologically resemble reactive astrocytes that are hypertrophic with thickened and increased processes (Ridet et al., 1997), which are observed in both

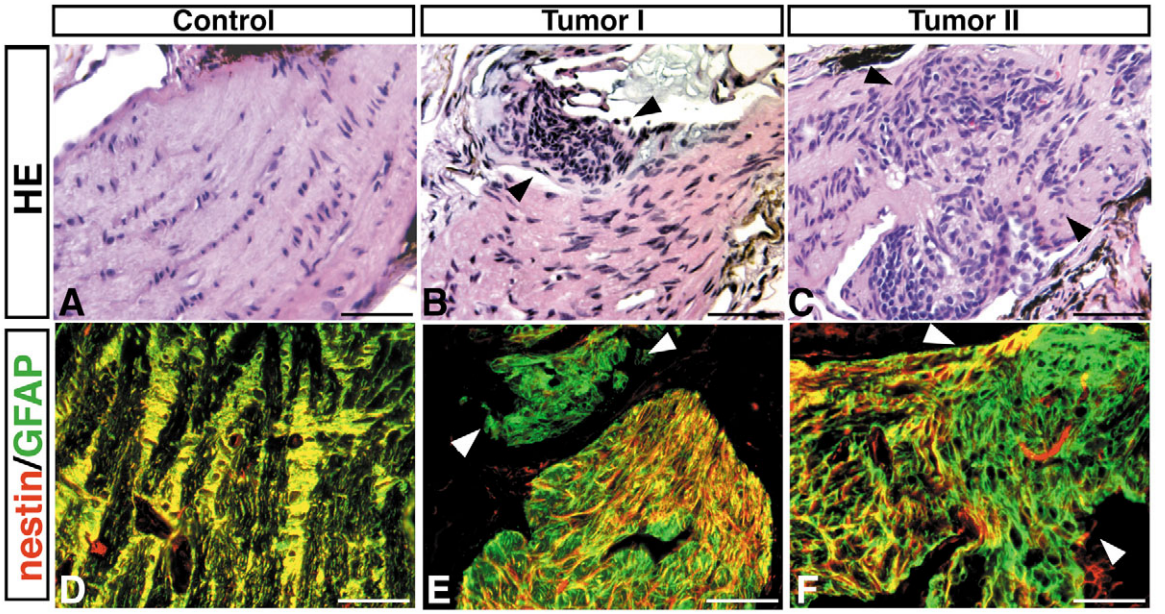

Fig. 8. *Nf1*^{hGFAP}*KO* mice develop optic pathway gliomas. Two independent optic gliomas (B,C) are shown with Hematoxylin and Eosin staining and compared with the control (A). Adjacent sections from control (D) and mutant nerves with gliomas (E,F) were stained with anti-nestin (red) and anti-GFAP (green). Unlike the well-organized normal astrocytes that express both nestin and GFAP in control (D), most of the cells in optic gliomas express only GFAP (E,F, arrowheads). Scale bars: 100 μm.

human and mouse NF1-deficient brains (Gutmann et al., 1999; Nordlund et al., 1995; Rizvi et al., 1999; Zhu et al., 2001). As these nestin/GFAP-positive cells were not observed in the brains of developing (P8) or young adult (P30) mutant mice, these observations suggest that NF1 may be required for the maintenance of the astrocytic differentiation state or possibly preventing mature astrocytes from undergoing abnormal differentiation. Previously, we have reported that neuronal loss of NF1 results in activation of MAPK in neurons but not in astrocytes, leading to reactive astrogliosis in a non-cell autonomous fashion (Zhu et al., 2001). Despite exhibiting morphological similarities, the reactive astrocytes observed in neuronal-specific NF1 (*Nf1*^{SynI}*KO*) mutant brains, do not express nestin (Zhu et al., 2001). Therefore, the aberrant expression of this CNS progenitor cell marker (nestin) could result in part from intrinsic loss of NF1 within astrocytes or its progenitor cells. This is consistent with the observation that astrocytes in *Nf1*^{hGFAP}*KO* brains have elevated levels of activated MAPK, while reactive astrocytes in *Nf1*^{SynI}*KO* brains do not (Zhu et al., 2001).

NF1, a tumor suppressor gene in optic nerve glial progenitor cells

The present results and previous reports indicate that loss of NF1 alone is insufficient to induce astrocytoma in the brain (Bajenaru et al., 2003; Bajenaru et al., 2002; Zhu et al., 2005). By contrast, *hGFAP*-cre-mediated NF1 inactivation results in fully penetrant glial cell hyperplasia and ~20% incidence of gliomas in the optic nerves. One likely reason for this optic nerve-specific neoplasia is that increased proliferation in the mutant brain is limited to development, while mutant optic nerves have sustained increased proliferation into adulthood. Our data indicate that the proliferating cells in mutant optic nerves express glial progenitor cell markers including nestin, BLBP and Pax2. These progenitor-like cells display nuclear atypia, a characteristic feature of neoplastic cells, and have increased levels of activated MAPK. Together, these observations suggest that NF1 deficiency regulates glial progenitor cell proliferation, which is likely to underlie optic glioma formation in this model.

A model for optic pathway glioma

Histologically, pilocytic astrocytomas may contain a surprisingly wide range of patterns (Kleihues and Cavenee, 2000). In addition to some of the more common features, including recognizable bipolar cytoplasmic processes, brightly eosinophilic Rosenthal fibers and hyaline granular bodies, pilocytic astrocytomas may also contain areas of substantial nuclear pleomorphism, oligodendroglioma-like regions, areas of infiltrative growth and cells similar to those of diffuse WHO grade II astrocytoma. In the case of lesions lacking Rosenthal fibers and hyaline granular bodies, the distinction between diffuse and pilocytic astrocytomas may be extremely difficult (Kleihues and Cavenee, 2000). Thus, within the accepted variability of pilocytic astrocytomas, the lesions found in the mutant mice are consistent with early stage optic pathway gliomas. This phenotype is further consistent with the fact that individuals with NF1 develop astrocytic neoplasms predominantly along the optic pathway (Listernick et al., 1999).

While this manuscript was in preparation, a mouse model for NF1-associated optic pathway glioma was published using the conditional NF1 flox mouse strain described here together with the GFAP-cre* transgene (see Fig. S3 in the supplementary material) (Bajenaru et al., 2003). The pathology described by Bajenaru et al. is less severe, reminiscent of that described as hyperplasia in this study (Fig. 7). In addition,

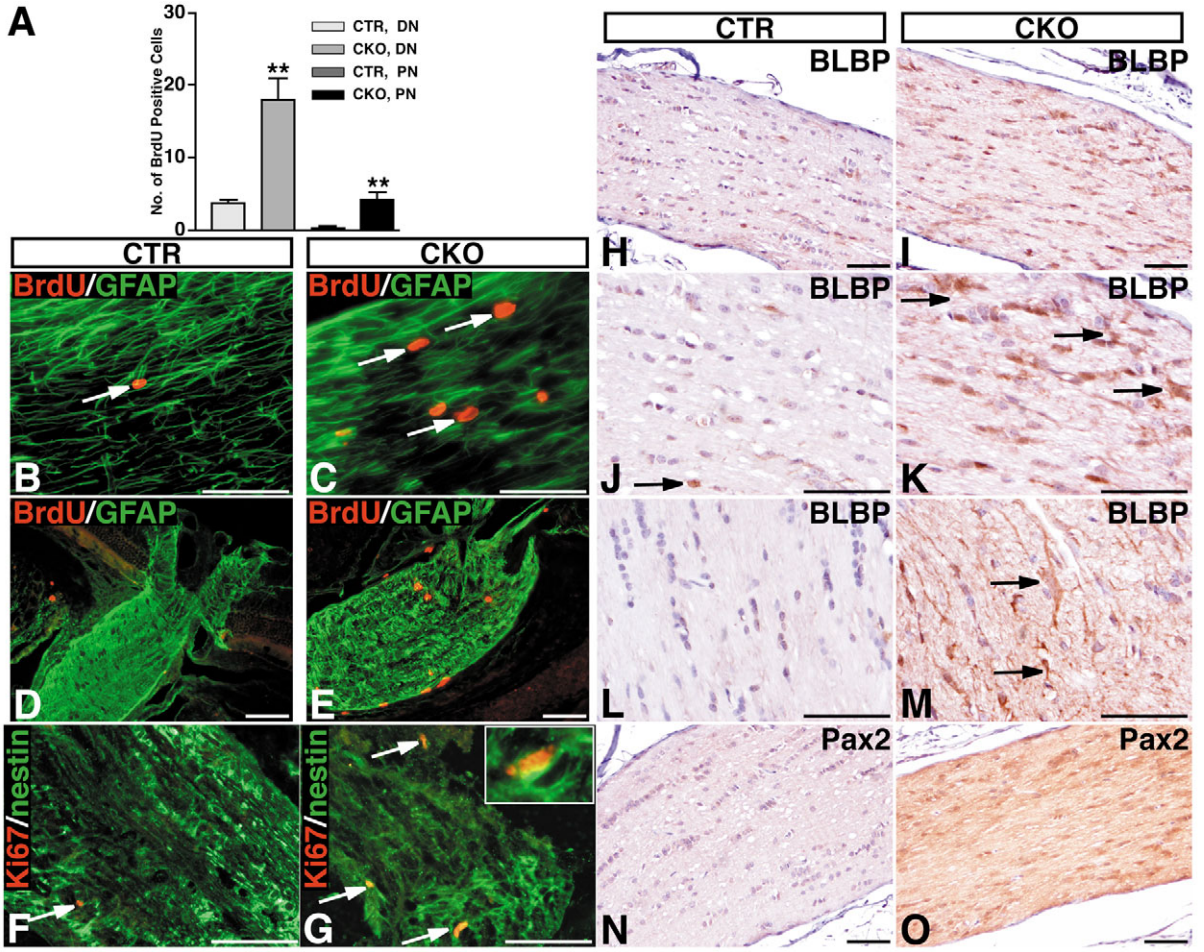

Fig. 9. *Nf1*^{hGFAP}*KO* hyperplastic nerves have increased proliferation and express glial progenitor cell markers. (A) The quantification of BrdU-positive cells in the adult control (CTR) and mutant (CKO) distal (DN) and proximal (PN) nerves. The data plotted are mean±s.e.m. (distal nerve, CTR, n=4, CKO, n=5, $^{**}P$<0.001; proximal nerve, CTR, n=3, CKO, n=6, $^{**}P$<0.001). Sections from control (B,D) and mutant (C,E) distal (B,C) and proximal (D,E) optic nerves were stained with anti-BrdU (red) and anti-GFAP (green). Sections from control (F) and mutant (G) nerves were stained with anti-Ki67 (red) and anti-nestin (green). Arrows in B and C indicate proliferating cells that do not express GFAP. Arrows in F and G indicate nestin-positive proliferating cells (inset in G provides higher magnification). Sections from control proximal (H,J), mutant proximal (I,K), control distal (L) and mutant distal (M) optic nerves were stained with anti-BLBP. Arrow in J indicates a BLBP-positive cells with normal nuclei in the normal nerve; arrows in K,M indicate BLBP-positive cells with atypical nuclei in the mutant nerve. Sections from control (N) and mutant (O) optic nerves were stained with anti-Pax2. Scale bars: 100 μm.

Bajenaru et al.'s study describes hyperplastic optic nerves only in the *Nf1*$^{flox/-}$ genetic configuration and not in the *Nf1*$^{flox/flox}$ configuration. Our *Nf1*^{hGFAP}*KO* mice exhibit fully penetrant hyperplasia in either the flox/- or the flox/flox configurations and, additionally, 20% incidence of optic pathway gliomas. Possible explanations for the discrepancy between these two studies include the timing of Cre transgene activation (E10.5 for *hGFAP-cre* versus E14.5 for GFAP-cre*), contributions of NF1 deficient neighboring cells in the tumor micro-environment and differences in genetic background. In line with this study, it is tempting to speculate that the timing of NF1 inactivation in the glial cell lineage during optic nerve development may account in part for the heterogeneous nature of the NF1-associated optic gliomas (Listernick et al., 1999; Rubin and Gutmann, 2005). Thus, our model may mimic a subset of individuals with NF1 who have severe tumor phenotypes as a consequence of loss of NF1 in a progenitor cell population, while the mouse strain developed by Bajenaru et al. may model less aggressive lesions owing to NF1 inactivation in more differentiated cells.

In this study, we compared Cre-mediated recombination in both GFAP-cre strains and found that the GFAP-cre* transgene is active only in the retinal surface layer where astrocytes are located (see Fig. S3 in the supplementary material). By contrast, the *hGFAP*-cre activity is also observed in the inner retinal layer (Fig. 6A). Interestingly, this layer contains another retina-specific glia, called Müller cells. This cell type can produce and secrete various kinds of trophic factors and cytokines, which may regulate glia-glia and glia-neuron network under pathological conditions (Harada et al., 2002; Harada et al., 2000). It is therefore possible that in the context of NF1 loss, an enhanced paracrine interaction occurs between Müller cells and glial progenitor cells in the optic nerve. This would account for the robust appearance of tumors with our

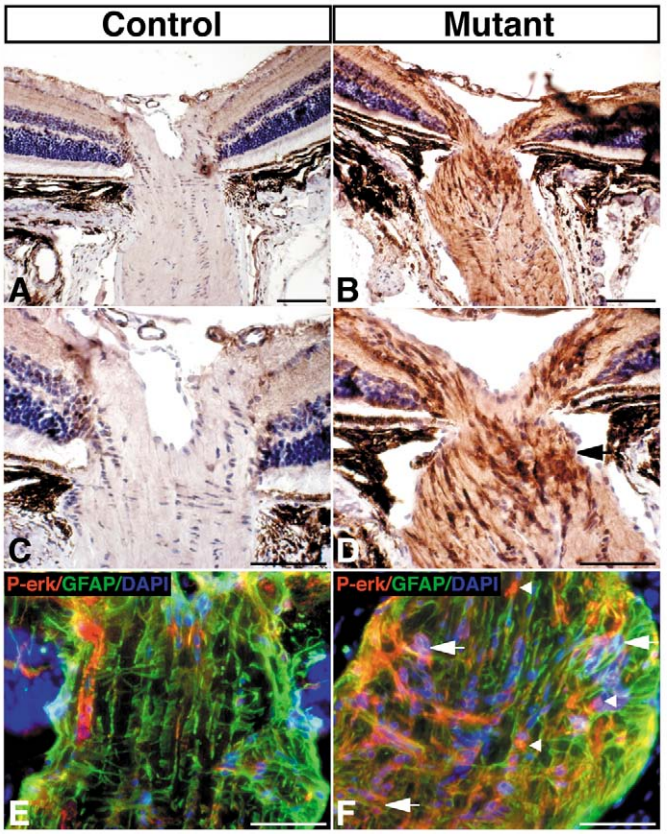

Fig. 10. Glial cells in mutant optic nerves have elevated levels of activated MAPK. Sections of the proximal optic nerves from control mice (A,C) and mutant mice (B,D) were stained with anti-P-erk. The arrow in D indicates the tumor cells with activated MAPK. Sections from control (E) and mutant (F) optic nerves were subjected to triple labeling with anti-P-erk (red), anti-GFAP (green) and DAPI (blue). DAPI was used to label the nuclei. In contrast to the control nerves where little or no cells had activated MAPK (E), mutant nerves contained numerous P-erk positive cells, some of which co-expressed GFAP (F, arrows) and some of which failed to express GFAP (F, arrowheads). Scale bars: 100 μm.

Nf1^{hGFAP}*KO* model that has NF1-null surrounding cells (e.g. Müller glia) compared with a partial hyperplastic response in the *Nf1*$^{flox/-}$;*GFAP*-cre*+ transgene where neighboring cells are heterozygous for NF1.

We thank P. Houston, A. DeShaw, S. McKinnon, W. Song and A. Wang for technical assistance; members of the Parada and Zhu laboratories for support; Dr N. Heintz for BLBP antibody; Dr G. Dressler for Pax2 antibody; and Dr S. Weiss for critically reading the manuscript. This work is supported by grants from the National Institute of Neurological Disorders and Stroke, the American Cancer Society and Department of Defense (L.F.P.); from the National Institutes of Health and DOD to D.H.G.; and by a NIH postdoctoral award to M.L.B. Y.Z. acknowledges support from National Neurofibromatosis Foundation (Young Investigator Award), the Biological Sciences Scholars Program and the Comprehensive Cancer Center of the University of Michigan Medical School.

Supplementary material

Supplementary material for this article is available at
http://dev.biologists.org/cgi/content/full/132/24/5577/DC1

References

Alvarez-Buylla, A., Garcia-Verdugo, J. M. and Tramontin, A. D. (2001). A unified hypothesis on the lineage of neural stem cells. *Nat. Rev. Neurosci.* **2**, 287-293.

Anthony, T. E., Klein, C., Fishell, G. and Heintz, N. (2004). Radial glia serve as neuronal progenitors in all regions of the central nervous system. *Neuron* **41**, 881-890.

Bajenaru, M. L., Zhu, Y., Hedrick, N. M., Donahoe, J., Parada, L. F. and Gutmann, D. H. (2002). Astrocyte-specific inactivation of the neurofibromatosis 1 gene (NF1) is insufficient for astrocytoma formation. *Mol. Cell. Biol.* **22**, 5100-5113.

Bajenaru, M. L., Hernandez, M. R., Perry, A., Zhu, Y., Parada, L. F., Garbow, J. R. and Gutmann, D. H. (2003). Optic nerve glioma in mice requires astrocyte Nf1 gene inactivation and Nf1 brain heterozygosity. *Cancer Res.* **63**, 8573-8577.

Ballester, R., Marchuk, D., Boguski, M., Saulino, A., Letcher, R., Wigler, M. and Collins, F. (1990). The NF1 locus encodes a protein functionally related to mammalian GAP and yeast IRA proteins. *Cell* **63**, 851-859.

Bayer, S. A. and Altman, J. (1991). *Neocortical Development*. New York: Raven Press.

Bennett, M. R., Rizvi, T. A., Karyala, S., McKinnon, R. D. and Ratner, N. (2003). Aberrant growth and differentiation of oligodendrocyte progenitors in neurofibromatosis type 1 mutants. *J. Neurosci.* **23**, 7207-7217.

Brannan, C. I., Perkins, A. S., Vogel, K. S., Ratner, N., Nordlund, M. L., Reid, S. W., Buchberg, A. M., Jenkins, N. A., Parada, L. F. and Copeland, N. G. (1994). Targeted disruption of the neurofibromatosis type-1 gene leads to developmental abnormalities in heart and various neural crest-derived tissues. *Genes Dev.* **8**, 1019-1029.

Dasgupta, B. and Gutmann, D. H. (2005). Neurofibromin regulates neural stem cell proliferation, survival, and astroglial differentiation in vitro and in vivo. *J. Neurosci.* **25**, 5584-5594.

Daston, M. M. and Ratner, N. (1992). Neurofibromin, a predominantly neuronal GTPase activating protein in the adult, is ubiquitously expressed during development. *Dev. Dyn.* **195**, 216-226.

Daston, M. M., Scrable, H., Nordlund, M., Sturbaum, A. K., Nissen, L. M. and Ratner, N. (1992). The protein product of the neurofibromatosis type 1 gene is expressed at highest abundance in neurons, Schwann cells, and oligodendrocytes. *Neuron* **8**, 415-428.

Feng, L., Hatten, M. E. and Heintz, N. (1994). Brain lipid-binding protein (BLBP): a novel signaling system in the developing mammalian CNS. *Neuron* **12**, 895-908.

Fraser, M. M., Zhu, X., Kwon, C. H., Uhlmann, E. J., Gutmann, D. H. and Baker, S. J. (2004). Pten loss causes hypertrophy and increased proliferation of astrocytes in vivo. *Cancer Res.* **64**, 7773-7779.

Frisen, J., Johansson, C. B., Torok, C., Risling, M. and Lendahl, U. (1995). Rapid, widespread, and longlasting induction of nestin contributes to the generation of glial scar tissue after CNS injury. *J. Cell Biol.* **131**, 453-464.

Gage, F. H. (2000). Mammalian neural stem cells. *Science* **287**, 1433-1438.

Gutmann, D. H., Loehr, A., Zhang, Y., Kim, J., Henkemeyer, M. and Cashen, A. (1999). Haploinsufficiency for the neurofibromatosis 1 (NF1) tumor suppressor results in increased astrocyte proliferation. *Oncogene* **18**, 4450-4459.

Gutmann, D. H., Donahoe, J., Brown, T., James, C. D. and Perry, A. (2000). Loss of neurofibromatosis 1 (NF1) gene expression in NF1-associated pilocytic astrocytomas. *Neuropathol. Appl. Neurobiol.* **26**, 361-367.

Gutmann, D. H., Hedrick, N. M., Li, J., Nagarajan, R., Perry, A. and Watson, M. A. (2002). Comparative gene expression profile analysis of neurofibromatosis 1-associated and sporadic pilocytic astrocytomas. *Cancer Res.* **62**, 2085-2091.

Harada, T., Harada, C., Nakayama, N., Okuyama, S., Yoshida, K., Kohsaka, S., Matsuda, H. and Wada, K. (2000). Modification of glial-neuronal cell interactions prevents photoreceptor apoptosis during light-induced retinal degeneration. *Neuron* **26**, 533-541.

Harada, T., Harada, C., Kohsaka, S., Wada, E., Yoshida, K., Ohno, S., Mamada, H., Tanaka, K., Parada, L. F. and Wada, K. (2002). Microglia-Muller glia cell interactions control neurotrophic factor production during light-induced retinal degeneration. *J. Neurosci.* **22**, 9228-9236.

Holland, E. C. (2001). Gliomagenesis: genetic alterations and mouse models. *Nat. Rev. Genet.* **2**, 120-129.

Huynh, D. P., Nechiporuk, T. and Pulst, S. M. (1994). Differential expression and tissue distribution of type I and type II neurofibromins during mouse fetal development. *Dev. Biol.* **161**, 538-551.

Jacks, T., Remington, L., Williams, B. O., Schmitt, E. M., Halachmi, S.,

Bronson, R. T. and Weinberg, R. A. (1994). Tumor spectrum analysis in p53-mutant mice. *Curr. Biol.* **4**, 1-7.
Jacobson, M. (1991). *Developmental Neurobiology*. New York: Plenum Press.
Kim, H. A., Ling, B. and Ratner, N. (1997). Nf1-deficient mouse Schwann cells are angiogenic and invasive and can be induced to hyperproliferate: reversion of some phenotypes by an inhibitor of farnesyl protein transferase. *Mol. Cell. Biol.* **17**, 862-872.
Kleihues, P. and Cavenee, W. K. (2000). *Pathology and Genetics of Tumors of the Nervous System*. Lyon, France: International Agency for Research on Cancer Press.
Kluwe, L., Hagel, C., Tatagiba, M., Thomas, S., Stavrou, D., Ostertag, H., von Deimling, A. and Mautner, V. F. (2001). Loss of NF1 alleles distinguish sporadic from NF1-associated pilocytic astrocytomas. *J. Neuropathol. Exp. Neurol.* **60**, 917-920.
Kurtz, A., Zimmer, A., Schnutgen, F., Bruning, G., Spener, F. and Muller, T. (1994). The expression pattern of a novel gene encoding brain-fatty acid binding protein correlates with neuronal and glial cell development. *Development* **120**, 2637-2649.
Lau, N., Feldkamp, M. M., Roncari, L., Loehr, A. H., Shannon, P., Gutmann, D. H. and Guha, A. (2000). Loss of neurofibromin is associated with activation of RAS/MAPK and PI3-K/AKT signaling in a neurofibromatosis 1 astrocytoma. *J. Neuropathol. Exp. Neurol.* **59**, 759-767.
Lendahl, U., Zimmerman, L. B. and McKay, R. D. (1990). CNS stem cells express a new class of intermediate filament protein. *Cell* **60**, 585-595.
Li, J., Perry, A., James, C. D. and Gutmann, D. H. (2001). Cancer-related gene expression profiles in NF1-associated pilocytic astrocytomas. *Neurology* **56**, 885-890.
Listernick, R., Louis, D. N., Packer, R. J. and Gutmann, D. H. (1997). Optic pathway gliomas in children with neurofibromatosis **1**, consensus statement from the NF1 Optic Pathway Glioma Task Force. *Annu. Neurol.* **41**, 143-149.
Listernick, R., Charrow, J. and Gutmann, D. H. (1999). Intracranial gliomas in neurofibromatosis type 1. *Am. J. Med. Genet.* **89**, 38-44.
Maher, E. A., Furnari, F. B., Bachoo, R. M., Rowitch, D. H., Louis, D. N., Cavenee, W. K. and DePinho, R. A. (2001). Malignant glioma: genetics and biology of a grave matter. *Genes Dev.* **15**, 1311-1333.
Malatesta, P., Hartfuss, E. and Gotz, M. (2000). Isolation of radial glial cells by fluorescent-activated cell sorting reveals a neuronal lineage. *Development* **127**, 5253-5263.
Malatesta, P., Hack, M. A., Hartfuss, E., Kettenmann, H., Klinkert, W., Kirchhoff, F. and Gotz, M. (2003). Neuronal or glial progeny: regional differences in radial glia fate. *Neuron* **37**, 751-764.
Mi, H. and Barres, B. A. (1999). Purification and characterization of astrocyte precursor cells in the developing rat optic nerve. *J. Neurosci.* **19**, 1049-1061.
Noctor, S. C., Flint, A. C., Weissman, T. A., Dammerman, R. S. and Kriegstein, A. R. (2001). Neurons derived from radial glial cells establish radial units in neocortex. *Nature* **409**, 714-720.
Nordlund, M. L., Rizvi, T. A., Brannan, C. I. and Ratner, N. (1995). Neurofibromin expression and astrogliosis in neurofibromatosis (type 1) brains. *J. Neuropathol. Exp. Neurol.* **54**, 588-600.
Qian, X., Shen, Q., Goderie, S. K., He, W., Capela, A., Davis, A. A. and Temple, S. (2000). Timing of CNS cell generation: a programmed sequence of neuron and glial cell production from isolated murine cortical stem cells. *Neuron* **28**, 69-80.
Ridet, J. L., Malhotra, S. K., Privat, A. and Gage, F. H. (1997). Reactive astrocytes: cellular and molecular cues to biological function. *Trends Neurosci.* **20**, 570-577.
Rizvi, T. A., Akunuru, S., de Courten-Myers, G., Switzer, R. C., 3rd, Nordlund, M. L. and Ratner, N. (1999). Region-specific astrogliosis in brains of mice heterozygous for mutations in the neurofibromatosis type 1 (Nf1) tumor suppressor. *Brain Res.* **816**, 111-123.
Rosenbaum, T., Boissy, Y. L., Kombrinck, K., Brannan, C. I., Jenkins, N. A., Copeland, N. G. and Ratner, N. (1995). Neurofibromin-deficient fibroblasts fail to form perineurium in vitro. *Development* **121**, 3583-3592.
Rubin, J. B. and Gutmann, D. H. (2005). Neurofibromatosis type 1 – a model for nervous system tumour formation? *Nat. Rev. Cancer* **5**, 557-564.
Soriano, P. (1999). Generalized lacZ expression with the ROSA26 Cre reporter strain. *Nat. Genet.* **21**, 70-71.
Temple, S. (2001). The development of neural stem cells. *Nature* **414**, 112-117.
Viskochil, D. H. (1999). The structure and function of the NF1 gene: molecular pathology. In *Neurofibromatosis: Phenotype, Natural History, and Pathogenesis* (ed. J. M. Friedman, D. H. Gutmann, M. MacCollin and V. M. Riccardi), pp. 119-141. Baltimore: Johns Hopkins Press.
Xu, G. F., Lin, B., Tanaka, K., Dunn, D., Wood, D., Gesteland, R., White, R., Weiss, R. and Tamanoi, F. (1990). The catalytic domain of the neurofibromatosis type 1 gene product stimulates ras GTPase and complements ira mutants of S. cerevisiae. *Cell* **63**, 835-841.
Zhu, Y. and Parada, L. F. (2002). The molecular and genetic basis of neurological tumours. *Nat. Rev. Cancer* **2**, 616-626.
Zhu, Y., Richardson, J. A., Parada, L. F. and Graff, J. M. (1998). Smad3 mutant mice develop metastatic colorectal cancer. *Cell* **94**, 703-714.
Zhu, Y., Romero, M. I., Ghosh, P., Ye, Z., Charnay, P., Rushing, E. J., Marth, J. D. and Parada, L. F. (2001). Ablation of NF1 function in neurons induces abnormal development of cerebral cortex and reactive gliosis in the brain. *Genes Dev.* **15**, 859-876.
Zhu, Y., Ghosh, P., Charnay, P., Burns, D. K. and Parada, L. F. (2002). Neurofibromas in NF1: Schwann cell origin and role of tumor environment. *Science* **296**, 920-922.
Zhu, Y., Guignard, F., Zhao, D., Liu, L., Burns, D. K., Mason, R. P., Messing, A. and Parada, L. F. (2005). Early inactivation of p53 tumor suppressor gene cooperating with NF1 loss induces malignant astrocytoma. *Cancer Cell* **8**, 119-130.
Zhuo, L., Theis, M., Alvarez-Maya, I., Brenner, M., Willecke, K. and Messing, A. (2001). hGFAP-cre transgenic mice for manipulation of glial and neuronal function in vivo. *Genesis* **31**, 85-94.